Universidade de Aveiro Departamento de Engenharia Cerâmica e do Vidro
2008

Zhi Fu

$BaNd_2Ti_5O_{14}$ Thick Films for Microelectronics Fabricated by Electrophoretic Deposition

Filmes espessos de $BaNd_2Ti_5O_{14}$ para a microelectrónica fabricados por deposição electroforética

Universidade de Aveiro Departamento de Engenharia Cerâmica e do Vidro
2008

Zhi Fu

$BaNd_2Ti_5O_{14}$ Thick Films for Microelectronics Fabricated by Electrophoretic Deposition

Filmes espessos de $BaNd_2Ti_5O_{14}$ para a microelectrónica fabricados por deposição electroforética

Dissertação apresentada à Universidade de Aveiro para cumprimento dos requisitos necessários à obtenção do grau de Doutor em Engenharia e Ciência de Materiais, realizada sob a orientação científica da Professora Dra. Paula Maria Vilarinho, Professora Associada do Departamento de Engenharia Cerâmica e do Vidro da Universidade de Aveiro e do Professor Angus I. Kingon, Professor Catedrático da Divisão de Engenharia da Universidade de Brown,nos Estados Unidos da America.

A dissertation presented to the University of Aveiro to obtain the Doctor degree in Materials Science and Engineering, under the scientific guidance of Professor Dr. Paula Maria. Vilarinho, Associate Professor of the Department of Ceramics and Glass Engineering of the University of Aveiro, and Professor Angus I. Kingon, Full Professor of the Division Engineering of Brown University, USA.

Financial support from FCT.

o júri

presidente

Prof. Luís António Ferreira Martins Dias Carlos, Departamento de Física da Universidade de Aveiro

Prof. Tim W. Button, The Interdisciplinary Research Centre (IRC) in Materials Processing, University of Birmingham, United Kingdom

Prof. Luís Manuel Cadillon Martins Costa, Departamento de Física da Universidade de Aveiro

Prof. Fernando Bico Marques, Departamento de Engª Cerâmica e do Vidro da Universidade de Aveiro

Prof. Angus I. Kingon, Division of Engineering, Brown University, USA, (co – orientador)

Prof. Paula Maria Lousada Silveirinha Vilarinho, Departamento de Engª Cerâmica e do Vidro da Universidade de Aveiro, (orientadora)

Acknowledgements

I am very grateful to my supervisor Prof. Dr. Paula M. Vilarinho for her guidance, support, discussion, suggestions and constant encouragement throughout this study. We always share our passion during this work. And under her critical supervision and powerful advisement, my PhD time was very enriching and profitable.

I am very grateful to my co-supervisor Prof. Angus I. Kingon for his wide knowledge; he was always open for discussions and ready to share his deep understanding of material science.

Many thanks to Dr. Aiying Wu for her selfless help during the course of this work. She is always willing to listen, discuss and give advice through. A lot of help I received from other members of the Department of Ceramics and Glass Engineering of the University of Aveiro. This concerns not only the scientific work but also the friendship and cheerful atmosphere of the Electroceramics Group and of the Department. In order not to miss some of their names, I want to thank all of them.

I would like to express thanks to Prof. Ian M. Reaney for the useful discussions on microwave materials and TEM characterization and also for inviting me to visit his group in Sheffield during my PhD program. Many thanks to Dr. Rosario Soares from the Central Laboratory of the University of Aveiro for the XRD studies and profitable discussions.

I would like to express thanks to Dr. Roger Wordenweber, Dr. Anna Axelssson and Prof. Neil Alford for the measurements at MW frequencies.

I acknowledge FCT, the Portuguese Foundation for Science and Technology for financial support.

I am very grateful to my family and friends for their support over the years.

Last but not least, many thanks to my wife, Gao Jie for her patience, her enthusiastic support and her continuous understanding.

palavras-chave

Filmes espessos, deposição electroforética, $BaNd_2Ti_5O_{14}$, elevado Q, baixas perdas dieléctricas, microelectrónica, microondas, frequências elevadas

resumo

Nos dias que correm os engenheiros de circuítos na área da microelectrónica são confrontados com a necessidade de desenhar circuítos que permitam um maior transporte de informação numa menor largura de banda, que consumam menos energia e ao mesmo tempo com a necessidade de criar produtos de dimensões menores e mais flexíveis, com maiores níveis de integração, operação a frequências mais elevadas e a custos mais reduzidos. Neste contexto, a substituição de componentes dieléctricos cerâmicos na forma de monolitos, que são parte integrante de determinados dispositivos microelectrónicos que operam a frequências elevadas (filtros e antennas, por exemplo), por dieléctricos processados na forma de filmes espessos está sob consideração. Com esta aproximação espera-se, por um lado conseguir uma redução do tamanho do dispositivo e dos custos associados à sua produção e por outro lado, e de particular relevância, explorar as oportunidades criadas pela possibilidade de processar filmes conformes com substratos de diferentes formas e de natureza metálica. Novas estruturas e concepções para dispositivos que operam a frequências elevadas deverão ser criadas. Ao mesmo tempo, crê-se contribuir para o desenvolvimento de processos de fabrico de produção em massa de filmes de materiais dieléctricos com desempenho reproductível e a baixos custos.

As técnicas de preparação de filmes finos incluem a fabricação por cinta (“tape casting”), por impressão em tela (“screen printing”), por jacto de tinta (“jet printing”) e por deposição electroforética (“electrophoretic deposition”, EPD). A importância da deposição electroforética advém das suas características únicas, que incluem a simplicidade e flexibilidade na aplicação a vários tipos de materiais e combinações de materiais numa gama alargada de formas e dimensões de estruturas, na relação fabricação – custos e na capacidade de dimensionar o processo à escala industrial para fabricação de volumes elevados de produtos e de grandes dimensões. Concomitantemente, quando comparado com os outros processos de fabricação de filmes espessos, a deposição electroforética permite a produção de camadas de uniformidade excepcional com um fácil controlo da sua espessura. Desta forma a fabricação de filmes espessos por deposição electroforética vai de encontro às actuais necessidades da indústria da microelectrónica no que respeita à substituição dos componentes dieléctricos monolitos em uso hoje em dia.

Em relação aos materiais, os dieléctricos que podem ser utilizados como componentes de dispositivos de operação às frequências das microondas, deverão possuir perdas dieléctricas baixas, factor de qualidade (definido como o inverso das perdas dieléctricas) elevado, permitividade dieléctrica elevada e coeficiente de temperatura da permitividade baixo. De entre os dieléctricos com baixas perdas, o sistema $BaO\text{-}Nd_2O_3\text{-}TiO_2$ representa uma importante família comercial de materiais para utilização às frequências das microondas, em particular a composição 1:1:5, que, porque reúne as características acima

mencionadas, é um material de referência para estas aplicações. Embora cerâmicos de $BaO\text{-}Nd_2O_3\text{-}TiO_2$ estejam actualmente em produção e comercialmente disponíveis em resonadores, filtros e substratos, entre outras aplicações, o uso de filmes espessos de BNT não foi até à realização deste estudo, referido.

Neste trabalho, é explorada a fabricação por deposição electroforética de filmes espessos de $BaNd_2Ti_5O_{14}$ (BNT). Para tal é conduzido um estudo sistemático do processo de deposição, desde a prova de conceito de aplicação do processo de deposição electroforética até à definição de condições reprodutíveis e optimizadas de deposição. São utilizados pós comerciais e pós fabricados em laboratório que foram depositados sobre folhas metálicas flexíveis de platina e substratos de alumina.

Inicia-se o trabalho pela prova do conceito de aplicação da deposição electroforética ao fabrico de filmes de BNT. Filmes de BNT com 12 a 52 μm de espessura são fabricados a partir de pós de BNT comerciais sobre substratos de platina. Para melhorar a densidade em verde e a microestutura dos filmes obtidos recorre-se a uma etapa intermédia de prensagem isostática dos filmes em verde. O efeito da espessura dos filmes nas propriedades dieléctricas a baixas frequências é analisado. À medida que a espessura do filme aumenta, as propriedades dieléctricas dos filmes de BNT aproximam-se das propriedades dos cerâmicos de BNT em termos de permitividade e perdas dieléctricas. Filmes de BNT com 52 μm de espessura e sinterizados a 1300 ℃ durante 1 h exibem uma constante dieléctrica e uma perda dieléctrica de 107 e 0.0006 ou um factor de perda Q de 1600 a 1 MHz, respectivamente. A variação de permitividade dieléctrica é inferior a 0.02 % a um campo eléctrico de ±8 kV/cm e na gama de temperatura entre 30-120 ℃ é abaixo de +58.5 ppm/℃. O estudo revela ainda que não há degradação das propriedades dos filmes de BNT até 1.4 GHz, relativamente às propriedades medidas à frequência de 1 MHz.

Após a prova de conceito, são conduzidos estudos de optimização do processo de deposição. Para tal foram especificamente sintetizados por processo convencional de reacções no estado sólido pós de BNT.

O sucesso no processo de fabricação por EPD está intimamente relacionado com a escolha do meio de suspensão e aditivos, que devem originar uma suspensão estável com um grau de dispersão das partículas elevado. Neste trabalho são estudados quatro meios suspensores diferentes, que incluem, água, acetona, etanol e ácido acético. As propriedades físico – químicas das diferentes suspensões foram analisadas pelo determinação do potencial zeta, da distribuição do tamanho de partícula e transmitância de luz. Os resultados experimentais revelam que o potencial zeta é uma medida directa da estabilidade das suspensões, visto que o máximo do potencial zeta corresponde ao máximo de dispersão da suspensão que se reflecte também na distribuição do tamanho de partícula e no comportamento em termos de

transmissão de luz através da suspensão. O máximo de potencial zeta (61 mV) é obtido para o meio suspensor de acetona com adições de I_2, a que corresponde uma transmitância de 10%. O efeito dos diferentes meios suspensores é estudado na deposição, microestrutura e propriedades dieléctricas dos filmes de BNT. De entre os vários meios suspensores, apenas o ácido acético e a acetona com I_2 apresentam a capacidade para formação de depósitos e as limitações do ácido acético são analisadas em termos da reproductibilidade do processo. Camadas depositadas de homogeneidade e taxa de deposição elevadas e com superfícies macias foram obtidas com o meio suspensor à base de acetona. Para este caso, o efeito de vários parâmetros de processamento, que incluem o campo eléctrico aplicado, o tempo de deposição e a composição da suspensão e a espessura e morfologia dos filmes é investigada e a discutida.

Conjuntamente, e sob as condições optimizadas de deposição é estudado o efeito da temperatura de sinterização na estrutura, microestrutura e propriedades dieléctricas dos filmes espessos de BNT. Para tal filmes de BNT com 10 a 80 μm de espessura foram fabricados por EPD sobre folhas de Pt em diferentes condições. O impacto dos parâmetros de processamento: campo eléctrico, substrato e temperatura de sinterização são analisados e discutidos. Observa-se que um aumento da temperatura de sinterização aumenta acentuadamente a razão de aspecto dos grãos, decresce a permitividade dieléctrica relativa e o coeficiente de temperatura da permitividade $TC\varepsilon_r$ varia de -114 para +12 ppm/℃. É então proposto que a anisotropia do grão observada é facilidade pelas condições de sinterização restrictas (“constrained sintering”). Através do controlo da temperatura de sinterização filmes espessos de $TC\varepsilon_r$ quase nulo, Q elevado com $45< \varepsilon_r<70$ podem ser fabricados. Esta descoberta é de especial relevância tecnológica visto que demonstra que o controlo da tensão originada pelo substrato e as condições de sinterização podem ser usadas para controlar a anisotropia do cerscimento do grão e consequentemente as propriedades dieléctricas dos filmes de $BaO\text{-}Re_2O_3\text{-}TiO_2$. Ao mesmo tempo o fabrico de filmes com propriedades controladas contribui para a diminuição das dimensões dos dispositivos que operam a frequências elevadas. Esperam-se observações semelhantes em outros sistemas de materiais, o que abre ainda mais o leque de oportunidades em termos tecnológicos.

Para aplicações específicas, camadas espessas de dieléctricos sobre substratos isoldaores podem ser necassárias. Contudo a fabricação de filmes por deposição electroforética é incompatível com o uso de substratos isoladores; assim sendo foi desenvolvido e é apresentado neste trabalho um método de fabricação de filmes sobre substratos isoladores por deposição electroforética. Para ultrapassar esta dificuldade, substratos de alumina foram recobertos com uma “camada sacrífício” de grafite. Filmes uniformes e densos

foram então depositados sobre substratos de alumina (Al_2O_3). A influência da espessura da camada de grafite e a sua interacção com os filmes de BNT na estrutura, microestrutura e resposta dieléctrica é avaliada e discutida. Intercações marcadas entre os filems de BNT e os substratos de alumina foram observadas a temperaturas superiores a 1300 ºC. A difusão dos iões de Al para o interior dos filmes origina a formação de segundas fases de aluminatos de neodimio. Contudo filmes de BNT de espessura de 100 μm e sinterizados a 1250 ºC durante 1h exibem uma permitividade dieléctrica relativa e valores de Q de146 e 1161 a cerca de 10 GHz, respectivamente. Crê-se que esta aproximação do uso de uma "camada sacrífício" de grafite sobre substratos não condutores é muito importante e válida, já que pode ser extendida para a deposição de filmes espessos e finos a uma variedade alargada de materiais funcionais sobre um leque também alargado de substratos não condutores.

Um outro desafio em termos de industria microelectónica, em particular a relacionada com o fabrico de dispositivos sintonizáveis de operação a frequências elevadas, é a fabricação de dieléctricos de perdas baixas e sintonabilidade elevada. Neste trabalho propõe-se uma aborgadem de engenharia para ultrapassar esta limitação. Assim reporta-se a preparação e caracterização de compósitos de $BaNd_2Ti_5O_{14}$ (BNT) - $Ba_{0.5}Sr_{0.5}TiO_3$ (BST) sobre folhas de Pt, através da combinação do processo de deposição electroforética com o processo sol gel.

Filmes compósitos de BNT – BST com espessuras de 9μm sobre Pt, homogéneos, densos e uniformes exibem permitividade e perda dieléctrica de 287 e 0.0013 a 1MHz, e sintonização da permitividade dieléctrica de 12% a 33 kV/cm, e coeficiente de temperatura da permitividade de 0.26% entre 28 ºC e 120 ºC, respectivamente. Acima de tudo estes filmes exibem um dos facoters de qualidade K mais elevados referidos na literatura. Assim, a actual limitação de dieléctricos sintonizáveis de baixa perda é de certo modo ultrapassada e considera-se que estes resultados têm uma implicação alargada na comunidade microelectrónica de dispositivos sintonizáveis a frequências elevadas.

keywords

thick films, electrophoretic deposition (EPD), $BaNd_2Ti_5O_{14}$, high Q, low loss, microelectronics, microwave, high frequency

abstract

Currently RF and MW design engineers are being asked to send more bits over less bandwidth, use less battery power, and create products that are smaller and more flexible, which include increased integration, operation at higher frequencies and reduced costs. In this context the replacement of the current bulk ceramic dielectric components of some microelectronic devices (filters, baluns and antennas) by dielectrics processed as thick films is now being considered. With this methodology it is expected, besides reducing device size, to reduce processing costs and of particular relevancy are the opportunities created by the possibility to process thick films conformally on substrates and on metal foils. New structures and designs for such devices to operate at high frequencies are then expected. At the same time, this drives the search for fabrication processes for films materials to be mass-produced with repeatable performance at very low costs.

The techniques for the preparation of thick films include tape casting, screen printing, jet printing or electrophoretic deposition (EPD). The importance of EPD comes from its unique features, such as the high flexibility and simplicity for application with various materials and combinations of materials, and on a wide range of shapes and 3D complex and porous structures, its cost-effectiveness, and its ability to be scaled-up to the fabrication of large product volumes and sizes. In addition, when compared with the other methods, EPD enables the fabrication of highly uniform layers with an easy control of the layer thickness. As so, EPD matches well with the current considerations of the microelectronics industry of replacement of bulk dielectric components by dielectrics processed as thick films.

Pertaining to materials, dielectrics which may be employed as microwave components must exhibit low loss or high quality factor Q, high relative permittivity and small temperature coefficient of relative permittivity ($TC\varepsilon_r$). Within low loss dielectrics, the $BaO\text{-}Nd_2O_3\text{-}TiO_2$ system represents an important commercial family of microwave materials, particularly the 1:1:5 composition, that because it exhibits low dielectric losses, high quality factor, high relative permittivity and small temperature coefficient of resonant frequency, have been known as an important microwave dielectric material. Although $BaO\text{-}Nd_2O_3\text{-}TiO_2$ ceramics are currently being produced for resonators, filters and substrates, among others applications, the use of BNT thick films have not been reported until the realization of this PhD program.

In this work, the fabrication of $BaNd_2Ti_5O_{14}$ (BNT) thick films by EPD is exploited. For that a systematic research study of the EPD process is conducted from the proof-of-concept till the definition of reproducible and optimised process conditions. Commercial and “home made” $BaNd_2Ti_5O_{14}$ powders were used to fabricate BNT films on platinum foils and polycrystalline alumina substrates.

The technological feasibility of using EPD for the fabrication of BNT thick films

was firstly studied. 12 to 52 μm thick BNT films were fabricated from BNT commercial powders on platinum metallic foils by EPD. To improve the microstructure and density of the films a post deposition isostatic pressing step was used. The effect of film thickness on the dielectric properties at low frequencies was investigated. As the film thickness increases, the dielectric properties of BNT films approach those of BNT ceramics in terms of permittivity and loss tangent. 52 μm-thick BNT film sintered at 1300 ℃ for 1 h exhibit a dielectric constant and a loss tangent of 107 and 0.0006 (or Q of 1600) at 1 MHz, respectively. The variation in permittivity is less than 0.02 % at a bias voltage ±8 kV/cm. The change of film permittivity with the temperature within the range 30-120 ℃ is below +58.5 ppm/℃. Compared to at 1 MHz, the dielectric properties of 52 μm thickness BNT films do not show tremendously degradation till up to 1.4 GHz.

After the proof-of-concept, the optimization of the EPD process was conducted. For that BNT powders were specifically synthesised by the conventional solid state reaction method.

The success in the EPD process is intimately related to a careful choice of the suspension media and additives, which should lead to well-dispersed and stable suspensions for EPD. Four different suspension media, which included de-ionized water, acetone, ethanol, and glacial acetic acid (HAC), were studied. The physicochemical properties of the different suspensions were evaluated and analyzed by zeta potential, particle size distribution and light transmittance. Experimental results revealed that the zeta potential is a straightforward indication of the stability of these suspensions, since the maximum absolute zeta potential corresponds to a maximum of the suspension dispersibility, also reflected in the particle size distribution and suspension light transmittance behaviour. The maximum zeta potential was obtained for acetone with iodine suspensions (61 mV), and the corresponding transmittance was 10%. The effect of different solvents was studied on the deposition, microstructure and dielectric properties of BNT thick films. Among the used solvents, only the acetic acid and acetone with I_2 based suspensions showed the ability of forming deposits and the limitations of acetic acid solvent was analyzed in terms of the process reproducibility. Deposits with homogeneous, smooth surface and high deposition yield were obtained upon adding I_2 to the acetone based suspension. For the case of acetone with I_2 suspensions, the effect of EPD process parameters such as deposition voltage, deposition time and suspension composition, deposited thickness of BNT and film morphology was investigated and discussed.

In addition, under the definition of the optimal conditions for EPD BNT thick films, the effect of the post deposition sintering temperature was addressed on the structure, microstructure and dielectric properties of BNT thick films. For that 10 to 80 μm thick $BaNd_2Ti_5O_{14}$ (BNT) films were fabricated by electrophor-

-etic deposition on Pt foils under different conditions. The impact of the processing parameters: electric field during EPD, the substrate effect and the sintering temperature were analyzed and discussed. It was observed that the increase of the sintering temperature increases markedly the aspect ratio of the grains, decreases the dielectric permittivity and TCε_r changes from -114 to +12 ppm/℃. It was then proposed that the observed anisotropic grain growth is facilitated by the constrained sintering. By controlling the sintering temperature, near – zero TCε_r, high Q thick films can be fabricated with 45< ε_r<70. These findings are of technological relevance since they demonstrate that control of substrate constraint and sintering conditions can be used to control grain anisotropy and thus microwave properties of the $BaO\text{-}Re_2O_3\text{-}TiO_2$. The thick films facilitate scaling to small device sizes for high frequency operation. Similar observations are expected in other MW systems thus opening further technological opportunities.

For some specific applications, such as multilayer microstrip for band-pass microwave filter applications, thick dielectric layers on insulating substrates may be required. However the fabrication by EPD is incompatible with the use of insulating substrates, so a method of performing EPD on non-conducting substrates was developed and is reported in this work. To overcome the requirement of a conducting substrate, insulating polycrystalline alumina substrates were covered with a sacrificial graphite layer. Uniform and dense BNT layers have been then deposited on alumina (Al_2O_3) substrate by EPD. The influence of the graphite layer thickness and the interactions between the BNT films and alumina substrates on the final structure, microstructure and dielectric response were addressed and discussed. Severe interactions between the BNT films and alumina substrates were observed for sintering temperatures >1300 ℃. The diffusion of Al ions into the films resulted in the formation of neodymium aluminates second phases. However 100 μm thick BNT films sintered at 1250 ºC/1h show relative permittivity and Q values of 146 and 1161 at about 10 GHz, respectively. It is believed that this approach of using sacrificial graphite layers for EPD on non-conducting substrates is extremely valuable since it can be extended for both thin and thick film deposition on a large variety of other non-conducting substrates.

Another challenge for the microelectronics agile / tunable industries is the fabrication of low loss tunable microwave dielectrics because lower loss tangents provide lower insertion loss in the device. In the work an approach to overcome this limitation is proposed. The preparation and characterization of $BaNd_2Ti_5O_{14}$ (BNT) - $Ba_{0.5}Sr_{0.5}TiO_3$ (BST) composite thick films on flexible platinum foil substrate, via an EPD process combined with a sol gel one was reported. Homogeneous, dense, and uniform 9μm-thick BNT-BST composite thick films on flexible Pt foils exhibit dielectric constants and loss tangent of 287 and 0.0013 at 1MHz, and dielectric tunability of 12% at 33kV/cm, and tempera-

-ture coefficient of relative permittivity of 0.26% between 28ºC to 120ºC, respectively. Above all these films exhibit one of the highest quality factor (*K* = 70) reported for dielectric films. As such the actual limitation of low loss high tunable dielectrics is somehow surmount and these results are expected to have broad implications in the community of microwave agile devices.

Table of Contents

List of Figures

List of Tables

List of Symbols

α - Length

α_l – Linear thermal expansion coefficient

d – Spacing

D - Diameter

E - Dc bias electric field

f – Frequency

k_B - Boltzmann constant (1.38066· × 10^{-23} J/K)

L_{dB} - Insertion loss in dB

n - Tunability

n_r - Relative tunability

P - Polarization

P_r - Remnant polarization

P_s - Spontaneous polarization

p - Isostatic pressure

Q - Quality factor

T – Temperature

ΔT - Temperature change

Tanδ - Loss tangent or dissipation factor

T_c - Temperature of the phase transition (Curie temperature)

TCC – Temperature coefficient of capacitance

$TC\varepsilon_r$ – Temperature coefficient of relative permittivity

V – Voltage

ε_r - Relative permittivity or dielectric constant

ε_0 - Dielectric constant of vacuum (8.854 × 10^{-12} F/m)

ε^* - Complex dielectric permittivity

ε' - Real part of dielectric permittivity

ε'' - Imaginary part of dielectric permittivity

ε'(0) - Zero-field dielectric constant

ε'(E) - Dielectric constant under bias electric field

$\dot{\varepsilon}$ - Strain rate

η – Viscosity

μ - Electrophoretic mobility

τ_f - Temperature coefficient of resonant frequency

χ' - Real part of dielectric susceptibility

χ'' - Imaginary part of dielectric susceptibility

ψ - Angle 90°-δ

ω - Angular frequency

λ - Wave length

ρ - Density

ν^p - Poisson's ratio

List of Abbreviations

AES - Atomic Emission Spectrometry

BET - Brunauer, Emmett and Teller

BMT - $Ba(Mg_{1/3}Ta_{2/3})O_3$

BCZN - $Ba(Co,Zn)_{1/3}Nb_{2/3}O_3$

BRT - $BaO\text{-}Re_2O_3\text{-}TiO_2$ (R- rare earth)

BNT - Barium Neodymium Titanate ($BaO\text{-}Nd_2O_3\text{-}TiO_2$)

BST – $(Ba_xSr_{1-x})TO_3$

BT – $BaTiO_3$

CIP- Cold Isostatic Press

CMM - Ceramic Multicomponent Modules

CNT - Carbon Nano Tube

DLS - Dynamic Light Scattering

DLVO - Derjaguin, Landau, Verwey and Overbeek

DR-Dielectric Resonator

DTA - Differential Thermal Analysis

DC - Direct Current

ED - Electron Diffraction

EDS - Energy Dispersive Spectroscopy

ELS - Electrophoretic Light Scattering

EPD - Electrophoretic Deposition

FWHM - Full Width at Half Maximum

GPS - Global Positioning System

IC - Integrated Circuit

ICP - Inductively Coupled Plasma

LAN - Local Area Network

MIC - Microwave Integrated Circuit

MIM - Metal Insulator Metal

MMIC - Monolithic Microwave Integrated Circuit

MW – Microwave

PCS - Personal Communication Systems

ppm - Parts Per Million

PSD - Particles Size Distribution

PZT - $(Pb_xZr_{1-x})TiO_3$

RF - Radio Frequency

RT - Room Temperature

SEM - Scanning Electron Microscopy

SPDR - Split Post Dielectric Resonator

ST - Sintering Temperature

TEM - Transmission Electron Microscopy

TG -Themogravimetry

UV - Ultraviolet Light

WLAN - Wireless Local Area Networks

XRD - X-ray Diffraction

YBCO - Yttrium Barium Cuprate

YSZ – Ytrria Stablized Zirconia

ZST - $(Zr,Sn)TiO_4$

Chapter 1
An Introduction to Low loss (High Q) Dielectric Ceramic Materials, Properties and Applications

Abstract:
Low loss dielectric ceramics are playing a very important role in the microwave communication systems. These materials are key factors in realization of low-loss temperature-stable components for satellite and broadcasting equipment, and in many other microwave devices. High dielectric-constant materials are critical to the miniaturization of wireless systems, both for the terminals and base-stations, as well as for handsets. This chapter reviews the sequential evolution of the dielectric ceramics applications in microwave devices, and the development of low loss dielectrics, such as, $BaO\text{-}Nd_2O_3\text{-}TiO_2$ (BNT) systems. The recent advances in the applications of low loss dielectric ceramics in electronic circuits and systems are also described.

1.1 Definitions

For microwave dielectrics, there are three important properties to be considered: the relative permittivity, the loss tangent (or quality factor), and the temperature coefficients of the resonant frequency. The relative permittivity determines the size of the electronic component, the temperature coefficient of resonant frequency determines the temperature stability, and the loss tangent (or Q factor) determines the selectivity and performance of the device. [Scotta A. W.-1993]

1.1.1 Relative Permittivity

Relative Permittivity is of paramount importance when discussing dielectric materials. Relative permittivity is a physical quantity that describes how an electric field affects and is affected by a dielectric medium, and is determined by the ability of a material to polarize in response to the field, and thereby reduce the total electric field inside the material.

The overall net polarization experienced in a material, P, creates a dipole moment which augments the total displacement flux of dipole, D. Thus,

$$D = \varepsilon_0 E + P \qquad (1\text{-}1)$$

where E stands for the applied field; ε_0 for the permittivity of free-space. And the net polarization can be written in terms of the susceptibility, χ,

$$P = \varepsilon_0 \chi E \tag{1-2}$$

thus the relative permittivity can be defined in terms of the susceptibility that is directly related to the polarization mechanisms in a material:

$$D = \varepsilon_0 (1+\chi) E = \varepsilon_r \varepsilon_0 E \tag{1-3}$$

where

$$\varepsilon_r = \frac{\varepsilon}{\varepsilon_0} = \text{relative permittivity} \tag{1-4}$$

the relative permittivity, ε_r, is then the ratio of the natural permittivity of the material (ε) to the permittivity of free-space (ε_0). The natural permittivity, ε, is considered to be a direct measure of the polarizability of a material and will govern both the phase variation and attenuation of an imposed field to the material. Thus, the permittivity, ε, is a complex quantity with both real and imaginary parts and can be written as,

$$\varepsilon = \varepsilon' + j\,\varepsilon'' \tag{1-5}$$

the real part of the relative permittivity, ε', is termed the dielectric constant and is determined by the magnitude of P. It defines the amount of electrostatic energy stored per unit volume in a material for a given applied field, i.e. the amount of charge stored in a capacitor. The imaginary component of the permittivity, ε'', is called the loss factor and is governed by the lag in polarization upon application of the field and the energy dissipation associated with charge polarization. It represents the energy loss in a material.

In microwave application, ε_r reflects the capability of a material to confine a microwave. The higher this parameter, the better the confinement. The ceramic microwave component is divided by the square root of the relative permittivity. High relative permittivity dielectric materials permit the miniaturization:

$$D=\lambda_0 \cdot \frac{1}{\sqrt{\varepsilon_r}} \tag{1-6}$$

where D stands for the diameter of the dielectric component, and λ_0 stands for the wavelength at the resonant frequency. As a consequence, the size reduction of a dielectric component requires materials with a high relative permittivity.

1.1.2 Loss tangent, tanδ, relates to the electrical losses in the material. And are represented by:

$$\tan\delta = \frac{\varepsilon''}{\varepsilon'} \tag{1-7}$$

where δ stands for the loss angle. In terms of an electrical circuit, tanδ represents the resistive part of the impedance and is directly proportional to the electrical conductivity. Q gives definition name and is equal to:

$$Q = 1/\tan\delta \tag{1-8}$$

as shown above, the concepts of Q-factor and loss tangent can be used interchangeably. The latter is more correct in terms of solid state physics; however the former is more commonly used in microwave circuit design. The Q of the dielectrics determines the steepness of the filter skirts, the power requirements and the selectivity of frequency. High Q values reduce the risk of cross-talk within a given frequency range. The higher the materials Q factor, the better the material, which relate to the frequency selectivity in microwave devices. Q decreases with increasing frequency and the theoretical relationship between the two is such that Qf should be constant for any given material, and, often, Qf values are quoted when comparing low loss (high Q) dielectric microwave ceramics. So, a common way for expressing losses within the microwave community, as they are linear with the frequency, is to use the "Q times frequency" factor called Qf, where f is the measurement frequency. [Reaney I. M. - 2006]

1.1.3 Temperature coefficient of resonance frequency, defined as τ_f, is a measure of the ‘‘drift’’ with respect to the temperature of the resonant frequency:

$$\tau_f = \frac{\Delta f}{f_0} \cdot \frac{1}{\Delta T} \tag{1-9}$$

where f_0 stands for the resonant frequency at ambient temperature, Δf for the frequency variation among the ΔT temperature range. It is self-evident that a material with a significantly non-zero τ_f is useless in microwave circuits as it cannot maintain its resonant frequency as the operating temperature changes.

The τ_f is a composite parameter related to temperature coefficient of relative permittivity and the linear expansion coefficient of dielectric materials, according to the following equation holds: [Moulson A. J. -1990]

$$\tau_f = -(1/2TC\varepsilon_r + \alpha_l) \tag{1-10}$$

where $TC\varepsilon_r$ stands for the temperature coefficient of relative permittivity, and α_l is the linear thermal expansion coefficient of the dielectric materials, respectively. The τ_ε describes the maximum change in relative permittivity over a specified temperature range. The presented τ_f and τ_ε are established at a reference temperature of room temperature, i.e. 25 ^oC. The τ_f should always be considered for applications operating above or below this temperature. The specification of τ_f will always specify the resonant frequency change in parts per million per degrees centigrade (ppm/^oC). The adjustment of a τ_f value must be accomplished with high accuracy (0.5-1 ppm/°C) and must be easily reproducible in production.

1.2 Important groups of low loss dielectric ceramics and applications

Microwave dielectric ceramics are characterized by high ε_r, low loss, and very small τ_f, making them attractive as electronic components in microwave applications. These unique dielectric properties permit to revolutionize the microwave-based wireless communications industry by reducing the size and cost of filter and oscillator components in systems ranging from cellular telephones to global positioning technologies.[Hirade K.-1992] In the mid-1960s, Cohn and his co-workers performed the first extensive theoretical and experimental evaluation of the low loss dielectric

resonators [Cohn S. B. -1968], based on rutile ceramics. The poor temperature stability of rutile dielectrics prevented the development of practical components for commercial applications. A real breakthrough in ceramic technology occurred in the earlies 1970s when the first temperature-stable low-loss barium–tetratitanate ceramics were developed by Masse [Masse D. J. -1971]. Later, a modified barium–tetratitanate with improved performance was reported by Bell Laboratories [Plourde J. K. -1975]. These important results led to the actual use of low loss (high Q) ceramics as microwave components. The next major breakthrough came from Japan when the Murata Manufacturing Company produced $(Zr_{0.8}Sn_{0.2})TiO_4$ ceramics [Wakino K.-1977, Wakino K.-1975], which offers adjustable compositions so that the temperature coefficient could be varied between 10 and 12 ppm/°C. These low loss dielectric devices became commercially available at reasonable prices. Afterwards, the use of low loss dielectric ceramic components expanded rapidly. [American Technical Ceramics Ltd.]

Today, low loss dielectric ceramics are commercially important as enabling materials for resonators, filters, and other key components in microwave communications systems. The global market for the low loss dielectric ceramics is on the order of $400 million, and the markets for the resulting devices and components, and for the end-user systems, are ~10 and ~100 times of that size, respectively. [Vanderah T. A.-2002]

Low loss dielectric ceramics are very popular as the substrates for microstrip lines and coplanar waveguides for microwave and millimeter-wave integrated circuits. A microstrip antenna (or patch antenna) for the receivers of a global positioning system (GPS), that use a relative high permittivity dielectric substrate has several advantages such as small size, narrow frequency band, and good temperature stability. Other microwave components, such as forward directional couplers and simple phase shifters can be fabricated from low loss dielectric ceramics. The most successful fabricated components have been in the area of antennas, either surface-wave antennas or leaky-wave antennas. [Hessel A.-1969] Several types of miniature antennas are now in use.

Application of dielectric materials in microwave components is very cost effective and leads to a significant miniaturization of the device, particularly when microwave integrated circuit (MIC) or monolithic microwave integrated circuit (MMIC) structures are used. Excellent performance in filters and oscillators is currently being achieved. Dielectric resonators (DRs) are widely used in wireless communication systems. Additional applications include radar, satellite, portable telephone, satellite broadcasting,

ultra-high speed wireless local area network (LAN), intelligent transport system (ITS) including ladder for anti-collision, security systems detectors and so on.[Ohsato H. -2007, Matthaei G.-1980]. Miniature dielectric-filled coaxial resonators are commonly used in wireless headsets (cellular and personal communication system (PCS) phones). Recently available very high-Q materials will extend commercial applications of DRs to much higher frequencies. Applications as high as 100 GHz are being reported. [Fiedziuszko S. J. -2002]

Future improvements of communication devices require new low loss dielectric ceramic materials. As the electronic community develops new concepts and designs for tomorrow's communication systems, they will be relying on progress in understanding and controlling these low loss (high Q) dielectric ceramics materials.

1.2.1 Materials Requirements for high frequency application

For a material to be considered as candidate for a microwave components, there are three critical requirements: [Moulson A. J-1990]

(i) Theoretically, the relative permittivity (ε_r) should be as large as possible, since the size of microwave dielectric components is inversely proportional to the square root of relative permittivity. In reality the range of materials is restricted to approximately $20 < \varepsilon_r < 100$, in order that other conditions can be met.

(ii) The dielectric loss tangent ($\tan \delta$) should be as small as possible to ensure maximum signal discrimination. This is more commonly described in terms of the dielectric Q value ($1/\tan \delta$) which should be maximized. For many current practical applications today, Q> 5000 at 1 GHz is essential.

(iii) To ensure temperature stability in communications systems, the microwave dielectric components need to have a temperature coefficient of resonant frequency (τ_f)~20 ppm/$^{\circ}$C, so that the signal does not drift during device operation.

However, obtaining optimal values of these three properties simultaneously is difficult; for example, high ε_r materials often possess a large τ_f and low Q.

Over the years, low loss dielectric ceramic materials were developed for applications in the three main categories, 1) mobile phone handsets, 2) base station application and 3) passive integration. In the first category high ε_r is mainly demanded for miniaturization of the portable device, while in the second group high Q is on

demand for increasing signal/noise ratio for base station applications and for the last group of applications in which passive integration using multilayer ceramic technology with Ag or Cu electrodes are required, moderate Q and ε_r are tolerated if the ceramic will be fired at low temperature (about 900 °C).

The variation of the Qf versus ε_r is plotted in Figure 1-1 for the three main categories of applications.

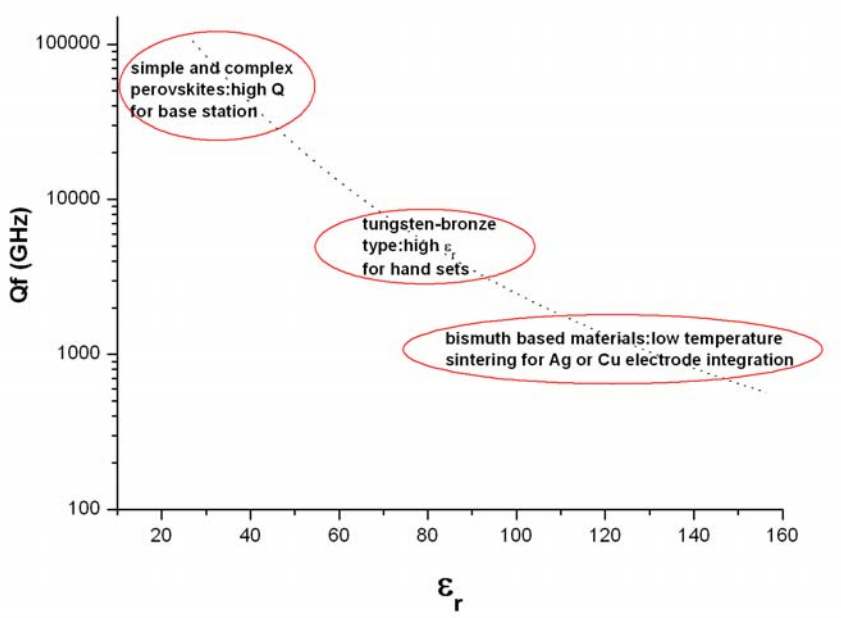

Figure 1-1 Qf versus ε_r for the three main categories of applications of low loss dielectrics

Table 1-1 lists those typical low loss (high Q) microwave ceramics that have gained the most technical importance and commercial applications so far. As mentioned before, the earliest studies of low loss dielectric materials commenced with the work of Cohn [Cohn S. B.-1968] on titania in the 1960s but also include pioneering investigations by Bolton on high relative permittivity tungsten bronze-structured $BaTiO_3$–Ln_2O_3–TiO_2 (Ln-Lathanide, i.e. Nd, Sm, La etc). [Bolton R. L.-1968] By the late 1970s and early 1980s there interest in materials such as $MgTiO_3$–$CaTiO_3$, $(Zr,Sn)TiO_4$(ZST) and $BaTi_4O_9$ appeared. $BaTi_4O_9$ was one of the first microwave ceramics to fulfill the technical requirements, with ε_r=38, τ_f=15ppm/°C and Q=5000 at 2GHz [Masse D. J.-1971]. Shortly after this, it was shown that $Ba_2Ti_9O_{20}$ ceramics possess even better properties.

The growth of the mobile communications market in the 1990s stimulated the

research in microwave dielectrics, particularly looking for relative high permittivity materials for mobile telephone handset applications, and very high Q materials for base station applications. [Reaney I. M.-2006] As shown in Table 1-1, one obtains equally good values for ε_r and Q in the ceramic system zirconium titanate stannate (ZTS) with τ_f of zero, [Wersing W.-1991] which has led to the widespread use of ceramics from this system, in such a way that ZST ceramics are today termed standard microwave ceramics.

Table 1-1 Typical examples of low loss microwave dielectric ceramics

Materials	ST*(°C)	ε_r	Qf(GHz)	τ_f(ppm/°C)	Reference
$BaTi_4O_9$	1350	38	10,000	15	Masse D. J.-1971
$Ba_2Ti_9O_{20}$	1300	40	36,000	2	Choy H.-1995
$(Zr,Sn)TiO_4$	1450	34-37	50,000	0	Hirano S.-1991
$(Ma,Ca)TiO_3$	1400	21	70,000	0	Jantunen H.-2000
$Ba(Mg_{1/3},Ta_{2/3})O_3$	1650	24	300,000	-4	Ohuchi H.-1996
$Ba(Co,Zn)_{1/3}Nb_{2/3}O_3$	1400	34	90,000	0	Reaney I. M.-2006
$BaO-R_2O_3-TiO_2$	1350	80-90	7000-13,000	<10	Ohsato H.-2003
$Bi_{1.5}ZnNb_{1.5}O_7$	950	150	1000	400	Nino J. C.-2001

*: ST means sintering temperature, R indicates rare earth element.

As indicated in Table 1-1, the highest dielectric quality factors Q have been found among microwave ceramics based on complex perovskites, such as $Ba(Mg_{1/3}Ta_{2/3})O_3$ (BMT), which provided materials with the highest Q values for base stations applications, however the commercial application interest of these materials is limited because of the high cost of tantalum raw materials. Recently $Ba(Co,Zn)_{1/3}Nb_{2/3}O_3$ (BCZN)-based ceramics have been developed as an alternative cost effective substitute of the more expensive $Ba(Mg_{1/3}Ta_{2/3})O_3$ (BMT)-based compositions. On the other hand, for the mobile telephone handset markets, the high ε_r tungsten bronze-structured materials remained the primary choice. Ceramics based on $BaO-Re_2O_3-TiO_2$ (Re-rear earth, BRT) oxides afford the highest permittivity values, of approximately 90, among the microwave ceramics, being the Nd and Sm based compositions the most frequently studied.

In summary five main families of microwave dielectrics have been identified and developed: (1) $Ba_2Ti_9O_{20}$ system, (2) $(Zr,Sn)TiO_4$ system, (3) $BaO-R_2O_3-TiO_2$ (R=rear earth) system, (4) Ba $(B_{1/3}Ta_{2/3})O3$ (B=Mg, Zn), (5) other dielectrics.

In addition, the highest miniaturization degree at the lowest cost is achieved by using multilayer ceramic technology suitable for passive integration. For microwave

ceramic multicomponent modules (CMM) ceramics are required to be sintered at low temperatures (<900 ^{o}C) to enable the cofiring with copper or silver electrodes. One important example of this group of so-called low-fire microwave ceramics is bismuth based composition (Table 1-1). Details on the sintering temperature, electrical properties of low loss microwave dielectric ceramics can be found in literature. [Sebastian M.T.-2008]

Most recently, the use of ferroelectrics has been investigated to produce novel electronic controllable devices to operate at high frequencies. Ferroelectrics are distinctive dielectric materials characterized by the existence of spontaneous polarization that is reversible under electric fields. Ferroelectrics usually exhibit high dielectric constant with a strong dependency on the applied electric fields and temperature. The relationship between the applied field and the polarization in non linear and is described by a hysteresis loop. In addition ferroelectrics can undergo a phase transition adopting a non-polar centrosymmetric structure at a temperature called T_c (the temperature of the phase transition or Curie temperature). Above T_c, with the loss of the polar structure, the material does not exhibit spontaneous polarization and it is said to be paraelectric. Below T_c, due to the appearance of the spontaneous polarization and to the mutual interaction between the dipoles, which causes a significant increase of the local field, the material exhibits ferroelectricity. The structural phase transition from the paraelectric to the ferroelectric phase is reversible. Near T_c due to a distortion in the crystalline lattice as the phase structure changes, the thermodynamic properties, including dielectric, elastic, optical, and thermal constants show an anomalous behaviour; the permittivity raises, reaching a maximum at T_c. In the ferroelectric region the increase of the thermal agitation as the temperature approaches Tc facilitates the growing of the domains oriented along the field. Above T_c the permittivity of the material decreases and at the same time a sudden reduction of the resistivity and a marked increase in the losses are observed. [Vilarinho P. M. – 2005] A detailed description of the physics of ferroelectrics is beyond the scope of the current work and several literature reviews and text books should be used for further details.

Due to the distinctive properties, ferroelectrics have many uses in electronics and microelectronics. They are often used as the dielectric in capacitors because of their high relative dielectric permittivity, and in memory applications due to the hysteresis of the polarization with the electric field and the ability to use this feature to store information. Ferroelectrics are also piezoelectric and pyroelectric, enabling their use as

mechanical transducers, actuators and or sensors and thermal detectors, such as infrared detectors.

Though ferroelectrics have the highest dielectric permittivity values, their associated high dielectric losses were traditionally a handicap for their use at high frequencies. However recently, microwave circuits that take advantage of the ability to control the relative permittivity by varying an applied electric field have been developed, in which ferroelectric materials look very promising. [Tagantsev A. K. -2003] A very good example is application such as phase shifters, which are the most widely studied tunable ferroelectric components. The importance of using ferroelectric component is owing to the role in phased array antennas. A phased array antenna consists of thousands of radiating elements which should be served by thousands of phase shifters. The phase shifters are used to modify and control the width and angle of the steered radar beam. At present each phase shifter is a housed microwave semiconductor module. The employment of ferroelectric materials enables the integration of the phase shifters with the microwave circuits on one substrate thus substantially reducing the size, mass, and cost of the antennas.

Barium titanate-$BaTiO_3$ (BT) was recognized as a very important ferroelectric material for practical applications in 1942–1943 by Von Hippel and co-workers at the Massachusetts Institute of Technology (MIT) [Hippel V.-1954]. Since then a huge number of applications have been developed for BT ceramics, thin and thick films. However, BT has a limited application in the microwave electronic industry, since the adequate tunability (change in the relative permittivity induced by a dc field) is achieved only at about 120 °C, that corresponds to the ferroelectric phase transition. The temperature range of high tunability can be shifted towards low temperature by means of Ba-site substitution by Sr, for example. Such shift corresponds to induced ferroelectric phase transition in $(Ba_xSr_{1-x})TiO_3$ (BST) solid solutions at temperatures in the range of 0-400 K. However, higher insertion loss and thermal instability of BST impose serious restrictions to its application in phased array antennas.

The efforts in using ferroelectric materials in microwave devices have been concentrated on the development of phase shifters, tunable filters, oscillators, and antennas. [Tagantsev A. K-2003] and a key aspect relates with the need to reduce the relatively high dielectric losses of ferroelectric at microwave frequencies, which has been the main barrier to implementation. However, in the long run, the tunability of the relative permittivity possible in ferroelectric materials by the changing of the electric

filed promises to enable a number of simple low-cost microwave control devices.

1.3 $BaO\text{-}Nd_2O_3\text{-}TiO_2$ (BNT) microwave dielectric ceramic materials

As stated previously, one of the most important trends in wireless technology is the miniaturization of the electronic systems. To achieve this, ceramic components such as oscillating or filtering devices must be manufactured from high-relative permittivity materials.

Among the materials listed in Table 1-1, $BaO\text{-}Nd_2O_3\text{-}TiO_2$ (BNT) system stands out and has attracted the interest of researchers and industrialists due to its high relative permittivity. [Kolar D.-1978] This interest has spread quickly to other rare earth elements besides neodymium, $BaO\text{-}R_2O_3\text{-}TiO_2$ systems (R = rare earth, such as La, Sm, Nd, Pr, BRT). And at the present the only commercially available group of high relative permittivity microwave materials are ceramics based on BRT solid solutions with relative permittivities ranging from 80 to 90. The earliest work on these systems is credited to Bolton [Bolton R. L.-1968] and Kolar et al. [Kolar D.-1978]

The BNT with stoichiometries near to $BaNd_2Ti_5O_{14}$ and $BaNd_2Ti_4O_{12}$ have been widely studied. [Ratheesh R.-1998, Rawn C. J.-1998] Following earlier reports the $BaNd_2Ti_4O_{12}$ (BaO: Nd_2O_3: $4TiO_2$) and $BaNd_2Ti_5O_{14}$ (BaO: Nd_2O_3: $5TiO_2$) are represented as BNT114 and BNT115 compounds, respectively, for convenience. Later on `1:1:4' compound was shown to belong to the solid solubility region with the general formula $Ba_{6-3x}Nd_{8+2x}Ti_{18}O_{54}$. [Rawn C. J.-1998]

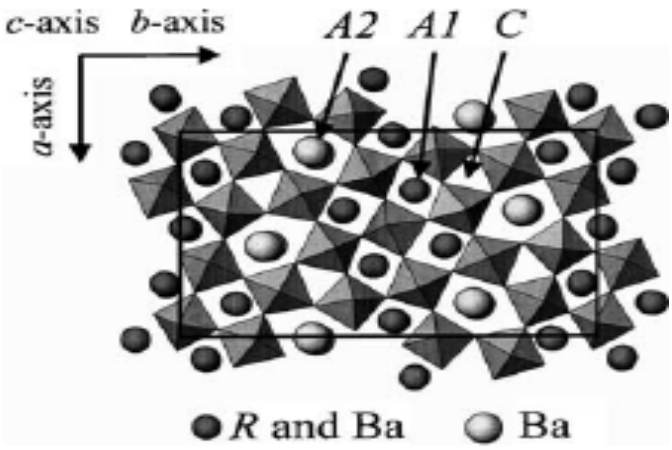

Figure 1-2 Tungsten-bronze type like crystal structure of the $Ba_{6-3x}R_{8+2x}Ti_{18}O_{54}$ solid solutions, in which R-rare earth, A1-rhombic site, A2-pentagonal site, C-trigonal site [Ohsato -2001]

The crystal structure of BRT compounds are composed of three types of large cation sites. It essentially consists of a three-dimensional framework of corner-sharing perovskite-like octahedra joined together according to a pattern similar to that of the tetragonal tungsten bronzes. The structure is typified by oxygen octahedra linked at the corners in a complex way to yield three types of channels: large pentagonal sites; diamond sites; and tiny triangular sites (Figure 1-2). The rare earth, i.e. Nd^{3+}, cations occupy the rhombic channels (diamond sites); Ba^{2+} cations fill the pentagonal channels and the remaining Ba^{2+} ions share the rhombic channels with the Nd^{3+}. The triangular channels are empty. [Ohsato H.-2001]

The crystallography of BRT solid-solutions has been reported by different authors. Gens et al.[Gens G. A.-1981] firstly suggested Pba2 (No. 32) or Pbam (No. 55) as possible space groups for the solid solution. The lattice parameters calculated for the Nd-analogue are a = 22.21 Å, b = 12.30 Å, c = 3.84 Å. These results were later confirmed by Matveeva et al. [Matveeva R. G. -1984] and Kolar et al.'s works [Kolar D. -1993]. Ohsato et al. [Ohsato H. -1992] observed superlattice XRD peaks in Nd-based 15:19:72 crystals and the space group of their fundamental lattice agreed with the previously reported. [Matveeva R.G. -1984]. Azough et al. [Azough F. -1995] also determined the space group to be either Pna21 (No. 33) or Pnam (No. 62). Later, Rawn [Rawn C. J. -1996] accounting for the c-axis doubling and re-orienting the unit cells into the standard setting for each space group, used Rietveld analysis on powder XRD data of La- and Gd-1:1:4 analogues to determine the space groups as Pna21 (No. 33) for La-1:1:4 and Pnma (No. 62) for Gd-1:1:4. The space groups suggested for the phase have included Pbam (No. 55), Pba2 (No. 32), Pbn21 (No. 33), and Pbnm (No. 62). Finally, Reaney reported that the actual space group is almost perfectly described as Pbnm (No. 62), [Ubic R.-1998] but is probably more accurately given by Pb21m (No. 26). Clearly, no general consensus has yet emerged on the space group of these solid-solutions.

In BRT family materials, the BaO-Nd_2O_3-TiO_2 (BNT) series was extensively studied by Kolar and coworkers, who discovered the ternary phases $BaNd_2Ti_3O_{10}$ (1:1:3) and $BaNd_2Ti_5O_{14}$ (1:1:5) [Kolar D.-1981]. Later, an intermediate compound with the compositional ratio of 1:1:4 ($BaNd_2Ti_4O_{12}$) was reported by Razgon and Mudrolyubova. [Razgon S. -1980, Mudrolyubova P.-1981] A summary of the dielectric data of these compositions is plotted in Table 1-2, highlighting the dependence on the stoichiometry and the inconsistency of the values. The dependence of the dielectric properties on the

composition of the BNT system is also shown in Figure 1-3 which is an isothermal section of the ternary phase diagram for BNT system.

Table 1-2 Summary of $BaO\text{-}Nd_2O_3\text{-}TiO_2$ typical compounds and their dielectric properties

Materials	Ratio*	ε_r	Qf	Frequency (GHz)	τ_f (ppm/^{o}C)	Reference
$Ba_{4.2}Nd_{9.2}Ti_{18}O_{54}$	~	88	8315	3.44	76	Ohsato H.-1995
$BaNd_2Ti_3O_{10}$	1:1:3	60	5300	4.19	140	Ratheesh R.-1998
$BaNd_2Ti_4O_{12}$	1:1:4	84	7800	6.5	88	Ubic R. thesis-1997
$BaNd_2Ti_4O_{12}$	1:1:4	45	13500	4.7	~	Wu M. C.-2007
$BaNd_2Ti_4O_{12}$	1:1:4	76	5600	3.7	77	Solomon S.-2000
$BaNd_2Ti_5O_{14}$	1:1:5	78	8900	3.7	82	Solomon S.-2000
$BaNd_2Ti_5O_{14}$	1:1:5	90	6100	4.7	3.62	Jung B. H.-2004
$BaNd_2Ti_5O_{14}$	1:1:5	81	3500	3	93	Wakino K.-1984
$BaNd_2Ti_5O_{14}$	1:1:5	88	5500	5	5	Fuji Titanium Industry Co., Ltd.
$BaNd_2Ti_5O_{14}$	1:1:5	81	12479	4.46	90	Ioachim A.-2001

*: Ratio indicates the molar proportion of the oxides (BaO: Nd_2O_3:TiO_2)

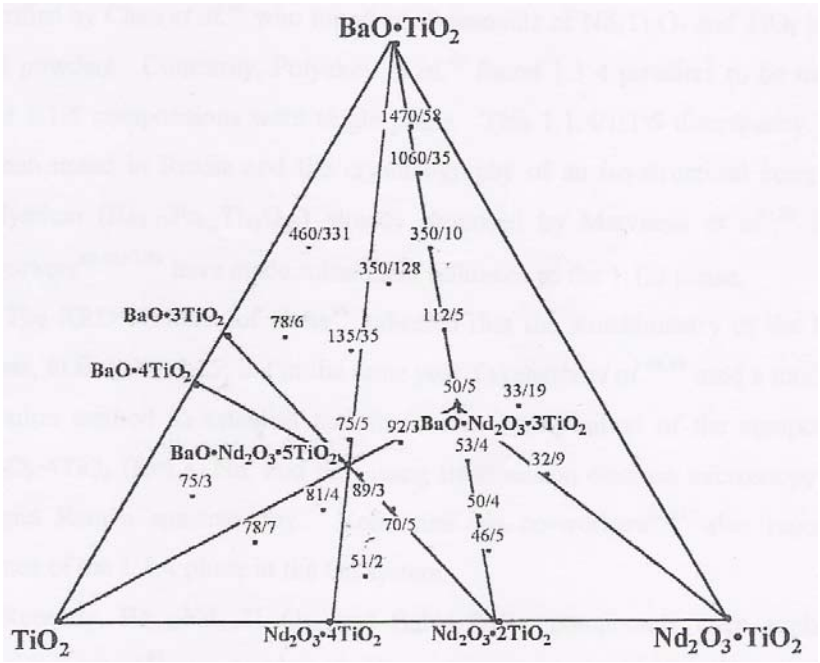

Figure 1-3 Isothermal section (1300 °C) for $BaTiO_3{\cdot}Nd_2O_3{\cdot}TiO_2$ subsystem based on room-temperature powder x-ray diffraction data of quenched samples showing variation of relative permittivity and loss tangent ($\varepsilon_r/\tan\delta\times10^{-4}$ at 1 MHz) with composition [Kolar et al-1978]

The composition and stoichiometry of the ternary phases of BNT have been the subject of some debate between different research groups. As mentined before, the existence of both 1:1:3 and 1:1:5 compounds were claimed by Kolar et al. [Kolar D.-

1981] and the 1:1:4 stoichiometry was first suggested by Razgon et al.[Razgon Y. S.-1980]. In 1986 Jaakola et al. [Jaakola T.-1986] proposed that the true stoichiometry for the 1:1:4/1:1:5 phase must be closer to 15:19:72 ($Ba_{3.75}Nd_{9.5}Ti_{18}O_{54}$), who found that the 1:1:5 composition did not lead to a single phase, but contained ~15% $BaTi_4O_9$ and TiO_2 as impurity phases. These results were later verified by Chen et al. [Chen X. M -1995] who found small amounts of $Nd_2Ti_2O_7$ and TiO_2 impurities in 1:1:5 powders. Contrarily, Polyakov et al. [Polyakov S.M.-1983] found 1:1:4 powders to be multiphasic and those of 1:1:5 composition to be single phase. Although it is now accepted that BNT 114 is the correct nominal formula and is commonly referred to as 1:1:4 phase, based on the stoichiometry of its constituent oxides ($BaO\text{-}Nd_2O_3\text{-}4TiO_2$) BNT 114 ceramics were found to be characterized by a poor densification degree and hence to possess high losses. This explains why BNT 1:1:5 ceramics have been often reported as having higher Q value than the single phase 1:1:4 compound. Indeed BNT115 ceramics are currently used in commercial applications (Fuji Titanium Industry Co., Ltd, Japan). Although the debate on the stoichiometry and fundamental crystal structure of BRT systems is still on going, the dielectric performance oriented investigation and research on BRT family materials is progressing very quickly.

The main aspects in optimizing BNT tungsten bronze-type ceramics for microwave applications include tuning τ_f to zero while retaining a high ε_r and low losses. Three approaches have been used to achieve it: (i) improvement of τ_f by the use of additives; (ii) proper variation of the Nd : Ba ratio, and (iii) or combination of different rare earth elements. Frequently, these approaches have been used simultaneously. For example, by substituting Ba by Pb in BNT114, Wakino et al. achieved a high ε_r of 85-88, a τ_f near zero and a Qf = 6000GHz. [Wskino K.-1984] Starting with BNT115 composition and by replacing some Ti by Bi and decreasing the Ti content, a high ε_r of 90-92, a τ_f near zero (3ppm/°C) and a Qf of 6000GHz [Wersing W.-1991] was attained. By using Sm instead of Nd in a 1:1:4.7 composition, ceramics with Qf of 9000 GHz and a τ_f near zero for a relative permittivity of 77 were fabricated [Laffez P.-1992]

In addition, as a result of the anisometric crystal structure, BRT series tend to show anisotropic development of elongated grains in the microstructure at particular processing conditions. Therefore the dielectric properties of BRT ceramics display significant anisotropy as reported by Negas (Negas T.-1995), and Hoffmann and Waswe (Hoffmann C.-1997). The electrical anisotropy is especially pronounced in the temperature coefficient of permittivity. It was also reported that textured $BaO\text{-}Re_2O_3\text{-}$

TiO_2 ceramics (Re = Sm, La), by the template grain growth technique, exhibited enhanced thermal stability of the dielectric response. [Valant M.-2000, Wada K. -2003, Fukami Y.-2006] In anisotropic ceramics, nearly "zero" temperature coefficient of resonance frequency can be reached while maintaining an equivalent permittivity and Q values when compared to the non textured specimens. This suggests that BRT is at least partially "self-compensating" from the τ_f point of view: the intrinsic τ_f is likely to be different in different crystallographic directions, yielding the best τ_f for particular mixtures of orientations of the crystallites in a bulk sample. Thus it is evident that large anisotropy exists in the properties in BRT systems, the dependence of the electrical properties on the crystallographic anisotropy of BRT solid solution is then important subject of research with obvious practical repercussions.

1.4 Summary

Low loss (high Q) dielectric materials are being extensively used at high frequencies range. Availability of high relative permittivity materials accompanied with low loss and high temperature stability, such as in the bronzoid type structures like $BaO\text{-}Nd_2O_3\text{-}TiO_2$, has a significant impact on the miniaturization of wireless microwave devices both for the terminals and base-stations, as well as for handsets, allowing to meet the growing industrial demands for miniaturization of electronic devices.

1.5 References

1. Azough F., Champness P.E., and Freer R. (1995) J. Crystallography **28**, 577
2. Bolton R. L. (1968) PhD Thesis, University of Illinois, USA
3. Chen X. M., Suzuki Y., and Sato N. (1995) J. Mater. Sci.: Mater. Electron. **6**, 10
4. Choy H., Han Y. S., Sohn J. H. and Itoh M. (1995) J. Amer. Ceram. Soc. **78,** 1169
5. Cohn S. B. (1968) IEEE Trans. Microwave Theory Tech. **MT16**, 218
6. Fiedziuszko S. J., Hunter I. C., Itoh T., Kobayashi Y., Nishikawa T., Stitzer S. N.,
7. Wakino K. (2002) IEEE Trans. Microwave Theory Tech. **50**, 706
8. Fuji Titanium Industry Co., Ltd, Japan
9. Fukami Y., Wada K., Kakimoto K., Ohsato H. (2006) J. Eur. Ceram. Soc. **26**, 2055
10. Gens A. M., Varfolomeev M. B., Kostomarov V. S., and Korovin S. S. (1981) Russian J. Inorganic Chem. **26,** 482
11. Hessel A., (1969) General characteristics of traveling-wave antennas in Antenna Theory, New York: McGraw-Hill, **19,** 151
12. Hippel A. V. (1954) Dielectric Materials and Applications, Cambridge, MA: MIT Press
13. Hirade K. (1992) Electron Ceram. **23,** 64
14. Hirano S., Hayashi T. and Hattai A. (1991) J. Amer. Ceram. Soc. **74,** 1320
15. Hoffmann C. and Waser R. (1997) Ferroelectrics **201**, 127
16. Ioachim A., Toacsan M.I., Stoica G., Coca R., Vasiliu F., Banciu G., Jaakola T. Uusimäki A., Rautioahu R., and Leppävuori S. (1986) J. Amer. Ceram. Soc. **69**, C234
17. Jantunen H., Rautioaho R., Uusimaki A. and Leppavuaro S. (2000) J. Euro. Ceram. Soc. **20,** 2331
18. Kolar D., Gaberscek S., Barbulescu A. and Volavsek B. (1978) J. Less-Common Metals **60,** 137
19. Kolar, D., Gabersek, S., Volvasek, B., Parker, H. S., and Roth, R. S. (1981) J. Solid State Chem. **38,** 158
20. Kolar D. and Suvorov D. (1993) J. Euro. Ceram. Soc. **2**, 229
21. Laffez P., Desgsrdin G., Rsvesu B. (1992) J Mater. Sci. **27**, 5229
22. Masse D. J., Pucel R. A. and Readey D. W. (1971) Proc. IEEE **59**, 1628
23. Matthaei G. L., Young L., and Jones E. M. T. (1980) Microwave filters impedance-matching networks and coupling structures, Norwood, MA: Artech House
24. Matveeva R.G., Varfolomeev M.B, and Il'yushenko L.S. (1984) Russian J. Inorganic

Chem. **29,** 17

25. Moulson A. J. and Herbert J. M. (1990) Electroceramics, Chapman & Hall, London
26. Mudrolyubova P., Rotenberg B.A., Kartenko N.F., Borshch A.N., Prokhvatilov V. G., Kostikov Y. P., and Ivanova M.P. (1981) Trans. from Izvestiya Akademii Nauk SSSR Neorganicheskie Materialy **17**, 683
27. Negas T. and Dacies P. K. (1995) Ceram.Trans. **53**, 179
28. Nino J.C, Lanagan M.T. and Randall R.C. (2001) J. Appl. Phys. **89**, 89
29. Ohsato H. (2001) J. Euro. Ceram. Soc. **21**, 2703
30. Ohsato H. (2007) J. Euro. Ceram. Soc. **27,** 2911
31. Ohsato H.and Imaeda M. (2003) Mater. Chem. Phys. **79,** 208
32. Ohsato H., Kato H. and Mizuta M. (1995) Jap. J. Appl. Phys. Part 1 **34**, 5413
33. Ohsato H., Nishigaki S., and Okuda T. (1992) Japanese J. Appl. Phys. **31**, 3136
34. Ohuchi H., Okayama M. and Ito H. (1996) Electroceramics-V. Book-2, 1
35. Plourde J. K., Linn D. F., O'Bryan H. M., and Thompson J. (1975) J. Amer. Ceram. Soc. **58**, 418
36. Polyakov S.M., Gindin E.I., Prokhvatilov V.G. and Shtel'makh S.V. (1983) Russian J. Inorganic Chemistry **28**, 1686
37. Ratheesh R., Sreemoolandhan H., Monahan P. and Sebastian M. T. (1998) Ferroelectrics **211**, 1
38. Rawn C. J. (1996) J. Euro. Ceram. Soc. **2**, 67
39. Rawn C. J., Birnica D. P., Bruck M. A., Enemark J . H. and Roth R. S. (1998) J. Mater. Res. **13**, 187
40. Razgon Y. S., Gens, A. M., Varfolomeev M. B., Korovin, S. S. and Kostomarov V. S. (1980) Zhurn. Neorg. Khimii **25**, 1701
41. Reaney I. M. and Iddles D. (2006) J. Am. Ceram. Soc. **89,** 2063

42 Sebastian M.T. (2008) Dielectric materials for wireless communication, Elsevier Science and Technology Publishers, Oxford

43. Scotta A. W. (1993) Understanding Microwaves, New York: Wiley
44. Solomon S., Santha N., Jawahar I. N., Sreemoolanadhan H., Sebastian M. T. and Mohaman P. (2000) J. Mater. Sci.: Mater. in Electron. **11**, 595
45. Tagantsev A. K., Sherman V. O., Astafiev K. F., Venkatesh J. and Setter N. (2003) J. Electroceramics **11**, 5
46. Ubic R. (1998) PhD thesis, University of Sheffield, UK
47. Ubic R., Reaney I.M., and Lee W.E. (1998) Inter. Mater. Review **43,** 205

48. Valant M., Suvorov D. and Rawn C. J. (2000) Ferroelectrics **237,** 253

49. Vanderah T. A. (2002) Science **298**, 1182

50. Vilarinho P. M., Rosenwaks Y. and Kingon A. I. (2005), Scanning Probe Microscopy: Characterization, Nanofabrication and Device Application of Functional Materials, Kluwer Academic Publishers

51. Wada K., Kakimoto K. I., Ohsato H. (2003) J. Eur. Ceram. Soc. **23**, 2535

52. Wakino K., Katsube M., Tamura H., Nishikawa T., and Ishikawa Y. (1977) IEEE. Four Joint Conv. Rec. 235

53. Wakino K., Minai K. and Tamura H. (1984) J. Am. Ceram. Soc. **67**, 278

54. Wakino K., Nishikawa T., Tamura S., and Ishikawa Y. (1975) IEEE MTT-S Int. Microwave Symp. Dig. 63

55. Wersing W. (1991) High frequency ceramic dielectrics and their application for microwave components, In Electronic Ceramics. Edited by Steele B. C. H., London Elsevier Applied Science

Chapter 2
A Review of Ceramic Thick Film Technology and Electrophoretic Deposition Technique

Abstract:
The use of thick films is becoming more and more important in particular for microelectronic applications. A number of established and emerging thick film deposition techniques were reported and described in this chapter**.** Among them is the electrophoretic deposition (EPD) technology, which has been used to fabricate highly reliable, low cost and high performance products. This chapter provides a review on the most important techniques for the deposition and patterning of ceramic thick films, and in particular on EPD. The review on EPD technique encompasses the fundamental aspects of EPD process, including mechanisms of EPD, suspension properties, kinetic aspects, charging origin of particles, zeta potential and double layer model. Numerous applications of EPD technique, including coatings, laminated or graded materials, infiltration in porous matrix, etc., are described as well.

2.1 Thick film fundamentals

2.1.1 General information

Depositing materials in film form enhances their applicability, simplifies the production of devices, and respond to the most actual requirement of electronic device miniaturization. Compared with bulk materials, the advantages of using film form materials are related to easier miniaturization, higher reliability, and lower driving voltages. For example, integrated circuits or devices incorporating ferro/piezoelectric thick films found numerous applications as microsensors and actuators for medical, military, telecommunication, environmental, vehicle and office automation industry. [Ferrari V.-1997]

Thick films are considered to be films ranging in thickness between 1 to 100 μm, but sometimes the thickness of “thick films” goes up to millimeters. [Hiremath B. V.-1989] The term “thick film” does not relate so much to the thickness of the film but more to the type of deposition, which occupies a technological region between the thin film processing techniques and machining of bulk ceramics. [Whatmore R. W. -1998] The original concept for thick film technology was developed for a low-cost, mass

production method for relatively crude electronic components.

2.1.2 Thick films deposition techniques

Thick films are normally fabricated by low-cost processes such as tape casting (doctor blading), screen-printing, ink-jetting (or ink-jet printing) or electrophoretic deposition (EPD). The preparation of ceramic thick films by these methods generally implies a processing sequence of the following steps: preparation of the precursor powders; preparation of pastes or powder suspensions; printing/depositing of the pastes or suspensions onto a suitable substrate; drying at low temperature; and sintering at high temperature to get a consolidated layer. [Dahotre N. B. -2001] The distinction between these processes lies on the method to deliver the suspension to the substrate.

Tape casting or doctor blading is an economical method for producing large surface areas of ceramic films, which consists of printing, coating, or spreading paste with a blade onto a substrate. [Tok A. I. Y. -1998] In tape casting, the powder is suspended in an organic solution. This solution is, in general, composed of a solvent, a plasticizer, and a dispersant. The relative proportion of each of these constituents is crucial for the film processing, affecting directly the final product quality. The powder suspension is deposited onto a polymeric tape lying down under a glass or metallic surface. The green tape is cut with the required dimensions. After drying, the organic components still remain in the tape and must be removed by pyrolysis. The burning out of organic components generates open pores, which are eliminated by sintering (1000-1200 °C). Films with thickness in the range 10-500 μm have been prepared by tape casting. Tape casting is a common process to fabricate laminated thick layers in multilayer structures, such as $BaTiO_3$ (BT) -based multilayer capacitors and $Pb(Zr,Ti)O_3$(PZT)-based multilayer actuators. [Lubitz K.-2002] Moreover tape casting is a low-cost method that allows mass productions of laminates making it very convenient for manufacturing. However, the involved technical procedure is not easily compatible with the deposition onto rigid substrates and the suspension and firing without deflection are very difficult.

Figure 2-1 indicates the steps in a tape-casting process employed in the production of ceramic films. Ceramic powders and solvents are mixed to form a slurry, which is treated with various additives and binders, homogenized, and then pumped directly to a tape-casting machine. There the slurry is continuously cast onto the surface of a moving carrier film. The edge of a smooth knife, generally called a doctor blade, spreads the

slurry onto the carrier film at a specified thickness, thereby generating a flexible tape. Heat lamps gently evaporate the solvent, and the dry tape is peeled away from the carrier film and rolled onto a take-up reel for additional processing.

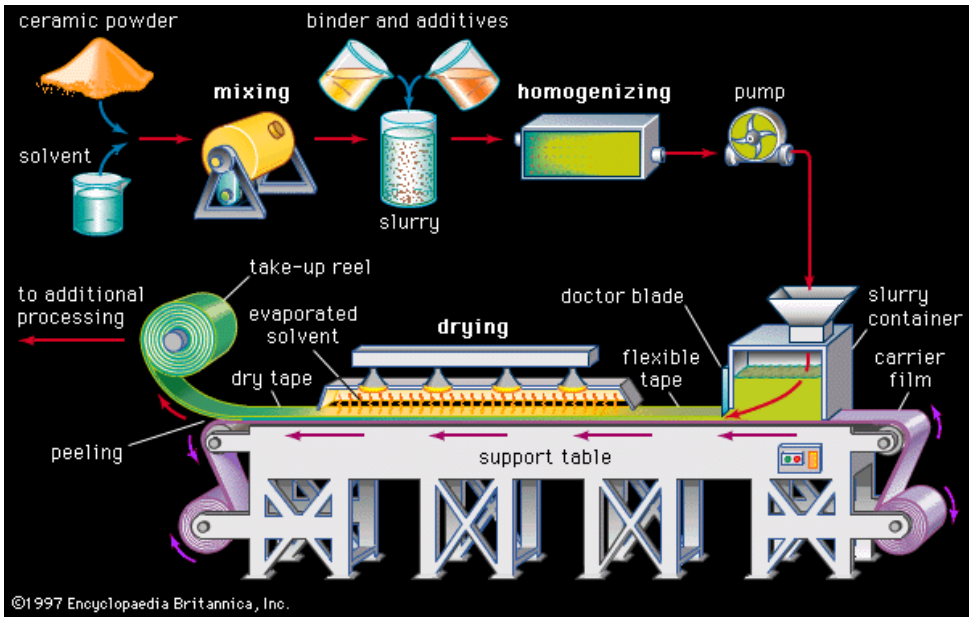

Figure 2-1 Schematic representation of the tape casting technique (www.britannica.com)

Screen printing is the most widely used thick film deposition technique, and prepare thick films with thickness ranging from 10 to 30 μm. In the screen printing technique the powder is also suspended in an organic solution composed of a solvent, a dispersant and a plasticizer. During the printing process a paste is forced through a fine mesh to deposit it onto the desired substrate. The thickness of the deposited layer depends on the viscosity of the suspension, rate of deposition, pressure applied on the screen, among other experimental variables. The as prepared film is then dried and sintered at elevated temperatures to yield a dense thick film. In the electronics industry, screen printing has been the dominant process for thick-film deposition. Since the end of the 1960s, several screen-printing models have been developed. [Owczarek J. A.-1990] One of the advantages associated with this technique is the ability to directly pattern the film by selectively masking certain areas of the mesh over the tape casting method. [Pan J.-1998] This direct patterning eliminates the need to pattern (typically by etching) the film at a later stage. Limitations in the maximum resolution are imposed by the size of the mesh used; hence this technique may not be suitable for producing very

fine features. Screen printing technique has been routinely applied for the preparation of piezoelectric thick films. For example, several compositions including (Pb,La)(Zr,Ti)O_3 (PLZT) [Kosec M.-1999] and PZT [Lee B. Y. -2002] have been successfully deposited by this technique onto Si substrates in order to be compatible with the standard routines used for the fabrication of microelectromechanical systems (MEMS). However, an important requirement in this technique is that the ink should contain a constituent which interacts with the ceramic and/or acts to promote adhesion between the ceramic phase and the substrate. In many cases this role is played by a glassy frit or by a metal oxide. However, the interactions between the adhesion promoter, film material and substrate limit the final properties of the films. [Bersani M.-1997]

Figure 2-2 shows the schematic process of screen printer: the screen is fixed just above the board, and the 'medium' (ink or glue, for example) lies in front of the flexible squeegee. The mesh of the screen is pushed down into contact with the board by the squeegee as it moves across the screen, rolling the medium in front of it. In screen printing, the screen employed as an image carrier consists of a rigid frame on which is stretched a mesh (or 'gauze') made from fine polyester or stainless steel wires. The mesh acts as a support for a stencil of the required image, which is produced in a photosensitive emulsion applied to the mesh. Emulsion is normally applied to both sides of the mesh, and 'built up' to a defined thickness on the underside (the side in contact with the board).

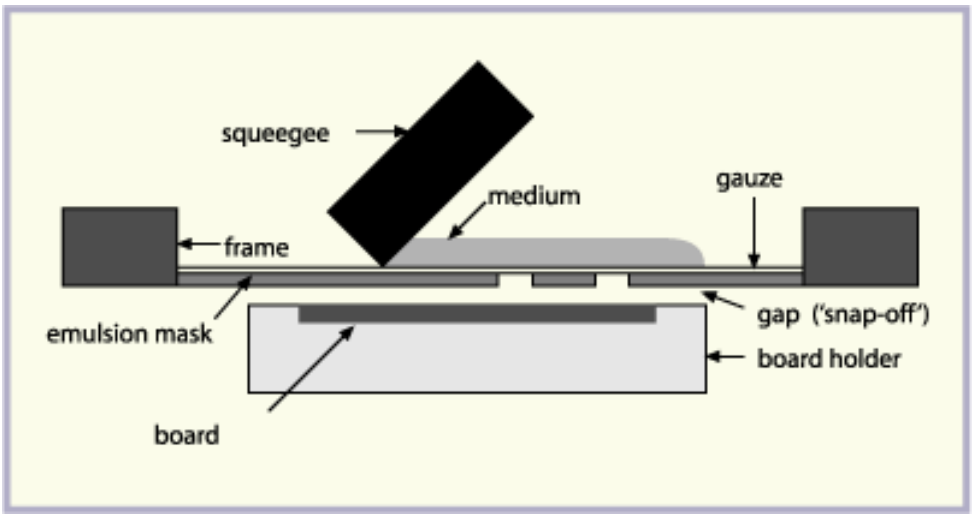

Figure 2-2 Schematic view of the screen printing technique
(www.ami.ac.uk)

Under the basis of screen printing, recent developments in the field of ink-jetting have enabled a range of microscale devices to be created. [King B. H.-1999] Compared to the screen printing, application of such technology has the benefit of eliminating the need to pattern the devices after deposition. [Riemer D. E. -1988] Ink-jet is a non-impact dot-matrix printing technology in which droplets of ink are jetted from a small aperture directly to a specified position on a media to create an image. As with other fluid-based printing methods, the ink used in ink jet printing is a complex formulation of solvents, plasticizers and surfactants in addition to the appropriate materials.

Generally, there are two designs of ink jetting techniques. The designs are i) continuous and ii) drop-on-demand (DOD). [John B. B.-2007] Here, the DOD type is used as an example to introduce this technique because DOD printers have been used in ink jet printing of electronics. In DOD ink jet printers, droplets are generated only when they are needed. The droplets can be generated by heating the ink to boil off a droplet (so called thermal ink jet). Alternatively, the droplets can be ejected mechanically through the application of an acoustic pulse or electrically stimulating a piezoelectric to elicit a deformation, which will generate a droplet as shown in Figure 2-3.

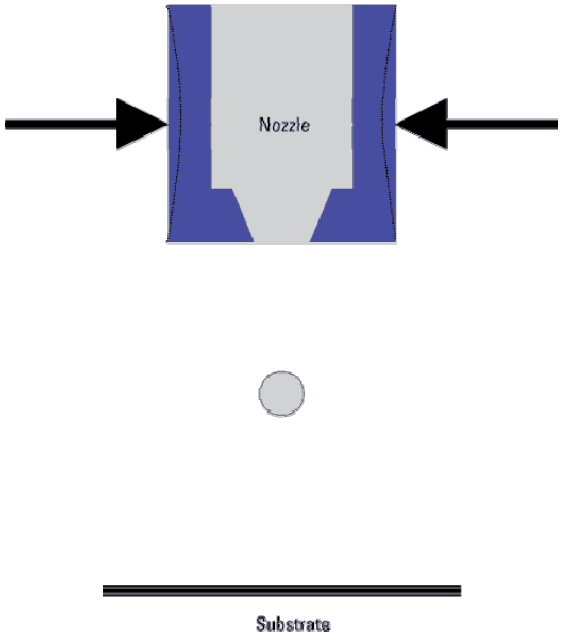

Figure 2-3 Schematic representation of ink jetting [after John B. B.-2007]

Ink jet printing has been used to produce conducting electrodes in electronic circuits, for example, of copper [Rozenberg G. G. -2002], silver [Smith P. J. -2006] and gold [Chung J. -2004]. The most important advantage of employing ink jet printing for

electronic circuits are that it is a digital process, allowing the patterning process to be directly computer controlled. No masks or screens are necessary. Changes can be made quite easily by altering the computer-controlled pattern rather than awaiting a new mask or screen, which eliminates the need to make expensive photolithographic masks and screens, as well as increasing the flexibility of the system. [Morissette S. L. -2001]

Electrophoretic deposition (EPD) is a simple, fast and inexpensive deposition technique for obtaining thick films. One of the advantages of EPD over other thick film deposition techniques is the ability to coat complex geometries, which allows easy deposition of the materials onto substrates of various shapes, including long wires, without organic residues being left in the coating after drying. [Ma J.-2002] The fabrication process by EPD includes three stages: i) the formation of a charged suspension; ii) the deposition of charged particles onto an electrode under the action of a DC voltage and iii) the final sintering. [Sweeney T.-1998]

In order to deposit thick films using EPD, it is necessary that for the substrate to be conducting or coated with an electrode. This may act somehow as a limitation for the use of this technique in the production of electronic circuits. A further limitation is the high density of some specific element as it is very difficult to maintain large (i.e. heavy) particles in suspension. [Tassel J. V. -1999] A thorough review of the EPD technique, as applied to many ceramic films, is given in the following section.

2.1.3 Precursors for thick film deposition

The quality of the initial powder material is a crucial point in processing ceramic thick films. This is the reason why so many investigations have been carried out on how to prepare tailored powders in terms of purity, homogeneity, reactivity, grain size, and grain size distribution. [Ueltzen M.-1995] Among them, the simplest method is the conventional solid state reaction in which the precursors, metallic oxides, carbonates, or nitrates are mixed according to the required stoichiometry and heat treated at elevated temperatures to obtain the required crystalline compounds. Specific alternative routes such as “reactive mixtures” or the “flakes method” have been tested in particular for the preparation of superconductor powders. [Altenburg H.-2001] Besides the conventional methods two other main kinds of powder preparation by wet chemistry—co-precipitation method and sol-gel process, have been used. Indeed, solution chemistry solves much better the problems associated with agglomeration, grain sizes, and distribution ranges and leads to reactive and homogeneous fine-grain powders.

Besides the powders quality, other prerequisites for thick films preparation such as the chemical and physical nature of the paste/suspension are also of fundamental importance for the final product performance in thick films fabrication process. Suspension/paste are multicomponent systems that include the solid powders to be deposited and a variety of additives, ranging from inorganic binder glasses, various dopants to organic suspension vehicles, binders, plasticizers, homogenizers and surface activating agents. [Rose A.-1988] Solvents, or suspension media, can be either aqueous (thus, inexpensive), incombustible, and nontoxic or non-aqueous of low viscosity, low boiling point, low evaporation heat, and high vapor pressure. Non-aqueous systems are used for high-performance materials and are commonly highly polar organic compounds such as alcohols, ketones, hydrogenated hydrocarbons, and mixtures of them. [Tok A. I. Y. -1998] In principle, a good suspension or paste for thick-film materials must meet the following conditions: good printing or depositing and leveling properties and the absence of pinholes. Besides the paste preparation considerations, the used substrate has to fulfill several conditions, such as no chemical reaction with the coating, or minimal chemical inter-diffusion, or minimal thermal stress by matching thermal coefficients with the coated layer, providing good coating, surface adhesion, among other specific aspects.

2.1.4 Constrained sintering

A common characteristic between the several thick film fabrication processes, where the coatings are applied as powder, is the need for a cofiring step of the coated layer with the substrate to obtain the highest possible density and to develop the necessary strength and bond with the substrate. The high firing temperature ensures that the atoms and ions have sufficient mobility to diffuse to the pores and densify the coating.

One of the key issues associated with the coating on a rigid substrate is that of shrinkage during the sintering. Constrained shrinkage occurs when the coating undergoes a reduction in volume while the dimensions of the substrate remain unchanged. This occurs initially during the drying of the film when fluid between particles is removed through evaporation. A further volume reduction occurs during the sintering of the particles when pores are eliminated. In an unconstrained body the volume reduction is accomplished via isotropic shrinkage. However, when the film is supported on a rigid substrate the shrinkage in the in-plane of the film is prevented,

which leads to the generation of in-plane stresses within the film. [Tzeng S.-Y. -2002] Such as, for an isotropic freestanding body, shrinkage will occur along all three perpendicular directions such that the sintered density (ρ_i) of the compact can be expressed as [Tzeng S.-Y.-2002]

$$\rho_i = \rho_0 \left(\frac{\alpha_0}{\alpha_i}\right)^3 \tag{2-1}$$

where ρ_0 stands for the initial density, α_0 for the initial characteristic length and α_i for the length corresponding to ρ_i. The equation can be expressed also in terms of the relative sintered density $\overline{\rho}$ as

$$\overline{\rho} = \frac{\rho_i}{\rho_{th}} = \overline{\rho_0} \left(\frac{\alpha_0}{\alpha_i}\right)^3 \tag{2-2}$$

where ρ_{th} stands for the theoretical density of the bulk material. If the film or coating is constrained from shrinking in the plane of the substrate, then any shrinkage will have to take place normal to the plane. The relative density then can be expressed as

$$\overline{\rho_i} = \overline{\rho_0} \frac{d_0}{d_i} \tag{2-3}$$

where $\overline{\rho_0}$ stands for the initial relative density and d_0 and d_i are now the corresponding thicknesses of the coating. For the same amount of densification, the constrained film will experience a larger amount of shrinkage than a free-standing body. The inhibition of shrinkage along the other directions leads to stresses in the film that can influence the sintering kinetics. There have been attempts to formulate models to predict the densification rate and the resulting stress in the coating. The general sintering behavior of a “green” film supported on a rigid substrate and subjected to a constant heating rate has been modeled by Zhao [Zhao Y.-1994] using a viscoelastic finite element simulation. Scherer [Scherer G. W.-1985] used the viscous analogy whereas Bordia [Bordia R. K.-1985] used the spring-dashpot model. Both models predict a reduced densification rate and the presence of in-plane stresses that reach a

maximum early in the sintering process when the amount and rate of shrinkage are highest.

Large differences in the thermal expansion coefficients of the substrate and film will lead to the generation of stresses in the film. These stresses will either arise during heating prior to sintering ($\alpha_{substrate}>\alpha_{film}$) or during cooling after sintering ($\alpha_{substrate}<\alpha_{film}$) [Zhao Y.-1994]. Hence care must be taken when using substrates with high thermal expansion coefficients (i.e. metals). Therefore, the constrained sintering is a concern because its effect may allow a degree of particle reorientation and influence the grains growth and arrangement during the constrained sintering. Moreover, the constraining effect of the substrate can lead not only to higher residual porosity but also to other defects such as cracks, warping and debonding due to residual stresses.

2.2 Electrophoretic Deposition (EPD)

2.2.1. Introduction

The phenomenon of electrophoresis was discovered in 1807 by the Russian physicist F.F. Reuss, who observed that when an electric current was passed through a suspension of clay in water, the clay particles migrated towards the anode. [Binner J. G. P.-1990]

170 years later, the first industrial application of electrophoresis in ceramic fabrication was developed on aqueous clay suspensions. Since then, EPD has been studied and applied in a wide variety of systems, especially as a technique for the coating of metal components. Later, oxides, phosphors, inorganic and organic paints, rubber, dielectrics and glasses have been deposited by this technique using both aqueous and non-aqueous media. And among these, some have found large scale applications in manufacturing, in particular rubber products, and the application of paints in the automotive industry. In ceramic manufacturing industry, EPD of ceramics was first studied by Hamaker [Hamaker H. C. -1940], and only in the 1980s this process received attention in the preparation of advanced ceramics. More recently, the number of applications has quickly developed, and as noted by Boccaccini and Van Tassel [Boccaccini A.R.-2008, Van Tassel-2004] in the last 10 years there has been a considerable increase of the areas of application of EPD, denoted by the existence of more than a thousand articles and patents related to EPD. Figure 2-4 shows the extraordinary increase of the number of published scientific papers, identified searching in Web of Science® by the keyword “electrophoretic deposition”, from only less than

100 papers before 1970s to more than 1800 papers published since 2000.

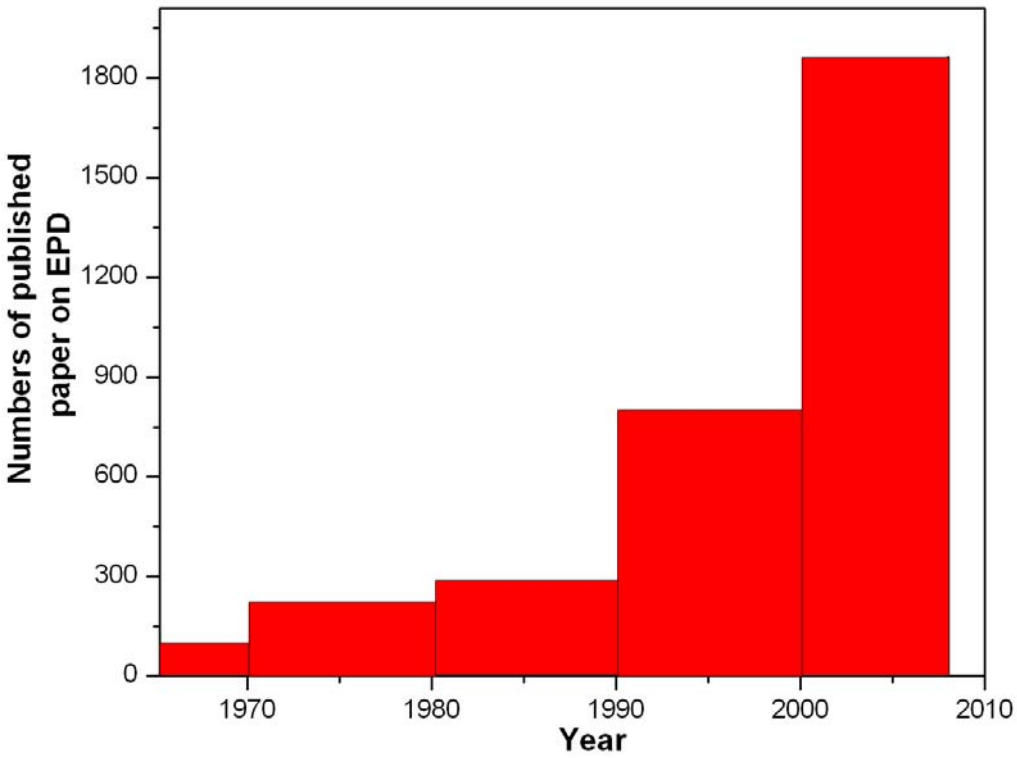

Figure 2-4 Number of published scientific papers on EPD from 1930 until 2008. The search was conducted by the keyword “electrophoretic deposition” in Web-of-Science®

EPD is a particulate forming process. It begins with a randomly arranged powder material and then uses an electric field to move the powder particles into a desired arrangement on an electrode surface. This arrangement can be either zero, one, two or three dimensions. As mentioned above, there are three basic steps in EPD: formation of a stable suspension of the particles, electrophoretic migration of the particles to the deposition electrode, and deposition of the particles in the desired arrangement on the electrode surface. The first step is to place the particles into a suspension where each of the particles can move independently. In the second step a DC electric field is applied to the suspension causing the electrophoretic motion of charged particles toward the oppositely charged electrode. In the final step, deposition, the interparticle repulsion that keeps the particles stably suspended must be overcome. However, EPD is purely a method of moving and arranging particles. To produce a dense, mechanically strong layer or object it must be combined with some other process such as sintering to eliminate the pores between the particles in the deposition.

2.2.2 Fundamentals of EPD

2.2.2.1 Definitions

The term “electrodeposition” is often used somewhat ambiguously to refer to either electroplating or electrophoretic deposition, although it more usually refers to the former.

In Table 2-1 the distinction between the two processes is indicated. In the electroplating processes a coating is produced by the diffusion and migration of individual ions in the solvent to the deposition electrode where they are electrochemically converted to an insoluble form, in which the reaction is the reduction of metal ions in solution to form the metal. In contrast, EPD uses charged particles, that move under an external electric field to form consolidated films onto the opposite electrode. [Zhitomirsky I. -2002] There are two types of EPD depending on which electrode the deposition happens. When the particles are positively charged, the deposition is formed on the cathode and the process is called cathodic EPD. On the contrary, the deposition formation on positive electrode (anode) is termed as anodic EPD. By suitable modification of the surface charge on the particles, both of the two modes of deposition are possible. [Zhitomirsky I. -2002]

Table 2-1 Characteristics of electrodeposition techniques. [Heavens N-1990]

	Electroplating	Electrophoretic Deposition
Moving species	ions	solid particles
Charge transfer on deposition	ion reduction	none
Required conductance of liquid medium	high	low
Preferred solvent	water	organic
Deposition rate	small(~1 μm/min)	high(~10 μm/min)

2.2.2.2 Origins of particles charging in suspension

Charged particles are then a prerequisite for EPD process and the particle charging process or step decisive for a successful EPD.

When different phases come into contact, some redistribution of positive and negative charge invariably occurs, leading to a potential difference between the phases (such as, solids and liquids) and to creation of charged particles. The charge on the particles surface can be formed from the liquid by one or more of the following mechanisms [Sigmund W. M.-2000]: (a) selective adsorption of ions onto the surface of

solid particle from the liquid, (b) dissociation of ions from the solid phase into the liquid, (c) adsorption or orientation of dipolar molecules at the particle surface, and (d) electron transfer between the solid and liquid phase due to differences in the substances work function.

In the case of ceramic or glass particles in water or organic liquids, the last mechanism is not applicable but the first two invariably occur. The sign of the net charge on the particle will depend not only on whether the ions involved are positive or negative, but also on whether mechanism (a) or (b) is dominant. Also, a positively-charged particle may even behave like a negative one, which is attracted to a positive electrode, if an excess of negative ions are attracted to the vicinity of the particle. Consequently, it is difficult to predict whether a deposition will occur on positive or negative electrodes in an unknown system. In water most solid particles acquire a negative charge, but in organic liquids charging may be either positive or negative. [Yates D. E.-1974, Labib M. E.-1986]

2.2.2.3 Electrical double layer concept and Zeta potential

The electric double layer concept is a very important one for the surface chemistry of materials in colloidal science field, i.e. in EPD. It describes the variation of the electric potential near a surface, and has a large bearing on the behavior of colloids. Development of a net charge at the particle surface affects the distribution of ions in the surrounding interfacial region, resulting in an increased concentration of counter ions (ions with opposite charge to that of the particle) close to the surface. The liquid layer surrounding the particle consists of two parts: an inner region where the ions are strongly bound and an outer (diffuse) region where they are less firmly associated. Within this diffuse layer is a boundary known as the slipping plane, within which the particle acts as a single entity. [Stern O. Z.-1924]

An assumed negative charge particle in a suspension is surrounded by ions with a positive charge in a concentration higher than the bulk concentration of these ions; this is the so-called electrical Double-Layer as illustrated in Figure 2-5 (a). The double layer thickness is of great importance in colloid stability and for that matter on flocculation since it controls the range of the double layer interaction. The thickness is determined by the concentration and valence of the ions in suspension. A high concentration of ions (high ionic strength) in the medium generally results in a decrease in the double layer thickness and consequent decrease in the potential. [Sennet P.-1965] When an electric

field is applied, the charged particle and surrounding ions will move in opposite directions. However, the ions are also attracted by the particle, and as a result, a fraction of the ions surrounding the particle will not move in the opposite direction but move along with the particle. Hence, there is a surface of shear between the particles and the surrounding ions. As shown in Figure 2-5 (a), the potential at the surface of slipping plane is termed the zeta-potential or electrokinetic potential. [Lyklema J.-1977]

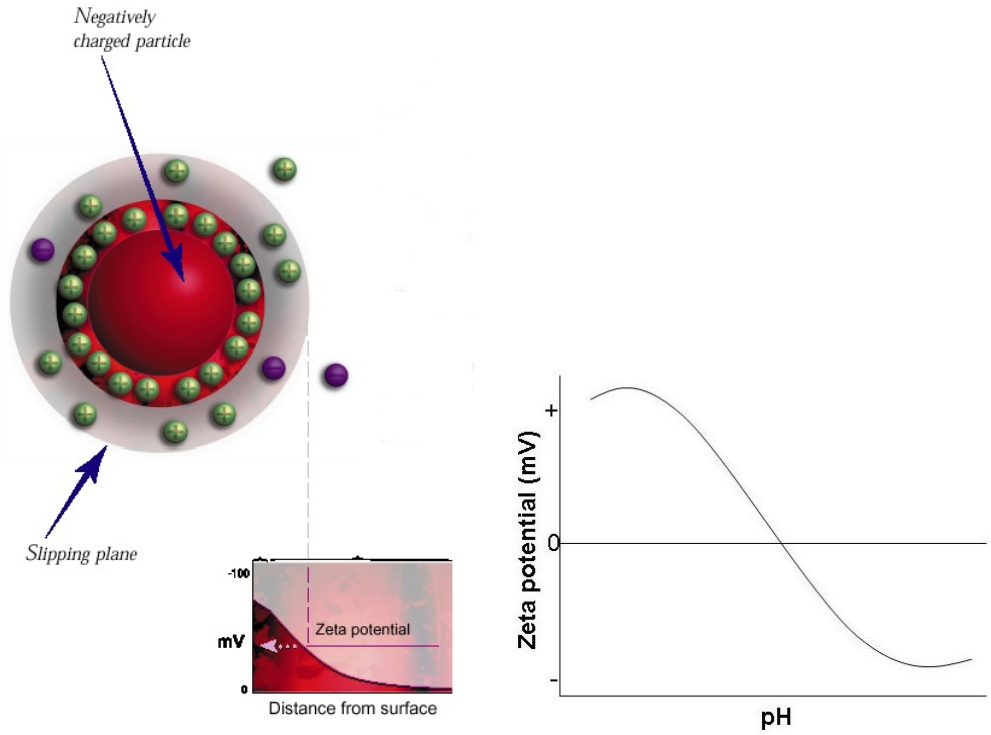

(a) (b)

Figure 2-5 (a) Schematic representation of the double layer surrounding a charged particle and evolution of the electric potential from the surface potential, [Weise N. L.-1985], and (b) Zeta potential versus pH value

Figure 2-5 (b) shows the schematic curve of zeta potential versus pH value. The zeta potential is affected by pH environment and is usually positive for low pH values and negative at high pH, as shown in Figure 2-5 (b). The zeta potential is the main parameter determining the electrokinetic behavior of particles in suspension, and as a consequence is a key factor in the EPD process. It is imperative to achieve a high zeta potential and a uniform surface charge density on the surface of suspended particles for a successful EPD. Zeta potential plays a role in: (i) the stabilization of the suspension by determining the intensity of repulsive interactions between the particles, (ii) determining the direction and migration velocity of particles during EPD, (iii) determining the

quality of the deposit. As zeta potential is closely related to the particle's double layer thickness, it provides also information on the agglomeration of the particles in the suspension. In general, the higher the absolute value of the measured zeta potential, the better is the dispersion of the particles in the suspension. [Lyklema J.-1977]

Numerous physical and chemical factors can influence the magnitude and sign of the zeta potential. It may depend on the presence or absence of added electrolytes, or on the concentration of the suspension itself. In addition, zeta potential can be controlled by a variety of charging agents such as acids, bases and specifically adsorbed ions or polyelectrolytes, to the suspension. [Zarbov M.-2002] Thus it is possible to use a variety of additives that affects the charge magnitude and its polarity in the suspension on EPD. Generally, the main criteria for selection of a charging agent are the preferred polarity and deposition rate of the particles.

2.2.2.4 Mechanisms of EPD

The basic mechanism of EPD has been extensively considered in the literature mainly in the framework of the Derjaguin-Landau-Vervew-Overbeek (DLVO) theory. [Derjaguin B. V. and Landau L. D.-1941, Vervew E. J. W.and Overbeek J. T. G.-1948] This theory is very important for modern colloid science, and predicts the stability of colloidal particles suspended in polar liquids. However, numerous other theories (particle flocculation, particle charge neutralization, electrochemical particle coagulation, distortion and thinning mechanism of electrical double layer) have been proposed to explain the mechanism of EPD as well. Additional theoretical and modelling studies are still being carried out in order to clarify the mechanisms of deposition and the role of electrochemical parameters on the complex interactions between solvent, particles and electric field. [Van Tassel -2004] Although the EPD has been applied successfully for many applications, the exact mechanisms that allow a deposit to be formed are still not entirely clear, because the deposition step is preceded by a complex electrochemical and aggregation phenomena during EPD. [Van der Biest O. O.-1999] The following are some representative proposals for the mechanisms of EPD:

1) Flocculation by particle accumulation mechanism

Hamaker and Verwey [Hamaker H. C.-1940] firstly attempted to explain the phenomenon of EPD. The authors suggested that the formation of deposits by EPD is like to the formation of sediment due to gravitation. It was supposed that the primary

function of the applied electric field in EPD is to move the particles towards the electrode to accumulate. The pressure exerted by the incoming particles enables next coming particles to the deposit to overcome the interparticle repulsion. [Vanderperre L.-1998] However, this theory cannot be applied to explain the mechanisms of deposition of monolayer films or individual particle deposition by EPD.

2) Particle charge neutralization mechanism

Grillon et al. [Grillon F.-1992] suggested that particles would neutralize upon contact with the deposition electrode and then become static to form a deposit. The function of the applied electric field is to push charged particles to move towards the electrode. The charged particles are adsorbed on the electrode and become neutralized so as to form a static deposite on that. This mechanism is important for single particles and monolayer deposits. But this mechanism does not hold on the following conditions: (a) longer time EPD (thick deposits), (b) deposition that does not occur at the electrode, e.g. deposition on a dialysis membrane between the electrodes. [Heavens N.-1990]

3) Electrochemical particle coagulation mechanism

This mechanism supposes that the deposition is formed due to the reduction of the repulsive forces between particles because of the change of the ionic strength close to the electrode in the suspension. Koelmans calculated the ionic strength next to an electrode and found that the ionic strength was of the same order as required to flocculate a suspension. [Koelmans H.-1995] In his view, the interparticle repulsion decreases due to the increase in the electrolyte concentration near the deposition electrode. This in turn lowers the zeta potential and induces the flocculation of particles to form a deposit. This mechanism is plausible when the electrode reactions generate OH^- ions, e.g., suspensions containing water, and it is invalid when there is no increase of electrolyte concentration near the electrode.

4) Electrical double layer distortion and thinning mechanism

Sarkar and Nicholson proposed a model mainly based on the distortion of the particle double layer, in which fluid dynamics and applied electric field will distort the double layer during the particle movement. [Sarkar P.-1996] In detail, when a positive particle and its shell are moving towards the cathode, the double layer is distorted (thinner ahead and wider behind), due to fluid dynamics and to the effect of the applied electric field. As a result the negative counter ions in the extended tail experience a smaller coulombic attraction to the positively charged particle and can more easily react with other cations moving towards the cathode. This process reduces the thickness of

the double layer and therefore decreases the zeta potential, when another particle with a thin double layer is approaching, the two particles come close enough to interact through London Van der Waal attractive forces and coagulate. This mechanism is plausible considering a high concentration of particles close to the electrode and works for incoming particles with thin double layer heads, coagulating with particles already in the deposit. [Fukada Y.-2004]

There is still no satisfactory and general theory that accounts for the mechanism of EPD.

In the meantime it would be desirable to find suitable physical/chemical parameters that characterize sufficiently a suspension that its ability to be deposited could be predicted. Most investigators use zeta potential or electrophoretic mobility, but these do not uniquely determine the ability of a suspension to be deposited. For example, in suspensions of alumina in alcohol the addition of an electrolyte causes no significant change in the zeta potential, but deposits can only be obtained in the presence of the electrolyte. [Brown D. R.-1965] Although the stability of the suspensions is evidently its most significant property, this is a somewhat an empirical property not closely related to fundamental processing parameters.

2.2.2.5 Kinetics of EPD

To make EPD process commercially more viable, knowledge of the kinetics of EPD process is necessary to take good use of this technique. Hamaker [Hamaker H. C. -1940] proposed that the amount of deposited films is proportional to the concentration of the suspension, time of deposition, surface area of deposit, and the electric field. This yield of deposition varies linearly with applied field according to Hamaker's equation [Hamaker H. C. -1940]

$$M=\int_0^t aACE\mu dt \tag{2-4}$$

where M stands for the mass deposited in time t (s), C for the particle concentration in the suspension (kg/m^3), E for the electric field (V/m), A for the electrode area (m^2), m for the electrophoretic mobility (m^2/V·s)), and α stands for a coefficient representing the fraction of particles deposited near the electrode.

Principally, EPD can be conducted under constant current or constant voltage

manner with either constant or variable concentration against deposition time. Sarkar et al. [Sarkar P.-2004] demonstrated the kinetic aspects of EPD through schematic plots of deposit weight versus deposition time for four possible deposition conditions (Figure 2-6): curve A (constant current and constant suspension solid concentration), curve B (constant current but decreasing suspension solid concentration), curve C (constant voltage and constant suspension solid concentration) and curve D (constant voltage but decreasing suspension solid concentration). The curve A shows that the rate of deposition is constant with time, differently, the rate of deposition decreases asymptotically against deposition time in either of the B, C, or D curves. Apparently, the deposition efficiency is highest in curve A, followed by curves B, C, and D, respectively in a certain deposition time. By comparison of the curves A, B, C and D, it clearly reveals that the highest efficiency is realized by constant current and constant suspension solid concentration in terms of the deposition weight or thickness. In addition, it is much easer prediction and precise control of the deposited yield or thickness in constant current and constant suspension solid concentration.

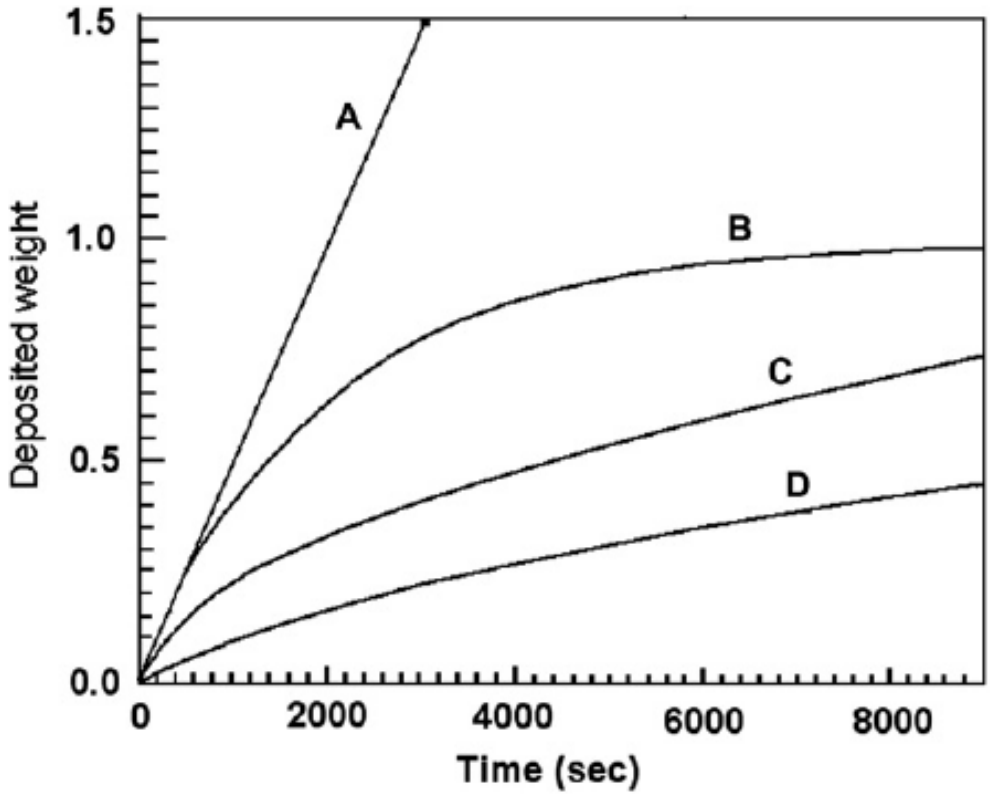

Figure 2-6 Representation of the deposited weight as a function of the deposition time (after Sarkar P. -2004)

2.3 Suspension media for EPD

In EPD process, the suspension medias play a key factor because the choice of suspension media determines the magnitude of the charge that is developed on the particle surface in the suspension, that ensures the stability of the suspension and as a consequence a successful deposition. A suspension media acts as a vehicle to transport the particles in the suspension to the substrate. Suspension media used in EPD should be inert with respect to the powder and two principal types of suspension media have been used, water and organic liquids. (Table 2-2)

Obviously, the use of water implies advantages associated to health, environmental, and cost aspects. However, the water-based suspensions cause a number of problems in EPD. [Moreno R.-2000] The main problem is related to the electrochemical reaction at the electrodes when a current is passed through, which seriously affects the efficiency of the process and the uniformity of the deposit. Electrolysis of water occurs at low voltages (> 2 V), and gas evolution is inevitable at the electrodes. This causes bubbles that will be trapped within the deposit. Meanwhile, current densities are high, leading to Joule heating of the suspension that results in the suspension instability. Moreover, when metallic electrodes are employed, the normal potential of the electrode is largely overpassed. This situation promotes the oxidation of the electrodes and formation of metallic impurities in the suspension. If these metallic particles will involved in the deposition process a degrading of the film properties may occur.

Compared with aqueous, organic liquids are generally preferable as suspension media for EPD. A variety of non-aqueous organic solvents are commonly used to prepare suspensions for EPD, as presented in Table 2-2. While the generally lower dielectric constant in organic liquids limits the charge on the particles as a result of the lower dissociating power, much higher field strengths can be used since the problems, such as, electrolytic gas evolution, joule heating and electrochemical attack of the electrodes, that happen in aqueous based suspensions, are greatly reduced or non-existent in organic based suspensions. Moreover, the organic liquids are preferred due to their higher density, good chemical stability and low conductivity. However there are a couple of disadvantages associated with organic solvents namely cost, toxicity, flammability and recycling. So the selection of a suitable organic solvent will taking into account these aspects.

Although many solvents were experimentally used for the EPD of specific

materials, unfortunately, there is not a universal suspension media for the fabrication of films by EPD yet.

Table 2.2 A non-exhaustive list of typical suspension medias for EPD

Suspension media	Deposited materials	Reference
Water	Al_2O_3	Hirata-1991
Acetone	$BaNd_2Ti_5O_{14}$(BNT)	Fu Z-2007
Ethanol	$(Ba,Sr)TiO_3$(BST)	Guo H. L.-2004
Acetic acid	$Pb(Zr,Ti)O_3$(PZT)	Wu A. Y.-2006
Isopropanol	ytrria stablized zirconia (YSZ)	Besra L.-2007
Dichloromethane	Hydroxyapatite	Ducheyne P.-1990
Mixture of ethanol and acetylacetone	$BaTiO_3$ (BT)	Louh R. F.-2003

2.4 Parameters related to the suspension

Due to the fundamental role of the suspension on the process its properties must be considered, such as the physicochemical nature of both suspended particle and the liquid medium, surface properties of the powders, and type and concentration of the additives (mainly dispersants). Particle size, dielectric constant of the suspension media, conductivity of the suspension, stability of suspension and zeta potential, have a direct effect on the EPD process and because of that will be addressed in detail in the following text.

1) Particle size

Although there is no general requirement to specify the ideal particle size for optimized EPD, it has been reported that good deposition occurs when the particle size lies in the proper range defined for the specific material. However, this does not mean that deposition of particles outside the reported size range will not be feasible. This is exactly the case of nanoparticles. Recently, with the increasing importance of nanomaterials and nanotechnologies, EPD is becoming more and more a technique to assemble / deposit nanoparticles. [Bocaccini A. R.-2006] As for the large particles, it is important that the nanoparticles are well dispersed and stable for homogeneous and smooth deposition.

When dealing with large particles (above 10 microns) the main problem is that they tend to settle due to gravity. In ideal suspensions, the mobility of particles due to electrophoresis must be higher than that due to gravity. Indeed it is difficult to get uniform deposits from flocculated (or less well deflocculated) suspensions since a

gradient in deposition will occur, for example the deposit will be thinner above and a thicker deposit at the bottom when the deposition electrode is placed in a vertical arrangement. In addition, with larger particles, either a very strong surface charge must be obtained, or the electrical double layer region must increase in size. Besides it was found that the particle size has a prominent influence on controlling the cracking of the deposit during drying. Sato et al. [Sato N.-2001] found that the reduction in the particle size of $YBa_2Cu_3O_{7-\delta}$ (YBCO) particles improved the morphology in terms of crack formation of the superconducting films fabricated by EPD.

2) Dielectric constant of liquid media

Powers [Powers R. W.-1975] determined the relationship between deposition and the dielectric constant of the liquid and the conductivity of the suspension for beta-alumina suspensions in various organic suspension medias. It was verified that the conductivity of the suspension rapidly increases with dielectric constant of the suspension media and deposits were only obtained with liquids for which the dielectric constant is in the range of 12–25. It is well known that the dielectric constant is related to the power of the dissociative ability for liquids. For very low dielectric constant, EPD fails because insufficient dissociative power led to low zeta potential in the suspension, while with a too high dielectric constant, the high ionic concentration in the liquid reduces the size of the double layer region with a consequent reduction of the zeta potential and stability of the suspension. So, there is a proper range of dielectric constant values of the liquid media for a successful EPD. In general, because the low ionic concentration is benefic for the high stability of the suspension, liquids of low dielectric constant are favored.

3) Conductivity of suspension

Ferrari et al [Ferrari B.-1996] proposed that the conductivity of the suspension is a key factor and needs to be taken into a careful consideration in EPD. The authors pointed out that too conductive suspensions led to very low particle motion, however if the suspension is too resistive its stability is lost. It was also observed that the conductivity of the suspension increases with both suspension temperature and polyelectrolyte (dispersant) concentration. Based on these studies the existence of a window of conductivity range at varying dispersant dosage and suspension temperature, in which the deposit is successfully formed by EPD, was indicated. Conductivities of the liquid media out of this range are not suitable for EPD, limiting the deposition ability. Worthwhile to point that the suitable region of conductivity is different for the

different liquid media.

4) Stability of suspension

It is well accepted that in colloidal processing, such as EPD, the stability of the colloid in the system is one of the most essential factors in the conformation process. [Adamczyk Z.-2003] [Lewis J. A. -2000] A stable colloidal suspension with well-dispersed particles will provide a dense and homogeneous powder compact upon subsequent consolidation processes such as EPD. An unstable one will result in agglomeration of particles, hence results in inhomogeneous packing of the particles.

Suspension stability is characterized by settling rate and tendency to undergo or avoid flocculation. Stable suspensions show little tendency to flocculate and settle slowly. On the country, flocculating suspensions settle rapidly. The stability of suspension has been described by the classical DLVO theory established by Derjaguin and Landau [Derjaguin and Landau-1941] and Verwey and Overbeek [Verwey and Overbeek-1948]. According to this theory, the stability of a colloidal system is determined by the total energy of interaction, determined by sum of the electrical double layer repulsive forces (VR) and the van der Waals attractive forces (VA) which the particles experience as they approach each other. Increasing the ionic strength can significantly reduce the repulsive force. The behavior of particle separations depends critically upon the ionic strength and hence the electrolyte concentration of the suspension. At very low ionic strengths, the potential energy is high, make strong repulsive forces producing a totally dispersed system. At a slightly higher but still low enough ionic strengths, the role of electrolytes, such as, coagulants or flocculants, is either to reduce the electrostatic repulsion and hence making it easier for the particles aggregation, thereby destabilizing the suspension. But, re-dispersion is also possible by diluting the electrolyte solution to decrease the ionic strength. Finally, in a high ionic strength, the colloid particles experience no repulsive forces. Consequently, fast coagulation occurs and the system is completely unstable under such circumstances.

The original DLVO theory only considered the van der Waals and electrostatic interactions in the suspension. Recently, it was proposed that the stabilization of colloidal dispersions might also be affected by steric stabilization and structural forces. [Lewis J. A.-2000] These mechanisms become important when long chain macromolecules are adsorbed to the particles surface. When these particles with polymer chains protruding from their surfaces come close to each other, sharp repulsive steric interactions will happen. In this case the chain configuration of the polymer is a

very important parameter in steric stabilization [Evens D. F. -1999] and determines the quality of the dispersant. Caution must be paid in using sterically stabilized suspension for EPD. For example, in extreme cases, adsorbed polymers can reverse the sign of surface charge, so the deposition may fail or could occur on the counter electrode.

5) Zeta potential

A key ingredient in most of the colloidal processing methods used for ceramic shaping, including EPD, is the achievement of well stabilized, deagglomerated, and homogeneous slurry [Adamczyk Z.-2003]. Through a careful choice of the suitable suspension media, stable colloidal suspensions can be prepared. This is a necessary but not a sufficient condition for a successful EPD. Though stable and well-dispersed suspensions are necessary to produce densely packed deposits [Bouyer F.-1999], the use of suspensions with high zeta ptential and low ionic conductivity are also determinant aspects. [Van der Biest O. O. -1999]

The zeta potential indicates the degree of repulsion between adjacent, similarly charged particles in dispersion. A high zeta potential will confer stability, i.e. the solution or dispersion will resist aggregation. So, colloids with high zeta potential (negative or positive) are electrically stabilized while colloids with low zeta potentials tend to coagulate or flocculate as outlined in the Table 2-3. A value of 25 mV (positive or negative) can be taken as the arbitrary value that separates low - charged surfaces from highly-charged surfaces.[ASTM Standard] Therefore, most investigators use zeta potential or electrophoretic mobility to determine the ability of a suspension to be deposited by EPD. However other parameters need to be considered also. For example, in suspension of aluminium in alcohol the addition of an electrolyte of Al^{3+} causes no significant changes of the zeta potential, but deposits can only be obtained in the presence of the electrolyte. [Brown D. R.-1965]

Table 2-3 Relation of zeta potential and stability behaviour of the colloid [ASTM Standard]

Zeta potential (mV)	Stability behavior of the colloid
0 to 5	rapid coagulation or floculation
10 to 30	incipient instability
30 to 40	moderate stability
40 to 60	good stability
more than 61	excellent stability

2.5 Parameters related to EPD process

1) Deposition time

Time of deposition controls the thickness of the deposited layer. Basu et al. [Basu R. N.-2001] and Chen et al [Chen F.-2001] found that the deposition rate for a constant applied field decreases with prolonged deposition times. The deposition is initially linear, but as the deposition time increases the deposition rate decreases and attains a plateau at very high deposition times. According to Zhitomirsky [Zhitomirsky I.-1997] when the applied voltage is maintained constant between the electrodes, the electric field on the suspension decreases with deposition time because of the formation of an insulating layer of ceramic particles on the electrode surface.

2) Applied voltage

Normally the amount of deposit is proportional to the applied potential during EPD process, according to the formula (2-1). Powders can be deposited more quickly under higher applied fields, but the quality (morphology and density) of the deposit can suffer from the applied high fields. In general the literature reports that more uniform films are deposited at moderate applied fields (25–100 V/cm), whereas the film quality degrades at relatively higher applied fields (>100 V/cm). [Basu R. N.-2001, Negishi H-2002, Van Tassel-2004) In EPD the accumulation rate of the particles influences their packing behavior in the coating. A high applied field may cause turbulence in the suspension and the coating may be disturbed by flows in the surrounding medium during its deposition. At the same time under high applied fields, particles move very fast so that they may not have enough time to sit in their best positions to form a close-packed structure. In addition, the increase of the current density of the suspension media in proportion to the applied voltage may originate unstable suspensions with increasing applied voltages that may influence the morphology quality of the deposit. [Negishi H.-2002]

3) Conductivity of substrate

The uniformity and conductivity of the substrate electrode, particularly for non-metallic electrodes is a critical parameter to the green quality of deposited of films by EPD. Substrate of low conductivity such as $La_{0.9}Sr_{0.1}MnO_3$ (LSM) leads to a decrease of the deposition rate and non-uniform green films. [Peng Z.-2001] [Chen F.-2001]

2.6 Practical consideration

a) Powders washing

As mentioned above, successful EPD performance requires a stable suspension wherein well dispersed particles have a controlled surface charge. Thus the preparation of a particulate suspension with a carefully defined chemistry before conducting EPD is essential. For that powder washing is a necessary step to remove any residual impurities incorporated during powder preparation, particularly for powders synthesized by chemical methods and commercial powders.

It is well known that commercial powders usually include some surfactants in order to have a good particle size distribution, but the surfactants have usually a negative influence on the stability of the suspension. On the other hand, for the chemically prepared powders they may retain residues of the used chemical precursors that will affect the stability of the powders when in suspension. For both cases these residual impurities on the powder's surface can be removed by a washing step in deionized water. The conductivity of deionized water is about 0.04 μ/cm. After several times washing in deionized water, if the supernatant of the suspension has a similar conductivity to the pure deionized water, then there are no residual impurities in the suspensions. The removal of the impurities is also very important because, besides affecting directly the stability of the suspension and deposition performance it can later affect the sintering process. It was reported that unwashed 8-YSZ (8-mol%-yttria-stabilized zirconia) powders led to unstable suspension, lower deposition yield, a gradient in the EPD film thickness (thinner coating at top, thicker on bottom) and a decrease of 15–25% in the overall green density of the deposited coating. [Basu R. N.-2001]

b) Drying and sintering

Another important area of concern when shaping by EPD is cracking and how to avoid cracking during drying and sintering. [Sarkar P. -2004] As discussed in above constrained sintering, the shrinkage of the deposit can be substantially different from the substrate during drying and sintering. Ceramic coatings typically suffer about 10 to 15% linear shrinkage during sintering. As a result, tensile/compressive stresses are developed in the coating/substrate and are usually relieved by the formation and propagation of cracks that originate from flaws or defects in them. In a recent review Sarkar et al. [Sarkar P-2004] outlined strategies to avoid cracking of EPD deposits during sintering. For example, cracking can be avoided by using a low surface tension solvent, or by

preventing fine pore structure in the coating, to minimize capillary stresses. Capillary stresses can also be removed altogether by adopting freeze/supercritical drying since the solvent phase is sublimed in this process. Furthermore, slow drying will help to control the capillary stresses by adjustment of the vapor pressure in the drying medium. For aqueous EPD, the use of a high humidity oven for drying is generally found to prevent cracks. [Sarkar P.-2004]

There are various origins for the cracking in the sintered deposits. Well known is that if thermal expansion between the deposited layer and the substrate matches cracking during sintering can be avoided. So an appropriated choice of the substrate and deposited layer based on thermal expansion coefficients is important [Besra L.-2007]. The use of liquid phase during sintering is another way of avoiding cracking formation during sintering. Other methodologies have been used to overcome this problem and recently the use of polymer additives (poly diallyldimethylammonium chloride - PDDA) which insures a good adhesion of the deposits to the substrate was claimed to prevent crack formation. [Zhitomirsky I.-2000]

Therefore, a careful control of the drying and sintering step for each individual system, by the identification of the most relevant strategies will ensure a crack free film fabrication.

2.7 Design of the apparatus for EPD

The construction and design of an EPD facility is an important consideration of the process because it affects directly the feasibility of fabricating a determined shape and the quality of the green deposited.

Almost any shape can be deposited through a proper design of the mandrel or forming electrode, such as flat plates, crucible shapes, and tubes of circular or rectangular. [Heavens N.-1990] Although the equipment requirements for EPD are simple, (Figure 2-7) a number of design features need to be taken into account. In terms of materials those selected to construct the cell should avoid the neutralization of the charges on the suspended particles. In terms of the cell design the geometry of the cell should guarantee a uniform distribution of the electric field between the electrodes to yield uniform wall thickness in complex-shaped deposits and patterns, since the thickness profile can be influenced by the field distribution in the cell, as discussed in section of EPD dynamics. To keep the stability of the suspension, a continuous agitation (magnetic stirring) to avoid gravitational settling is usually required and should be

contemplated in the EPD apparatus design. [Powers R. W.-1974] As shown in Figure 2-7, the EPD cell can de designed in the horizontal or vertical position, and that more recently more complex apparatus have been designed in which the application of magnetic fields have been introduced for example for the purpose of alignment.

To the author knowledge, there is no specific commercial design of any EPD apparatus. Different research groups have employed a variety of different designs depending on their own requirements. Most of the designs are based on deposition on flat surfaces.

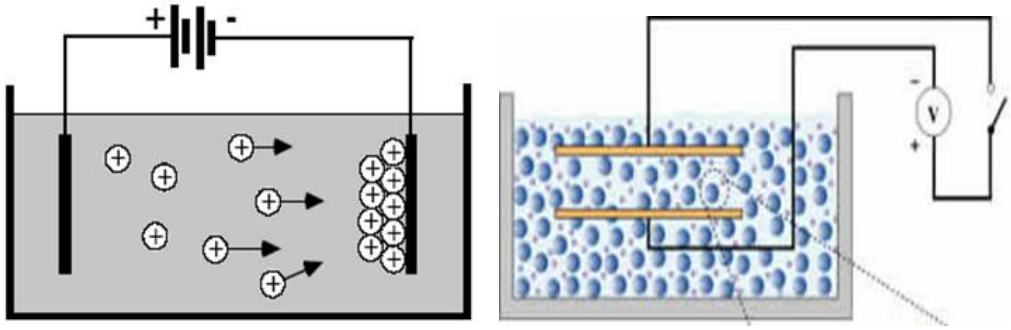

(a) (b)

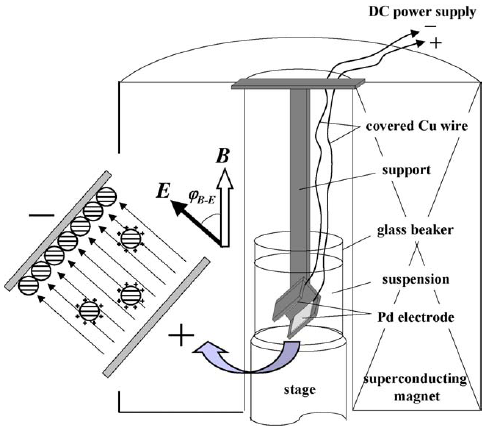

(c)

Figure 2-7 Schematic of EPD cell (a) horizontal, (b) vertical configuration, and (c) in a superconducting magnet (after Uchikoshi T.-2006)

2.8 Application of EPD

In general, EPD can be applied to any solid that is available in the form of a colloidal suspension. Examples of EPD can be found for any class of materials, including metals, polymers, carbides, oxides, nitrides and glasses. Compared to other

thick film techniques, EPD demonstrates substantial technical advantages due to the fact that it can be easily scaled up using inexpensive equipment and, consequently, it has the potential to lead to commercial success and large-scale production.

Figure 2-8 provides a comparison of processing techniques versus devices application over a range of size scales for the microelectronic industry. Even with commercially available sub-micron powders, the smallest devices can be produced via traditional thick film methods range from 5-10 μm. While thin film techniques are able to achieve sub-micron devices, deposition times can be very long for thicknesses above 1.0 μm, and stoichiometry can be difficult to control in the forming complex oxide films. It would be advantageous to have a processing technique which ranged from thin to thick films while maintaining the stoichiometric of the compositions. As is shown in Figure 2-8, EPD is such a technique. With EPD thin to thick layers can be deposited by controlling the deposition parameters, principally the suspension concentration. The adequate choice of the suspension media will guarantee the stoichiometry of the initial powders. These are the reasons that EPD have been used for the fabrication of a wide range of materials and is becoming now more and more important for the fabrication of nanomaterials and nanostructures. [Boccaccini A. R.-2008]

The following are some examples for specific applications of EPD:

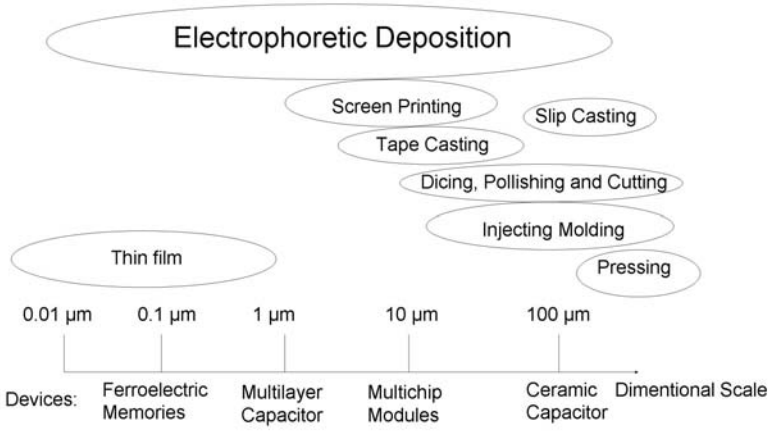

Figure 2-8 Comparison of processing techniques versus device application over a range of scales in terms of microelectronic industry

a) Coatings

Depending on the powder composition and size, EPD has the capability to fabricate from a stable colloidal suspension films of a few μm up to more than 300 μm

on electrical conductive substrates of any shape.

EPD of coatings has already gained a world-wide acceptance for automotive, appliance, and general industrial (organic) coatings, namely painting industry. [Pierce P. E.-1981] The examples of coatings made by EPD include the deposition of phosphor coatings in the manufacture of screens for cathode ray tubes (CRTs) for advanced display applications, deposition of insulating glass for electronic applications, and superconductive coatings. [Siracuse J. J.-1990, Sussman A.-1981, Miziguchi J.-1991] First reports on the use of EPD to prepare advanced ceramic coatings were published in the late 1980s. Moreover, by performing EPD in a magnetic field, some authors were able to create a desirable textured microstructure in the coatings. [Hein M.-1989] Some examples of relatively complex shapes were reported to be coated, such as, taps coated with carbides, metal cones coated with a ceramic glaze, platinum grids coated completely with ferrite [Ortner M.-1964, Barraclough M.-1967, Van der Biest O. O.-2004] More recently, selective EPD has been achieved with good resolution for the deposition of silver interconnects. The high resolution patterns (16 μm pattern line width, 10 μm line-pitch) for interconnects and circuit components made by EPD was reported by an advanced ceramic company (Cerel—Ceramic Technologies Ltd, Israel), as shown in Figure 2-9. Some other significant recent developments of advanced functional materials coating include: the fabrication of $BaTiO_3$ thick films for sensor and actuator applications, [Zhang J.-2000] MgO-modified $Ba_{0.6}Sr_{0.4}TiO_3$ thick films for tunable microwave devices, [Ngo E.-2001] $(Pb,Zr)TiO_3$(PZT) coatings for embedded components or for optical switches. [Ng S. Y.-2005, Wu, A. Y.-2006, Shen I. Y.-2006]

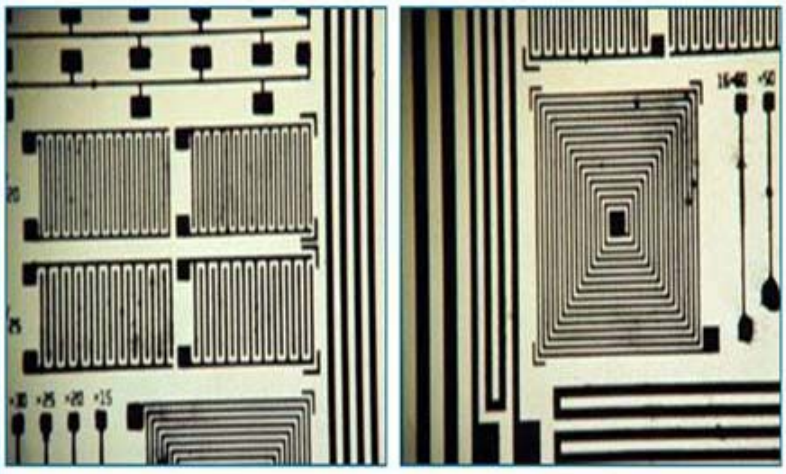

Figure 2-9 A pattern line width of 16 μm EPD silver interconnects
(after Cerel—Ceramic Technologies Ltd, Israel)

b) Monolithic or free standing objects

For traditional ceramics, such as sanitary ware, the main advantage of EPD lies in its higher speed and in the low wear of the moulds compared with tape casting. Tiles, closed and open end tubes, hemispheres, tubes with changes in diameter, and conical sections are some of the shapes that have been made by EPD. Technical ceramics such as alumina (Jean J. H.-1995), silicon carbide (Vandeperre L. J.-1998), and aluminium nitride (Moritz K.-1993) have been shaped by EPD and are commercially available in the market for a long time. A good example of the classical use of EPD is the fabrication of Beta-alumina tubes, used as electrolyte in sodium sulfur batteries [Powers R. W.-1974]

c) Layered and Graded Materials

Layered materials can also be produced via EPD. When the desired thickness of the first layer is reached, the deposition electrode can be moved to a second suspension for the deposition of a layer of a different composition. By changing back and forth, a layered material can be obtained. Nicholson et al [Nicholson P. S.-1993] reported the production of ZrO_2/Al_2O_3 laminates in which the boundaries between the layers were straight and well defined, showing that although EPD can be a fast process, good control of the growth of the layers can be obtained. Later, the fabrications of alumina/lanthanum aluminate layered ceramics were reported by the same group. [Bissinger M. -1994]

Similarly to layered materials, by immersing the deposition electrode in different baths, graded materials can also be made by gradually changing the composition of the suspension from which EPD is carried out. Sarkar et al [Sarkar P.-1993] demonstrated the ability to form graded materials by slowly adding an ethanol-based suspension of an alumina powder to an ethanol-based suspension of an yttria-stabilized zirconia powder, during deposition gradual increase in the alumina content of the deposit was observed. Zhao et al reported the fabrication of alumina/ceria-stabilized zirconia-graded rods as well. [Zhao C.-1998]

d) Infiltration

EPD can be used to infiltrate objects with a matrix material or to apply an internal coating. Gal-Or reported the infiltration of porous graphite electrodes with silicon carbide and silicon oxide particles. [Gal-Or L.-1992] Ishihara applied an internal coating of yttria-stabilized zirconia to a porous Ni-CaO stabilized ZrO_2 cermet containing 40 wt% Ni for a solid oxide fuel cell. [Ishihara T. -1996] By repetitive

infiltration and sintering, a dense film of uniform thickness could be fabricated. Another application where EPD is gaining increasing interest is the infiltration of fiber preforms with a matrix material for composite production. [Boccaccini A. R.-1998] The advantage of using EPD for infiltration fabrication is that it allows considerable reduction of the costs and much higher rates of infiltrations, compared with, for example, chemical vapor infiltration.

e) Nanostructured materials

The production of materials with nanoscale patterns is of current importance in a range of applications, such as photonic materials, high density magnetic data storage devices, microchip reactors, and biosensors. [Dutta J.-2003] It is also foreseen that the importance of nanoscale patterns will quickly spread over other technological areas, such high frequency microelectronics.

Since the suspended particles are usually charged, the concept of EPD utilizing a directional force (external electric field) has recently created significant interest for patterned assembly of nanoparticles [Bailey R. C-2002]. EPD of nanoparticles was firstly used by Giersig [Giersig M.-1993] to prepare ordered monolayers of gold nanoparticles. In the last 10 years there has been a considerable increase of the areas of application of EPD for nano structured materials, such as manipulation and arrangements of nanoparticles, and other nano structured films and coatings. The processing of novel nanomaterials is reported by Limmer et al. [Limmer S. J.-2004], who present the growth of Titania nanorods by sol-gel electrophoresis and by Matsuda et al., [Matsuda A.-2004] who use a combination of sol-gel and EPD to produce novel inorganic-organic films for micro-optical devices. In addition, the EPD technique can be readily extended to allow the coating of Carbon Nano Tubes (CNTs) onto large planar substrates, wires, individual fibers, fibrous structures, and porous components. Boccaccini et al. have deposited Multi-Walled Carbon Nano Tubes (WCNTs) onto highly porous bioactive glass scaffolds with the intention of imparting a monotopography to the pore wall surface, as shown in Figure 2-10. [Boccaccini A. R.-2007] The growth of single crystalline PZT nanorods arrays ware presented by Limmer et al. (Figure 2-10) [Limmer S. J.-2005] The progress of EPD based methods on nano structured materials was recently reviewed in detail by Cao and Boccaccini et al. [Cao G. Z.-2004, Boccaccini A. R.-2008]

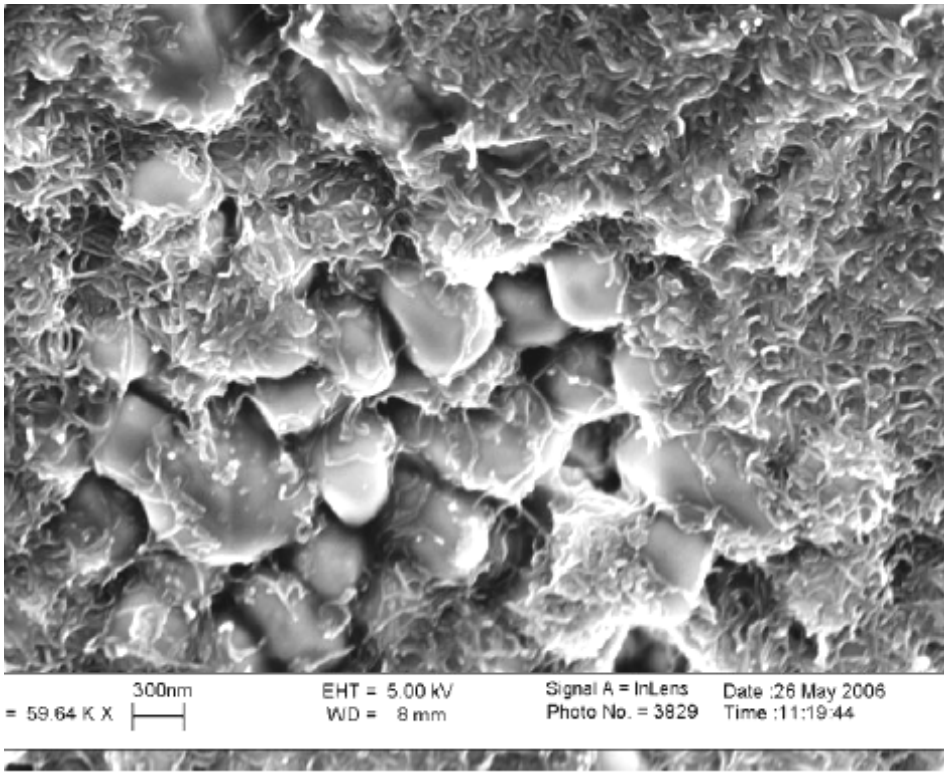

(a)

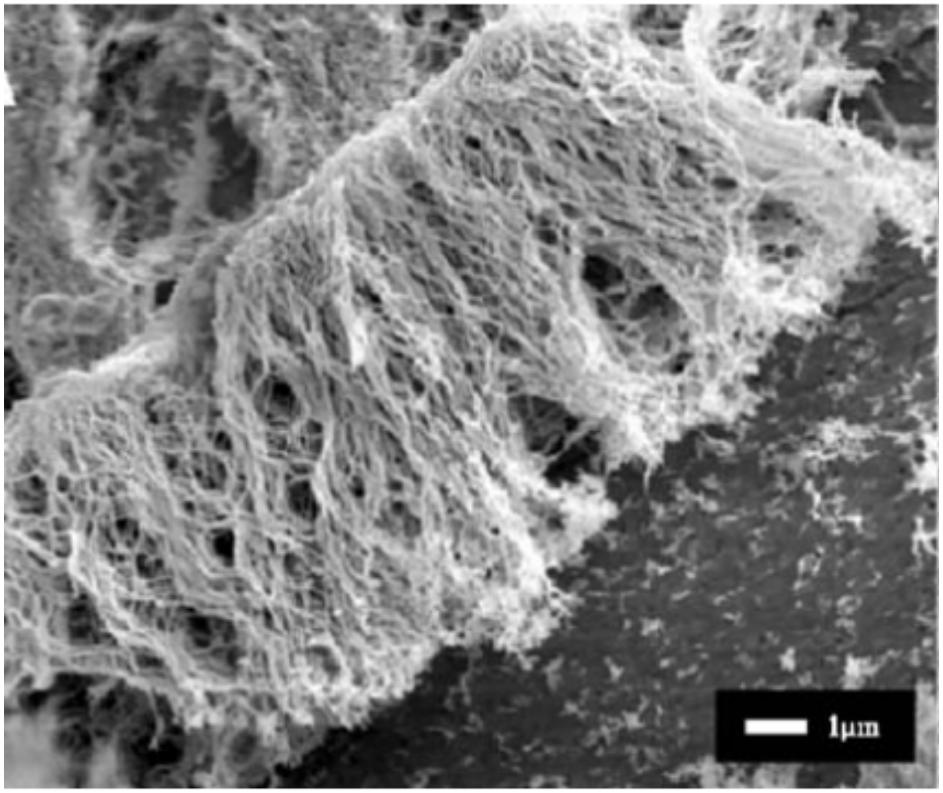

(b)

Figure 2-10 SEM micrographs of (a) a Bioglass® scaffold coated with CNTs (after Boccaccini A. R.-2007), (b) PZT nanorods (after Limmer S. J.-2005)

2.9 Summary

Over recent years, advances in thick-film technology have enabled this cheaper process to become significantly useful in many applications. This chapter reviewed the different thick films technology currently available. Among these, EPD stands out as a versatile and cost effective materials processing technique for a wide range of technical applications. It offers control over the microstructure, stoichiometry, and properties. An overview of the state-of-the-art of the knowledge on EPD and in the use of EPD for the fabrication of materials was presented. In addition the fundamental EPD mechanisms and theories proposed for EPD are explained and their limitations highlighted.

2.10 References

1. Adamczyk Z. (2003) Adv Colloid Interface Sci. **100**, 267
2. Altenburg H., Plewa J., Schultze W. and Vilics T. (2001) BMBF. Forschungs bericht, VDI
3. ASTM Standard (1985) Zeta Potential of Colloids in Water and Waste Water, American Society for Testing and Materials
4. Bailey R. C., Stevenson K. J., Hupp J. T. (2002) Adv Mater. **12**, 1930
5. Barraclough M., Bolton N. E., Collins A. H. and Andrews J. H. (1967) IEEE Trans. Magnet. **3**, 531
6. Basu R. N., Randall C. A., Mayo M. J. (2001) J. Am. Ceram. Soc. **84**, 33
7. Bersani M., Morten B. and Prudenziati M. (1997) J. Mater. Res. **12**, 501
8. Besra L. and Liu M. (2007) Progress in Mater. Sci. **52**, 1
9. Binner, J.G. P. (1990) Advanced Ceramic Processing and Technology, William Andrew Publishing
10. Bissinger M., Prakash O., Sarkar P. and Nicholson P. S. (1994) Ceram. Sci. Eng. Proc. **15**, 1084
11. Boccaccini A. R., Chicatun F., Cho J., Bretcanu O., Chen Q., Roether, J. A., Novak S., and Chen Q. Z. (2007) Adv. Funct. Mater. **17**, 2815
12. Boccaccini A. R., Roether J. A., Thomas B. J. C., Shaffer M. S. P., Chavez E., Stoll E., Minay E. J. (2006) J. Ceram. Soc. Jap. **114**, 1
13. Boccaccini A. R. and Trusty P. A. (1998) J. Mater. Sci. **33**, 933
14. Bordia R. K. and Raj J. (1985) J. Am. Ceram. Soc. **68**, 287
15. Bouyer F. and Foissy A. (1999) J. Am. Ceram. Soc. **82**, 2001
16. Brown D. R. and Salt F. W. (1965) J. Appl. Chem. **15**, 40
17. Cao G. Z. (2004) J. Phys. Chem. B **108**, 19921
18. Chen F. and Liu M. (2001) J. Euro. Ceram. Soc. **21**, 127
19. Chung J., Ko S., Bieri N. R., Grigoropoulos C. P., and Poulikakos D. (2004) Appl. Phys. Lett. **84**, 801
20. Corni I., Ryan M. P., Boccaccini A. R. (2008) J. Euro. Ceram. Soc. **28**, 1353
21. Dahotre N. B., Kadolkar P. and Shah S. (2001) Surf. Interface Anal. **31,** 659
22. Derjaguin B. V. and Landau L.D. (1941) Acta Physicochemi. URRS **14**, 633
23. Ducheyne P., Radin S., Heughebaert M., Heughebaert J. C. (1990) Biomaterials **11**, 244
24. Dutta J., Hofmann H. (2003) Self organization of colloidal nanoparticles In:

Nalwa H. S Editor, Encyclopedia of nanoscience and nanotechnology, vol. X. American Scientific Publishers, P1–32

25. Evens D.F. and Wennerstrom H. (1999) the Colloidal Domain, Wiley-VCH
26. Ferrari B. and Moreno R. (1996) Mater. Lett. **28**, 353
27. Ferrari V., Mariolli D. and Taroni A. (1997) Meas. Sci. Technol. **8**, 42
28. Fukada Y., Nagarajan N., Mekky W., Bao Y., Kim H. S. and Nicholson P. S. (2004) J. Mater. Sci. **39**, 787
29. Fu Z., Wu A. Y., Vilarinho P. M., Kingon A. I. and Wordenweber R. (2007) Appl. Phys. Lett. **90**, 052912
30. Gal-Or L., Haber S. and Liubovich S. (1992) J. Electrochem. Soc. **139**, 1078
31. Giersig M., Mulvaney P. (1993) Langmuir **9**, 3408
32. Grillon F., Fayeulle D. and Jeandin M. (1992) J Mater. Sci. Lett. **11**, 272
33. Guo H. L. (2004) Current Appl. Phys. **4**, 385
34. Hamaker H. C. (1940)Trans Farad Soc **36**, 279
35. Heavens N. (1990) Electrophoretic deposition as a processing route for ceramics, In: Binner GP, editor. Advanced ceramic processing and technology, vol. 1, Park Ridge (NJ), USA: Noyes Publications, P255–283 [chapter 7]
36. Hein M., Peiniger M., Piel H., Ponto L., Becks M. and Klein U. (1989) J. Appl. Phys. **66**, 5940
37. Hirata Y., Nishimoto A. and Ishihara Y. (1991) Nippon Seramikkusu Kyokai Gakujutsu Ronbunshi **99**, 108
38. Hiremath B. V. (1989) Symposium on Ceramic Thin and Thick Films, Indianapolis, Indiana
39. Ishihara T., Takita Y. and Sato K. (1996) J. Am.Ceram.Soc.**79**, 913
40. Jean J. H. (1995) Mater. Chem. Phys. **40**, 285
41. John B. B. (2007) Printed Circuit Design & Manufacture **24**, 38
42. King B. H., Dimos D., Yang P., and Morissette S.L. (1999) J. Electroceramics **3**, 173
43. Koelmans H. (1995) Phillips Res Rep **10**, 161.
44. Kosec M., Holc J., Malic B., Bobnar V. (1999) J. Euro. Ceram. Soc. **19**, 949
45. Labib M. E., Williams R. (1986) Colloid Polymer Sci. **264**, 533
46. Lee B. Y., Cheon C. I., Kim J. S., Bang K. S., Kim J. C., Lee H. G. (2002) Mater. Lett. **56**, 518
47. Lewis J. A. (2000) J. Am. Ceram. Soc. **83**, 2341
48. Limmer S. J., Chou T. P. and Cao G. Z. (2004) J. Mater. Sci. **39**, 895

49. Limmer S. J., Chou T. P. and Cao G. Z. (2005) J. Sol Gel Sci. Tec. **36**, 183
50. Louh R. F. (2003) Mater. Chem. Phys. **79**, 226
51. Lubitz K., Schuh C., Steinkopff T.and Wolff A. (2002) in piezoelectric materials for the end user, Conference notes, Polecer Meeting, Interlaken
52. Lyklema J. (1977) J. Colloid Interface Sci. **58**, 242
53. Ma J. and Cheng W. (2002) J. Am. Ceram. Soc. **85**, 1735
54. Matsuda A., Tanaka T., Tadanaga K., Minami T. and Tatsumisago M. (2004) J. Mater. Sci. **39**, 903
55. Miziguchi J., Matsumura M., Suzuki M. and Yamato H. (1991) J. Electrochem. Soc. **138**, 2942
56. Moreno R. and Ferrari B. (2000) Mater Res Bull. **35**, 887
57. Morissette S. L., Lewis J. A., Clem P. G., Cesarano J., and Dimos D. B. (2001) J. Am. Ceram. Soc. **84**, 2462
58. Moritz K. and Reetz T. (1993) In Third Euroceramics, Ed: Duran P., Fernandez J. F., P425–30, Castell´on de la Plana, Spain
59. Negishi H., Yanagishita H., Yokokawa H. (2002) Proceedings of the electrochemical society on electrophoretic deposition **21**, 214
60. Nicholson P. S., Sarkar P. and Huang X. (1993) J. Mater. Sci. **28**, 6274
61. Ngo E., Joshi P. C., Cole M. W. and Hubbard C. W. (2001) Appl. Phys. Lett. **79**, 248
62. Ng S. Y. and Boccaccini A. R. (2005) Mater. Sci. Eng. B-Solid State Mater. Adv. Technol. **116**, 208
63. Ortner M. (1964) Plating **9**, 885
64. Owczarek J. A. and Howland F. L. (1990) IEEE Trans. On Components Hybrid and Manufacturing Tech. **13**, 358
65. Pan J., Tonkay G. L. and Quintero A. (1998) International Symposium on Microelectronics, 264
66. Peng Z. and Liu M. (2001) J. Am. Ceram. Soc. **84**, 283
67. Pierce P. E. (1981) J. Coat. Tech. **53**, 52
68. Powers R. W. (1974) Am. Ceram. Soc. Bull. **53**, 619
69. Riemer D. E. (1988) Solid State Tech **85**, 107
70. Rose A. (1988) Proceedings of the 38th Electronics Components Conference 636, Digital Object Identifier: 10.1109/ECC.1988.12660
71. Rozenberg G. G., Bresler E., Speakman S. P., Jeynes C., and Steinke J. H. G. (2002) Appl. Phys. Lett. **81**, 5249

72. Sarkar P., De D. and Rho H. (2004) J. Mater. Sci. **39**, 819

73. Sarkar P. and Nicholson P. S. (1996) J. Am. Ceram. Soc. **79**, 1987

74. Sarkar P., Nicholson P. S. and Huang X. (1993) J. Am. Ceram. Soc.**76**, 1055

75. Sato N., Kawachi M., Noto K., Yoshimoto N., Yoshizawa M. (2001) Physica C **357**, 1019

76. Scherer G. W. and Garino T. (1985) J. Am. Ceram. Soc. **68**, 216

77. Sennet P., Olivier J. P. (1965) Colloidal dispersions, electrokinetic effects and the concept of zeta potential, In: Ross S, editor. Chemistry and physics of interfaces, Washington (DC): Am Chem Soc. P73–93

78. Shen I. Y., Cao G. Z., Wu C. C. and Lee, C. C. (2006) Ferroelectrics **342**, 15

79. Sigmund W. M., Bell N. S. and Bergstroem L. (2000) J. Am. Ceram. Soc. **83**, 1557

80. Siracuse J. J., Talbot J. B., Sluzky E. and Hesse K. R. (1990) J. Electrochem. Soc. **137**, 346

81. Smith P. J., Shin D. Y., Stringer J. E., Derby B., and Reis N. (2006) J. Mater. Sci. **41**, 4153

82. Stern O. Z. (1924) Electrochem **30**, 508

83. Sussman A, Ward T. J. (1981) RCA Review **42**,178

84. Sweeney T. (1998) Ph.D. Thesis, Cranfield University, UK

85. Tassel J. V. (2004) PhD thesis, Pennsylvania state university, USA

86. Tassel J. V. and Randall C.A. (1999) J. Euro. Ceram. Soc. **19**, 955

87. Tok A. I. Y., Boey F. Y. C. and Khor K. A. (1998) Proc. Fabric. Advanced Materials VI, 1791

88. Tzeng S. Y. and Jean J. H. (2002) J. Am. Ceram. Soc. **85**, 335

89. Uchikoshi T., Suzuki T. S., Iimura S., Tang F. Q. and Sakka Y. (2006) J. Euro.Ceram. Soc. **26**, 559

90. Ueltzen M., Altenburg H., Seega C., Litzkendorf D., Fischer F. and Görnert P. (1995) EUCAS **148**, 179

91. Van der Biest O. O. and Vandeperre L. J. (1999) Ann. Rev. Mater. Sci. **29**, 327

92. Van der Biest O. O., Put S., Anné G. and Vleugels J. (2004) J. Mater. Sci. **39**, 779

93. Vanderperre L. (1998) PhD thesis, Katholieke University, Belgium

94. Vandeperre L. J., Biest V. B., Bouyer F., and Foissy A., (1998) Ceram. Bull. 7753

95. Vervew E. J. W.and Overbeek J. T. G. (1948) Theory of stability of lyophobic colloids, Elsevier, Amsterdam, the Netherlands

96. Weise N. L. (1985) Mineral processing handbook, New York: Society of Mining

Engineers

97. Whatmore R. W. (1998) Ferroelectrics **225,** 179

98. Wu A. Y., Vilarinho P. M. and Kingon A. I. (2006) J. Am. Ceram. Soc. **89**, 575

99. Yates D. E., Levine S. and Healy T. W. (1974) J. Chem. Soc. Faraday Trans **170**, 1807

100. Zarbov M., Schuster I., Gal-Or L. (2002) Methodology for selection of charging agents for electrophoretic deposition of ceramic particles, In: Proceedings of the international symposium on electrophoretic deposition: fundamentals and applications, the Electrochemical Society Inc, USA, Proc. **21**, 39

101. Zhang J. and Lee B. I. (2000) J. Am. Ceram. Soc. **83**, 2417

102. Zhao C., Vandeperre L., Vleugels J. and Biest O. V. (1998) J. Mater. Sci. Lett. **17**, 1453

103. Zhao Y. and Dharani L.R. (1994) Thin Solid Films **245**, 109

104. Zhitomirsky I. (2002) Adv Colloid Interface Sci. **97**, 279

105. Zhitomirsky I. and Gal L. (1997) J. Mater. Sci.: Mater Med. **8**, 213

106. Zhitomirsky I. and Petric A. (2000) Mater. Lett. **46**, 1

Chapter 3
Objective of This Thesis

3.1 Introduction

Wireless applications, based in part on radio frequency (RF) devices and integrated circuit (IC) technologies, have grown quickly to become significant markets for semiconductor manufacturers.[Bennett H. S.-2005] Such applications include multifunctional portable phones, blue tooth, office voice, video and data transmission through wireless local area networks (WLAN), global positioning system (GPS), and automotive safety control among others. [Gerhard G.-2001]

Though the advancement of wireless electronics has placed continuous demand on the electronics industry to develop new, multi-functional, and miniaturized circuits, miniaturization of passive components has not matched the advancement of semiconductor-based active components yet. The integration of active electronic components has resulted in the miniaturization and improvement of electronic circuits, however the majority of the passive elements still remain discrete. Transition from surface mount discrete components to integrated components into the substrate will result in enhanced reliability, better electrical performance, and miniaturization.

The rapidly growing wireless industry needs new advanced technology to build low loss, lower phase noise integrated circuits with low cost, high density, small size and lightweight. [Stephens D.-2005] One of which is miniaturization of systems such as planar circuits, antennas, filters, couplers, baluns etc. Because of this demanding development of smallness, thin and/or thick dielectric films are now considered to replace dielectric components currently utilized in bulk ceramic form. This drives the search for fabrication processes for films to be mass-produced with repeatable performance at very low costs.

Why ceramic thick film technology?

Future volume consumer communications products, such as WLANs, will all push the frequency and performance requirements further. The increase in required Q coupled with increasing frequency makes current FR4 (Flame Retardant 4), which is the current type of material used for printed circuit boards (PCB), progressively more difficult to use, and will undoubtedly result in an increasing use of modules containing subcircuits

fabricated on different substrates. An alternative to this approach is to combine these various subcircuits onto a single substrate allowing the benefits of the ceramic thick film (size, tolerance etc.) to be utilized for additional circuits such as filters and antennas.

Although thin film technologies are being explored for the wireless circuit technology, they are expensive processes with limited suitability for commercial applications. [Barnwell P.-1998] Alternatively, thick films technology offers advantages such as low cost and feasibility to be produced mass production. Thick films allow designers to combine microwave and digital functions on proper substrates and to incorporate components to the main structures, which offers increased potentials in terms of reliability, miniaturization of circuits, circuit design capabilities, continuous flow in production processes, and hence a reduction in cost. [Abe K.-1979]

Besides the low cost competition, thick film dielectrics have the capability of withstanding high voltages and the high thermal conductivity, which led to applications in mobile phone RF power amplifiers where small physical size and high power handling is necessary; in addition, thick dielectric film can also be used as a substrates in microelectronic devices to support mechanically the other materials and to ensure their adhesion on it, which may be difficult to achieve with thin film materials. [Caulton M. -1971]

Why EPD?

Among the thick-film fabrication techniques, for instance tape casting and screen printing, EPD technique offers unique features of precise pattern on complex shape substrate without high–cost etching and polishing step, besides the advantages of simplicity and low cost equipment, EPD allows a rigid control of the coating thickness and deposition rate. [Corni I.-2008] Thick film capacitors can be directly deposited and integrated on the pattern structure by EPD process, which will give higher reliability than soldered discrete capacitors. Another specialized application is a connector for the interconnection of different electrical component in electronic devices. In this case EPD derived thick dielectric films can be patterned to form an integral part of the connector.

Consequently, by applying EPD techniques, passive elements can be integrated in monolithic modules, and high density package and small size circuits are achieved with good performance at low cost.

The advantages of the use of EPD technology to the fabrication of wireless

systems as somehow already proved. As an example, EPD of ferroelectric (Ba, Sr) TiO_3 (BST) thick film has been reported and the potential application for tunable microwave devices. Phase shifters, tunable filters and antennas etc. have been demonstrated. [Ngo-2001] Improvements in technology of BST electronic tunable materials, including suitable lower loss and middle tunability, will be expected for leading a new class of wide-range tunable devices.

Why BNT?

Based on the description of chapter 1, dielectrics to be employed as microwave components must exhibit low loss or high quality factor Q (high Q allows signal distribution or storage with minimum loss), high relative permittivity (ε_r) (the size of the dielectric resonator is proportional to $1/\varepsilon_r^{1/2}$) and small temperature coefficient of relative permittivity ($TC\varepsilon_r$) (low $TC\varepsilon_r$ avoids drift in frequency due to temperature variations).[Cava R. J.-1997] So, it is believed that the main focus in the development of new small size microwave devices is related to the employment of low loss dielectric materials with relative dielectric permittivity as high as possible.

Within the low loss dielectrics family, $BaO\text{-}Nd_2O_3\text{-}TiO_2$ system represents an important commercial family of microwave ceramics due to the highest relative permittivity values, low loss and high temperature stability among microwave ceramic materials. Especially, $BaNd_2Ti_5O_{14}$ composition with Qf-6199, ε_r-91.9 at 3.5 GHz. [Wakino K.-1984, FuJi Titanium Industry Co., Ltd, Japan] has already been commercially employed in microwave devices. Availability of BNT materials with higher relative permittivity has a significant impact on the miniaturization demand of portable systems at specific frequency microwave devices (1-5 GHz region), such as cellular and personal communication systems (PCS) base-stations.

Why metal foil substrate?

Although rigid substrates, such as Al_2O_3 etc, are typically employed as the substrate for thick film fabrication.The ability to process thick films conformally on metallic substrates, and also directly on flexible metallic foils, opens up the possibility of innovative structures and designs. Such as, electronic components on flexible foil substrate can be embedded inside hybrid circuits, with obvious advantages over surface mounting techniques (SMT) because embedding the components can be very attractive in many ways in that it enhance the reliability by increasing the electrical contact area, it

can conserve board surface area, and reduce the overall volumes. Also it could be quite attractive in its ability to decrease the indirect manufacturing cost and increase the throughput in the manufacturing process. [Kingon A. I. -2005]

3.2 Motivation of this research

Although low loss (high Q) microwave ceramics, such as BNT bulk ceramics, have been developed and are currently part of commercial microwave devices, there is no available knowledge on the processing and properties of low loss dielectric thick films. In addition, EPD has been widely investigated in the fabrication of high k dielectric thick films, such as $(Ba_{1-x}Sr_x)TiO_3$ (BST), $BaTiO_3$ (BT), $Pb(Zr_{1-x}Ti_x)O_3$ (PZT), [Wu A. Y.-2006, Van Tassel -2004], but not on the preparation and dielectric properties of high Q (low loss) dielectric thick films. Consequently, it is of the most importance to fill this gap of knowledge. In the present work, BNT materials were chosen as representative to study low loss dielectric thick films fabrication by EPD technique.

The main purpose of this research effort is to develop a processing route for the fabrication of low loss dielectric $BaNd_2Ti_5O_{14}$ (BNT) thick films at a low cost for high frequency applications, and to establish the processing-properties relationship. For that, an electrophoretic deposition (EPD) process was investigated since it matches the objective of low-cost and offers the advantages of complex pattern to address the miniaturization trend of integrated circuits. This research was directed towards the understanding the low loss dielectric BNT thick film processing and utilizing this knowledge to design a methodology for achieving low loss dielectric BNT thick films.

The thesis describes a technology by which low loss dielectric thick films belonging to the system of $BaNd_2Ti_5O_{14}$ (BNT) can be processed and developed by using EPD technique. The specific objectives of this work include the following aspects:

1) Exploitation of the EPD process for the fabrication of BNT thick films
2) Establishment of the effects of the processing parameters on the final properties of BNT thick films
3) Exploitation of the ability of fabrication of BNT thick films on insulating, particularly Al_2O_3 substrate and systematic characterization of the obtained films
4) Exploitation of the fabrication of tunable low loss dielectric thick films by the combination of EPD with sol gel deposition in the BNT-BST ($(Ba,Sr)TiO_3$) system.

3.3 References

1. Abe K., Ikegami A., Sugishita N., Taguchi N., Isogai T., Tsubokawa I. and Ohtsu H. (1979) IEEE Trans. On Components Hybrids and Manufacturing Tech. **2**, 434
2. Barnwell P., Wood J. (1998) Fabrication of low cost microwave circuits and structures using an advanced thick film technology, IEMT/IMC Proceedings
3. Bennett H. S., Brederlow R., Costa J. C., Cottrell P. E., Huang W. M., Immorlica A. A. J., Mueller J. E., Racanelli M., Shichijo H., Weitzel C. E. and Zhao B. (2005) IEEE Trans. Electron Devices **52,** 1235
4. Caulton M., Hersheno B., Knight S. P. and Debrecht R. E. (1971) IEEE Trans. on Microwave Theory and Tech. **MT19**, 588
5. Cava R. J., Peck W. F., Krajewski Jr., J. J., Roberts G. L., Barber B. P., O'Bryan H. M. and Gammel P. L. (1997) Appl. Phys. Lett. **70**, 1396
6. Corni I., Ryan M. P. and Boccaccini A. R. (2008) J. Euro. Ceram. Soc. **28**, 1353
7. Gerhard G. and Koch S. (2001) IEEE Trans. Microwave Theory and Tech. **49**, 559
8. Kingon A. I. and Srinivasan S. (2005) Nature Mater. **4**, 233
9. Ngo E., Joshi P. C., Cole M. W. and Hubbard C. W. (2001) Appl. Phys. Lett. **79**, 248
10. Stephens D., Young P. R., and Robertson I. D. (2005) IEEE Trans. On Microwave Theory and Tech. **53**, 3832
11. Van Tassel (2004) PhD thesis, Pennsylvania state university, USA
12. Wakino K., Minai K. and Tamura H. (1984**)** J. Am. Ceram. Soc. **67**, 278
13. Wu A. Y., Vilarinho P. M. and Kingon A. I. (2006) J. Am. Ceram. Soc. **89**, 575

Chapter 4
Experimental Procedures

Abstract:
In this chapter, a detailed description of the experiments, including the BNT powders preparation, suspension preparation and characterization, EPD process, ceramics fabrication, characterization of the structure and microstructure of BNT thick films and measurements of the dielectric properties is presented. A brief description of the instrumentation used for studying the structural, microstructural and dielectric characteristics of low loss BNT thick films and ceramics is included as well.

4.1 Introduction

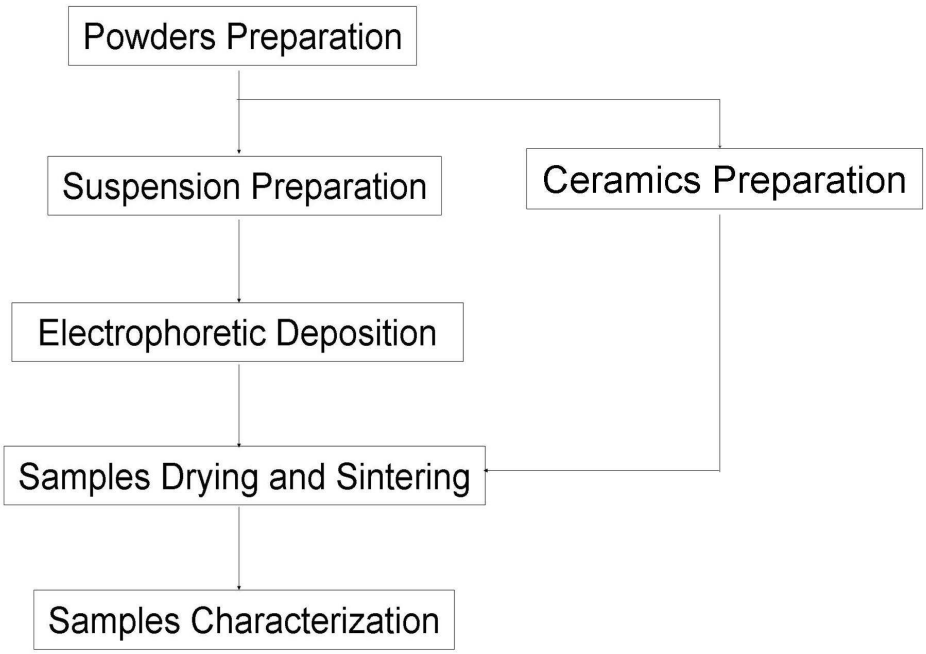

Figure 4-1 Flowchart of the experimental procedure carried out in this work

The experimental work carried out in this work is schematically represented in the flowchart of Figure 4-1. The first experimental conducted step was the preparation of $BaNd_2Ti_5O_{14}$ powders to be used in the fabrication of the films and two types of powders were used: commercial BNT powders [MBRT-90M(B), Fuji Titanium Industry Co., Ltd] and “home made” BNT powders, synthesised by conventional solid state method. Both powders were characterised in terms of their chemical composition,

structure, morphology and rheological behaviour. The next step was the preparation of the suspensions to be used in the deposition. As clearly indicated in the introduction of this work, a great part of the success in preparing EPD films depends on the quality of the starting suspension. Systematic studies were conducted to choose the right suspension media. The deposition of BNT thick films was then conducted by EPD in a home-made EPD set up and under different processing conditions. The films were dried and sintered under different conditions. For comparison BNT ceramics were prepared from the same powders and sintered under the same conditions of the thick films. Finally the structure, microstructure and electrical properties of the films and ceramics at RF and MW frequencies (for some of the samples) and at different temperatures were analysed.

4.2 Processing of the samples

4.2.1 Materials

1) BNT Powder:

a) Commercial BNT powders

$BaNd_2Ti_5O_{14}$ commercial powders (MBRT-90M(B), Fuji Titanium Industry Co., Ltd) were used in the fabrication of BNT films for the proof of concept of preparation of low loss dielectric thick films for high frequency applications by EPD, described in chapter 5.1. The product specification of these commercial powders indicates besides the main constituents, barium, neodymium and titanium, the presence of bismuth, which was also confirmed by our ICP analysis (Table 4-1). The particle size distribution is shown in Figure 4-2. The surface area determined by single point BET is 1.36 m^2/g. From the morphological point of view the particles are spherical (Figure 4-3) with an average diameter of 0.4 μm as determined by light scattering after a 12h of ball milling in ethanol. The X-ray diffraction pattern of these powders is depicted in Figure 4-4, which indicates that these powders are monophasic with the 1:1:5 stoichiometry ($BaNd_2Ti_5O_{14}$ (BNT115), JCPDS Card 33-0166).

Table 4-1 Composition analysis of commercial BNT powders by ICP

Elements	Ba % (m/m)	Nd % (m/m)	Ti % (m/m)	Bi % (m/m)	Pb % (m/m)
	11.1	10.8	52.7	2.42	<0.02

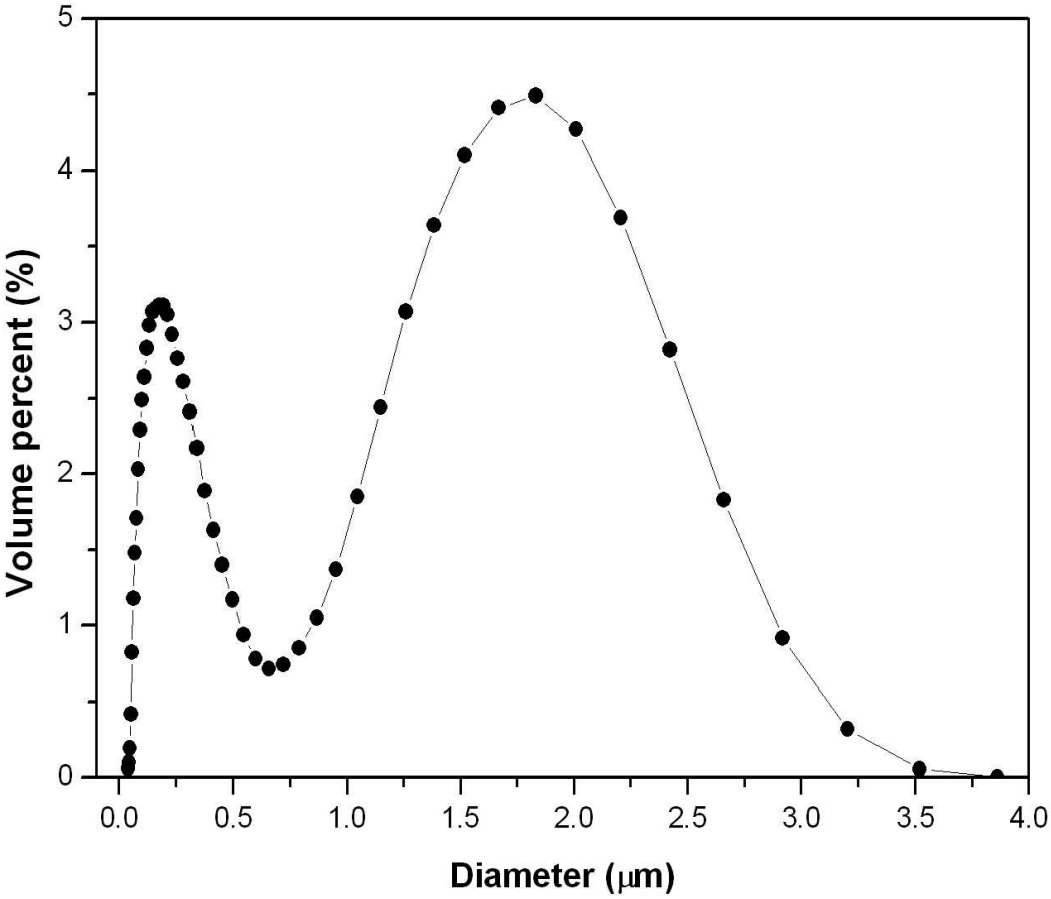

Figure 4-2 Particles size distribution of ball milled commercial BNT powders

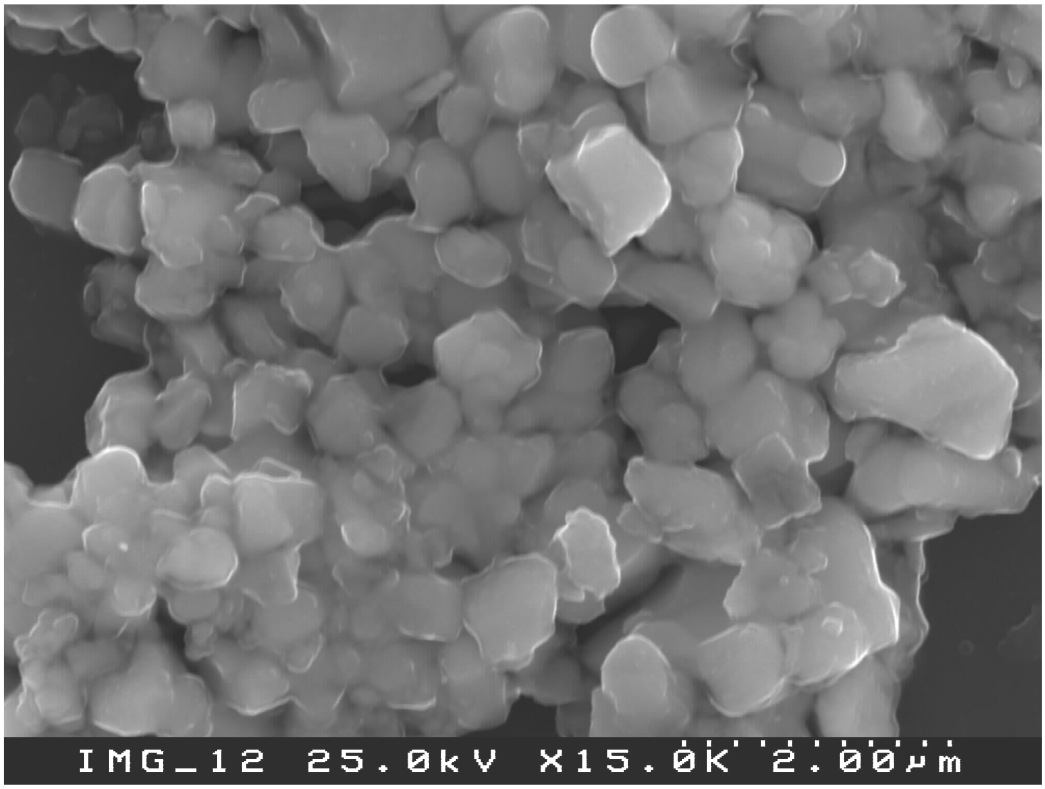

Figure 4-3 SEM micrograph of ball milled commercial BNT powder

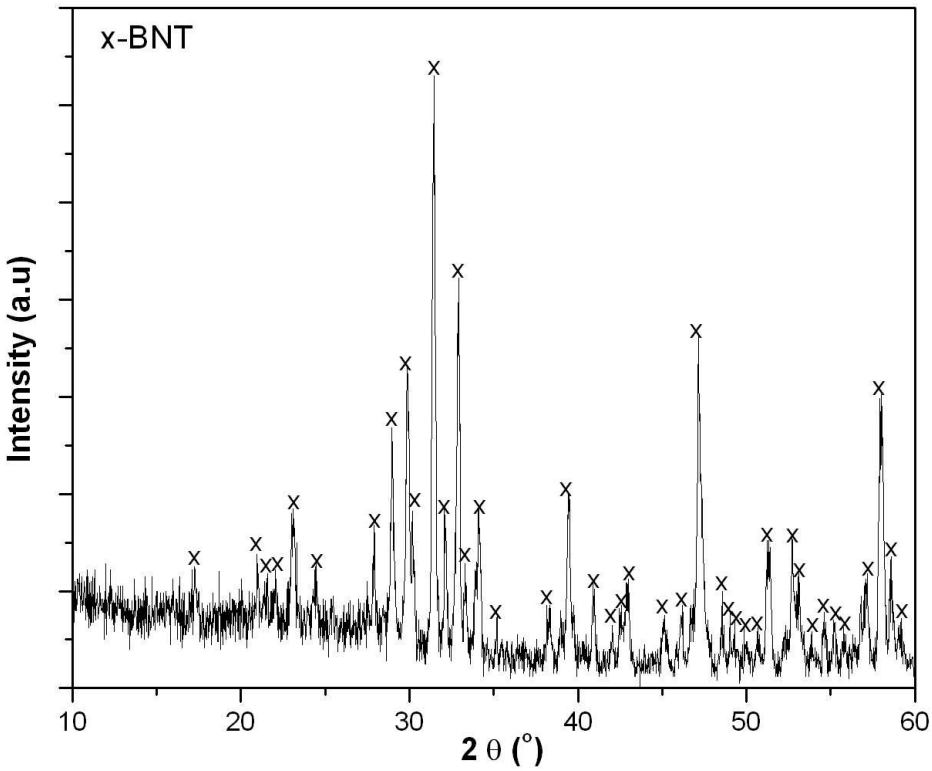

Figure 4-4 XRD pattern of commercial BNT powders

b) Home-made BNT powders

A solid-state reaction method was employed to synthesize $BaNd_2Ti_5O_{14}$ (BNT) powders. Reagent-grade powders of $BaCO_3$ (Aldrich, Product No.: 513-77-9, purity>99.9%), Nd_2O_3 (Aldrich, Product No.:1313-97-9, purity >99.9%) and TiO_2 (Aldrich, Product No.:1317-80-2, purity >99.9%) were mixed in the correct stoichiometry in ethanol. These materials were ball-mixed in Teflon pots with zirconia balls for 24 h on a planetary mill, and dried at 120 ºC/24h in air. Once dry, the powders were grounded by hand with a mortar and pestle, and closely packed in alumina crucibles, and then calcined in a programmable furnace equipped with an automatic temperature controller.

Differential Thermal Analysis (DTA) / Themogravimetry (TG) of the stoichiometric mixture of $BaCO_3$, Nd_2O_3 and TiO_2 were conducted with a heating rate of 5 ºC/min and a representative curve is shown in Figure 4-5. The reaction between the starting precursors and the BNT phase formation is completed before 1200 °C, so to ensure the synthesis of monophasic powders the calcination temperature of 1200 ºC was selected. Monophasic BNT powders were obtained after a calcination at 1200 ºC for 3 hours with a heating and cooling rate of 5 ºC /min, as depicted in the X-Ray diffraction of Figure 4-6.

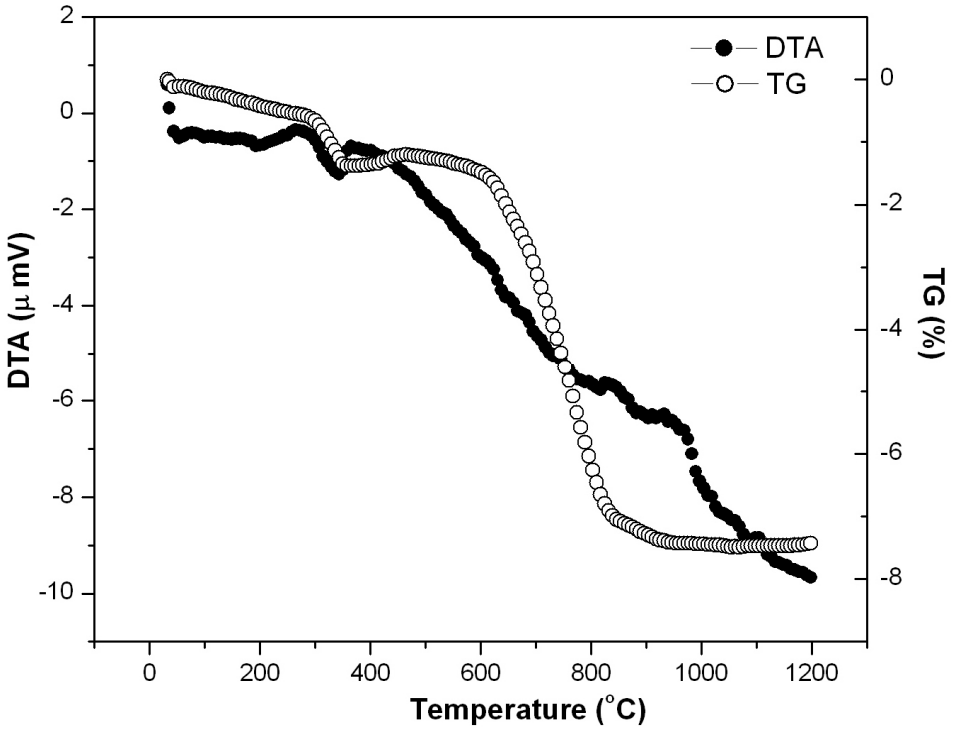

Figure 4-5 TG-DTA thermal curve of $BaCO_3$-Nd_2O_3-TiO_2 mixtures

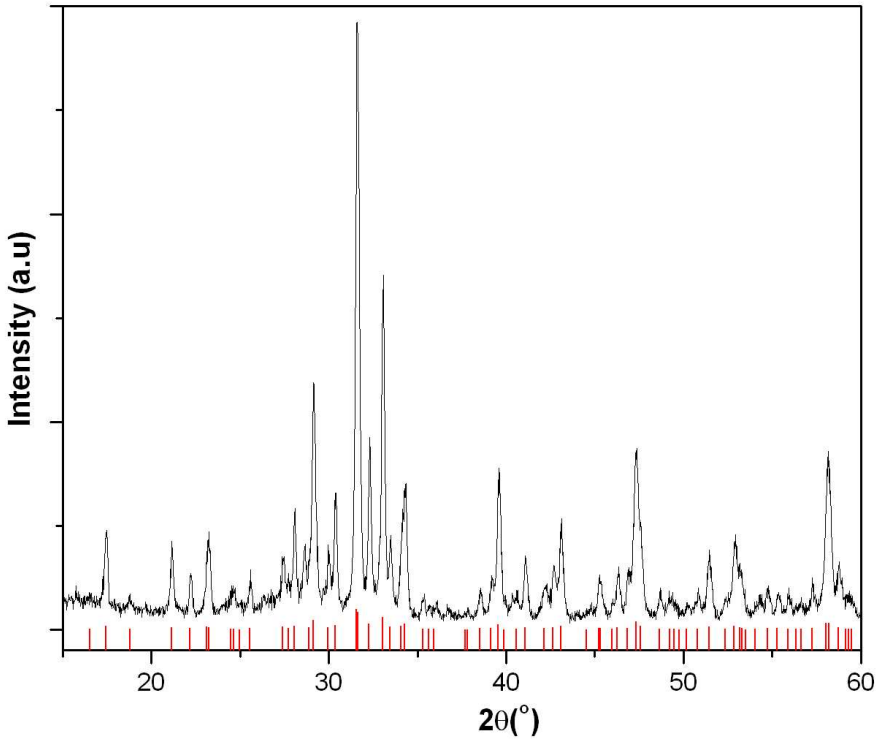

Figure 4-6 XRD pattern of home made BNT powders calcined at 1200 °C for 3h (the bottom red line corresponds the JSPDS file of $BaNd_2Ti_5O_{14}$ (BNT115), Ref.33-0166)

In order to get fine particles to optimise the suspension stability and sinterability of the green films, a ball milling step was further performed. The calcined powders were milled in alcohol on a planetary mill with zirconia balls for 2-24 hours. The particle size distribution after the ball milling was determined using a Particle Size Analyzer (Coulter LS 230). The diameter of average particle size was also determined from the mass specific surface area measurements (BET, Gemini 2370 V5.00). After a set of experiments 12h of milling time was selected. For milling times longer than 12h there is no appreciable decrease of the powders average particle size and high levels of agglomeration occurred, as determined by particle size distributions obtained by the Coulter measurements (Figure 4-7). The milled BNT powders were dried at 120 ºC for 24 h and kept in closed glass recipients to avoid surface reactions with air that could lead to the aging of the powders. The powders morphology was observed with a scanning electron microscope (SEM) Hitachi, S-4000 SEM / EDS. Figure 4-8 depicts the SEM micrographs of BNT home made powders after 12h of milling.

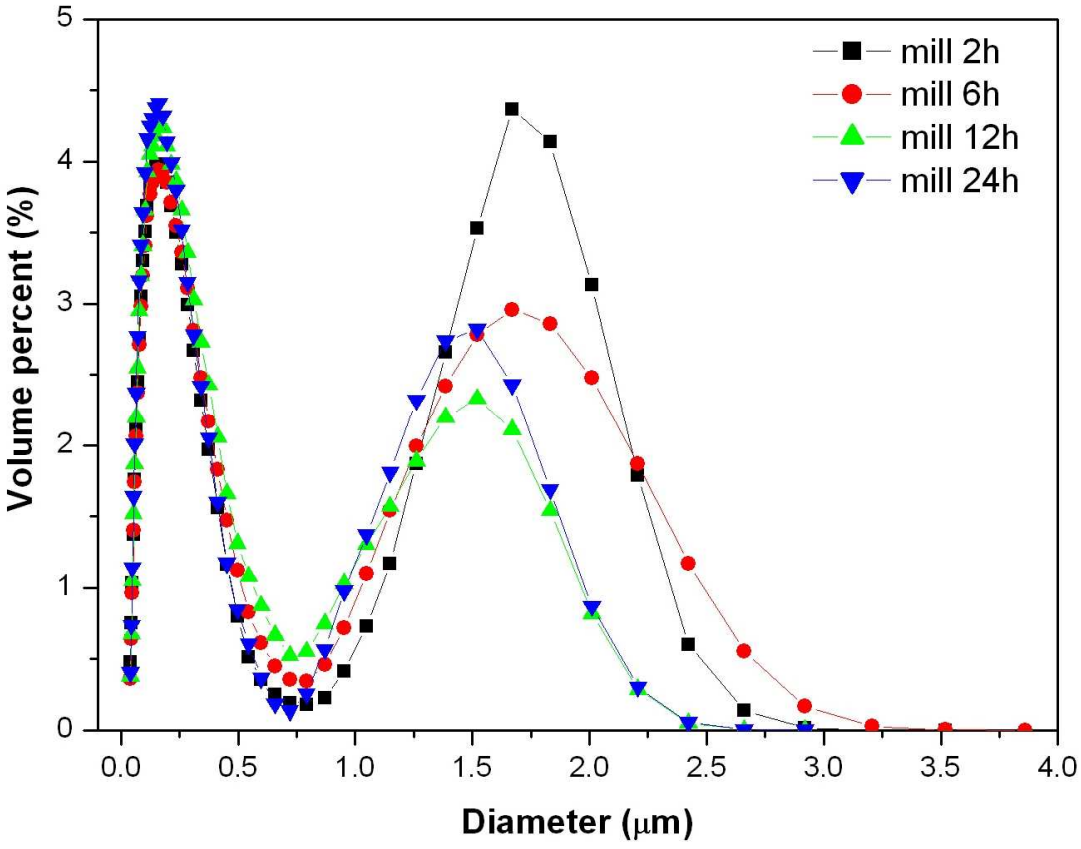

Figure 4-7 Particle size distribution of home made BNT powders as a function of milling time

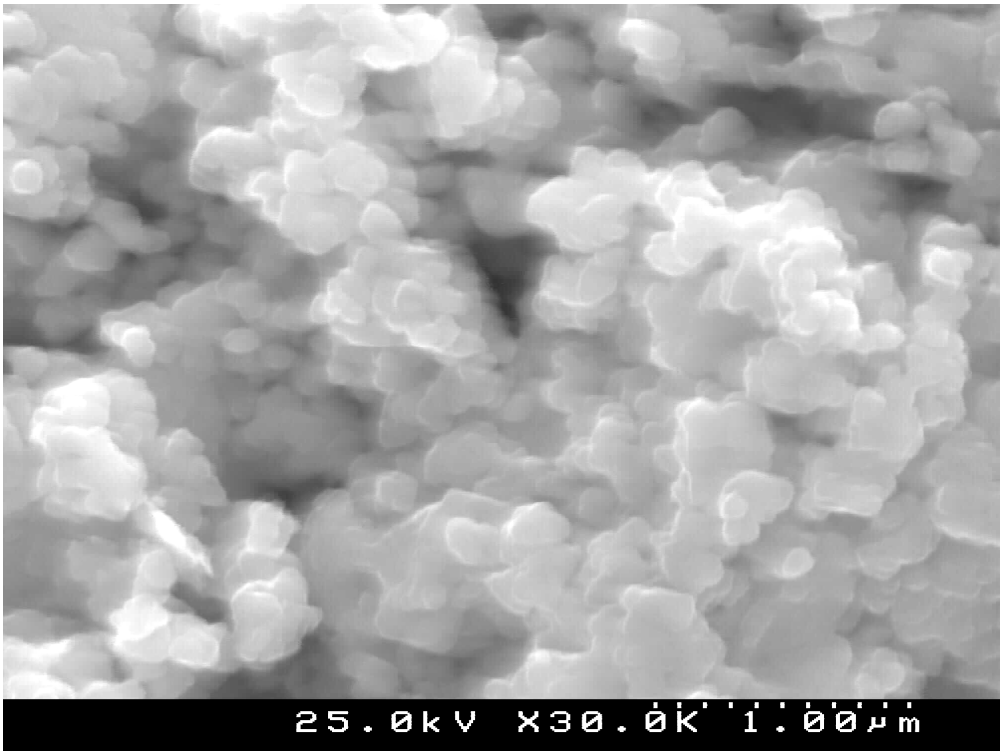

Figure 4-8 SEM micrograph of home made BNT powders
after 12h of milling

2) Suspension media

The preparation of stabilised BNT suspension for a successful deposition by EPD was tried in four different suspension media: de-ionized water, acetone (>99.9%, Merck), ethanol (>99.9%, Merck), and glacial acetic acid (>99.9%, Merck), respectively. For the case of acetone medium, I_2 (≥99.8%, Aldrich) dissolved in iso-propanol (>99.9%, Merck) was used as an additive to adjust the pH value of the BNT suspension. This iodine solution consisted of 0.92 g iso-propanol containing 0.5 wt % dissolved I_2. The stability of the suspensions was analysed by transmittance of the UV light, particles size distribution and zeta potential of suspensions.

3) Substrates and electrodes

Platinum foil (11 ×11 × 0.025 mm, 99.95%, Good fellow, UK) and polycrystalline Al_2O_3 substrates (25.4 × 25.4 × 0.0254 mm, 99.6%, Coors Ceramics Co. UK, with the remaining 0.4 wt. % assumed to be a silicate based sintering aid) were used as substrates for the preparation of BNT films.

The counter electrode was Pt as well.

As previously referred EPD requires two conducting electrodes (anode and cathode), so in order to use insulating substrates, such as Al_2O_3, it was necessary to

deposit a conducting layer on the substrate surface. In the current work, graphite layers were used for that purpose. The graphite layer acted as a temporary bottom electrode being burnt out high sintering temperatures without leaving any residual contaminations. A radio frequency (RF) magnetron sputtering (CRIOLAB, Portugal) was used to deposit the graphite layer. For that, a graphite target (purity>99.9%, Sofacel Inc., Spain) of 5.5 cm diameter disc with 3 mm thick was used. The graphite coatings were prepared at a substrate–magnetron distance of 120 mm under Ar pressure of 5.8 x 10^{-3} mbar, with a magnetron current of 0.3 A and substrate bias of 470 V. The thickness of graphite layer is controlled by the deposition time.

4) BST sol and powders

For preparation of BNT-BST composite thick films by EPD combined sol-gel process, $(Ba_{0.5}Sr_{0.5})TiO_3$ solutions are prepared by a sol-gel method. $Ba(CH_3COO)_2$ (Merck, 99%), $Sr(CH_3COO)_2 \cdot 1/2H_2O$ (ABCR, 98%), and $Ti(OC_4H_9)_4$ (Merck, >98%) are used as starting materials. Glacial acetic acid (CH_3COOH, Merck, >99.8%) and ethylene glycol ($HOCH_2CH_2OH$, Merck, >99.5%) are used as the solvent, and acetylacetone ($C_5H_8O_2$, Merck, >99.5%) as the stabilizer for Ti alkoxide. $Ba(CH_3COO)_2$ and $Sr(CH_3\text{-}COO)_2 \cdot 1/2H_2O$ powders with a molar ratio of 5:5 are dissolved in acetic acid and heated to 80 °C under constant stirring. $Ti(OC_4H_9)_4$ is stabilized with a mixture of ethylene glycol and acetylacetone. The stabilized $Ti(OC_4H_9)_4$ solution is mixed with $Ba(CH_3COO)_2/Sr(CH_3COO)_2$ solution with a molar ratio of 1:1 under constant stirring. After stirring for 2 h, the solution concentration is adjusted to 0.25 mol/l and stirred for 1 h more.

For comparison, BST thick films were also prepared on Pt foils by EPD. BST powders are obtained from the same sol used for the infiltration step. The dried sol was calcined at 1200 °C for 1h. The calcined BST powders were ball milled for EPD experiments and BST thick films were prepared under identical protocol as the one used for the fabrication of BNT thick films by EPD.

4.2.2 Suspension preparation and deposition

1) Suspension preparation

Suspensions of 10g / liter of BNT powders were prepared in 200 ml glass beakers. The BNT powders were slowly added into the solvent under constant stirring to promote the dispersion of powders in the suspension. A further dispersion of the suspension was conducted in ultrasonic bath for more 10 min.

Based on the colloidal chemistry analysis, namely the zeta potential curves, the pH of the suspension media is regulated in order to achieve the highest degree of dispersion and homogenization of the suspension.

2) Deposition device

As mentioned in chapter 2, in the EPD process, a DC electric field is applied to the suspension causing the electrophoretic motion of the charged particles towards the oppositely charged electrode.

Figure 4-9 illustrates the EPD set up used in this work. It is composed of the EPD cell, the ultrasonic bath and the power source. The EPD cell was home made and designed for the current work. The EPD cell itself includes three main parts: the base, the mask and the metal pole for conductive connection, as presented. The substrates, Pt foil or alumina, were placed in the mask chamber and pressed by the back screw. The two equal masks were mounted on the base, and the two steel poles provide the electrical connection to the external power source.

A DC power source (EPS, Stromversorgung Gmbh, Germany), ultrasonic bath (Branson, USA) and magnetic stirrer (Yellowline, IKA Werke GmbH & Co. KG Germany) were employed for the EPD experiments.

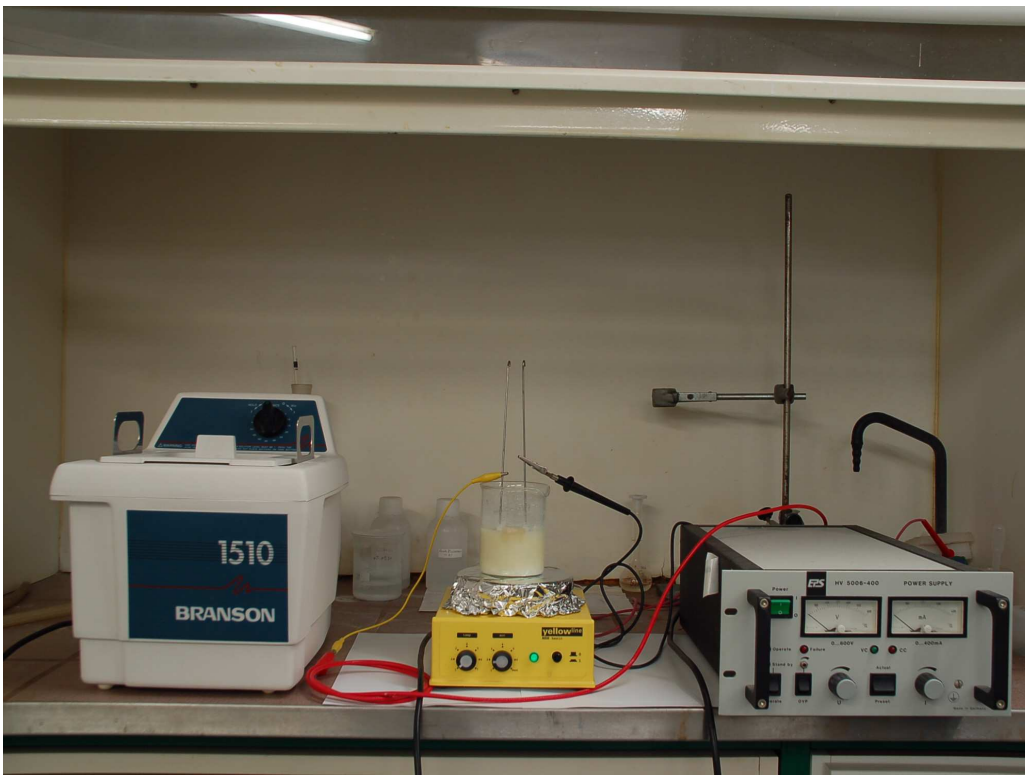

(a)

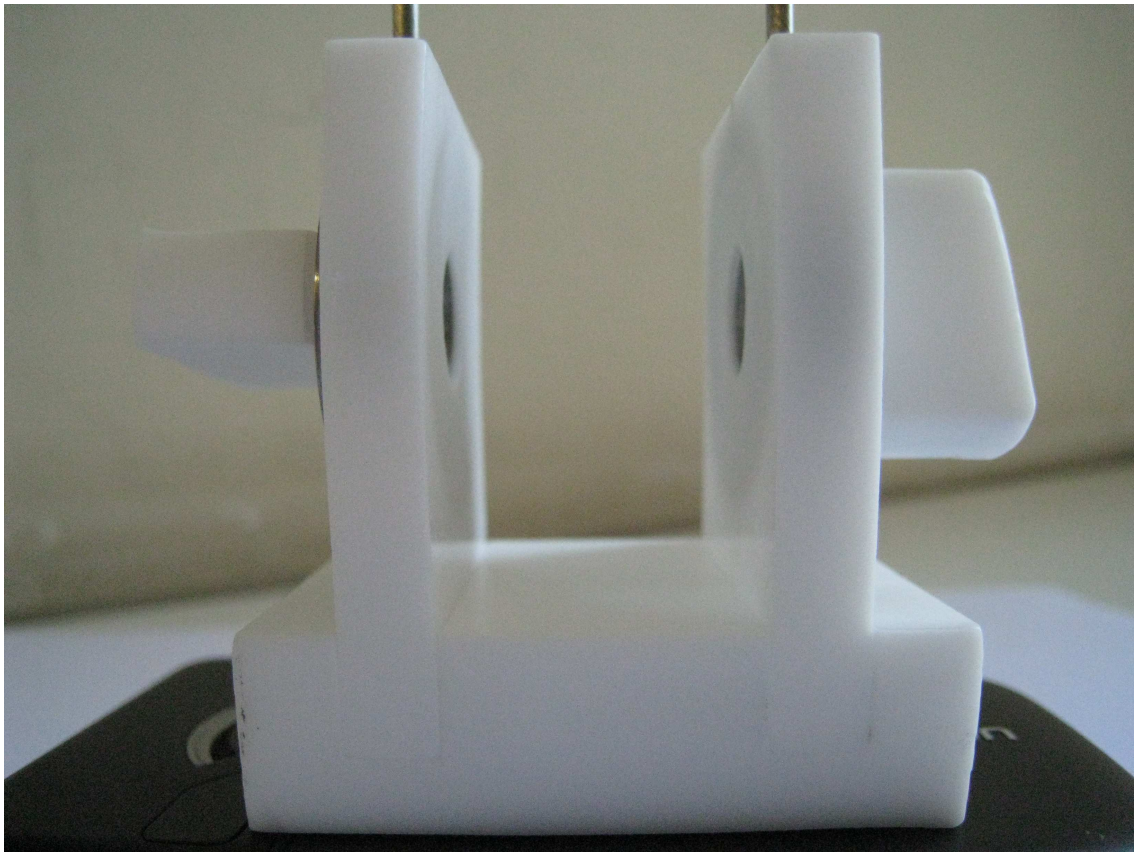

(b)

(c)

Figure 4-9 Representative images of the equipment (a) used in this work for the EPD process, of the EPD cell (b), and of the components of the EPD cell (c)

3) Deposition

For the deposition the EPD cell of Figure 4-9 was immersed in the suspension in a 200 ml glass beaker. The platinum foil as working electrode (cathode) was separated 2 cm from the Pt counter electrode (anode) in EPD cell.

Prior to each EPD cycle the suspensions were ultrasonically dispersed and magnetically stirred for 5 and 10 min, respectively, followed by settling for 5 min in order to sediment the coarse particles.

Constant voltage mode was used in the current work to deposit BNT films by EPD at various deposition times. The electric current through the EPD cell was monitored by a digital multimeter (MY-64, MASTECH, Hong Kong) located in series with the EPD circuit, during the EPD process.

4.2.3 Post deposition treatment

1) Drying and Cold Isostatic Press (CIP)

The as-deposited films were dried at 120˚C for 24 h in an oven. After that some of the green films were pressed under a cold isostatic pressure (CIP) of 200 MPa to enhance the green density of the films, using a Stansted (Fluid Power Ltd., England / Autoclave Engineer, Inc., USA)

2) Sintering

To determine the sintering temperature of the films, dilatometric analysis of BNT powders were conducted. Pellets of 5x5x7 mm were pressed and analysed in a computer assisted vertical dilatometer (Linseis, mod. 4 L70-2000) Figure 4-10 depicts the change in the length ($\Delta l/l_0$ x 100%, l_0 stands for the initial length and Δl for the variation of the length) with the temperature. After a small expansion the shrinkage of BNT powders is initiated slightly after 1000 ºC and continues steadily until 1350 ºC. Based on these results the interval between 1200 and 1450 °C was chosen for the sintering of BNT films. The as-prepared samples (BNT films and ceramics) were sintered in air at different temperatures to investigate the sinterability of the BNT films samples. The procedure adopted for the sintering step is as follows: heating at 5 ^{o} C/min from room temperature to the sintering temperature, and followed by a dwelling time (1h for BNT films and 3h for BNT ceramics), the samples are cooled in the furnace at 5 ^{o} C/min.

3) BNT ceramics fabrication

For comparison, corresponding BNT ceramics were prepared. The BNT powders were pressed with a steel die into green pellets of 1 cm of diameter and about 2 mm in thickness under a pressure of 20 MPa (Carver Laboratory Press, Fred S. Carver Inc., USA). The pellets were then isostatically pressed under 200

MPa and sinter under identical conditions to the ones above indicated for films.

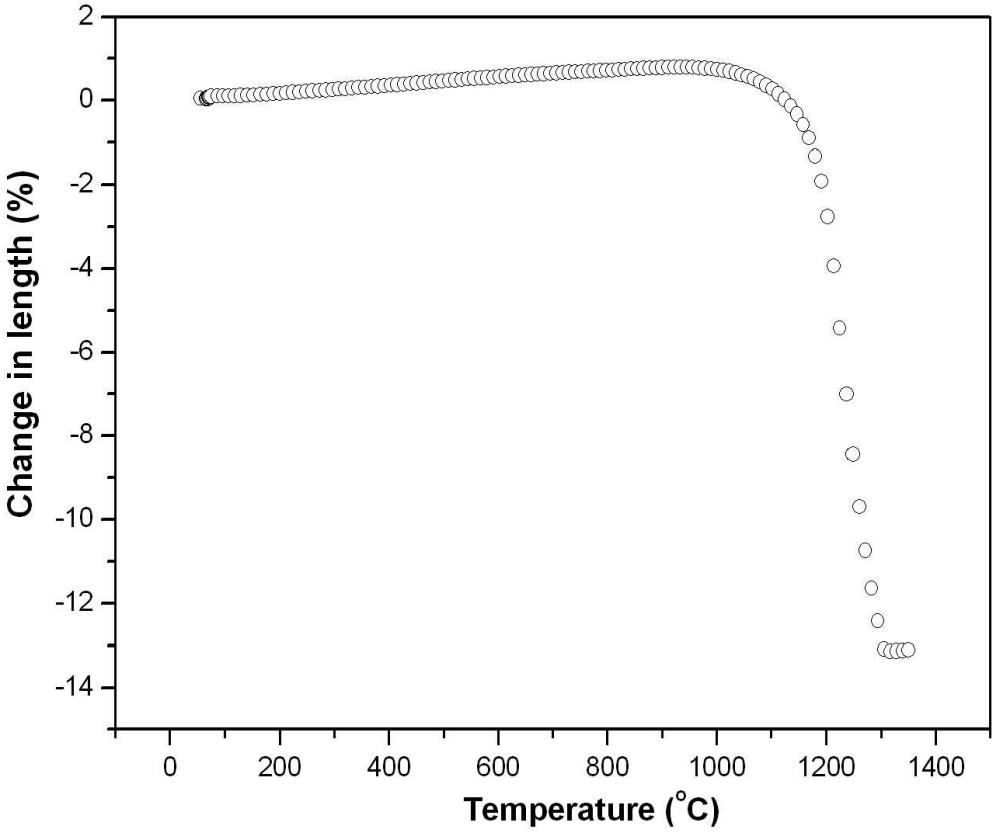

Figure 4-10 Dilatometric curve of BNT powders

4.3 Characterization techniques

4.3.1 Suspension analysis

4.3.1.1 Particle morphology

A laser particle size device (LS230, Beckman Coulter, Inc., USA) was used to determine the particle size and particle size distribution of as prepared BNT powders. Based on the effect of light scattering, this method enables the measurement of particles from 0.04 μm to 2000 μm without the risk of missing either the largest or the smallest particles in the sample. The analysis is conducted in suspension with concentrations of 1g per liter, previously ultrasonicated (Branson, USA) for 5 min before each measurement. The average particle size was also determined from mass specific surface area measurements (BET, Gemini 2370 V5.00), and from the morphology analysis of the powders by scanning electron microscope (SEM) Hitachi, S-4000 SEM / EDS.

Because LS230 equipment can only be used in water medium, a Malvern

Dynamic Light Scattering instrument (Zetasizer nano ZS, Malvern, UK) was employed to measure the distribution of particles size in the organic solvent, such as, (acetone, acetic acid and ethanol). Dynamic light scattering (DLS) is a non-invasive, well-established technique for measuring the size of particles typically in the submicron region from 0.4 nm to 6 μm. For this analysis a diluted suspension (10 mg BNT/100 ml solvent) was placed in the sample holder after 5 min ultrasonic dispersion (Branson, USA). A laser illuminates the sample in the cell, and most of the laser beam passes through the sample. A detector measures the scattered light and the scattering intensity signal at successive time intervals is compared, the rate at which the intensity is varying is derived and based on this information the particle size and particle size distribution is computed.

4.3.1.2 Zeta potential

Zeta potential, as defined as in chapter 2, is an abbreviation for electrokinetic potential in colloidal systems. In the colloidal chemistry literature, it is usually denoted using the Greek letter zeta, hence ζ-potential. From a theoretical viewpoint, zeta potential is the electric potential in the interfacial double layer (DL) at the location of the slipping plane versus a point in the bulk fluid away from the interface.[Hunter R. J. -1989]

Zeta potential is not directly measurable but it can be calculated using some theoretical models and the experimentally-determined dynamic electrophoretic mobility. In practice, the zeta potential of a dispersion is measured by applying an electric field across the dispersion. Under the electric field particles within the dispersion will migrate towards the electrode of the opposite charge with a velocity proportional to the magnitude of the zeta potential. This velocity is measured using the technique of the Laser Doppler Anemometer. The frequency shift or phase shift of an incident laser beam caused by these moving particles is measured as the particle mobility, and this mobility is converted to the zeta potential by inputting the dispersant viscosity, and the application of the Smoluchowski theory [Smoluchowski-1903]:

$$\mu=\zeta\varepsilon/\eta \tag{4-1}$$

where μ stands for the measured electrophoretic mobility, η for the viscosity of the solvent, ε for the permittivity of the solvent.

In this work, an electrophoretic light scattering (ELS) spectrophotometer (Delsa-440 SX, Beckman Coulter, Inc., USA) was used to determine the zeta potential of the BNT suspensions. To make a measurement, a sample is typically placed in a disposable plastic cuvette and platinum electrodes inserted. The entire cell is placed into the internal chamber of Delsa 440 SX. Since ELS requires the use of heterodyned light, the scattered light must be properly mixed with a reference beam (split off from the incident light beam) prior to entering the detector. The software will begin a measurement by automatically adjusting the incident light intensity to optimize the mixing between the scattered light and the reference beam.

4.3.1.3 Transmittance measurement of UV light

In order to evaluate the dispersibility of BNT suspensions, the transmittance measurement of UV light was conducted to reflect the dispersion degree of the BNT suspensions. Transmittance is the fraction of incident light at a specified wavelength that passes through a sample and is given as a percentage. Well dispersed suspension show low percentage of transmittance. In this work, UV Spectrophotometer (UV-2101/3101PC, Shimadzu scientific instruments. Inc, USA) was employed to determine the transmittance and evaluate the dispersibility of BNT suspension.

4.3.1.4 ICP-AES analysis

In order to analyze the chemical composition of BNT powders and suspensions, namely the concentration metallic elements in the suspension supernatant, inductively coupled plasma atomic emission spectrometry (ICP-AES, ISA Ins., Germany) was used. ICP-AES is an analytical technique used for the detection of trace metals that uses the inductively coupled plasma to produce excited atoms and ions that emit electromagnetic radiation at wavelengths characteristic of a particular element. The intensity of this emission is indicative of the concentration of the element within the sample. [Stefánsson A.-2007, Mermet J. M.-2005]

4.3.2 Structure and microstructure characterisation

4.3.2.1 XRD

The phase assemblage of calcined powders and sintered samples is examined by powder X-ray diffraction (XRD) technique. Because the wavelength

of X-rays (from few angstroms to 0.1 angstrom) is comparable to the size of atoms, they are ideally suited for probing the structural arrangement of atoms and molecules in a wide range of materials. A monochromatic X-ray beam with a wavelength λ incident onto a crystalline material at an angle θ leads to diffraction when the distance travelled by the rays reflected from successive planes differs by a complete number k of wavelengths. By varying the angle θ, the Bragg's law conditions are satisfied for different d-spacings in polycrystalline materials.[Jenkins R.-1996] according to the equation[Bragg W.L.-1913]:

$$2d\sin\theta = k\lambda \qquad (4\text{-}2)$$

In the current work the X-ray diffraction analysis of BNT powders, films and ceramics was carried out with a Rigaku (D/Max-C series) X-ray diffactometer, using Cu-Kα radiation (λ=0.15064 nm). The XRD was typically operated at 50 kV and 30 mA. θ-2θ scans at rate of 1 ^{o}/min with step 0.02 between 4-80^{o} were adopted in the current experiments. The degree of orientation of BNT films was characterized using XRD rocking curves and pole figures aquired with a Philips XPert MRD diffractometer. X-ray rocking curves were obtained by tilting the BNT films through the Bragg angle of the selected plane. The X-ray pole figure measurements were performed, using a Cu Kα X-ray source with a crossed slit incident optic and open receiving slit of 1 mm before the proportional detector. The samples were rotated 180° about the cp axis (azimuthal rotation) and 90° about the yr axis (tilt). In the pole figure measurements the diffracted intensity was collected at a step of 5° in the tilted and rotated angles in the whole hemisphere, at a fixed θ-2θ angle of the open detector, that corresponds to the selected reflections of BNT thick films, while the specimen is tilted and azimuthally rotated in relation to the incident beam. Partial pole figures were plotted. [Kocks U. F.-1998]

4.3.2.2 SEM

The microstructures of fractured and / or polished and thermally etched sections of the films were studied with scanning electron microscopy couple with energy dispersive spectroscopy (SEM / EDS).

In SEM, an electron beam source emits electrons which are then collected and focused by lenses to form few nanometres sized probes. Deflection coils are used to

operate the electron beam and to scan the sample surface. Simultaneously, another electron beam runs over a TV monitor screen in a synchronized mode. The image magnification is the ratio of the scanned monitor range to the scanned sample range, and it is easily controllable by beam deviation elements. Primary electron beam interacts with the specimen surface in a complicated manner resulting in different emitted signals (secondary and back scattered electrons, X-ray radiation, etc.), which could be registered with the appropriate detector. [Goldstein J. I.-1992]

In the current work, film thickness, surface and cross section morphologies and the microstructure in general of BNT films were analyzed by a Hitachi S-4100 SEM coupled with energy dispersive spectroscopy (EDS) [Hitachi, Japan]. Film specimens were mounted on aluminium stubs using carbon glue. Carbon paint was applied to the specimen to provide a conductive path to the stub, and an evaporated carbon surface coating was deposited to prevent sample charging inside the microscope. These samples were investigated using an operation voltage of 25 kV.

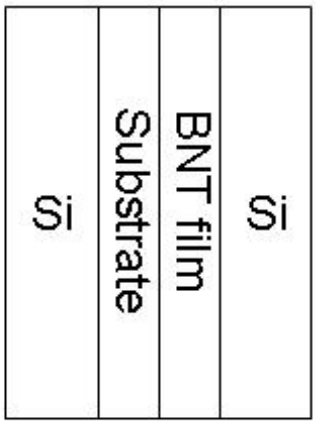

Figure 4-11 Schematic representation of the cross structure
for SEM samples preparation

The polished and etched sections of sintered samples and films were prepared according to the following steps. Films and small pieces of samples were firstly inserted in resin and, after a coarse polishing with silicon carbide paper, the surfaces were polished using a sequence of fine diamond pastes (15 μm, 6 μm, 3 μm, 1 μm and 0.25 μm). The polished samples removed from the resin were thermally etched at temperatures 80 ºC below the corresponding sintering temperature for 5 min. For the cross section preparation, a sandwich structure of samples on Pt foil was constructed

(Figure 4-11). The flexible BNT films were supported by gluing a rigid silicon slide on both sides of the BNT films. After the polishing, using the same procedure described above, an acid mixture of (10% HF + 37% HCl, 50:50 vol%) was used to chemically etch the polish cross sections. Finally, the as-etched samples were cleaned by ultrasonication in acetone.

4.3.2.3 TEM

The analysis of the interfaces between BNT films and the substrates was carried out on sintered films by transmission electron microscopy / energy dispersive spectroscopy (TEM / EDS).

In a TEM setup, a thin specimen is illuminated with electrons (the primary electrons). Whatever part is transmitted is projected onto a phosphor screen for the user to see. The darker areas of the image represent those areas of the sample, where fewer electrons were transmitted through (they are thicker or denser). The lighter areas of the image represent those areas of the sample that more electrons are transmitted through (they are thinner or less dense). An image in TEM can be formed by using the central spot of unscattered electrons, or by some or all of the scattered electrons. The type of the electrons is chosen by an insertion of aperture into the back focal plane of the objective lens, thus blocking out most of the diffraction pattern except that which is visible through the aperture. If the direct beam is selected, the resultant image is called a bright-field image, and if scattered electrons of any form are selected, a dark-field image is formed. If no aperture is inserted, electron diffraction pattern is observed. [Williams D. B.-1996]

In the current work, BNT film / substrate interfaces were analyzed by a Hitachi, Model H9000-NA, TEM equipped with an energy dispersive X-ray (EDS) detector.

The cross section of film samples were prepared in the following way: to protect the ceramic layer, two pieces of sample were glued face to face using an epoxy resin (M-band 610 glue) and under applied pressure to ensure that the amount of glue is as reduced as possible. The glue was cured at 100 ºC for 2 hours. The sample stacks were mechanically polished on both sides down to a thickness of around 15 µm using SiC grinding papers. Extra mechanical support is provided by a copper grid of 3 mm diameter and 50 µm thickness, glued onto the sample. The thin samples were then removed from the glass on a hot plane. The remaining epoxy is dissolved in acetone. A Gatan Duo ion Mill [Gatan, Inc, USA] was then used to thin the sample to electron

transparency at a low angle of 15° and a gun voltage of 6 kV.

4.3.3 Electrical measurements

4.3.3.1 Low frequency measurements

The complex permittivity at RF frequency was measured as a function of temperature and frequency in the capacitive cell illustrated in Figure 4-12.

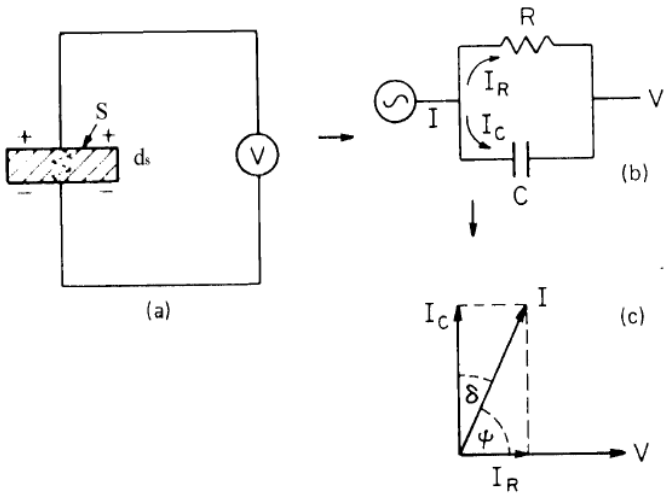

Figure 4-12 Equivalent circuit diagrams of capacitive cell (a) of charging and loss current (b) and of loss tangent for a typical dielectric (c) (after Buchanan-1991)

For the case of sinusoidal applied voltage V, the current discharge flow I of the capacitive cell may be written as:

$$I = i\omega\varepsilon^{*}V\varepsilon_0 S/ds = i\omega(\varepsilon^{'}-i\varepsilon^{''})V\varepsilon_0 S/ds = I_C + I_R \qquad (4\text{-}3)$$

where i stands for the imaginary operator, $\omega = 2\pi f$ for the angular frequency, ε_0 for the relative permittivity of the vacuum with the value 8.85×10^{-12} F/m, S for the area of the electrodes for a sample capacitor, ds for the distance between electrodes or sample thickness, ε^* for the complex permittivity, ε' for the real part of the permittivity, and ε'' is the imaginary part of the permittivity, related to dielectric loss. The dielectric loss existing in a dielectric material can then be represented by the analogue circuit of a resistance in parallel with a capacitor, and being I_C and I_R of the vector components the current of the I_C and I_R, as illustrated in Figure 4-9 (b, c). The I_C current represents a

capacitive current proportional to the charge stored in the capacitor. It is frequency dependent. The current I_R is an ac conduction current in phase with the voltage V, which represents the energy loss or power dissipated in the dielectric. From the ratio of the magnitude of I_R to magnitude of I_C, one can define a dissipation factor $\tan\delta = \varepsilon''/\varepsilon'$ [Buchanan R. C.-1991]

In this work, the electrical measurements at RF frequency were conducted via a metal-insulator-metal (MIM) configuration using Au as the top electrode for both films and ceramics. For the case of films, Au top circular electrodes were sputtered using a shadow mask of 0.6 mm diameter. BNT films with top electrode were post-annealed at 200 ºC for 30 min to improve the interface between the metal and the films. The ceramics were polished until 0.8 mm thickness, and top and bottom Au electrodes of 6 mm diameter were sputtered. The electrical properties were evaluated using an impedance bridge (HP 4284A, Agilent, USA) over a frequency range of 1 kHz to 1 MHz. The oscillation level of the applied voltage was set to 1.0 V. The analysed electrical properties include the relative permittivity, loss tangent, temperature dependence of relative permittivity ($\Delta\varepsilon_r/\varepsilon_{r0}\Delta T$,) and relative permittivity-voltage variation (ε_r-V).

4.3.3.2 Microwave frequency measurements

The microwave methods of measuring the dielectric properties can be divided into two main categories [Krupka J.-2001]:

i) Transmission-Reflection methods

ii) Resonance methods

Transmission reflection techniques have swept frequency capability, which allow for measurement over the range of the network analyzer (1 MHz to 26 GHz). This methods offer swept measurement at “any” point in the frequency range over which they operate. A wide range of dielectric constant values can be measured; however, dielectric loss values are limited to $\tan\delta > 0.01$. On the other hand, resonant cavity techniques are generally limited to a single frequency measurement which is defined by the cavity dimensions. Low loss samples of ($\tan\delta < 0.01$) range can be easily measured by resonant techniques.

For the BNT films on Pt foil substrates prepared in this work, the analysis of microwave dielectric properties was performed by transmission-reflection technique. The microwave transmission coefficients were determined with a

network analyzer (HP 8720D, Agilent, USA) using two separated Au contacts on the top BNT film for the rf input and rf output, respectively. The measurement resembles a rf line with two BNT capacitors in series. Modifications of the losses will affect the transmission and reflection signal. This measurement was conducted in the Division of Superconductivity and High Frequency Sensors, of the Institute of Thin-films and Interfaces, Forschungszentrum Jülich GmbH, Germany, with in the group of Dr. Roger Wordenberger.

For the BNT films on Al_2O_3 substrate, the split post resonance cavity technique, one of the resonance methods for microwave measurements, was employed to characterize the microwave properties. The split-post dielectric resonator (SPDR) has been shown to be a useful, accurate and convenient tool for complex permittivity measurements of various dielectric materials. It offers accurate measurements with quantifiable uncertainties for wide ranges of permittivity and loss values in the frequency range of 1-30 GHz. The method is especially useful for measurements of flat laminar specimens without any need for machining of their shape, as shown in Figure 4-13. Besides the SPDR fixture, a vector network analyzer and software package are required for the measurements. These measurements were conducted at the Department of Materials, Imperial College London, UK, within the group of Prof. Neil Alford.

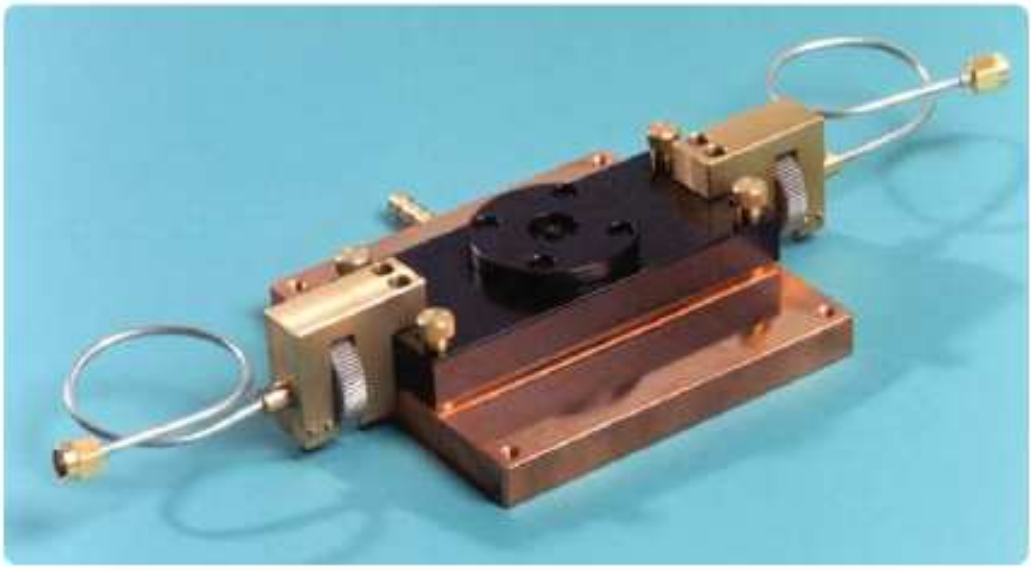

Figure 4-13 Photograph of split post cavity resonator
(after Agilent product information)

4.4 Reference

1. Agilent product information, www.agilent.com/find/materials
2. Bragg W. L., (1913) Proceedings of the Cambridge Philosophical Society, **17**, 43
3. Buchanan R.C. (1991) Ceramic Materials for Electronics - Processing, Properties and Applications, Marcel Dekker, New York
4. Goldstein J. I. (1992) Scanning electron microscopy and X-ray microanalysis, Plenum, New York
5. Hunter, R. J. (1989) Foundations of Colloid Science, Oxford University Press
6. Jenkins R. and Snyder R. L. (1996) Introduction to X-ray Powder Diffractometry, John Wiley and Sons, New York
7. Kocks U. F., Tomé C. and Wenk H. R. (1998) Texture and Anisotropy, Cambridge University Press, Cambridge, UK
8. Krupka J., Gregory A. P., Rochard O.C., Clarke R. N., Riddle B. and Baker J. J. (2001) J. Euro.Ceram.Soc. **10**, 2673
9. Mermet J. M. (2005) J. Anal. At. Spectrom. **20**, 11
10. Smoluchowski M. V. (1903) Bull. Int. Acad. Sci. Cracovie, **184**
11. Stefánsson A., Gunnar son I., Giroud N. (2007) Anal. Chim. Acta **582**, 69
12. Williams D.B. and Carter C.B. (1996) Transmission electron microscopy: a textbook for materials science, Vol. 1: Basics, Plenum, New York

Chapter 5
Thick Films of $BaNd_2Ti_5O_{14}$ on Pt Foils

5.1 Development of Low Loss $BaNd_2Ti_5O_{14}$ Dielectric Thick Films by EPD technique: Proof of Concept

Abstract:

The technological feasibility of applying electrophoretic deposition (EPD) for low dielectric loss thick-film materials is studied in this chapter. 12 to 52 μm thick BNT films were fabricated on platinum metallic foils by EPD. To improve the microstructure and density of the films a post deposition, cold isostatic pressing step, was used. The effect of film thickness on the dielectric properties at low frequency is investigated. As the film thickness increases, the dielectric properties of BNT films approach those of BNT ceramics in terms of relative permittivity and loss tangent. 52 μm-thick BNT films sintered at 1300 °C for 1 h exhibit a relative permittivity and a loss tangent of 107 and 0.0006 (or Q of 1600) at 1 MHz, respectively. The variation in relative permittivity is less than 0.02 % at a bias voltage 8 kV/cm. The change of relative permittivity with the temperature within the range 30-120 °C is below +58.5 ppm/°C, indicating a good thermal stability. Microwave measurements indicate that the dielectric losses of a 52 μm thick BNT films do not show a remarkable degradation till up to 1.4 GHz, compared to at 1 MHz. The high relative permittivity, high Q (low loss tangent), and good bias and temperature stability make EPD derived BNT thick films on metallic foils attractive candidates for new microwave communication devices.

5.1.1 Introduction

As described before, among low loss dielectrics, the $BaO\text{-}Nd_2O_3\text{-}TiO_2$ system represents an important commercial family of microwave materials. Although BNT ceramics are currently being produced for resonators, antennas and substrates, as shown in Figure 5-1, the use of BNT thick films have not yet been reported. Moreover, the miniaturization and reduced cost is a major trend in the communications industry, and because of that electronic device designers are now considering the dielectrics processed as thick films to take the place of components currently utilized in bulk

ceramic form or even for new device applications.

On the other hand the fabrication of dielectric films on metal foils is presently of interest for devices integrated into electronic packaging due to cost and space benefits. [Borland W-2001] For example, as shown in Figure 5-1 (b), the current microstrip patch antenna usually requires the metallization of a ground plane on one side of the dielectric materials by screen printing. However, this metallization process can be avoided by directly depositing the dielectric layer on a metallic substrate. In this case, for the reasons above described and in particular the possibility of being scaled up, EPD looks like very appealing for this purpose. It is then very opportune and scientifically and technically especially interesting to prove the adequacy of the use of EPD to fabricate low loss BNT thick films on metal foils.

(a)

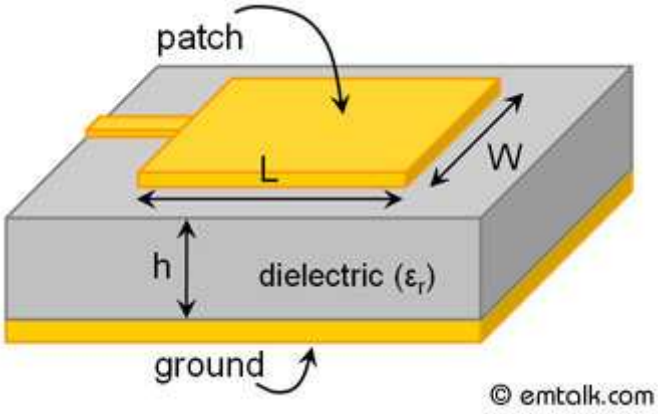

(b)

Figure 5.1-1 Photographs of commercially available microwave resonators and substrates (after Morgan Technical Ceramics Ltd) (a) and schematic representation of a microstrip patch antenna (b) (ww.emtalk.com)

In this chapter, the use of EPD on the preparation of BNT thick films for high frequency application is exploited. Commercial BNT powders were used to prepare the BNT films on Pt foils. The feasibility of using EPD technique to produce low loss BNT dielectric thick film is proved and discussed in this chapter.

5.1.2 Experimental

For this study BNT thick films were fabricated according to the process described in Chapter 4 and using the commercial BNT (1:1:5) powders (MBRT-90M(B), Fuji Titanium Industry Co., Ltd). The powders were previously milled for 12h in ethanol until an average particle size of around 0.4 μm was reached. For this particular study 12 to 52 μm-thick BNT films were deposited under 40V to 600V for 30s to 10min using the acetic acid based suspension. The as-deposited films were dried at 90˚C for 24h. Some of the green films were pressed under a cold isostatic pressure of 200 MPa to enhance the green density. At the same time BNT ceramics were prepared. For that BNT powders (the same used for films preparation) were pressed under a uniaxial pressure of 20 MPa followed by a cold isostatic pressure of 200 MPa. The films were then sintered in air at 1300 ˚C for 1 h, and the pressed disks at 1300 ºC for 3h.

5.1.3 Results and Discussions

As reviewed in chapter 2, the preparation of films by EPD comprises the preparation of a stable suspension of the powders of the starting material in appropriate suspension media system and the formation of a deposit onto the counter electrode by the movement of the charged particles under the influence of an electric field. The process parameters such as deposition time, applied voltage and suspension ageing, among others, have an important influence on the deposition efficiency and quality. [Corni I.-2008] The effects of these factors on the EPD of BNT films were studied and are reported as follows.

Deposition thickness of BNT films on platinum substrate as a function of deposition time is shown in Figure 5.1-2. The relationship between EPD thicknesses of BNT deposited films and deposition time is almost linear, and the thickness of deposited material increases with time, which is in accordance with the Hamaker equation at constant applied voltage. (Eq. 2-4) [Hamarker-1940] The relation between the thickness and deposition time for EPD derived BNT films will be discussed in detail in the chapter 5.2. According to it the thickness of the deposit can be predicted and precisely

controlled.

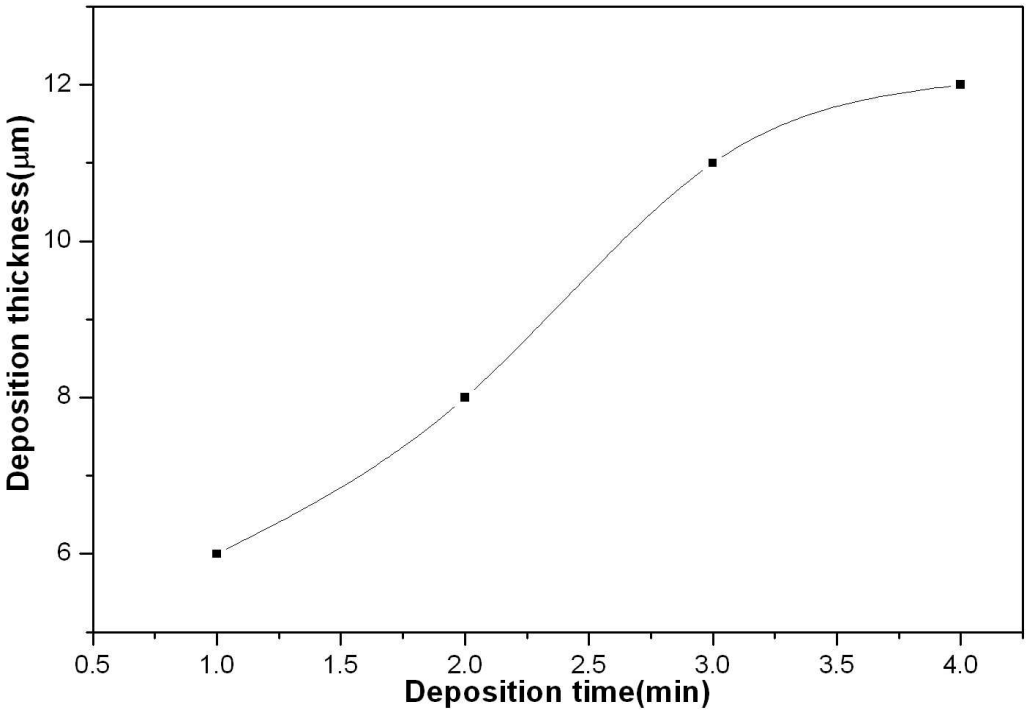

Figure 5.1-2 Deposition thickness of BNT films against deposition time for the suspension of BNT commercial powders in acetic acid and for an applied voltage of 200 V

Figure 5.1-3 depicts the effect of the applied voltage on the deposition weight of BNT films. The deposition weight is calculated by the difference of the substrate weight before and after coating. Under a constant deposition time of 1 min, the deposition weight increased till 800 V, and then decreased as further up to 1000 V. Under high electric fields charged particles will have an elevated velocity, so per unit of deposition time, more particles can be deposited on the substrate. In the meantime, for very high electric fields, the high mobility of the particles, the presence of flow currents together with the formation of bubbles that are facilitated under these conditions, the deposition becomes inhomogeneous, the edges irregular and the porosity of the films increases with a decrease of the film density. As a consequence, the deposition weight decreased after a critical applied voltage. This is a common effect, observed for many other systems, being the electric field threshold different depending on the system. [Basu R. N.-2001, Negishi H-2002]

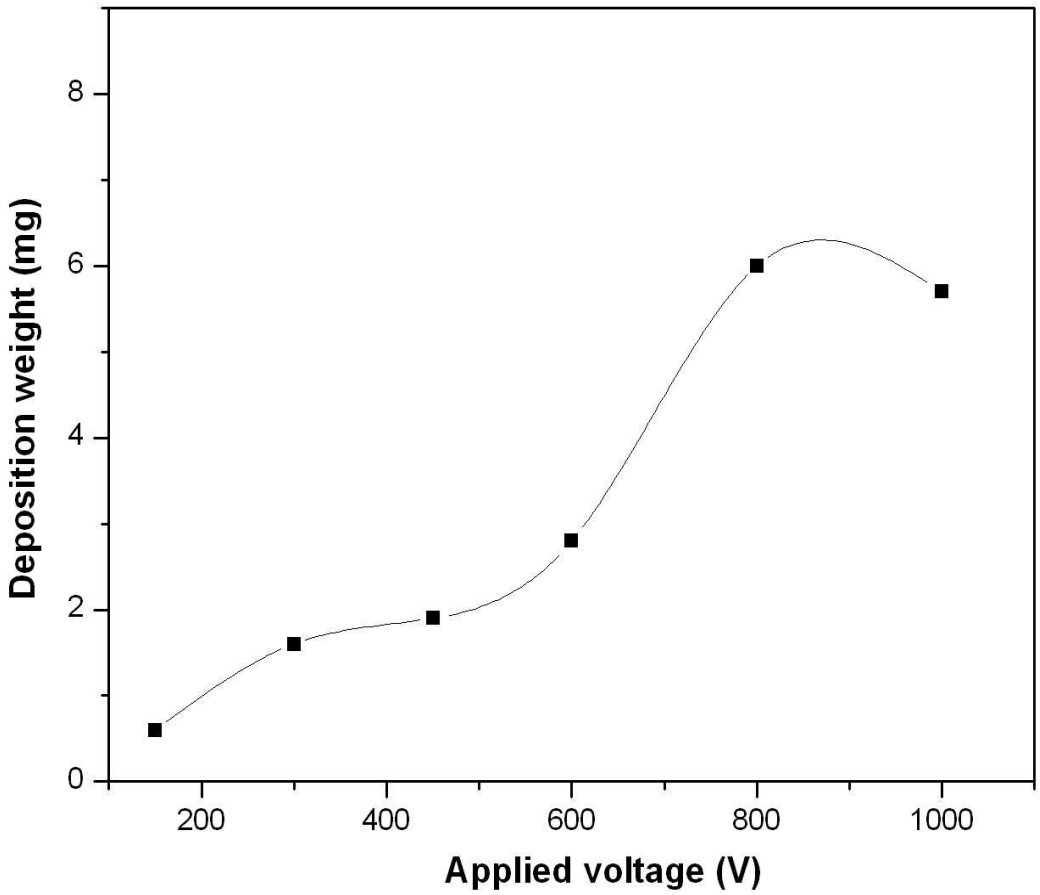

Figure 5.1-3 Deposition weight of BNT films against the applied voltage for the suspension of BNT commercial powders in acetic acid and for a deposition time of 1 min

For EPD process it is desirable that the suspension is stable for a long period of time to guarantee the reproducibility of the depositions. A long time stable suspension is of a crucial significance for an industrial EPD process. As illustrated in Figure 5.1-4, the variation of the deposition weight slightly increases until 24 hours as the suspension ages, declining after, which indicates that commercial BNT can be effectively stable for 24 hours in glacial acetic acid. There are several factors that can contribute to the observed variation of the deposition yield with the aging time, namely the change of the suspension electric nature and of the charge state of the particles in the suspension. Similar effects were reported for PZT thick films prepared in glacial acetic [Wu A. Y. - 2006] and attributed to the formation of water in the suspension and leaching of PZT powders. Further studies were conducted to clarify these dependences on BNT systems and will be presented in chapter 5.2.

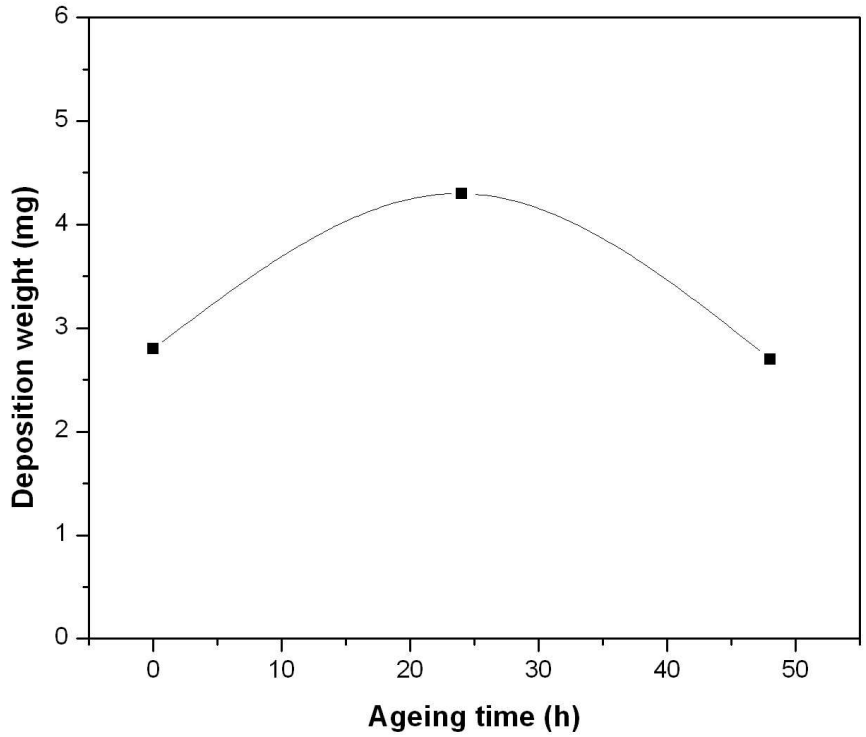

Figure 5.1-4 Deposition weight of BNT films against suspension ageing for the suspension of BNT commercial powders in acetic acid and for deposition conditions of 600 V for 1min

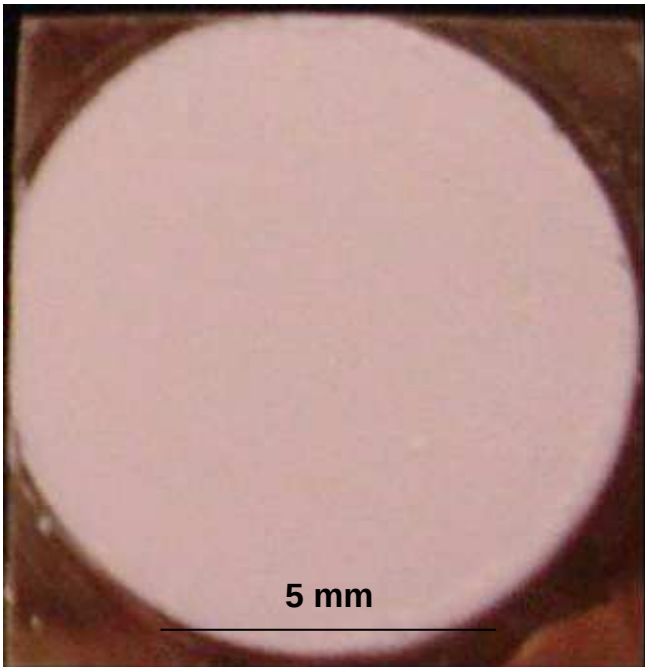

Figure 5.1-5 Optical micrograph of green BNT films deposited from the suspension of BNT commercial powders in acetic acid and under the deposition conditions of 200 V for 1min

Figure 5.1-5 depicts the optical micrograph of as deposited BNT film. A very homogeneous, crack-free, uniform and conformal deposition was achieved in the green films by EPD.

After deposition and sintering, the structure of BNT thick films was analysed by XRD. Figure 5.1-6 depicts the XRD patterns of BNT thick films and BNT bulk ceramics sintered at 1300°C for 1 and 3 h, respectively. Films and ceramics exhibit a well-crystallized phase that corresponds to the orthorhombic structure of $BaNd_2Ti_5O_{14}$ (JCPDS #33-0166) with no evidence of preferred orientation or secondary phases for both of them. The XRD results demonstrated that no detectable alteration of the materials composition occurred for BNT thick films and bulk ceramics.

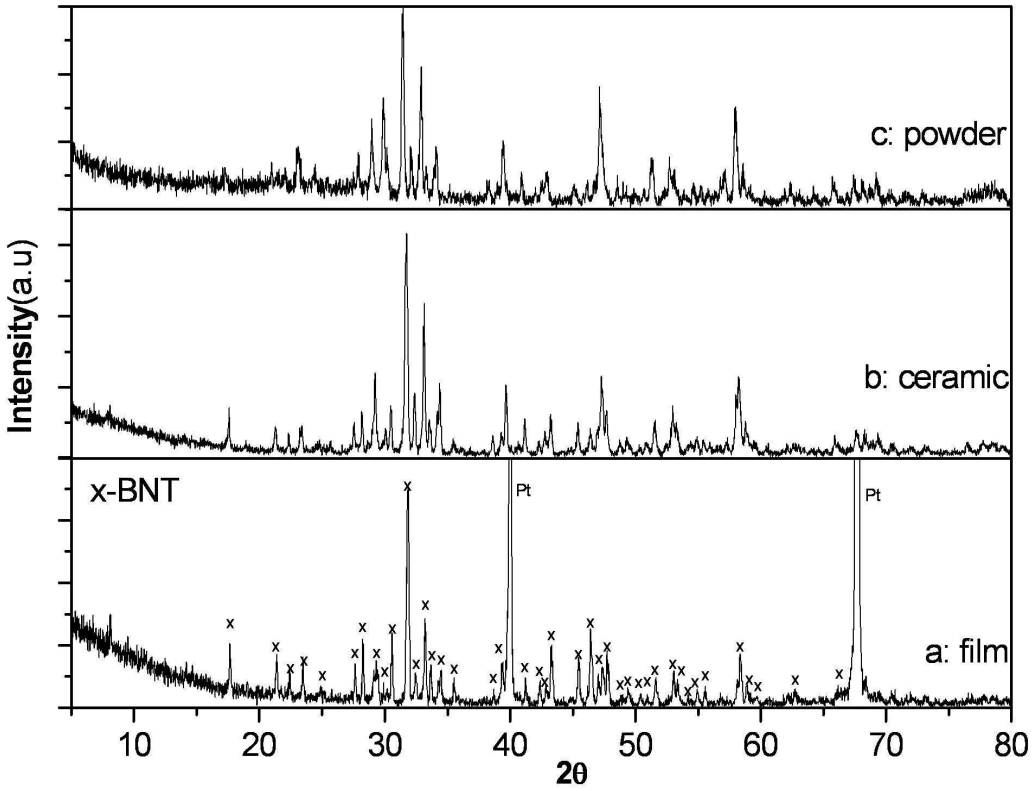

Figure 5.1-6 XRD pattern of: (a) EPD derived BNT thick films sintered at 1300 °C for 1h, (b) BNT ceramics sintered at 1300°C for 3h and (c) starting BNT powders

In generally, EPD process produces a porous layer of compacted powder and in order to enhance the density of BNT films, a post-deposition cold isostatic pressing (CIP) step was employed for that purpose. Although alternative approaches to enhance the sintered density of the films can be used, that include increasing the sintering temperature or introducing liquid phase sintering aids, these are not attractive for the present studies. Due to the thermal expansion mismatch between the films and the

substrate increasing the sintering temperatures will invariably lead to the formation of cracks and for case of sintering aids the dielectric losses can easily increase. Figure 5.1-7 illustrates the SEM micrographs of BNT films prepared without and with CIP treatment at 200 MPa, respectively. It is obviously seen that the porosity in the as prepared green BNT films is greatly reduced after a CIP step. The CIP step is proved to be a simple but effective method to achieve dense EPD derived films.

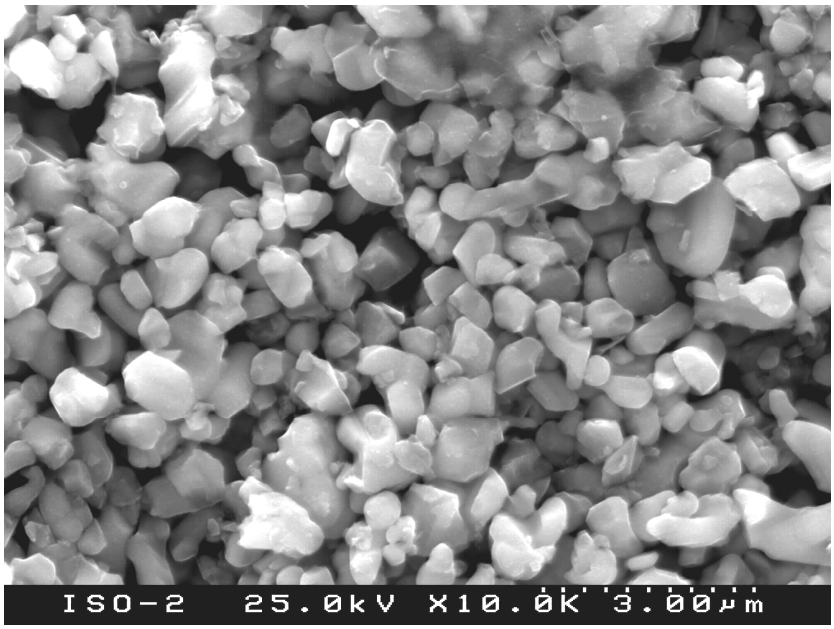

(a)

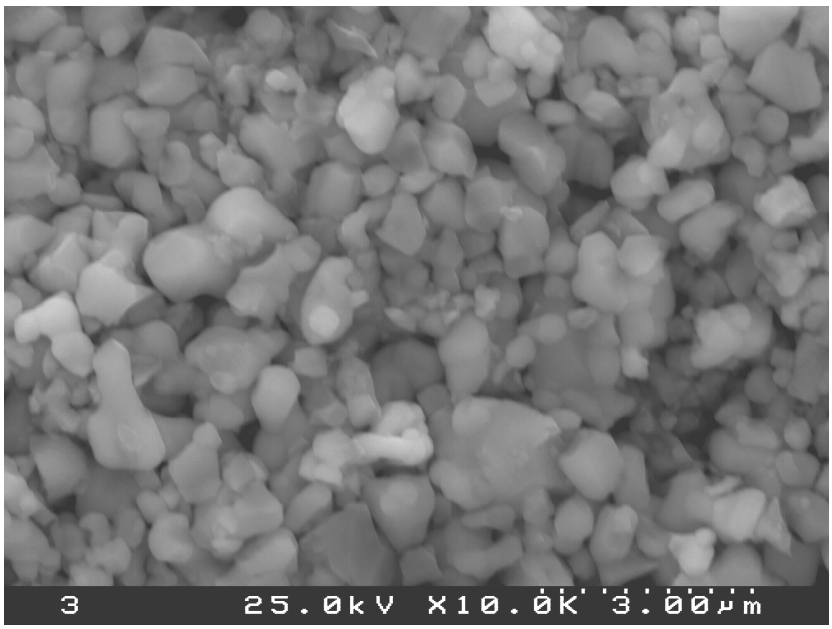

(b)

Figure 5.1-7 SEM micrographs of green BNT films (a) without and (b) with CIP treatment at 200 MPa

Figure 5.1-8 depicts the SEM fractured surface of sintered BNT films and the corresponding BNT ceramics. BNT ceramics exhibit a dense and homogeneous microstructure with rounded shaped grains (Figure 5.1-8 (a)). However the microstructure of EPD derived BNT thick films is substantially different from that of BNT bulk ceramics. The films without post deposition isostatic pressing step exhibit an obvious porous microstructure (Figure 5.1-8 (b)) that resulted as expected in unacceptable dielectric properties for these films. However the films with the CIP step and sintered under the same conditions exhibited a very dense microstructure, similar to the one observed for the ceramics however mainly composed of needle shaped grains, as clearly shown in Figure 5.1.8 (c). With regard to the origin of elongated grains in BNT thick films, it might arise from the constrained sintering of BNT films on Pt foil substrate. This effect is further addressed and elucidated in chapter 5.3.

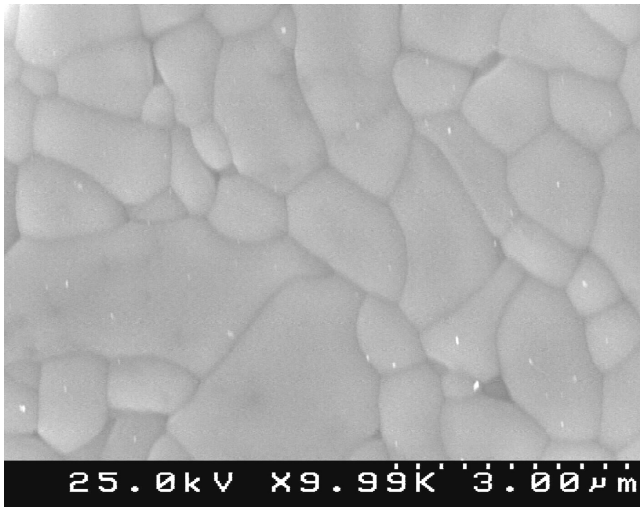

(a)

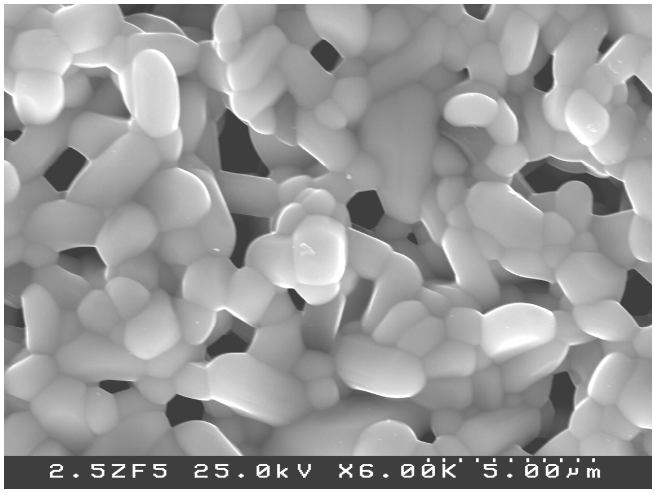

(b)

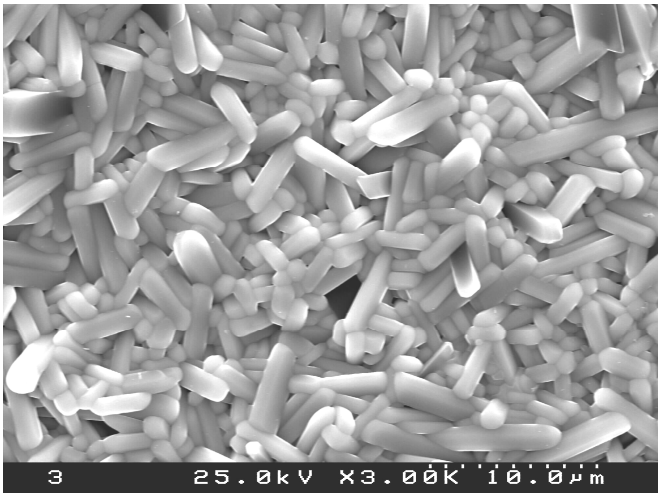

(c)

Figure 5.1-8 SEM micrographs of (a) BNT ceramics sintered at 1300 °C for 3h, BNT thick films (b) without, and (c) with post deposition CIP treatment sintered at 1300 °C for 1h

The relative permittivity and loss tangent of BNT thick films and the effect of film thickness are shown and compared with BNT ceramics in Figure 5.1-9 and Table 5.1-1. The relative permittivity (ε_r) and loss tangent ($\tan\delta$) at 1 MHz are 107 and 88 and 0.0006 and 0.0003 for 52 μm thick films and ceramics, respectively. As the film thickness is increased from 12 μm to 52 μm, the relative permittivity and loss tangent of BNT films approached that of BNT ceramics. However, BNT films without CIP treatment show a lower relative permittivity of 65 and higher loss tangent of 0.008 at 1 MHz due to the porous microstructure, compared with post CIP BNT films.

Q ($1/\tan\delta$) values of BNT films with different thickness are compared at 1 MHz with bulk ceramic values in Figure 5.1-9 (b). As shown, the Q of BNT thick films improved from 700 to 1600 when the film thickness increased from 12 μm to 52 μm. This trend with increasing film thickness is consistent with an ‘interfacial layer’ or interfacial region at the lower foil electrode interface that has lower relative permittivity and slightly increased dielectric loss. As the film thickness increases the macroscopic response of the capacitor tends to be ruled by the bulk of the film and the detrimental influence of the interfacial layer tends to be minimized. Besides the influence of the interfacial layer, the lower Q of BNT thick films compared with BNT ceramics might be also related with the microstructure of the films, which have particular grain morphology and some small volume of residual porosity. In current case, 52 μm thick BNT films show excellent Q value for high frequency applications.

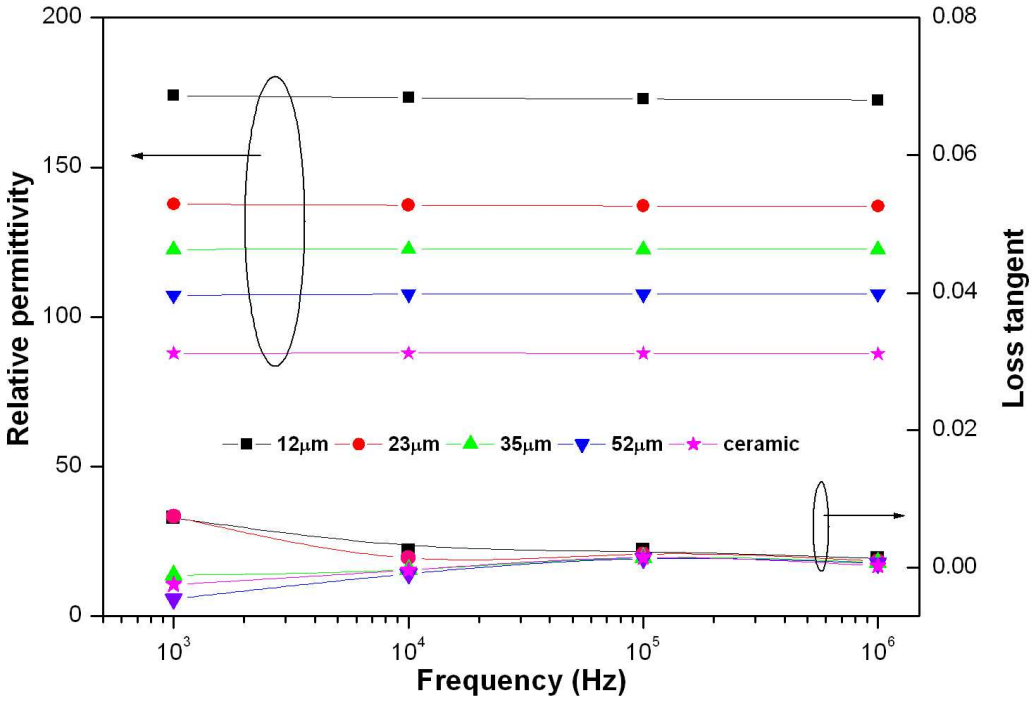

(a)

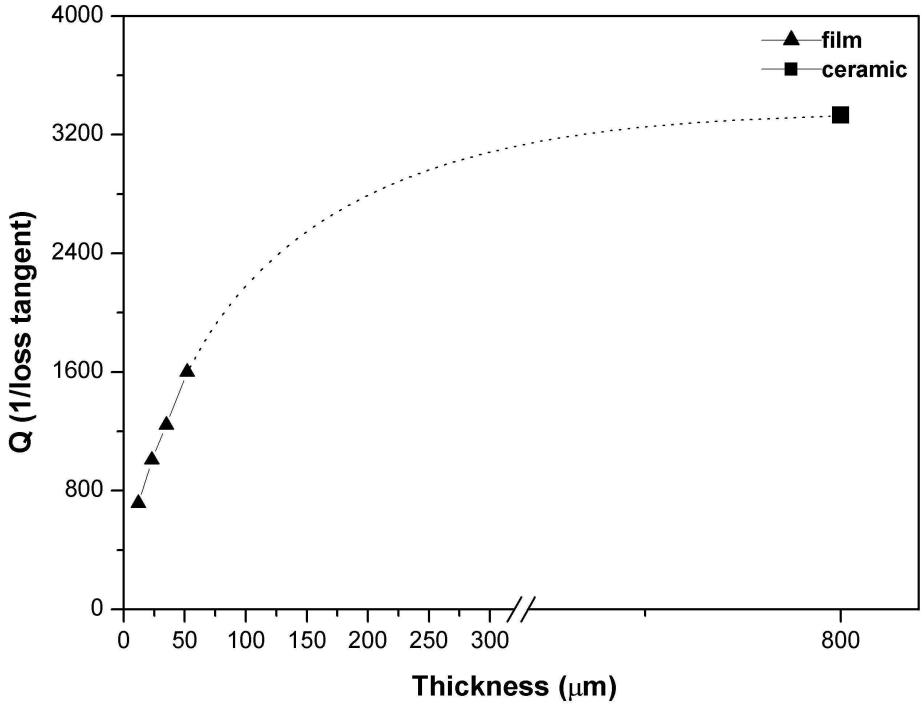

(b)

Figure 5.1-9 (a) Relative permittivity and loss tangent of ceramics and CIP BNT films with various thicknesses, sintered at 1300 °C for 3 and 1 h, respectively, (b) thickness dependence of Q (1/ loss tangent) of post CIP BNT thick films at 1 MHz and comparison with BNT ceramics

Compared with other reported microwave thin films, (Table 5.1-1) the BNT thick films prepared in this work demonstrated an excellent performance in terms of relative permittivity and loss tangent (high Q features). According to the authors' knowledge, this is the highest Q reported for thick films (> 1 μm) so far.

Table 5.1-1 Electrical properties of 52 μm thick BNT film and ceramics sintered at 1300 ºC for 1 and 3 h, respectively. Comparison with the dielectric properties of other analogue reported materials

System	Thickness	Electrical properties			Reference
		ε_r or Cp*	Tanδ and Q (1/tanδ)	TCε_r (ppm/ ^{0}C)	
BNT films by EPD	52 μm	107 at 1MHz	0.0006 or Q=1600 at 1MHz	+58.5 (30-120 ^{0}C)	Current work
BNT ceramics		88 at 1MHz	0.0003 or Q=3333 at 1MHz	-36.8 (30-120 ^{0}C)	Current work
BNT ceramics		91 at 3.5 GHz	Q=1771 at 3.5 GHz	-8 to -46 (-20-80 ^{0}C)	FuJi Titanium Ind.Co.,Ltd
$MgTiO_3$ films by MOD*	300 nm	21 at 100kHz	0.02 at 100kHz		Choi Y. H.-2001
$Ba_{0.7}Sr_{0.3}TiO_3$ by CVD*	30 nm	80 fF/μm^2 at 20GHz	0.006 at 20GHz		Baniecki J. D.-1998
$Ba(Mg_{1/3}Ta_{2/3})O_3$ by MOD*	300 nm	22.2 at 100kHz	0.009 at 100 kHz	-145 (25-125 ^{0}C)	Joshi P. C.-1998

MOD*: metalorganic deposition, CVD*: chemical vapour deposition,

Cp*: capacitance density

Figure 5.1-10 depicts the temperature dependence of relative permittivity and the applied DC voltage dependence of the relative permittivity and loss tangent for BNT thick films sintered at 1300 °C for 1h and the comparison with the corresponding BNT ceramics sintered at 1300 °C for 3h. The temperature dependence of the relative permittivity of MIM BNT film capacitors was analyzed between 30 °C to 120 °C at 1MHz. As shown in Figure 5.1-10 (a), the relative permittivity of BNT films is quite stable as a function of temperature. The temperature dependence coefficient of relative permittivity was measured in terms of the parameter $\Delta\varepsilon_r/\varepsilon_{r0}\Delta T$, where $\Delta\varepsilon_r$ stands for the change in relative permittivity in relation to the relative permittivity ε_{r0} at 30 °C. The temperature coefficient of relative permittivity of 52 μm-thick BNT films is calculated to be lower than +58.5 ppm/°C between 30 ˚C to 120 ˚C indicating a good temperature stability of EPD derived BNT thick films.

Figure 5.1-10 (b) shows the DC electric field dependence of the relative permittivity and loss tangent of 52 μm-thick BNT films sintered at 1300 °C/1h. The relative permittivity does not show substantial dependence on the bias voltage and its

variation is found to be less than 0.02% up to an applied voltage of 40 V (8 kV/cm).

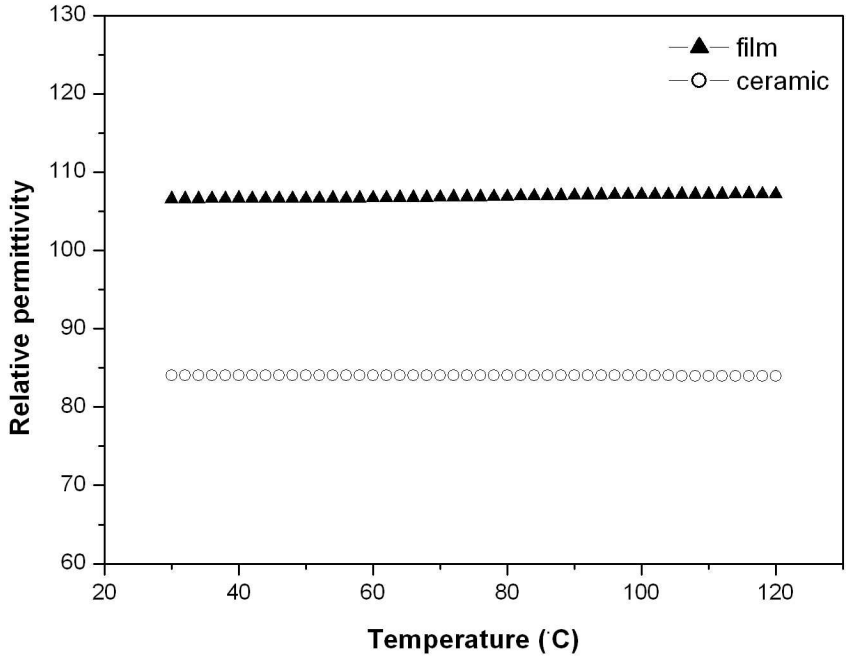

(a)

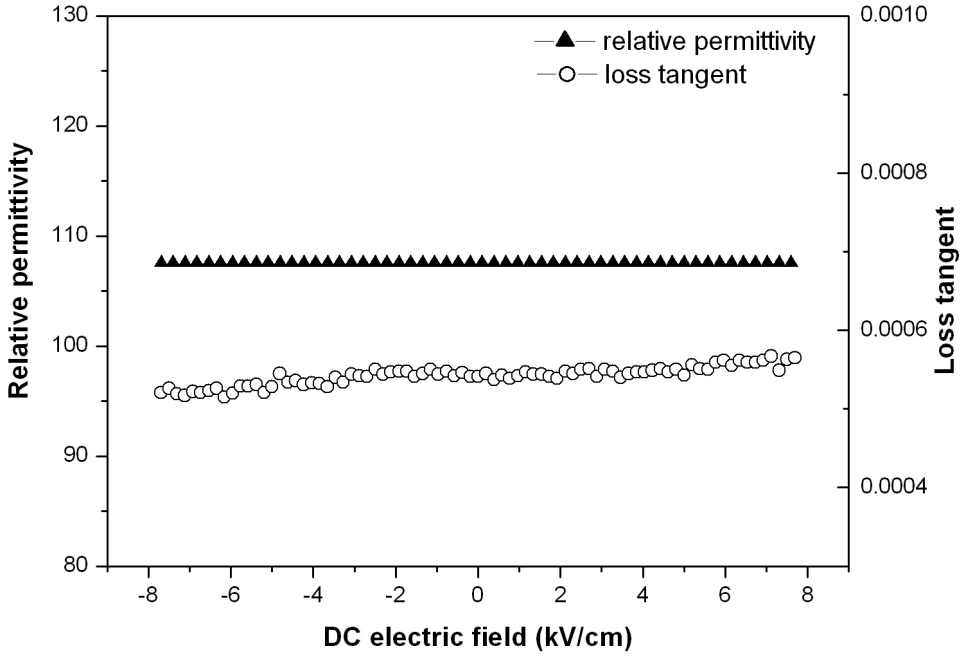

(b)

Figure 5.1-10 (a) Temperature dependence of the relative permittivity of 52 μm-thick CIP BNT films and ceramics sintered at 1300°C for 1 and 3 h, respectively, and (b) DC electric field dependence of relative permittivity and loss tangent of 52 μm-thick CIP BNT films sintered at 1300°C for 1h

The dielectric properties of BNT films sintered at 1300 °C for 1h were evaluated at microwave frequencies by a transmission-reflection technique, as described in chapter 4. Figure 5.1-11 depicts the qualitatively analysis of dielectric loss at specific microwave frequency. No significant increase of the losses takes place in BNT films up to 1.4 GHz i.e., the modification of the internal loss of the film was smaller than the resolution of the experiment of ~0.01 dB for this frequency range. This result indicated that the EPD derived BNT thick films are suitable to be used in some high frequency applications, such as mobile phone.

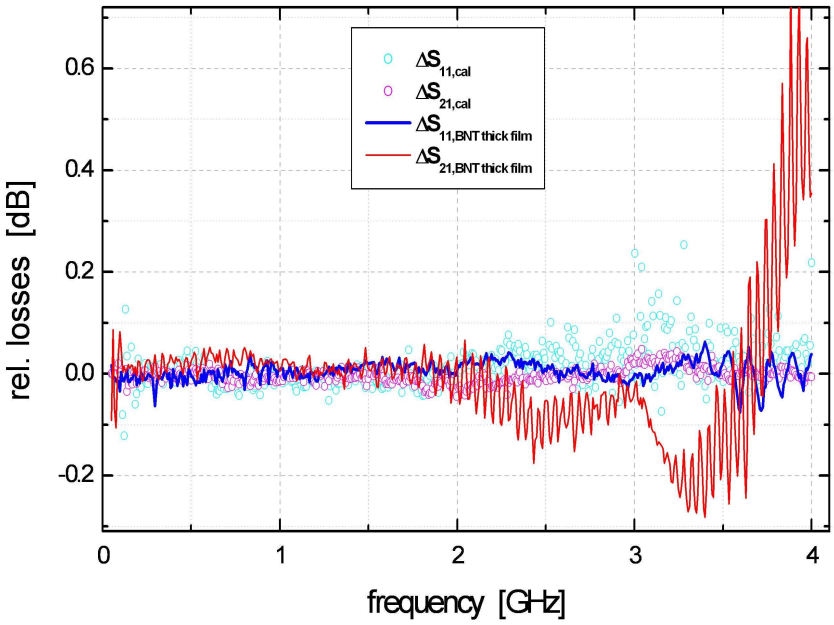

Figure 5.1-11 Change of loss tangent of 52 μm-thick BNT thick films sintered at 1300 °C for 1h as a function of frequency till to 4 GHz

5.1.4 Summary

BNT films on Pt foils were successfully fabricated by EPD using commercial BNT powders and an acetic acid based suspension. Moreover high quality BNT thick films were prepared by optimising the processing parameters. It is shown that the density of EPD derived BNT films can be greatly increased by applying a cold isostatic pressing step to the green films, which resulted in considerable enhancement of the density of the sintered films and as a consequence of the dielectric response. Dense BNT thick films displayed a homogeneous microstructure with a characteristic needle shape grain growth when compared with equivalent ceramic samples. Dense BNT thick films exhibit higher relative permittivity than bulk BNT ceramics prepared from the

same starting powders. The dielectric Q is higher than any previously reported for thick films. The excellent dielectric properties at RF and MW frequencies, including good thermal stability and bias voltage independent capacitance characteristics suggest the suitability of EPD derived BNT thick films for integrated capacitor and microwave device applications. EPD is thus proved to be a low-cost and efficient method to process low loss (high Q) coatings on metal electrodes for high frequency device, satisfying the objective previously defined.

5.1.5 References

1. Baniecki J. D., Laibowitz R. B., Shaw T. M., Duncombe P. R., Neumayer D. A., Kotecki D. E., Shen H., Ma Q. Y. (1998) Appl. Phys. Lett. **72**, 498
2. Basu R. N., Randall C. A., Mayo M. J. (2001) J. Am. Ceram. Soc. **84**, 33
3. Borland W. J. and Ferguson S. (2001) Embedded Passive Components in Printed Wiring Boards, a Technology Review, CircuiTree Magazine
4. Choi Y. H. and Lww J. C. (2001) Thin Solid Films **385**, 43
5. Corni I., Ryan M. P. and Boccaccini A. R. (2008) J. Euro. Ceram. Soc. **28**, 1353
6. Hamaker H. C. (1940)Trans Farad Soc **36**, 279
7. Joshi P. C. and Desu S. B. (1998) Appl. Phys. Lett. **73**, 1080
8. Negishi H., Yanagishita H., Yokokawa H. (2002) Proceedings of the electrochemical society on electrophoretic deposition **21**, 214
9. Wu A.Y., Vilarinho P. M., Kingon A. I. (2006) J. Am. Ceram. Soc. **89**, 575

5.2 Effect of Suspension Media on the Deposition of $BaNd_2Ti_5O_{14}$ Thick Films by EPD

Abstract:

A successful electrophoretic processing is intimately related to a careful choice of solvents and additives, which should lead to well-dispersed and stable suspensions for EPD. In this chapter, the influence of the suspension media on the EPD behaviour of BNT particles is investigated. For that, BNT powders were prepared by conventional solid state reaction, in order to avoid the influence on the stability of the suspension of the additives utilized in the commercial BNT powders previously used in chapter 5.1. Suspensions based on water, ethanol, acetone and acetic acid were employed and analyzed for the electrophoretic deposition (EPD) of BNT powders. Experimental results revealed that the zeta potential is a straightforward indication of the stability of these suspensions, since the maximum absolute zeta potential corresponds to a maximum of the suspension dispersibility reflected in the particle size distribution and suspension light transmittance as well. Among the used solvents, because of the easy formation of deposits, acetic acid and acetone are studied in detail. Deposits with a homogeneous, smooth surface and high deposition yield were obtained upon adding I_2 to the acetone based suspension. For these last suspensions, the effect of the EPD processing parameters, deposition voltage, deposition time and suspension composition, on the characteristics of BNT films is investigated. Optimized suspensions and deposition conditions allow the production of high quality BNT thick films in acetone with I_2 based suspensions.

5.2.1 Introduction

In order to fully utilize the advantages of the EPD technique, a number of processing parameters must be established, that include the selection of solvents and additives, deposition voltage, suspension composition, suspension ageing etc. In the search for the optimization of EPD, scientists and researchers concluded that the final properties of the films are greatly influenced by the powder composition, selection of the suspension media system to control the zeta potential and stability of the suspensions. [Negishi H.-2004, Xu Z. G.-2006, Zhitomirsky I.-2004]. In other words, the success in EPD is intimately related to the careful choice of the bath composition

and deposition conditions. [Zhitomirsky I.-2004] Although the preparation of films by EPD has been reported from a wide range of suspension media, unfortunately there is not a general suspension medium for the successful preparation of thick coatings by EPD.[Zarbov M.-2006] Usually, an appropriate medium for a given material is conventionally established through trial and approval attempts. The choice of the right suspension media is one of the most challenge aspects of EPD, in terms of reliability and reproducibility of the method. Therefore, for the EPD of the BNT powders of the present work to find an effective suspension media for the charging of the particles and stabilization of the suspensions to guarantee optimal processing conditions for BNT films is a crucial task. At the same time it is very important to clarify how the suspensions composition affects the deposition rate and the deposit morphology. In addition, the process parameters should be studied and optimized to satisfy the engineering requirements while minimizing the formation of process defects, which include variations in the particle packing density, loss of adhesion to the substrate, cracking of the deposit and surface roughness or thickness variations.

In the previous chapter of this work it was demonstrated that using acetic acid as a solvent, high quality low loss BNT thick films could be deposited by EPD. These studies were conducted with commercial BNT powders, but simultaneously it was verified that the reliability and reproducibility are critical issues when using acetic acid solvent. Based on these first observations, it became clear the need to conduct a systematic study on the effect of the suspension media on the deposition of BNT powders by EPD. Therefore, the aim of this chapter is to investigate the effect of suspension media on the EPD process and properties of fabricated BNT dielectric layers. Experiments led to optimized deposition conditions for the fabrication of dense, homogenous and reproducible BNT coatings on the platinum foil substrates. The electrochemistry of EPD suspensions is studied and discussed with regard to the electrophoresis behaviour of BNT suspensions. The relation between suspension media, process, microstructure and performance of EPD is established and discussed.

5.2.2 Experimental

In this chapter, all the BNT films were prepared from home-made powders prepared as described in Chapter 4. The EPD was attempted in four different solvent media: de-ionized water, acetone, ethanol, and glacial acetic acid (HAC), respectively. Particular attention was paid to the suspension properties using the characterization

techniques also described in the experimental chapter. All the green films were pressed under a cold isostatic pressure of 200 MPa to enhance the green density. The films were then sintered in air at 1300 ˚C for 1 h. The characterization of the films was as described.

5.2.3 Results

5.2.3.1 Suspension dispersibility

The physical properties of the suspension media used in this part of the work are shown in Table 5.2-1. The pH of water based suspension and operational pH of the organic-based suspensions is measured by means of a pH meter.

The operational pH is defined as:[Sarkar P.-1996]

$$P\alpha_H = pH - \frac{\Delta E_j}{0.05916} \text{ at } 25\ ^oC \qquad (5.2\text{-}1)$$

where $P\alpha_H$ is the negative logarithm of proton activity in organic solvent, which is the real pH in non-aqueous media, ΔEj is the difference between the liquid-junction potentials, pH is the operational readings by a standard pH meter. Thus, for a given solvent, the $P\alpha_H$ can be calculated from the operational pH reading in the non-aqueous medium. But, within convenience, the operational pH term is usually used in organic solvent.

Table 5.2-1 Physical properties and EPD performance of used suspension media

Suspension media	Dielectric constant	Viscosity (cP)	EPD performance
Water	80	0.89	No deposition
Ethanol	24.3	1.2	Bad
Acetone	20.7	0.306	Excellent
Acetic acid	6.19	1.22	Good

The effect of the suspension media on the BNT suspension stability is investigated by means of particle size distribution, suspension transmittance and zeta potential.

Figure 5.2-1 depicts the zeta potential of BNT particles in the different suspension media as a function of pH or operational pH. The surface of BNT particles is positively charged in acetic acid, pure ethanol and acetone. Compared with the organic solvents, the zeta potential of BNT particles in water is much lower. Although water is not suitable for EPD of BNT particles, the data of aqueous based suspension are used as reference for comparison and discussion. A positive zeta potential of 41 mV for BNT

particles in acetic acid has been measured at an operational pH of 0.8. For ethanol based suspension, the zeta potential increases from 25 mV to 46 mV when the operational pH value is decreased from 6.7 to 2.8 by adding a dilute 10^{-2} M HCl solution. In this study, iodine dissolved in isopropanol is used to adjust the operational pH value of acetone based BNT suspension. As shown in Figure 5.2-1, the zeta potential increases from 7 to 61 by adding I_2, accompanied with an operational pH change from 6.5 to 2.3, which means that iodine is very effective in charging and dispersing BNT powers in acetone based suspensions. This result indicates also that the amount of electrical charges on the surface of BNT powders in the acetone media increased with the iodine addition.

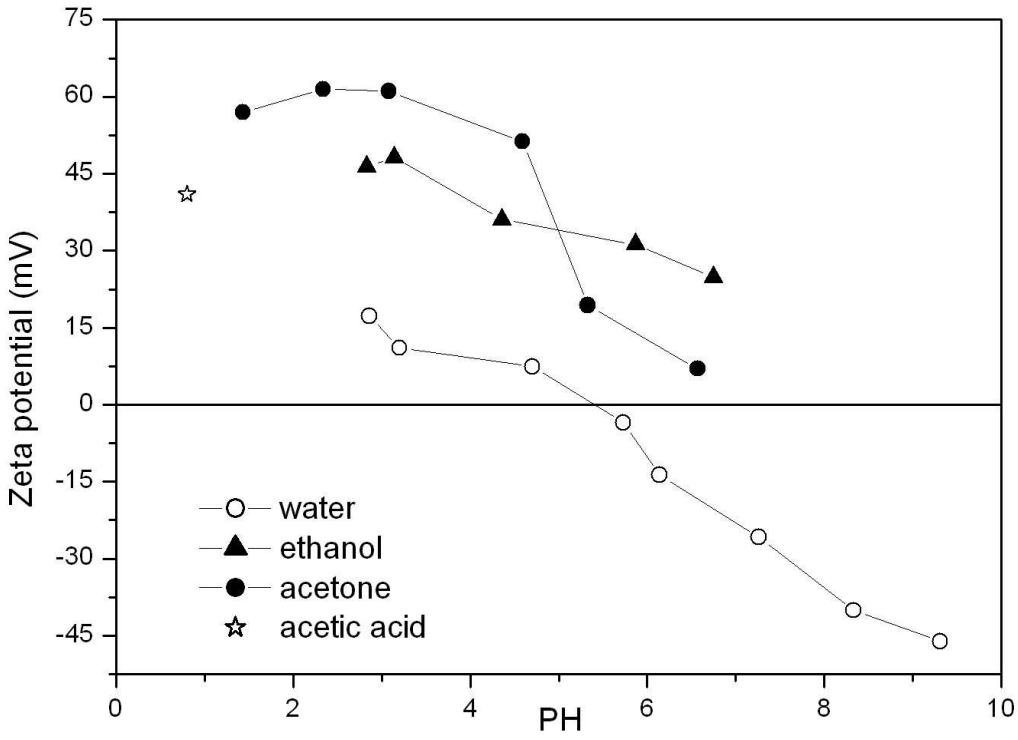

Figure 5.2-1 Zeta potential of different BNT suspensions

Figure 5.2-2 depicts the particle size distribution of the different BNT suspensions. As expected BNT particles show dissimilar dispersion characteristics in different suspension media. In the case of water based suspension, a bimodal distribution of the particles is obtained, which indicates the existence of particle agglomeration in water. But in organic solvents (acetone, ethanol and acetic acid), the BNT suspensions exhibit a monomodal narrow distribution of the particle size that peaks at approximately 0.7, 0.72, 0.45 and 0.2 μm in ethanol, pure acetone, acetic acid and acetone with I_2, respectively. To prepare a well dispersed BNT suspension for EPD to obtain a dense

BNT coating, a fine particle size suspension is required and BNT suspensions in acetic acid and acetone solutions present relative good results, in particular BNT acetone with I_2 based suspension.

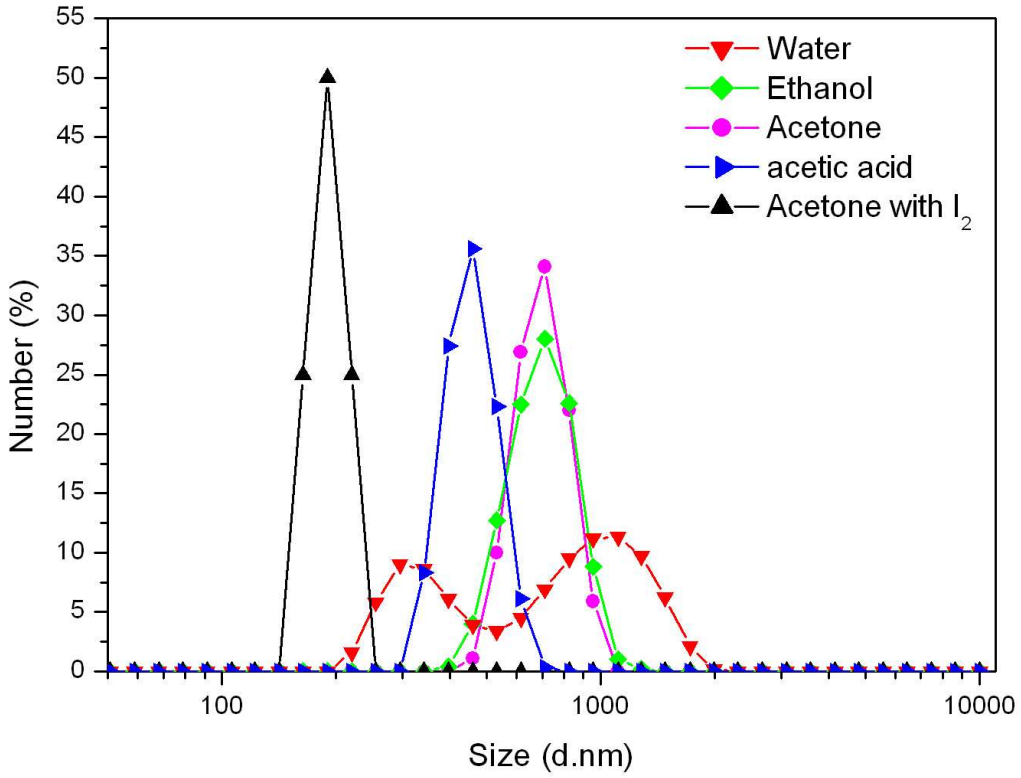

Figure 5.2-2 Particle size distribution of different BNT suspensions

Transmittance of UV light was recorded for the different suspensions of BNT particles, and is illustrated in Figure 5.2-3. Initial transmittance values of about 70%, 60%, 45% and 10% are obtained for water, ethanol, acetone (acetic acid) and acetone with I_2 addition suspensions, respectively. As the time increases, the transmittance slightly increases for the organic based suspensions. In opposition, this change is very obvious for the water based suspension. A small transmittance and transmittance change imply that the particles remain in a stable dispersed state for a long period of time, matching the optimized suspension conditions to be used for EPD. For water based suspension, besides presenting the highest values, the transmittance increases constantly with the time. In the water based suspension the majority of the particles continuously sediment and avoid the particle stabilization. These results are consistent with the above analysis of particles size distribution and the zeta potential curves in the different suspension media.

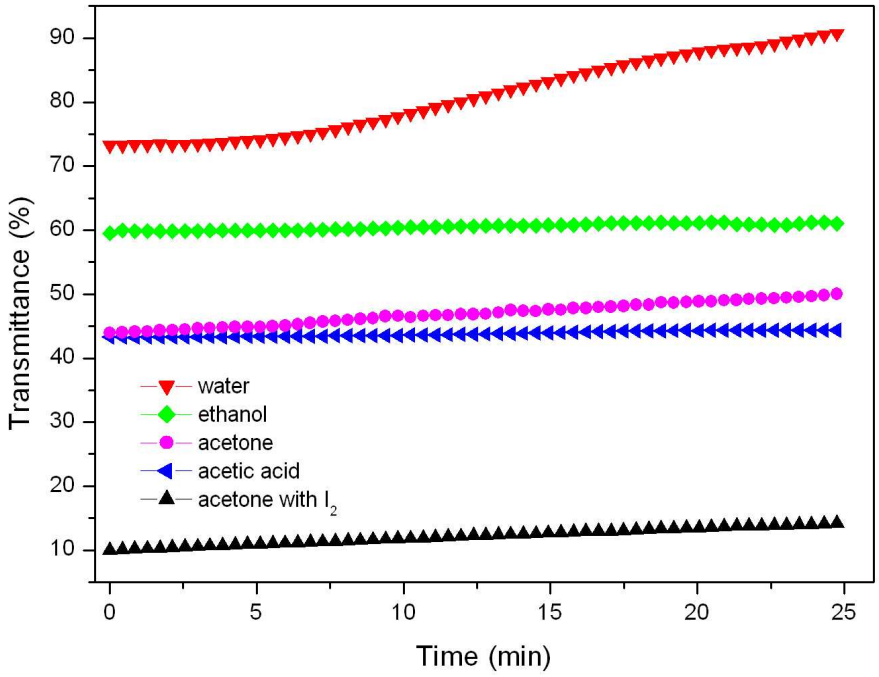

Figure 5.2-3 Transmittance of UV light versus time for the different BNT suspensions

In addition, it is found that acetic acid and acetone with I_2 based suspensions do not present the tendency to an immediate flocculation, settling slowly and forming a compact deposit at the bottom of the container. However, water and ethanol based suspensions, showing both the highest transmittance values, settle rapidly and form low density and loose compacts.

Based on above results, it is considered that BNT powders suspended in acetone with I_2 have excellent powder distribution and suspension dispersibility. Due to the marked effect of the colloidal stability on the quality of the obtained EPD compacts, high quality BNT compacts or films are expected to be produced with high reliability in acetone with I_2 based suspension.

5.2.3.2 EPD behaviour

EPD was attempted with all the studied suspensions, and because the particles are positively charged (Figure 5.2-1), cathodic deposition is performed. However, acceptable deposition is achieved only from acetic acid and acetone with I_2 suspensions. (Table 5.2-1) There is no deposition in water based suspension. Suspensions in ethanol and water exhibit rapid sedimentation when ultrasonic treatment is interrupted as predicted by the above suspension stability studies. Concerning ethanol, even for the operational pH value of 2.8 adjusted to obtain the highest zeta potential, there is still no

obvious deposition and the obtained deposited layers are particularly heterogeneous.

Figure 5.2-4 illustrates the optical micrographs of BNT films derived from ethanol, acetic acid and acetone with I_2 suspensions, respectively. The complete diameter of deposited films should be 10 mm. Very conformal and uniform BNT films are obtained from acetic acid and acetone with I_2 based suspensions. It is worthwhile to mention that experiments performed with suspensions of pure acetone have not yielded noticeable deposition. However, after the addition of I_2, quite uniform deposits are obtained. On the other hand, it is observed that a thin and fluffy layer with irregular edges covers some parts of the substrate in ethanol based suspensions.

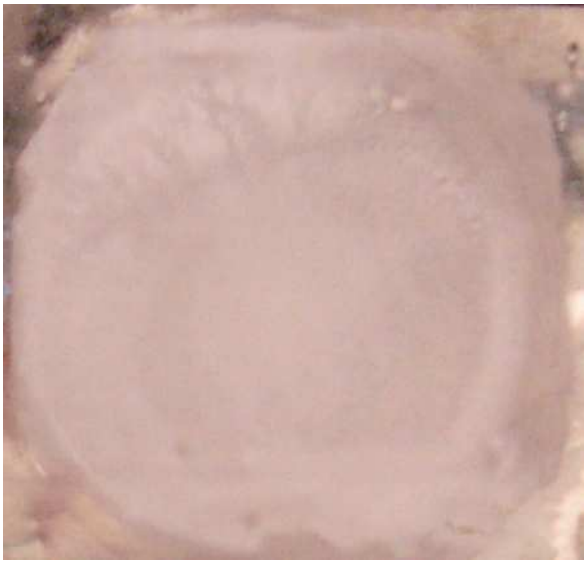

(a)

(b)

(c)

Figure 5.2-4 Optical micrographs of BNT films deposited from (a) ethanol, (b) acetic acid and (c) acetone with I_2 suspensions, respectively

Suspension media effect on the microstructure of as sintered BNT films was examined by SEM. Figure 5.2-5 depicts the microstructure of deposited BNT films derived from ethanol, acetic acid and acetone with I_2, respectively. For the two suspensions media, acetic acid and acetone with I_2, crack-free, dense, uniform and homogeneous microstructure were obtained (Figure 5.2-5 (b) and (c). A very porous microstructure was developed in ethanol, where BNT particles do not cover all the substrate (Figure 5.2-5 (a)).

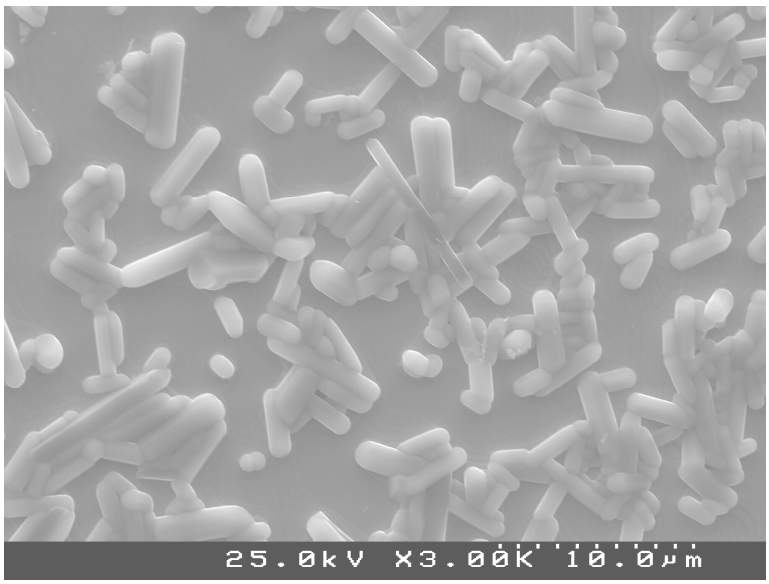

(a)

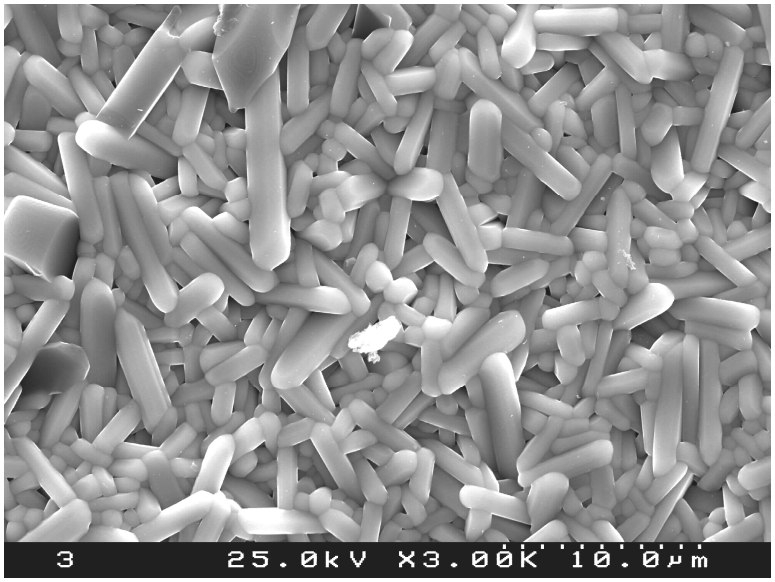

(b)

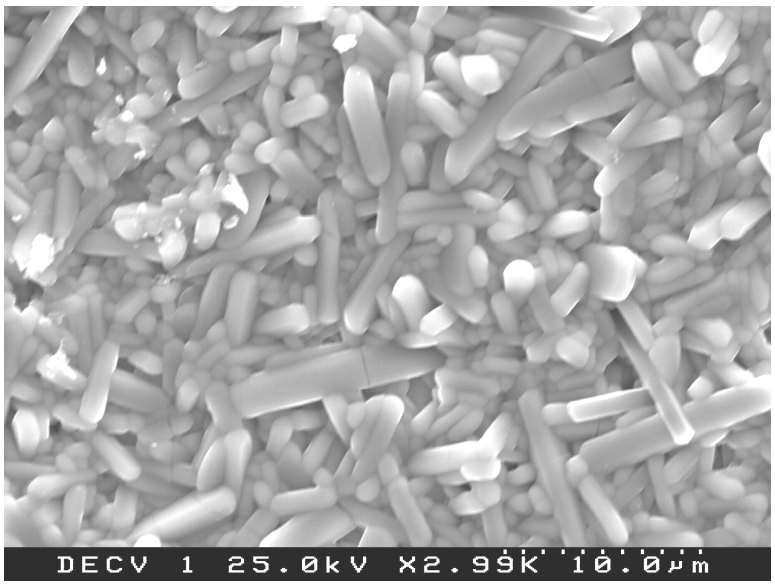

(c)

Figure 5.2-5 SEM surface micrographs of BNT thick films derived in (a) ethanol, (b) acetic acid, (c) acetone with I_2 suspensions and sintered at 1300 °C/1h

Ethanol is not a suitable solvent for EPD of BNT powders. The EPD performance of BNT powders in different suspension media is summarized in Table 5.2-1.

Based on the similar microstructures, it seems there is little difference between the behaviour BNT acetic acid and acetone with I_2 based suspensions in terms of EPD performance. Because of the good results obtained in term of deposition further studies were concentrated on both of these suspension media.

5.2.3.3 Characteristics of EPD of BNT films in acetic acid based suspension

As presented above, acetic acid can be used for EPD of BNT powders, but based on the previous experiments conducted with commercial BNT powders, reliability may be a critical issue for such suspension, because of that it deserve to be further inspected.

It was observed for the films derived from acetic acid based suspension that the conformal characteristics of the deposited layer degraded as the number of deposition cycles increased. Figure 5.2-6 depicts the optical micrographs of as deposited BNT films derived from acetic acid based suspension, at 200 V for 1 min, as a function of deposition times, in which this effect is quite clear.

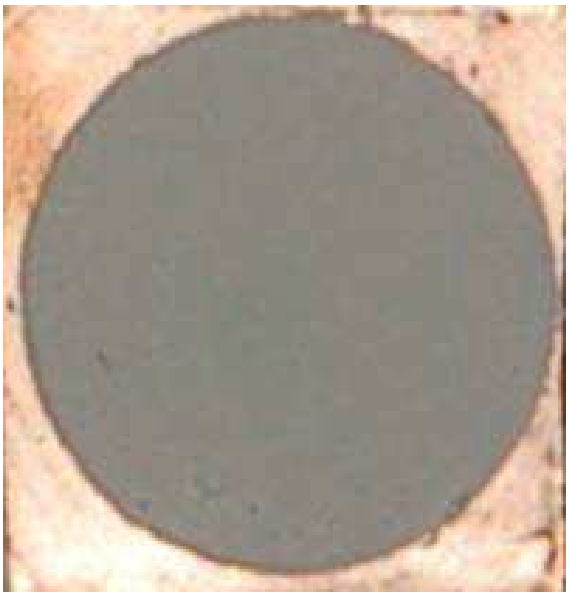

(a)

(b)

(c)

Figure 5.2-6 Optical surface micrographs of green BNT films deposited at (a) the first deposition, (b) the fourth deposition, (c) the sixth deposition in acetic acid based suspensions

For one deposition (Figure 5.2-6 (a)), very conformal, uniform and crack free layers were obtained. However, for further depositions the surface of the deposited films starts to become less smooth, uniform and conformal as observed for the fourth deposition (Figure 5.2-6 (b)) and if the deposition cycles continue, the surface of the deposited films became more and more rough till a non-continuous surface layer is formed, as shown in Figure 5.2-6 (c), for the sixth consecutive deposition. Although acetic acid based BNT suspension yield good EPD thick films, the quality of the obtained films is highly dependent on the number of consecutive depositions to which the suspension is submitted, i.e., on the number of consecutive times that voltages is applied to the suspension. In terms of production, the use of the acetic acid will require a systematic substitution of the suspension media, what is undesirable in terms of operation and cost.

The deposition weight and electric current through the suspension were further examined against deposition cycles in the EPD behaviour of BNT in acetic acid based suspension in order to track any changes occurring in the suspension and are illustrated in Figure 5.2-7. The deposition weight is 9, 6 to 1 mg for the first, forth and sixth depositions, respectively, and meanwhile, the corresponding current through the suspension is 0.05, 0.6 and 1.3 mA. The decreased trend of deposition weight is consistent with the above microstructure observations. The deposition becomes more

and more difficult as the current through the suspension increases with the increase of the deposition cycle. These results clearly show that the physical properties of the acetic acid based suspension change with the course of EPD.

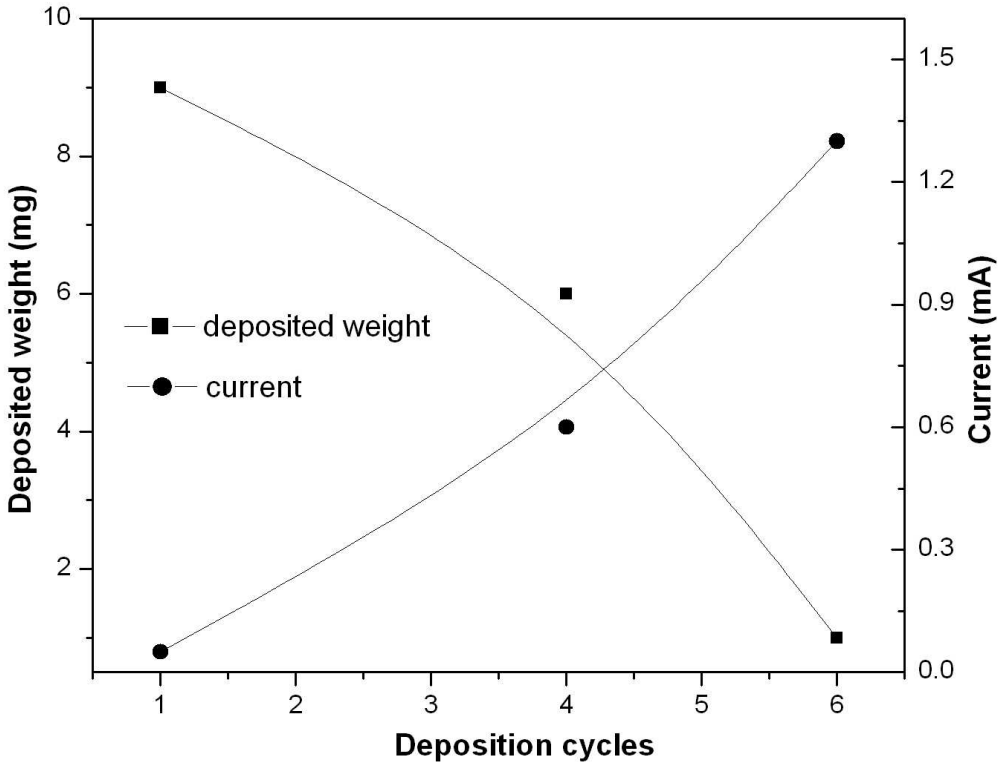

Figure 5.2-7 Deposition weight and current through suspension in acetic acid based suspension as a function of deposition cycles

In order to further analyze this suspension behaviour, a current loop against the applied voltage was recorded. Figure 5.2-8 shows the current loops of BNT suspensions in both acetic acid and acetone with I_2 when the applied voltage is increased from 100 to 600 V, and then decreased to 100 V. For both curves the current in the suspension increases and decreases when the applied voltage increases and decreases, respectively. However, for the acetic acid based suspensions (Figure 5.2-8 (a)) the current is always higher for the voltage decrease run (from 0.12 to 0.16 mA at 200 V), when compared with the voltage increase one, and contrary to the behaviour observed for the acetone with I_2 based suspensions. In this last case, the current is slightly lower for the decreasing voltage run (from 1.7 to 1.4 mA at around 300 V, Figure 5.2-8 (b)). These results clearly point to the conductivity change in the suspensions during EPD, and to their dependence on the suspension media.

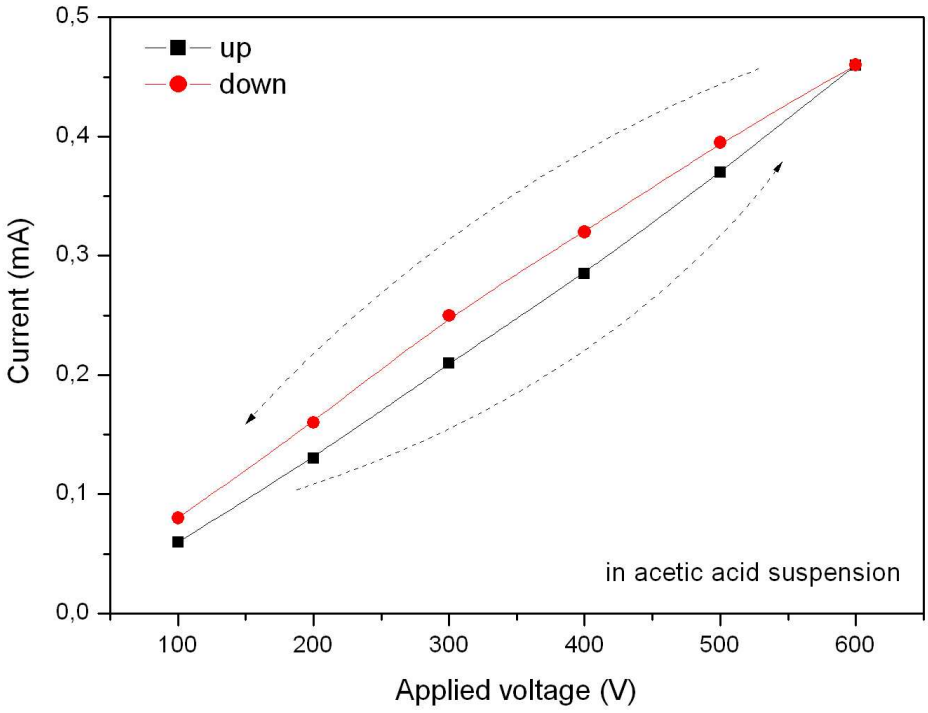

(a)

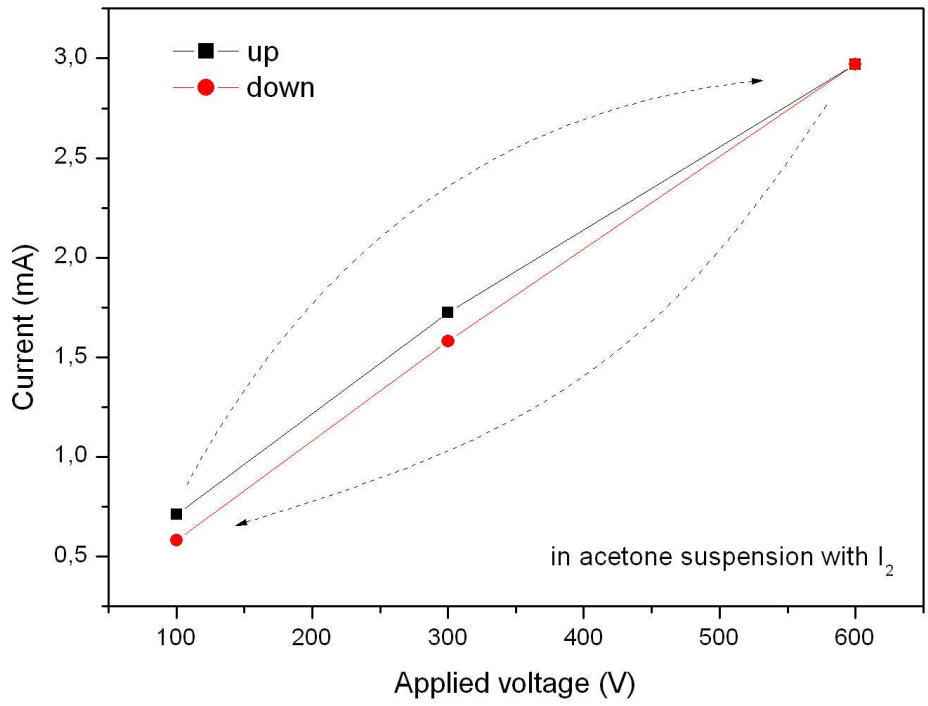

(b)

Figure 5.2-8 Current loop of (a) acetic acid, (b) acetone with I_2 based suspensions against applied voltage during EPD

The changes observed in the suspension current behaviour point to a change in the carriers that might come from a chemical modification of the suspension.

The results of ICP-AES analysis of the supernatant of fresh and aged suspensions are indicated in Figure 5.2-9, in which the concentration of Ba, Nd and Ti element in the solution and the deposition weight are plotted against the ageing time. The leaching of metallic elements from the solution is clearly seen. After ageing the acetic acid based suspension for 48 h, severe Ba leaching from BNT powders occurred. The concentration of Ba in the solution increases from about 10 mg/kg to 21 mg/kg (Figure 5.2-9 (a)). The concentration of Nd in the supernatant increases as well, following a similar trend to the observed for the Ba element, but with lower contents. The Ti ions is also verified but in a much smaller scale when compared with the previous elements. At the same time, the deposition weight decreases with the ageing time (Figure 5.2-9 (a)).

Leaching of BNT ions was also observed in the supernatant of acetone with I_2 based suspensions but in smaller amounts to those observed for the acetic acid based suspension (Figure 5.2-9 (b)). The highest concentration of metallic ions in the supernatant of acetone with I_2 BNT based suspension is Ti, followed by Ba and Nd, that increase with the ageing time increases. The concentration of titanium just increases from 0.329 mg/kg to 1.58 mg/kg in the supernatant of acetone with I_2 base suspension after ageing for 5 months (Figure 5.2-9 (b)). At the same time Ba concentration in the supernatant is 14 times higher for 48h of ageing in acetic acid based suspension than after 5 month of ageing in acetone with I_2 based suspension. These results clearly indicate the higher stability of acetone with I_2 suspensions and the longer shelf time of these suspensions that those prepared with acetic acid, which is an important aspect for industrial applications.

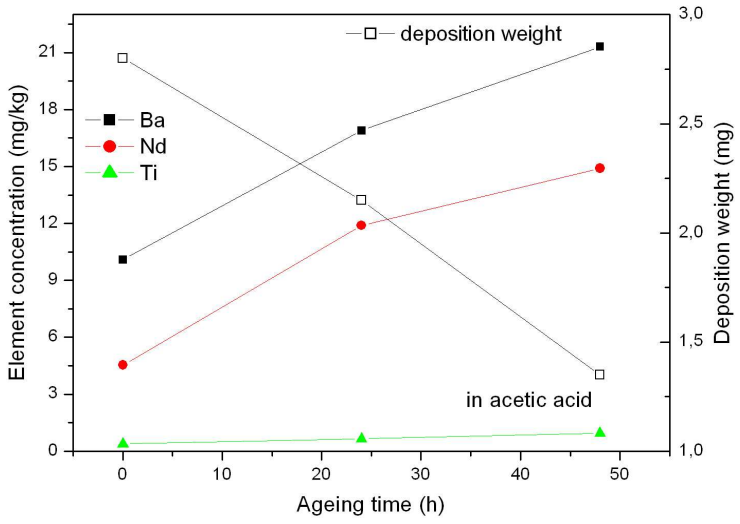

(a)

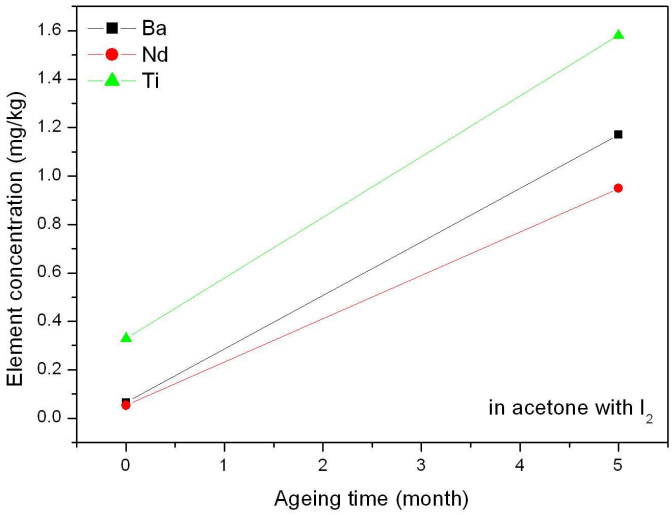

(b)

Figure 5.2-9 Ageing effect of (a) acetic acid and (b) acetone with I_2 based suspensions (note: at zero ageing, the elements are from the original pure suspension media)

5.2.3.4 EPD of BNT in acetone with I_2 based suspension

According to above results, among the studied suspension media, acetone with I_2 shows the best performance for EPD of BNT powders. In this section the process parameters, deposition time, operational pH and applied voltage, are studied for the optimization of EPD processing of BNT materials. The trial-and-error approach was used to determine the optimal processing conditions.

Figure 5.2-10 depicts the deposition thickness against the deposition time at a constant applied voltage of 200 V in which an asymptotic variation occurs. A significant and linear increase in deposition thickness is recorded for short deposition times (from 0.5 to 2.5 min) followed by a limited increase when the deposition time is increased from 2.5 to 3.5 min. From this variation it becomes obvious that EPD is a very efficient method to produce thick deposits when very short deposition times are required. Similar observations have been reported in the literature [Nicholson P. S.-1993] and attributed to the change in deposition rate and particle concentration as deposition continues. It is noted that in constant voltage EPD, the potential-induced electrophoresis decreases with increasing deposition on the electrode. This voltage drop across the electrodes hence results in decrease in the current density and, hence, in the deposition rate. Sarkar [Sarkar P.-1996] and others [Ma J.-2002] explained that this phenomenon in constant voltage EPD is mainly due to the building up of the insulating ceramic layer on the electrode as the deposition progresses.

From these variations the deposit thickness can be simply controlled by the variation of the deposition time at constant applied voltage.

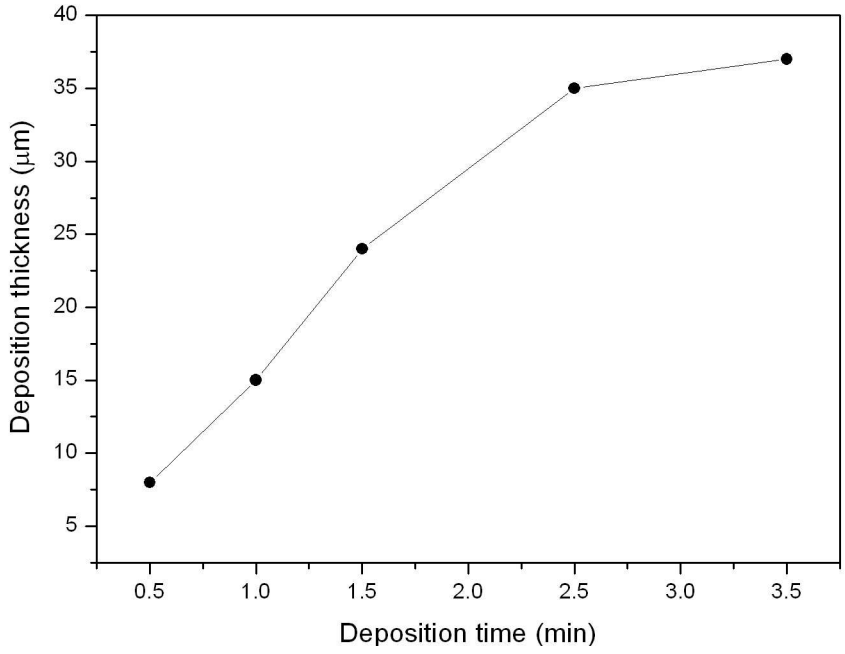

Figure 5.2-10 Deposition thickness versus deposition time in acetone with I_2 based suspensions

The operational pH in acetone based suspension was optimised based on the zeta potential curve (Figure 5.2-1). The surface of sintered BNT films deposited at 5.33, 2.34 and 1.43 operational pH of these suspensions is depicted in Figure 5.2-11. At high operational pH of 5.33, a quite porous microstructure is observed. As the operational pH value decreases to 2.34, a much denser and homogeneous BNT films is obtained, as shown in Figure 5.2-11 (b). It is worthwhile to note that this operational pH value, corresponds to the highest zeta potential. As the operational pH value continues to decrease to 1.3, a porous microstructure for the BNT films appeared again (Figure 5.2-11 (c). The results are summarised in Table 5.2-2. The deposition quality of the film is indeed consistent with the zeta potential of the suspension used in the preparation.

Table 5.2-2 Deposition quality at various operational pH

pH	Zeta potential (mV)	Deposition quality
<2	56.97	not uniform
3	61.47	uniform
4	51.27	uniform
>5	7.04	not uniform

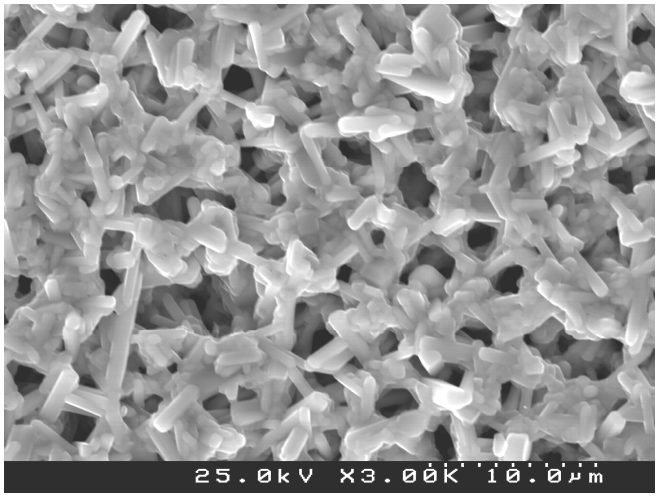

(a)

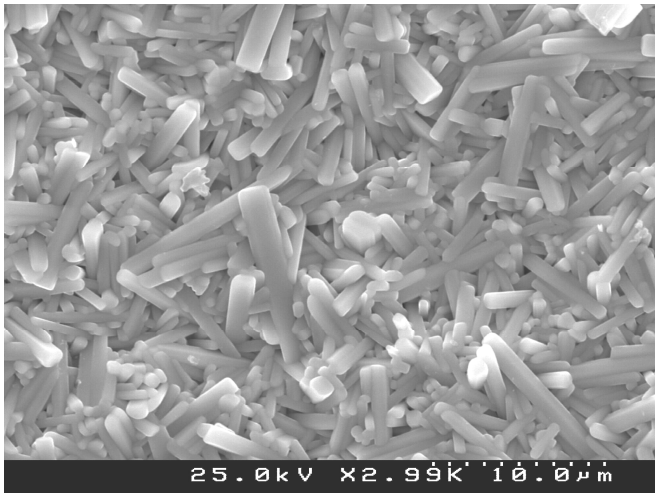

(b)

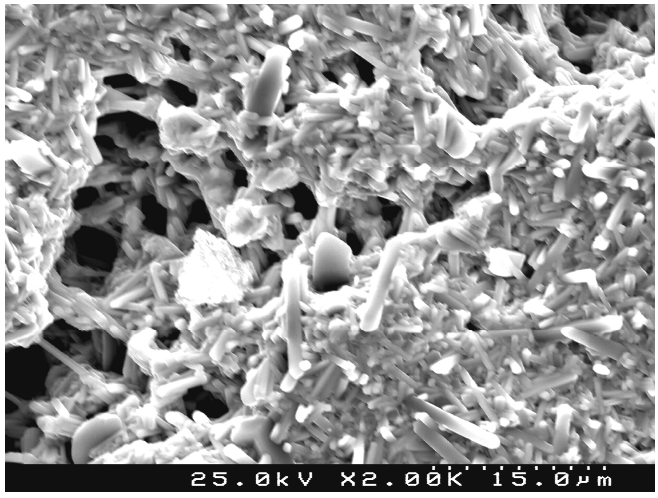

(c)

Figure 5.2-11 SEM micrographs of as BNT films deposited at operational pH of (a) 5.33, (b) 2.34 and (c) 1.43 in acetone with I_2 suspension and sintered at 1300 °C/1h

The driving force for EPD process is the electric field between the two electrodes and therefore it is important to know the effect of the applied voltage on the deposition performance. EPD of thick BNT films under constant applied voltage was performed and the effect of applied voltage on deposited mass was investigated. From Figure 5.2-12 one can see that, for the same initial particle concentration in the suspension, as the applied voltage increases the deposited thickness increases. However, the observed relation is not linear; for the case under study when the applied field exceeds 240 V there is a drop in the thickness deposited mass.

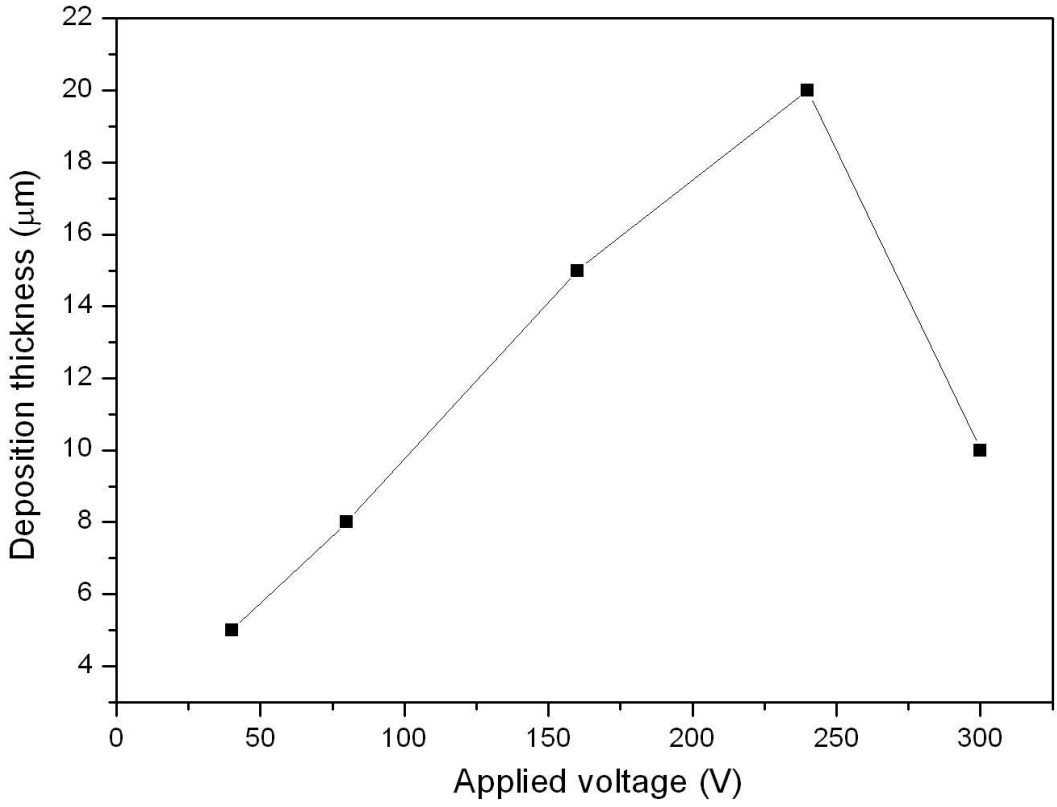

Figure 5.2-12 Deposition thickness of BNT films as a function of applied voltage in acetone with I_2 based suspension and 1 min deposition

The observed deterioration of the deposited thickness as the applied voltage increases above a certain value can be due to the high driving forces of the particles at high fields. Under these conditions the deposited mass is limited and the deposited layer is heterogeneous resulting in a lower powder packing density. 200 V is the adequate applied voltage for the present case.

Based on this set of experimental results the optimal conditions for EPD of BNT

powders were identified as: i) suspension media: acetone wit I_2, at pH: 2-3 and ii) applied voltage: 200 V. Using these parameters, high-quality, uniform BNT films on Pt foils were obtained.

The structure of sintered BNT thick films was analysed by XRD. Figure 5.2-13 illustrates the X-ray diffraction patterns of BNT films sintered at 1300 °C/1h and of the starting BNT powders for comparison. The BNT films exhibit a well-crystallized orthorhombic structure phase, and all the diffraction peaks are identified as belonging to $BaNd_2Ti_5O_{14}$ (JCPDS card 33-0166). No second phases were detected within the equipment detection limits and no detectable alteration of the materials structure occurred for sintered BNT thick films when comparing with the starting powders.

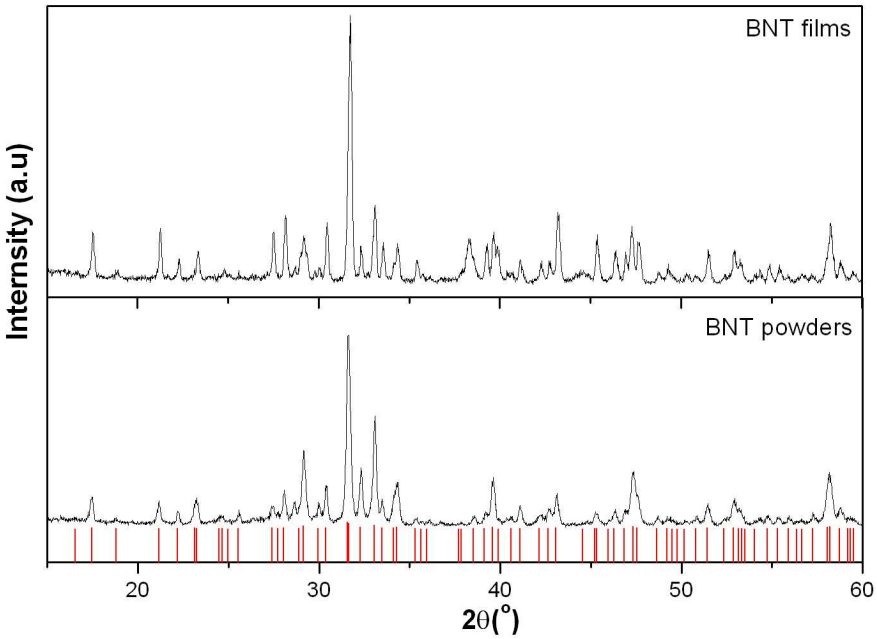

Figure 5.2-13 XRD patterns of BNT powders and films deposited from acetone with I_2 based suspension and sintered at 1300 °C/1h (XRD spectra lines for the JCPDS card 33-0166 are indicated at the bottom of the figure)

5.2.3.5 Dielectric properties

BNT films deposited from ethanol and acetone with I_2 based suspensions were chosen to study the effect of the suspension media on the dielectric properties of BNT films. This choice was related to the fact that under optimised conditions there is a little difference in the final quality of the films derived from acetic acid and acetone with I_2.

Figure 5.2-14 represents the frequency dependence of the relative permittivity and loss tangent of BNT thick films derived from ethanol and acetone with I_2 based

suspensions. At 1 MHz, the relative permittivity films is 96 and 62, the loss tangent is 0.0005 and 0.01 for BNT thick films derived from acetone with I_2 and ethanol based suspensions, respectively. As expected BNT thick films derived from acetone with I_2 suspensions exhibit enhanced electrical performance what is related with the more dense and homogeneous microstructure of these films when compared with those prepared from ethanol suspensions. (Figure 5.2-5)

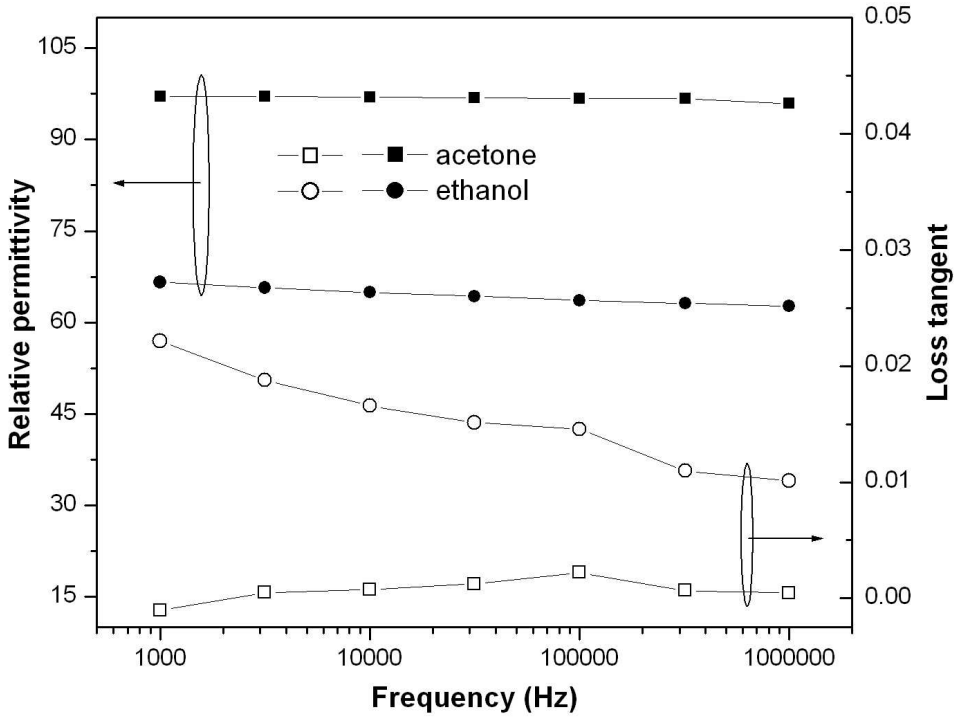

Figure 5.2-14 Relative permittivity and loss tangent of BNT films deposited from ethanol and acetone with I_2 based suspension as a function of frequency and sintered at 1300 °C/1h

5.2.4 Discussions

In this work the suspension stability was analysed in terms of zeta potential, particle size distribution and suspension transmittance (Figures 5.2-1, 2 and 3). The highest absolute zeta potential determined values are 61, 48, 41 and 17 for the acetone with I_2, ethanol, acetic acid and water suspensions, respectively, which are in agreement with the high stability and dispersibility, small particle size and narrow particle size distribution and low UV light transmittance of the acetone with I_2 suspension. So, according to Table 5.2-1, acetone with I_2 based suspensions correspond to the group of suspensions with excellent stability. Indeed the best films in terms of microstructure,

densification and dielectric properties were obtained with these suspensions.

5.2.4.1 Limitation of acetic acid based suspensions

Although acetic acid based suspensions can also be used for EPD of BNT materials, the reliability and reproducibility of the deposition was verified to be hard to control, limiting its utilization.

It was found that the current flow through the suspension markedly increases as the deposition times increases (Figure 5.2-7). Meanwhile as the aging time increases the leaching of metallic elements occurs (Figure 5.2-9). In the suspension of BNT powders dispersed in glacial acetic acid, barium ions on the surface of the BNT powder will react with the acid to form barium acetate and water, according to the reaction:

$$Ba^{2+} + 2CH_3COOH + 2OH^- \rightarrow Ba(COOCH_3)_2 + 2H_2O \qquad (5.2\text{-}1)$$

similar reactions occur between Nd^{2+} and Ti^{4+} ions and acetic acid.

Water is an electrolyte and undergoes electrolysis under the electric field that together with the increasing content of leached ions, causes the increase of the content of free ionic species and the current flow in the suspension, as observed in Figures 5.2-7, and 8. Concomitantly, as the EPD process continues and the electric field promotes the dissolution of BNT powders, the quality of the deposited films is markedly degraded.

At the initial stages of EPD, the double layer surrounding the dispersed particles is not greatly affected and particles remain well dispersed. The current flow through the suspension is very small during EPD and, consequently, a uniform deposition with high deposition mass rate is observed for the first depositions (Figure 5.2-6). As the EPD cycles proceed and the concentration of free ionic species in the suspension increases the level of particle agglomeration increases, the rate of deposited mass decreases and the quality of the deposited layers degrades.

According to the DLVO theory [Derjaguin B. V. -1941, Verwey E. J. W. -1948], the thickness of the double layer surrounding the particles characterized by the Debye length, is very sensitive to the electrolyte concentration. It is demonstrated that the potential energy peak decreases as the electrolyte concentration increases and as the energy barrier disappears, coagulation becomes favourable. In acetic acid based suspensions, the increase of water and leached metal ions increases the electrolyte concentration and causes the coagulation of particles. The same phenomenon was also

reported for EPD of PZT in acetic acid and other systems. [Wu A.Y.-2006, Biesheuvel P. M. -1999, Tassel J. V. -2004]

The increasing content of the leached elements and water, formed as a reaction by-product, are responsible for the observed augment of the current, and, as a consequence, for the gradual increase of the suspension instability. [Winslow W. M -1949]. These observations explained why EPD of BNT gradually degrades in acetic acid as the deposition times increases, as shown in Figure 5.2-6.

Although the leaching of the metallic elements is observed in acetone with I_2 suspensions as well, the content of leached elements is residual being 14 times smaller than in the acetic acid based suspension, and accordingly the variation of the current in the suspension is also inferior. At the same time the current loop presents the opposite behaviour to the one observed in acetic acid based suspensions, in which an increase of the current is verified for the reversed curve (Figure 5.2-8 (a)). This observation strongly supports the above presented explanation. The lower values of the current for the case of acetone with I_2 based suspensions indicate the absence of excess of free carriers in the suspension, as the EPD cycles proceed; as a consequence there is no visible degradation of the EPD performance during deposition in acetone with I_2 suspensions when compared with the observed for the acetic acid based suspensions.

It is then demonstrated that the aging of the acetic acid based suspension have quite negative effects on the EPD process of BNT materials, such as, leaching of the metallic elements with a consequent modification of the material stoichiometry and formation of water with associated formation of bubbles and degradation of the film compactness. These facts severely restrict the use of acetic acid for an industrial application. Compared with acetic acid based suspension, it was then identified that acetone with I_2 is the proper suspension media to perform EPD of BNT powders.

5.2.4.2 Role of iodine

BNT powders develop a positive surface charge in pure acetone (Figure 5.2-1). Due to the very week acidity of acetone in relation to water, thus generating a limited proton concentration in the solvent which adsorbs preferentially at the powder surface, in pure acetone most of the powder sediments immediately. This means that pure acetone is insufficient to stabilize and charge BNT powders for EPD.

A considerably more stable suspension is produced by adding a small amount of iodine solution. I_2 in acetone based suspensions was referred to be an effective additive

to disperse ceramic PZT, BST, YSZ, and YBCO for EPD process. [Nicholson P. S -1993, Zhitomirsky I.-1998] Iodine dissolves rapidly in iso-propanol where it reacts producing positively and negatively charged ions, according to the following equation: [Mathews T. -2000]

$$CH_3CHOHCH_3 + I_2 \rightarrow CH_3CHOICH_3 + H^+ + I^- \qquad (5.2\text{-}2)$$

it is then suggested that the protons generated by the above reaction are adsorbed on the surface of the suspended BNT particles, making them positively charged and enhancing the electrostatic repulsion force (Figure 5.2-1). Indeed, it can be seen that as the operational pH value decreases from 6.5 to 2.3, the value of the zeta potential increases considerably from 7 to 61 mV. However, as more iodine is added to the suspension, i.e., when operational pH value decreases from 2.3 to 1.4, the large amount of the free positive charges results in the reduction of the double layer thickness and, hence, in the decrease of the zeta potential to the value 51 mV.

In EPD the application of a dc field forces the positively charged BNT particles to move towards and deposited on the cathode. The deposited mass on the substrate is almost zero in the acetone based BNT suspension without I_2. For pH>5, a small amount of H^+ ions in the suspension is produced, the zeta potential is low, the suspensions are insufficiently dispersed and the transported mass is limited resulting in thin, porous and not homogeneous films (Figure 5.2-11). Indeed it is known that if the zeta potential is low, the particles tend to coagulate even for relative large inter-particle distances, leading to porous and sponge-like deposits. On the contrary the deposited mass increased rapidly with the addition of iodine, in a good agreement with the results of the zeta potential variation. If the particles have a high zeta potential, during the deposition the existing repulsive forces will keep them apart leading to a high particle packing density of the compact [Krueger H. G. -2004].

While the suspension stability is directly dependent on the zeta potential, which is determined in this case by the iodine addition, iodine content also affects the ionic conductivity of the suspension. And the ionic conductivity determines the interaction energy between the suspended particles in the bulk of the suspension, which influence the stability and dispersibility of the suspensions. With too much I_2 (at pH<2), the high ionic concentration results in the reduction of the double layer thickness of the BNT particles and in the drop of zeta potential (figure 5.2-2), which in turns results in particle

coagulation and sedimentation. The colloid particles experience no repulsive force in a high ionic strength. Under such circumstances, fast coagulation occurs and the system is completely unstable resulting in a low quality of the deposition.

As a result, the iodine concentration chosen for an operational pH of the suspensions was around 2-3, for which the highest zeta potential values and uniform depositions were obtained. Similar observations were found for the EPD of different materials. [Chen C. Y. -1999, Bouyer F.-1999]

5.2.4.3 Effect of deposition time and applied voltage

For the same initial powder concentration in the suspension, the yield of deposition increases as the dc voltage and deposition time increases. The relationship between deposition mass and dc voltage or deposition time fits a linear relationship. This yield of deposition varies linearly with the applied field and deposition time according to Hamaker's equation [Hamaker H. C. -1940]

$$M = \int_0^t aACm E dt \qquad (5.2\text{-}3)$$

where M stands for the mass deposited in time t (s), C for the particle concentration in the suspension (kg/m^3), E for the electric field (V/m), A for the electrode area (m^2), m for the electrophoretic mobility (m^2 /Vs), and a stands for a coefficient representing the fraction of particles deposited near the electrode.

In this work it was found that for fixed applied field the deposition becomes slower and slower with increased or prolonged deposition times (Figure 5.2-10). Similar observations were also reported by Chen et al [Chen F. L.-2001] for the deposition of YSZ. The relation between the deposited mass and the deposition time is linear for initial periods of deposition, but as the deposition time increases, the deposition decreases and attains a plateau at very high deposition times. In a constant voltage EPD, this is expected because while the potential difference between the electrodes is maintained constant, the electric field decreases with the deposition time due to the formation of an insulating layer of deposited particles on the electrode surface. [Zhitomirsky I.-1997] The decrease in the effective field strength during the EPD can be avoided under constant current conditions.

The other parameter that will also affect the mass deposition rate and which may

change during the course of the deposition is the solid content of the suspension. If the solid content is not kept constant, for example by a continuous inflow and outflow of the suspension, the decreasing powder concentration with time results in a decreasing deposition rate.

Because high applied electrical fields increase the particle flux and movement towards the counter electrode, the applied field affects the deposition rate and the structure of the deposit also. Normally the amount of deposited powders increases with the increase of the applied potential (Figure 5.2-12). In the meantime, for the present case, the deposited film thickness dropped when the applied voltage is increased from 240 to 300V what can be due to interactions between the particles and local turbulence in the suspension created under very high driving forces. Under these conditions the highly mobile particles will find difficulties in moving steadily towards the counter electrode and “sit and rest” on the substrate to form a close packed green structure. Under high electric fields the deposition process was greatly affected, a high level of non-uniformity developed and porous deposits were formed. Similar observations were reported for the deposition of zirconia electrolyte films in acetic acid [Basu R. N.-2001] and nanosized cordierite powders [Kaya C.-2002], in which more uniform films were deposited at moderate applied fields, whereas the film quality deteriorates if relatively high applied electric fields were used.

On the other hand, at very low applied voltage (40 V) porous BNT films are obtained. For voltage < 40 V the adherence is not acceptable and the deposits are partially washed away as the cathode is being extracted from the cell. This very porous microstructure can be attributed to the weak adherence of the deposit to the electrode under very low voltages. In the current work the adherence of the deposit to the cathode is adequate for voltage > 80 V.

According to above analysis of the applied voltage effect, an optimised uniform deposition is achieved for BNT acetone with I_2 within about 200 volt.

5.2.5 Summary

Suspension stability and zeta potential from different organic suspensions reveal that the suspension composition determines whether a deposition occurs at the electrode or not. Among the studied suspension medias, acetone with I_2 was found to be a suitable suspension media for the EPD of BNT thick films. Under the present conditions the results obtained in this work indicate that the acetone with I_2 - iso-propanol system is an

effective suspension media for the deposition of low loss BNT thick films. The limitation of acetic acid is related to the instability of the BNT suspension with the time and during the course of EPD. Owing to the more uniform, homogeneous and dense microstructure, BNT films deposited from acetone with I_2 based suspensions show higher relative permittivity and lower loss tangent than from ethanol based suspension.

The EPD parameters, i.e. applied voltage of about 200 V and I_2 concentration at operational pH of 2-3, were optimised to obtain high quality, uniformly deposited BNT films in acetone based suspensions.

5.2.6 References

1. Basu R. N., Randall C. A and Mayo M. J. (2001) J. Am. Ceram. Soc. **84**, 33
2. Biesheuvel P. M., Verweij H. (1999) J. Am. Ceram. Soc. **82,** 1451
3. Bouyer F. and Foissy A. (1999) J. Am. Ceram. Soc. **82**, 2001
4. Chen C. Y., Chen S. Y. and Liu D. M. (1999 Acta. Mater. **47**, 2717
5. Chen F. L. and Liu M. L. (2001) J. Euro. Ceram. Soc. **21**, 127
6. Derjaguin B. V., Landau L. (1941) Acta Physicochim. USSR **14**, 633
7. Hamaker H. C. (1940)Trans Farad Soc **36**, 279
8. Kaya C., Kaya F. and Boccaccini A. R. (2002) J. Mater. Sci. **37**, 4145
9. Krueger H. G., Knote A., Schindler U., Kern H. and Boccaccini A. (2004) J. Mater. Sci. **39**, 839
10. Ma J. and Cheng W. (2002) J. Am. Ceram. Soc. **85**, 1735
11. Mathews T., Rabu N., Sellar J. R., Muddle B. C. (2000) Solid State Ionics **128**, 111
12. Negishi H., Yamaji K., Sakai N., Hopita T., Yanagishita H., Yokokawa H. (2004) J. Mater. Sci. **39**, 833
13. Nicholson P. S., Sarkar P., Huang X. (1993) J. Mater. Sci. **28**, 6274
14. Sarkar P. and Nicholson P. S. (1996) J. Am. Ceram. Soc. **79**, 1987
15. Tassel J. V. (2004) PhD thesis, Pennsylvania state university, USA
16. Verwey E. J. W. and Overbeek J. T. G. (1948) Theory of the stability of Lyophobic colloids, Elsevier, Amsterdam
17. Wu A. Y., Vilarinho P. M. and Kingon A. I. (2006) J. Am. Ceram. Soc. **89**, 575
18. Winslow W. M. (1949) J. Appl. Phys. **20**, 1137
19. Xu Z. G., Rajaram G., Sankar J., Pai D. (2006) Surface & Coatings Tech. **201**, 4484
20. Zhitomirsky I. (1998) J. Mater. Sci. Lett. **17**, 2101
21. Zhitomirsky I., Petric A. (2004) J. Mater. Sci. **39**, 825
22. Zarbov M., Brandon D., Cohen N. and Shemesh E. L. (2006) J. Mater. Sci. **41**, 8115
23. Zhitomirsky I. and Gal L. (1997) J. Mater. Sci.: Mater. Med. **8**, 213

5.3 Effect of Sintering Temperature on the Structure, Microstructure and Dielectric Properties of $BaNd_2Ti_5O_{14}$ Thick Films

Abstract:

In this chapter, the effect of the sintering temperature on the structure, microstructure and dielectric properties of BNT thick films is studied. An alternative approach to tailor the temperature coefficient of the relative permittivity ($TC\varepsilon_r$) of low loss BNT dielectric thick films is presented. The anisotropic grain growth observed in these BNT thick films is facilitated by a constrained sintering. The increase of the sintering temperature markedly increases the aspect ratio of the grains, decreases the relative permittivity and $TC\varepsilon_r$ changes from -114 to +12 ppm/°C. By controlling the sintering temperature, near zero $TC\varepsilon_r$, high Q thick films can be fabricated with $45< \varepsilon_r<70$. These findings are of technological relevance since they demonstrate that the control of the substrate constraint and of the sintering conditions can be used to control the grain anisotropy and thus the dielectric properties of BNT thick films.

5.3.1 Introduction

Compared with the corresponding BNT ceramics, BNT thick films sintered under the same conditions and at 1300 ºC, exhibit an obvious textured microstructure characterised by markedly elongated grains (Figure 5.1-8). Because the microstructure of ceramics has an important impact on their final properties, the reasons for this elongated grained microstructure and its relation with the dielectric response, need to be understood and is the subject of the study of this chapter.

As reviewed in chapter 1, $BaO\text{-}Re_2O_3\text{-}TiO_2$ (Re-rare earth elements, e.g. Nd, Sm, La, Pr) materials (BRT) possess a tungsten bronze type structure with an orthorhombic unit cell (space group-$Pb2_1m$, No.26). [Ubic R. -1998] The framework of the corner-sharing TiO_6 octahedral in the ab-basal plane links along the c-axis with zigzag tilting. [Varfolomeev M. B. -1988] As a result of the anisotropic crystal structure BRT ceramics (and crystals) tend to exhibit, in particular processing conditions, the development of needle-like or elongated shaped grains, which grow along the preferred c-axis orientation. In the XRD pattern of these anisotropic polycrystalline ceramics the (hk0) diffractions will be stronger than the other diffractions. However, the consistent

presence of elongated grains in EPD films (sintered at 1300 ºC / 1h) and the equiaxed grains observed in the corresponding BNT ceramics, [Fu Z.-2007] implies that other aspects should be considered beyond the crystal structure, in order to understand the causes for the elongated grain growth of BNT films.

This chapter therefore investigates the impact of three effects on the anisotropic microstructure development of BNT films and thereby on the properties. These effects are: 1) the electric field used for EPD, 2) the substrate and 3) the sintering temperature. This knowledge will allow the tuning of the microstructure in order to optimise the final properties.

EPD derived BNT thick films were then prepared under different processing conditions to inspect the above effects on the evolution of the textured microstructure. The reasons behind the observed textured microstructure, the dependence on the processing parameters and the relations with the final dielectric properties are presented and discussed. Ultimately this chapter presents an alternative approach to control the $TC\varepsilon_r$ of high *Q* materials that, when combined with the possibility to scale down the size of the device, may be of practical utility.

5.3.2 Experimental

In this chapter, all the BNT films are prepared form home made powders and sintered between 1300 to 1450 °C for 1 h. In order to compare the final properties with those of BNT films, BNT ceramics were prepared and sintered at 1450 ºC /1h as well. The experimental details are as described in Chapter 4.

To exclude the effect of the electric field during the EPD process, BNT films were also prepared by the dip-coating technique, using the same suspension utilised in the EPD process. In addition, to further investigate the effect of the substrate a carbon layer was deposited on the top of some Pt substrates by dc sputtering that are then used to prepared partially “free-standing” sintered BNT films to be compared with constrained sintered ones. For more details about the deposition of graphite layer can be consulted in Chapter 4.

5.3.3 Results

5.3.3.1 Effect of the electric field

The electric field used during EPD is a possible cause for the development of textured growth on BNT materials. To clarify this effect BNT thick film were prepared

under different dc voltages.

Figure 5.3-1 shows the SEM micrographs of fractured surfaces of BNT films deposited at 40, 200 and 600 V and sintered at 1300 ºC / 1h. The microstructures are characterised by elongated shaped grains and some intergranular porosity. As observed there is no obvious difference in terms of grain size, grain shape or aspect ratio between the microstructure of the films prepared under different voltages, indicating a negligible effect of the voltage on the textured microstructure development.

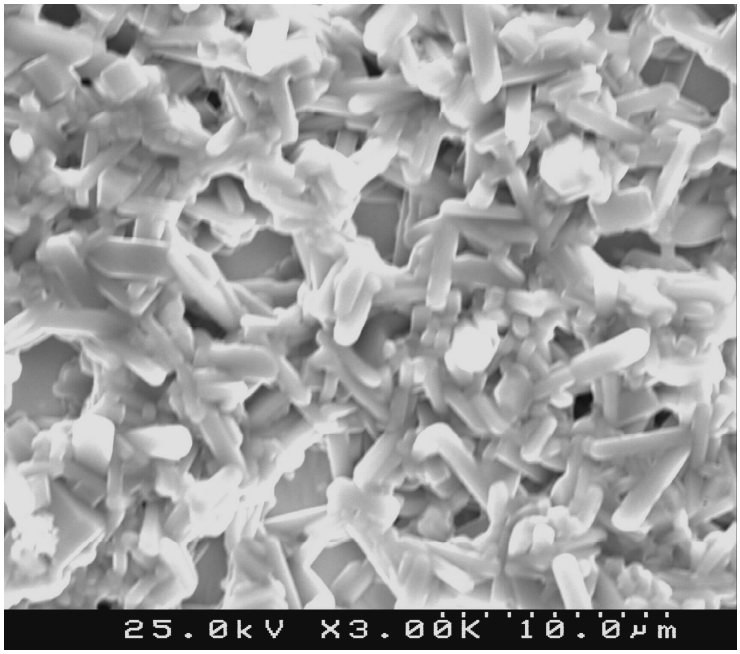

(a)

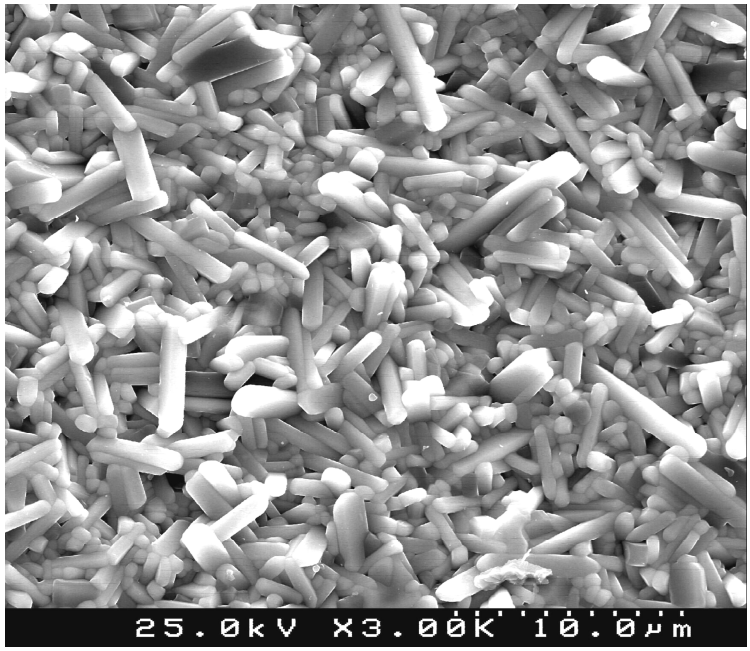

(b)

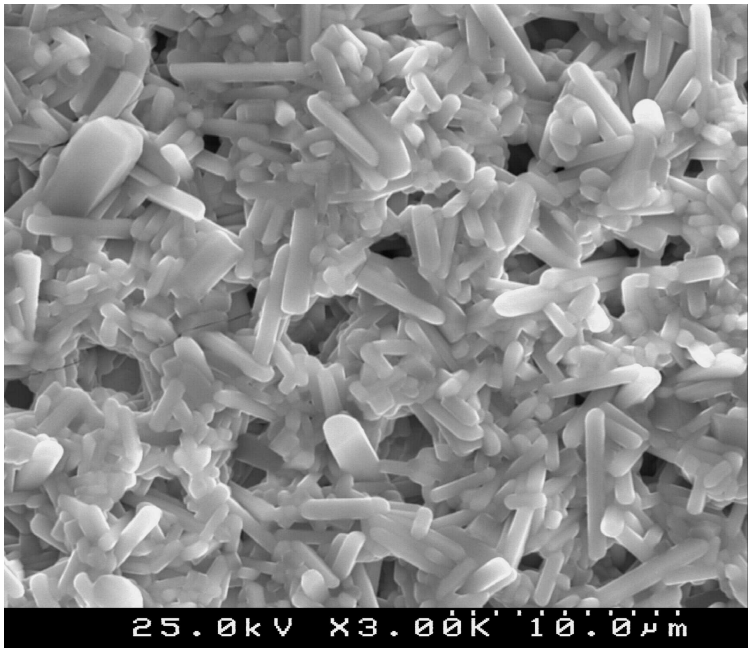

(c)

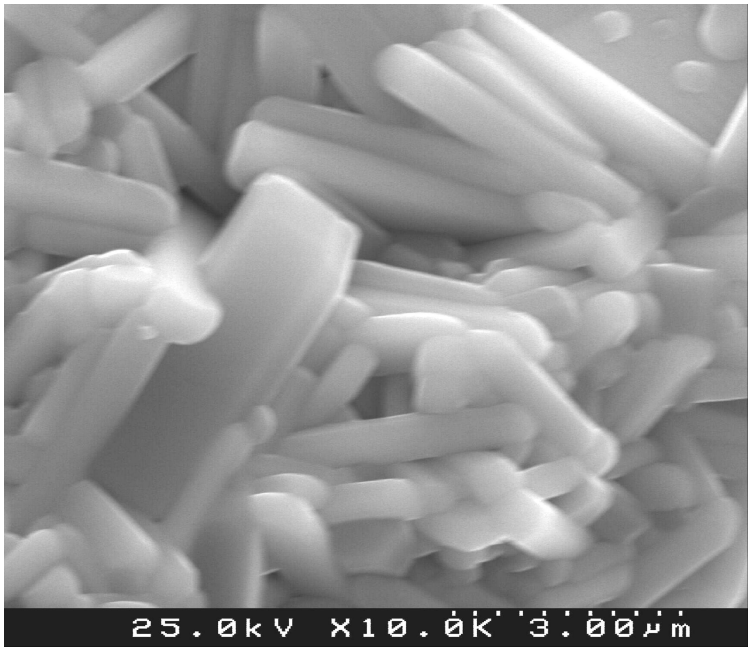

(d)

Figure 5.3-1 SEM micrographs of fractured surfaces of BNT films deposited under (a) 40V, (b) 200V, (c) 600V, and (d) by dip-coating and sintered at 1300 ºC / 1h.

The effect of the electric field was further analysed, by reducing it to zero. BNT films were prepared by dip coating to exclude the effect of the electric field. SEM fractured surface image of dip-coated BNT films sintered at 1300 ºC for 1h is also

depicted in Figure 5.3-1 (d). No significant differences are detected in the microstructure of these films; elongated grains very similar to the ones observed in EPD films characterise the microstructure of dip-coated BNT films. These results confirm that the electric field used in the EPD process has no significant influence on the textured microstructure development of BNT thick films. Based on previous and above observations 200 V was selected as the operational voltage for the fabrication of the films in this study.

5.3.3.2 Effect of the substrate

Compared with the ceramics, films are 2-dimensional structures, meaning that the densification process is not free in the directions of the plane as in the bulk materials, but instead is a constrained process in which films shrink preferentially along the out of-plane direction and differently from the in-plane direction. The clamping effect of the substrate on the film and the resultant mechanical stresses, induced by the different thermal expansion coefficient and lattice parameters between BNT films and the substrate and aroused during the sintering step, may also affect the microstructure development.

In order to remove or decrease the effect of the substrate a carbon buffer layer was deposited on the top of the Pt foil. During the sintering step the carbon interlayer is burnt out causing an intermediate free-floating stage during which the film sinters unconstrained and independently from the substrate. Figure 5.3-2 compares the microstructures of fractured surfaces of BNT films deposited onto carbon coated Pt and bare Pt substrates and sintered at 1350 °C/1h. As shown in the Figure 5.3-2, BNT films on bare Pt substrates present higher aspect ratio of the elongated grains than those observed on the carbon coated Pt substrate. The aspect ratio of elongated grains increased from 6 for BNT films on carbon-coated substrates to 8 for films on bare Pt ones. The aspect ratio, defined as the quotient between the length and the diameter of each grain, was computed using an imagine analysis software (analySIS 3.2) and lengths and widths of around 100 grains from several SEM micrographs were measured and average values computed. Though the difference in these aspects ratios is rather small due to the fact that the constrained effect is not completely removed (the removal of constraint is only partial and occurs primarily below 1000 ºC, and grain growth occurs predominantly during the last stages of the sintering process), these results point to the origin of the effect and suggest that the elongated texture is related to the

substrate and favoured by the constrained sintering.

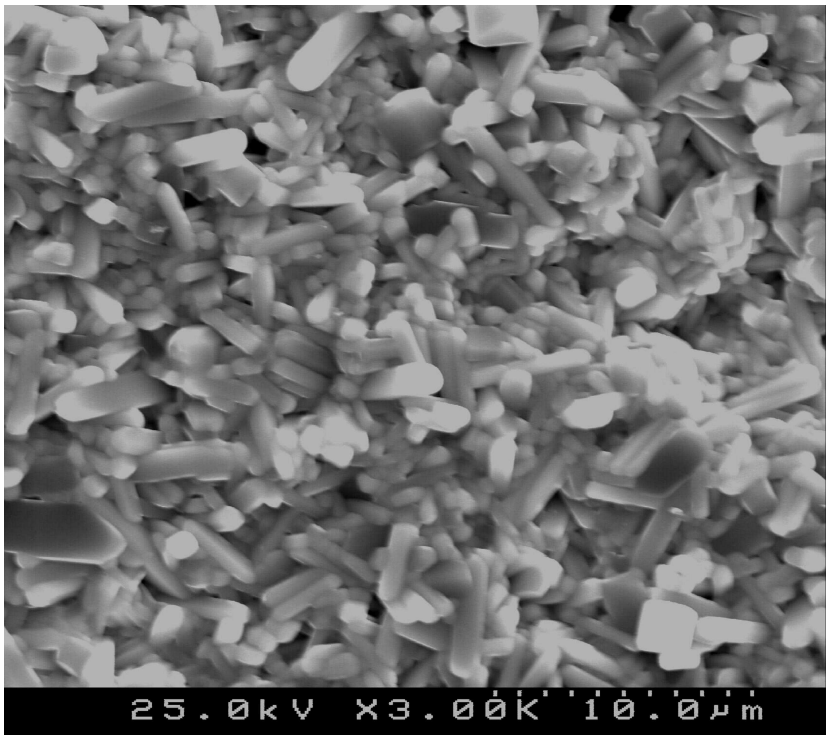

(a)

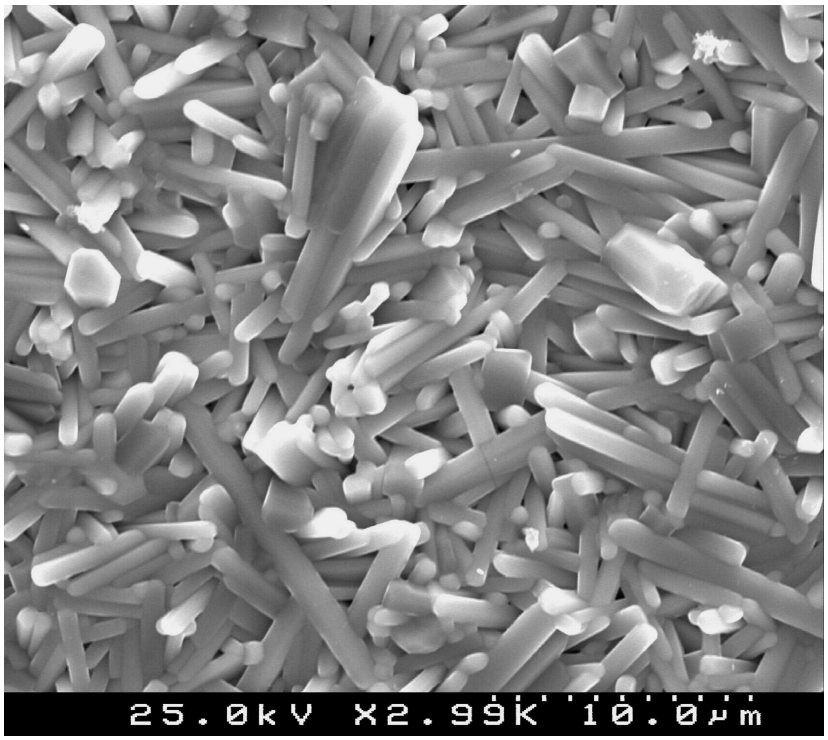

(b)

Figure 5.3-2 SEM micrographs of fractured BNT films sintered at 1350 ºC / 1h on (a) carbon coated Pt substrate and (b) pure Pt substrate

5.3.3.3 Effect of the sintering conditions

The influence of the sintering temperature on the microstructure evolution was then analyzed. SEM images of fractured and polished / thermal etched surfaces and polished cross sections of BNT films sintered at different temperatures are depicted in Figures 5.3-3 and 4. Anisotropic elongated grains are well developed in all the microstructures, but enhanced as the sintering temperature increases. After sintering at 1300 ºC the films present some porosity. As the temperature increases the elongation of the grains increases markedly, being maximised for the films sintered at 1450 ºC. From the surface images grain aspect ratio is calculated to quantify the texture degree of the films and the results are indicated in Table 5.3-1. The aspect ratio is increased from 5 to 23 when the sintering temperature is increased from 1300 to 1450 ºC, in agreement with the observations. This increment is more pronounced for the high sintering temperatures. The aspect ratio varied from 5 to 8 for films sintered at 1300 and 1350 ºC and from 8 to 18 for the films sintered at 1350 and 1400 ºC, respectively, which clearly indicates the strong dependence of the textured microstructure of BNT thick films on the sintering temperature.

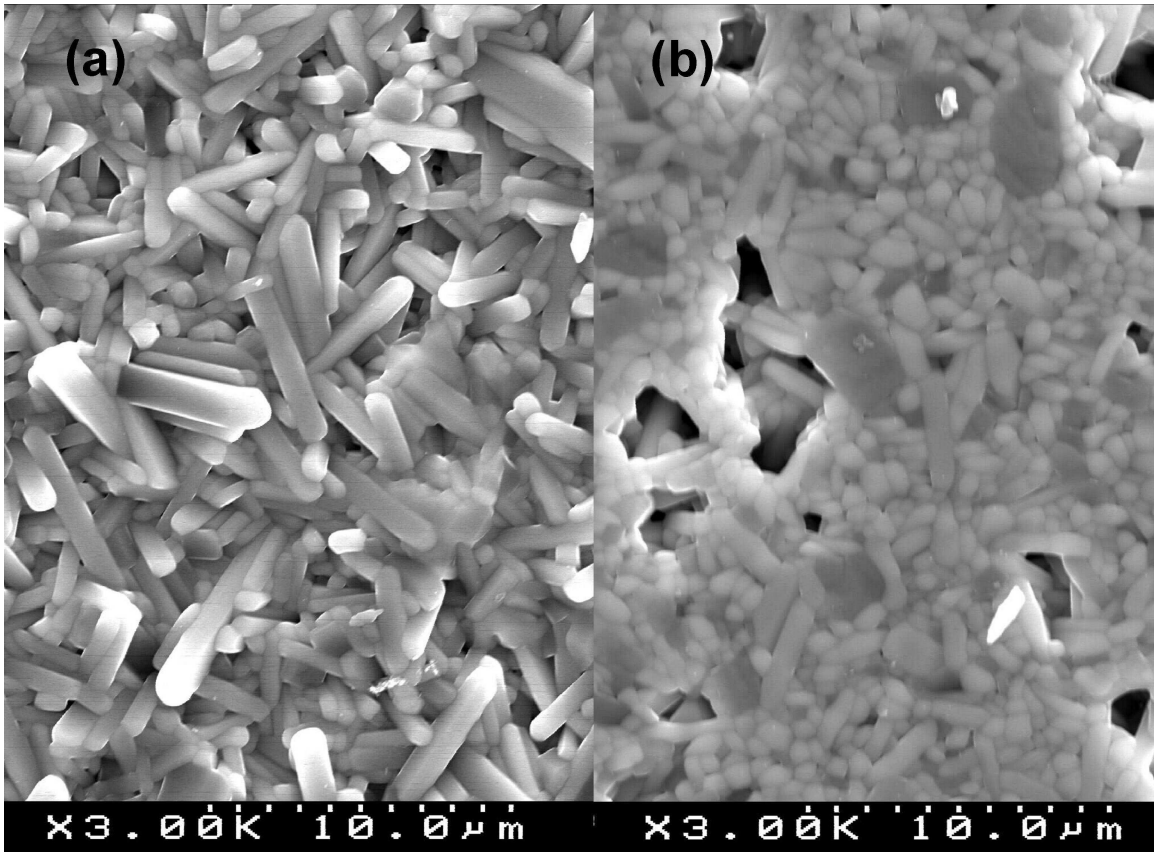

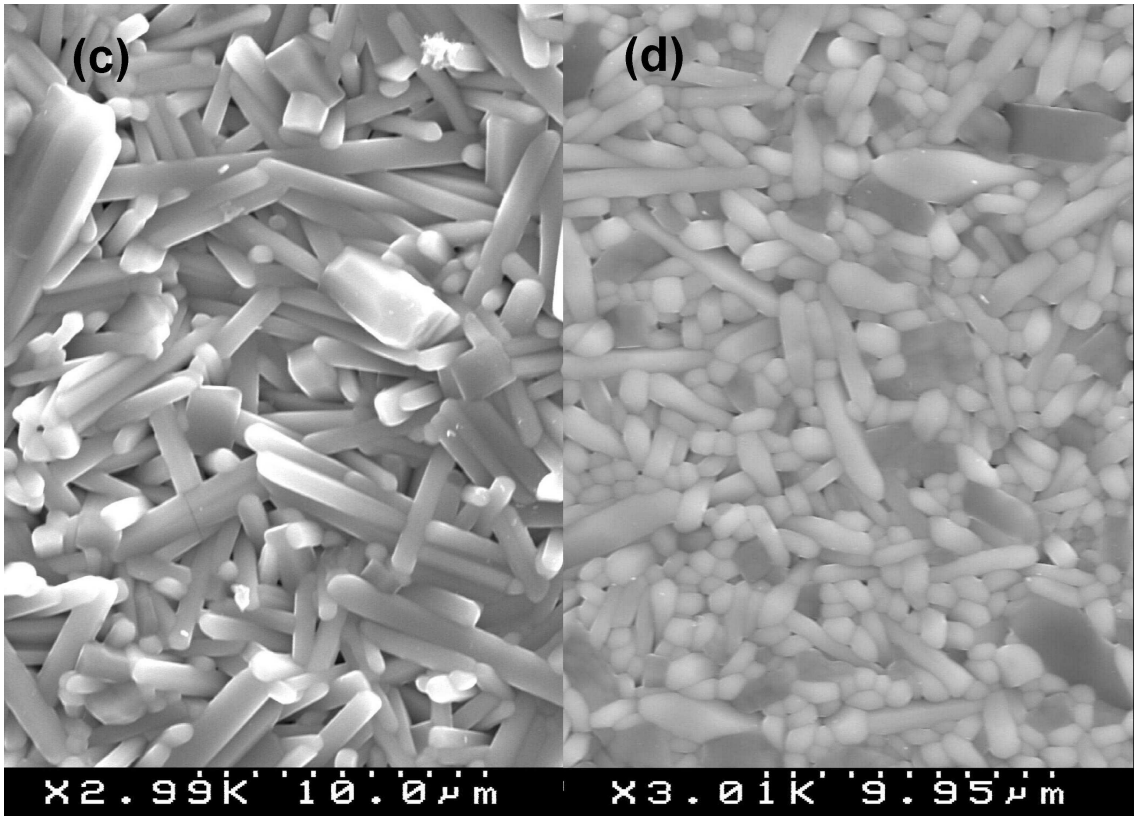
(c)
(d)
X2.99K 10.0µm
X3.01K 9.95µm

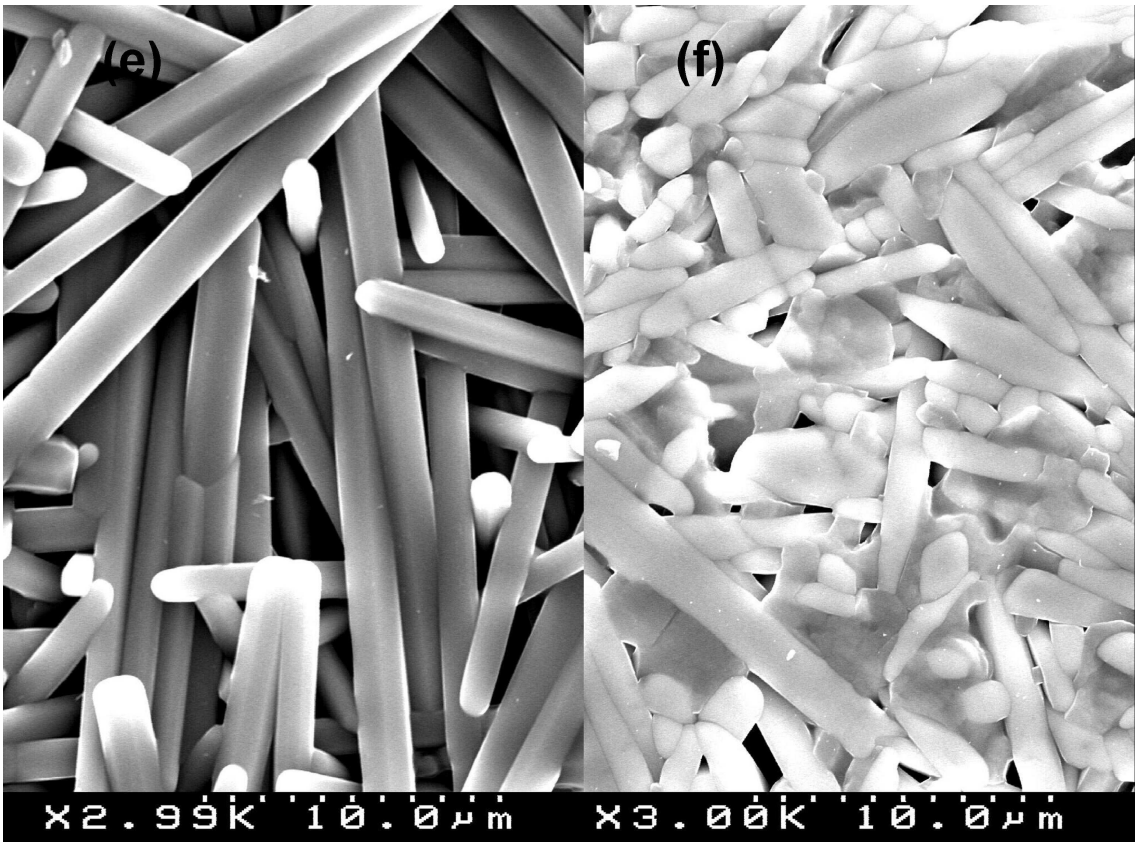
(e)
(f)
X2.99K 10.0µm
X3.00K 10.0µm

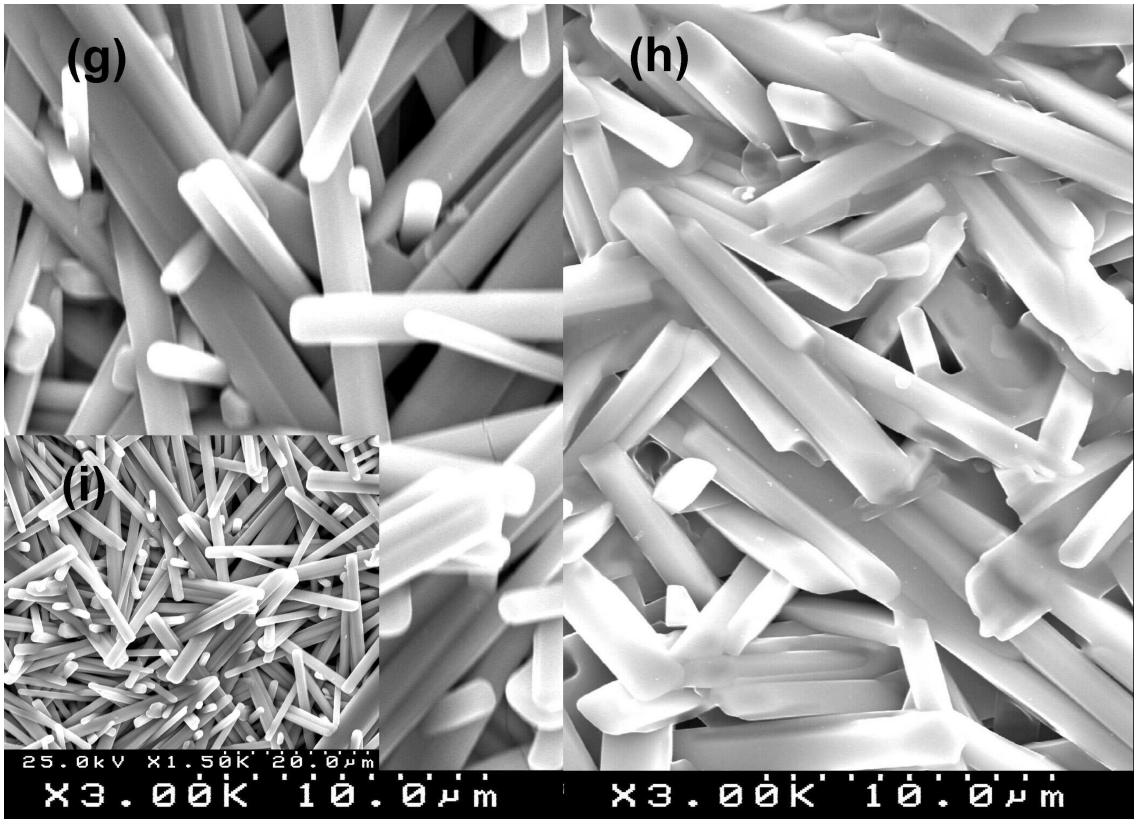

Figure 5.3-3 SEM micrographs of fractured (a, c, e, g) and polished and etched (b, d, f, h) BNT films sintered at various temperatures for 1 hour: 1300 ºC (a and b), 1350 ºC (c and d), 1400 ºC (e and f) and 1450 ºC (g, h and i). A low magnification of the films sintered at 1450 ºC is also presented (i)

Table 5.3-1 Aspect ratio of BNT films versus the sintering conditions

Sintering condition	1300 ^{o}C/1h	1350 ^{o}C/1h	1400 ^{o}C/1h	1450 ^{o}C/1h
Aspect ratio	5	8	18	23

From the polished cross sections of the films sintered between 1300 and 1450 ºC, a high degree of compactness with only remaining porosity is clearly seen from these images for all the films (Figure 5.3-4). As the sintering temperature increases the porosity decreases, being “residual” for the films sintered at 1400 and 1450 ºC. Corroborating the plane view images the SEM micrograph of the cross section of the film sintered at 1450 ºC (Figure 5.3-4 (d)) depicts a very dense microstructure in which the elongated grains are mainly lying in plane (parallel to the substrate). In addition it is obviously seen from these cross sections that the films have a good adhesion to the substrate, the interface between the film and the substrate is clear and no particular defects /effects are observed. For a more careful analysis of the interfaces TEM analysis

were conducted in some of the samples and the absence of interfacial reactions proved. As indicated in Figure 5.3-5, the interface between BNT and Pt is clear and clean.

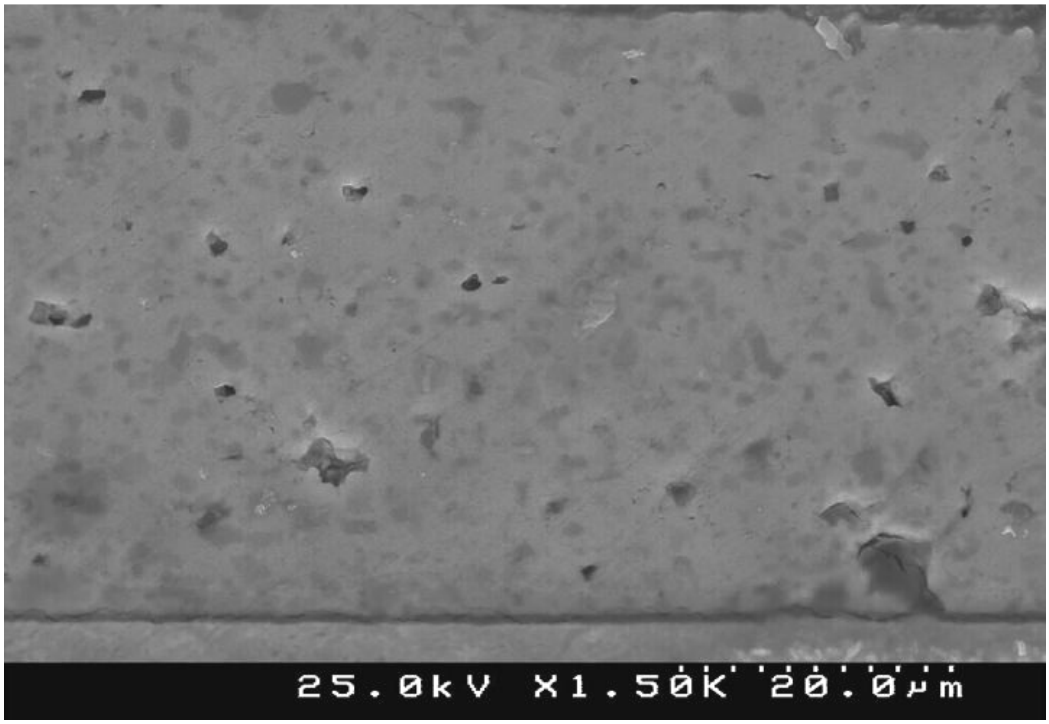

(a)

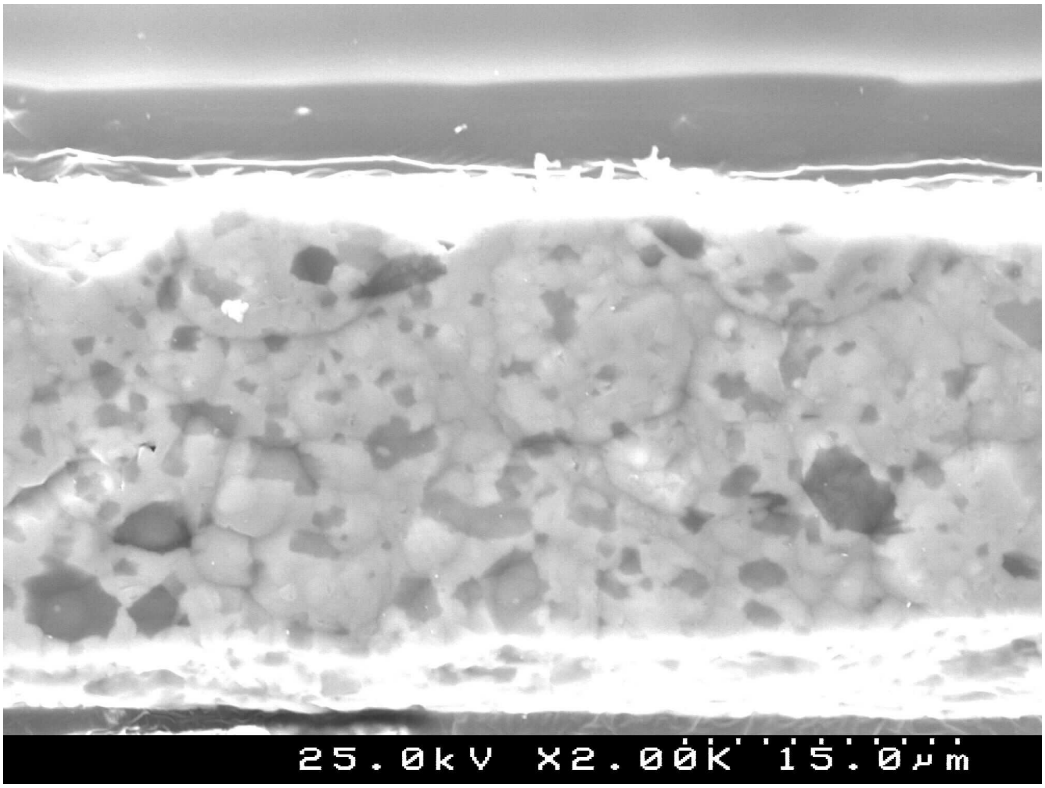

(b)

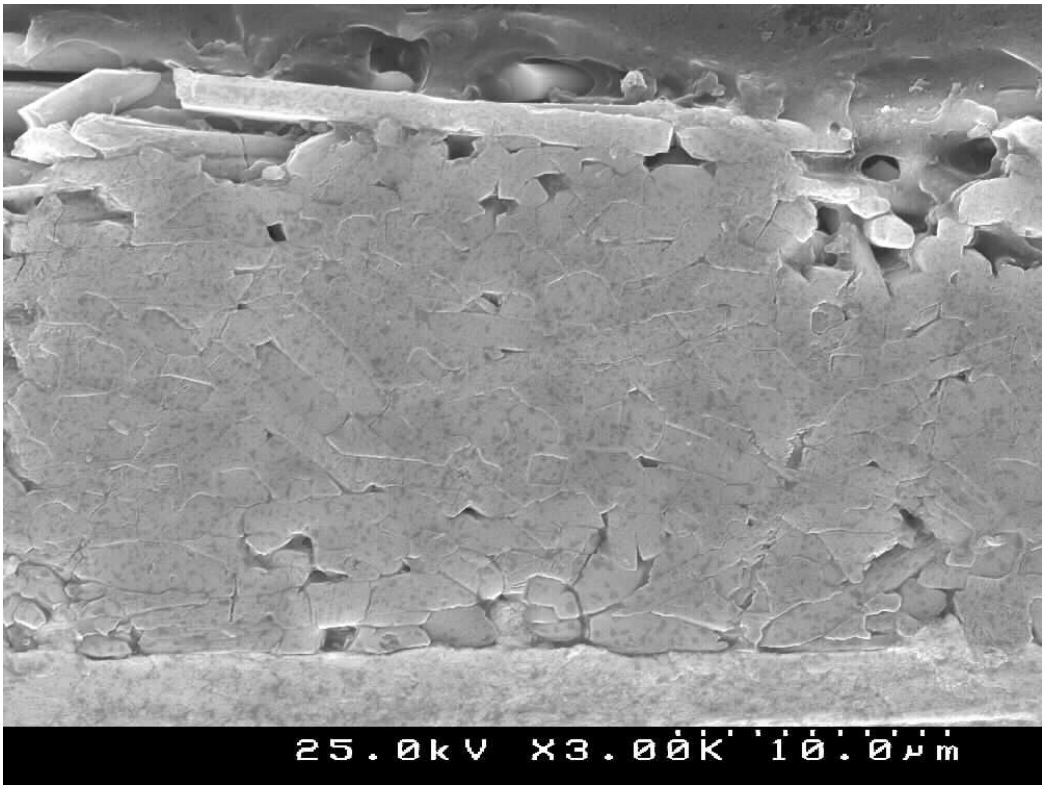

(c)

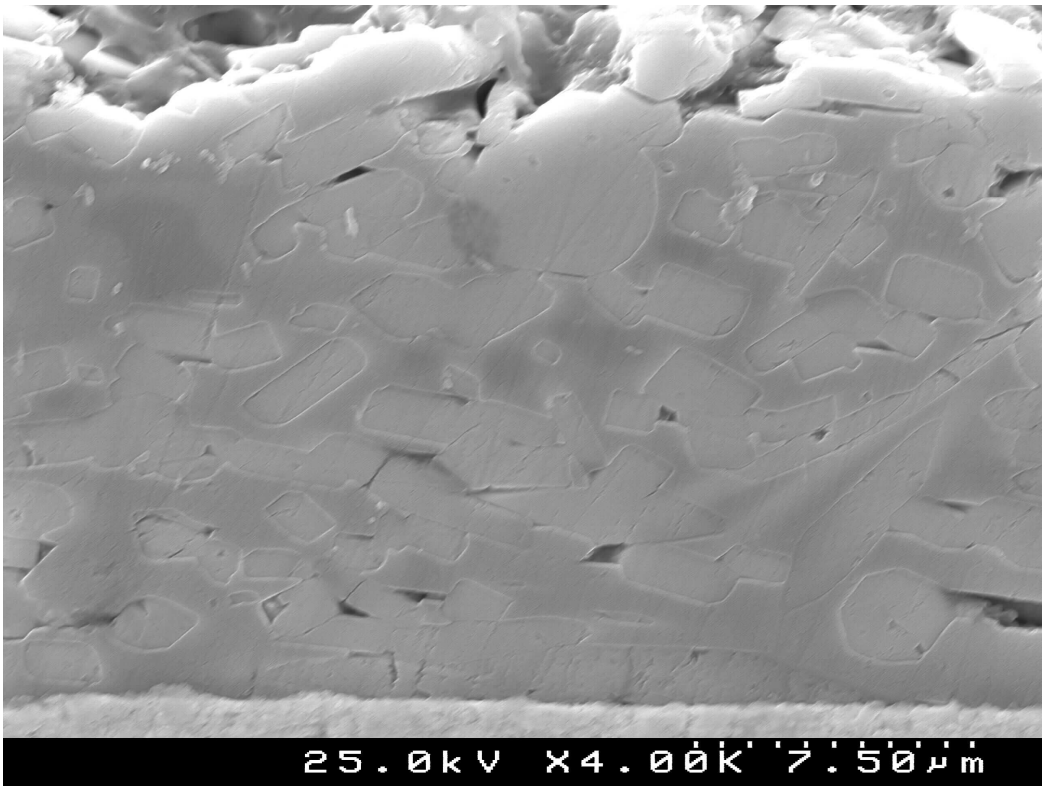

(d)

Figure 5.3-4 SEM micrographs of polished and etched cross sections of BNT films sintered at various temperatures for 1 hour:
(a)1300 ºC, (b) 1350 ºC, (c) 1400 ºC , and (d) 1450 ºC

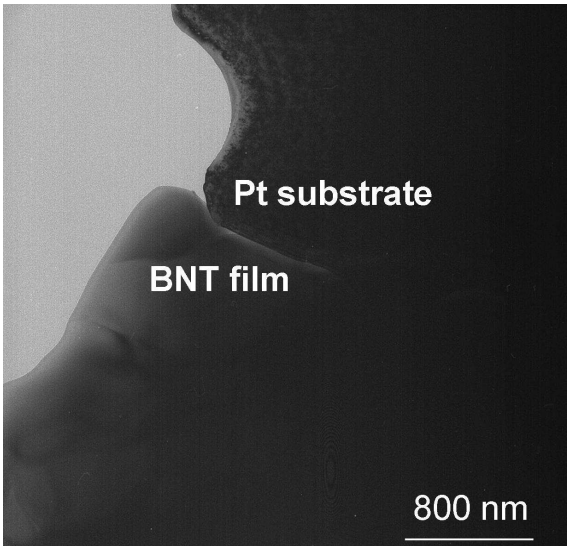

Figure 5.3-5 TEM interface micrograph between
BNT films and Pt substrate, sintered at 1350 °C/1h

From some of the polished and thermally etched film surfaces one can notice a group of equiaxed grains dispersed within the matrix of anisotropic grains. Figure 5.3-6 presents a high magnification SEM micrograph (Figure 5.3-6 (a)) and the EDS analysis (Figure 5.3-6 (b)) of one of these equiaxed grains (indicated as “A”) observed in a film sintered at 1350 ºC/1h. EDS analysis points to that “A” grains are rich in Ti and deficient in Ba and Nd species, compared with the BNT matrix grains (indicated as “B”) (Table 5.3-2). TEM technique was employed to further analyze the structure of the grains “A” and “B” in BNT films sintered at 1350 °C/1h. As illustrated in Figure 5.3-7, the electron diffraction shows that the “A” grains is much amorphous; on the other hand, the grains “B” are quite crystallized.

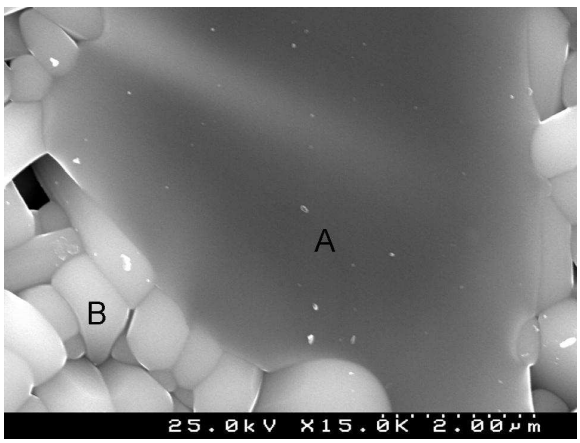

(a)

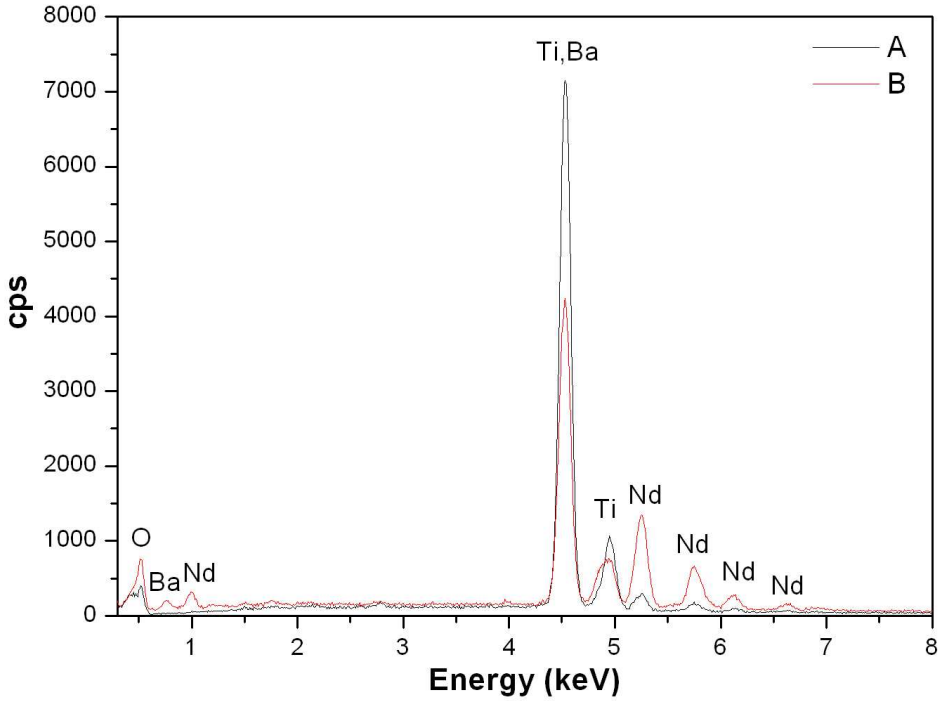

Figure 5.3-6 SEM micrograph of polished and etched surface

(a) and EDS analysis (b) of BNT films sintered at 1350 ºC/1h

Table 5.3-2 Atomic composition of A and B phases determined by EDS of BNT films sintered at 1350 °C/1h

	Ba (atm%)	Nd (atm%)	Ti (atm%)
A	1.81	1.48	43.59
B	6.66	12.16	40.79

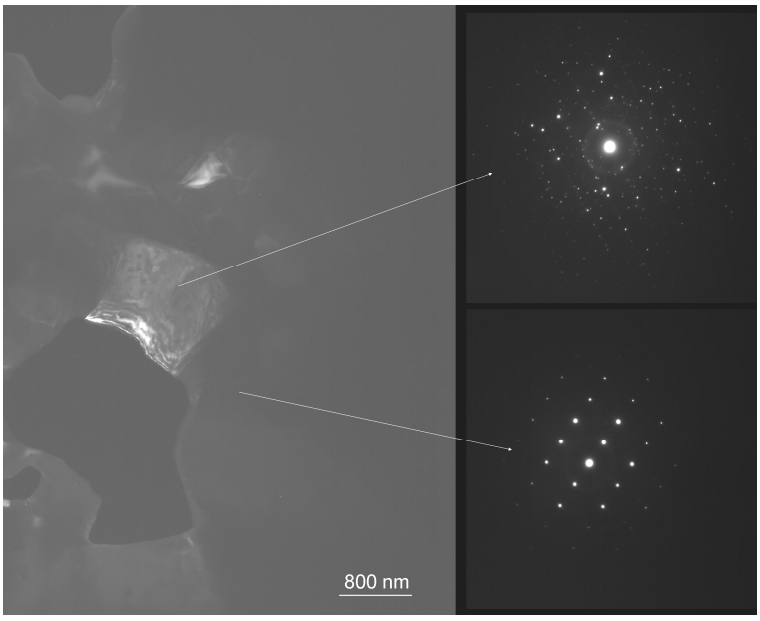

Figure 5.3-7 Electron diffraction pattern of BNT thick films sintered at 1350 °C/1h

For comparison BNT bulk ceramics were sintered under identical conditions at 1450 ºC for 1h and the microstructure is illustrated in Figure 5.3-8. As expected BNT ceramics sintered at 1450 ºC present an elongated grain growth. However, this grain elongation is obviously less intense than the one observed for the equivalent sintered films. (Figure 5.3-3 g-h)

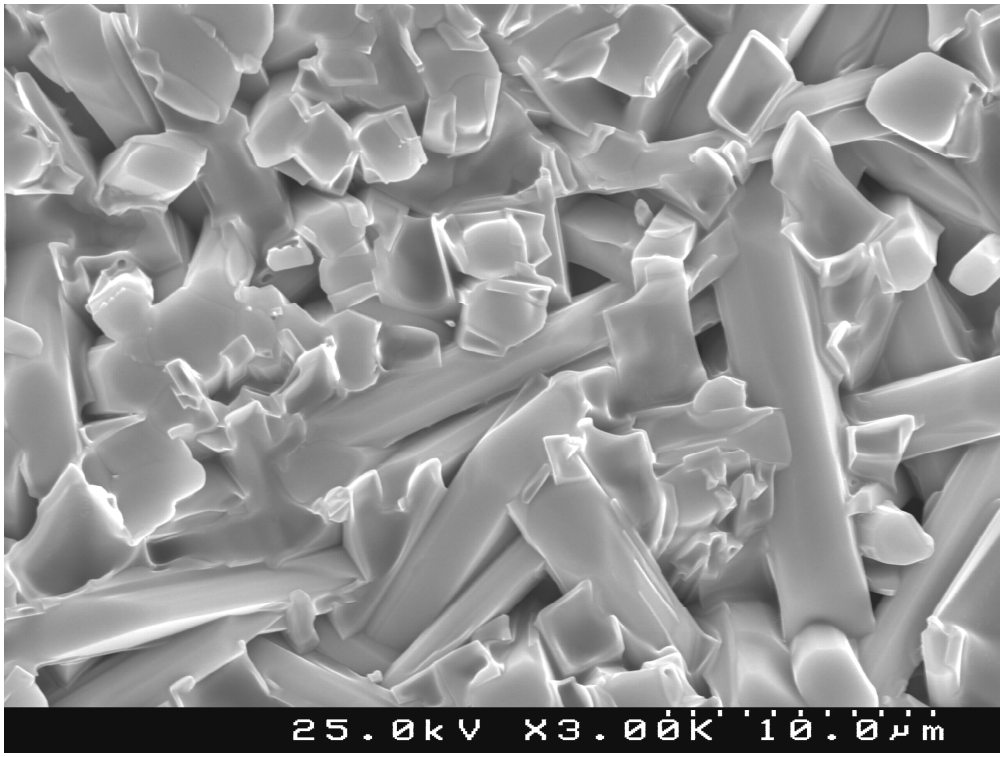

Figure 5.3-8 SEM micrograph of a polish and thermal etched surface of BNT ceramics sintered at 1450 ºC/1h

Figure 5.3-9 illustrates the X-ray diffraction pattern of BNT films sintered at various temperatures. Also depicted is the X-ray diffraction pattern of BNT powders for comparison. For every film all the diffraction peaks were identified as belonging to BNT (JCPDS card 33-0166) within the equipment detection limits. No second phases are detected. However some differences in the intensity of the diffraction lines at 2θ of 32.3º and 43.1º are observed which seems to be linked to the microstructure anisotropy. The intensity of (hk0) peaks such as (2 10 0) at 2θ of 43.1º increases with increasing sintering temperature from 1300 to 1450 ºC. In contrast, the peak intensity corresponding to (hkl), such as (311) at 2θ of 32.3º becomes weaker. These observations indicate a (hk0) preferred orientation of BNT thick films, which is dependent on the sintering temperature and deserve to be further inspected.

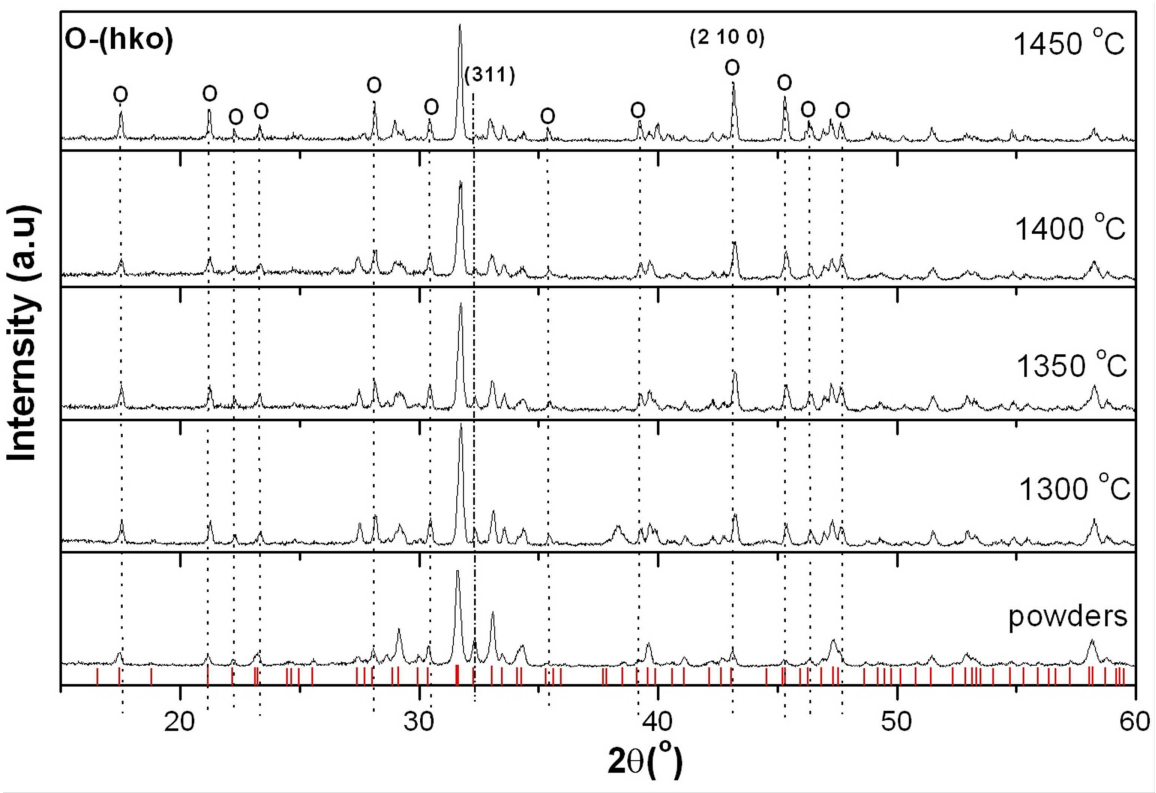

Figure 5.3-9 XRD patterns of BNT films sintered at various temperature and BNT powders calcined at 1200 ºC for 3 h (JCPDS card 33-0166 are indicated at the bottom of the figure)

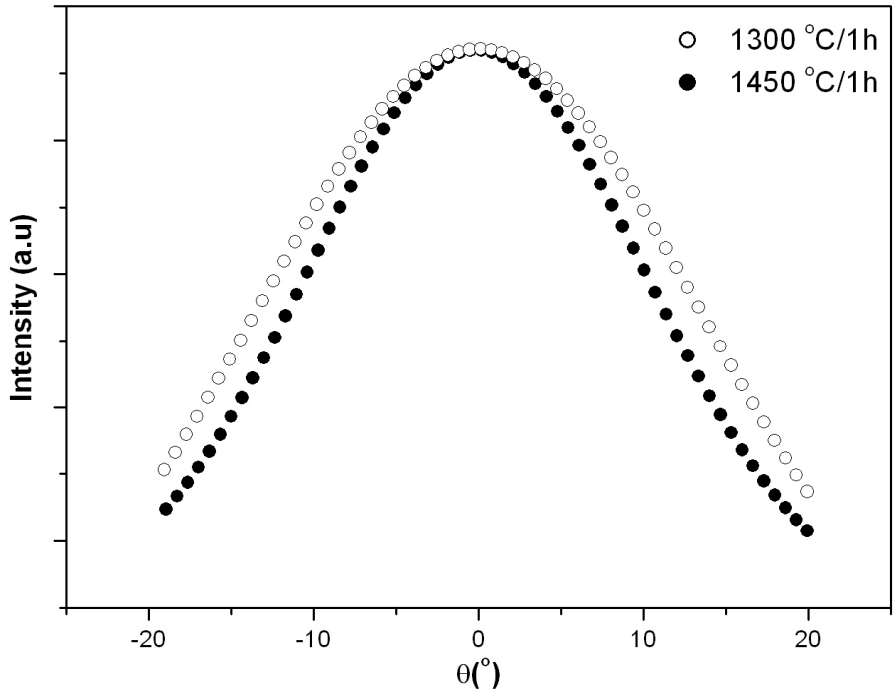

Figure 5.3-10 Rocking curves of (2 10 0) peak of BNT films sintered at 1300 ºC / 1h and 1450 ºC / 1h

The rocking curve of (2 10 0) peak is illustrated in Figure 5.3-10 in which a relatively intense and narrow peak is displayed for BNT films sintered at 1450 ºC/1h when compared to the less intense and broadened peak of the films sintered at 1300 ºC/1h, in which FWHM is 22 degree for BNT 1450 ºC/1h and 28 degree for BNT 1300 ºC/1h. Although the difference in terms of FWHM is not very high, it reflects the textured microstructure differences between these two films. It is worthwhile to emphasise here that these are ceramic films with a "textured" microstructure and not epitaxial.

Figure 5.3-11 portrays the X-ray pole figures of BNT films sintered at 1450 °C/1h in (150) (2θ = 21.2°) and (121) (2θ = 25.5°), which are two isolated diffractions representing (hk0) and (hkl) crystallographic directions, respectively. In the pole figure for (150) direction the projected piercings are grouped in a central band whereas in the pole figure for (121) direction the projected piercings are spread all over the sphere. Thus an obvious (150) texture is present in these BNT films. These results confirm the (hk0) preferred orientation of BNT films and its dependence on the sintering temperature, and are consistent with the SEM and XRD analysis shown in Figures 5.3-3, 9 and 10.

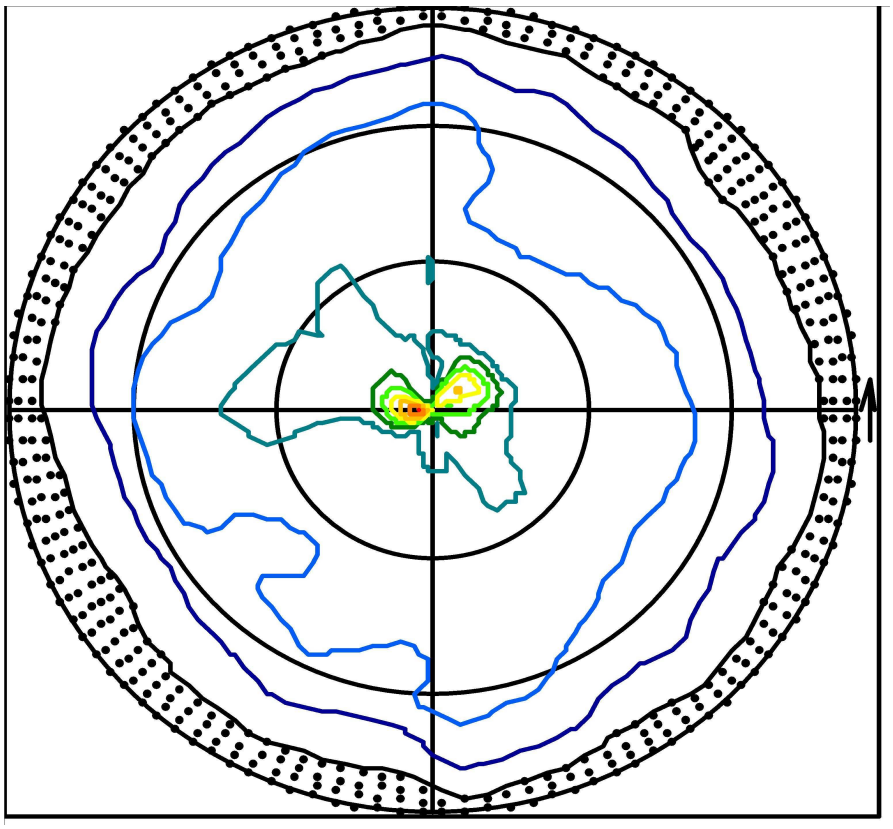

(a)

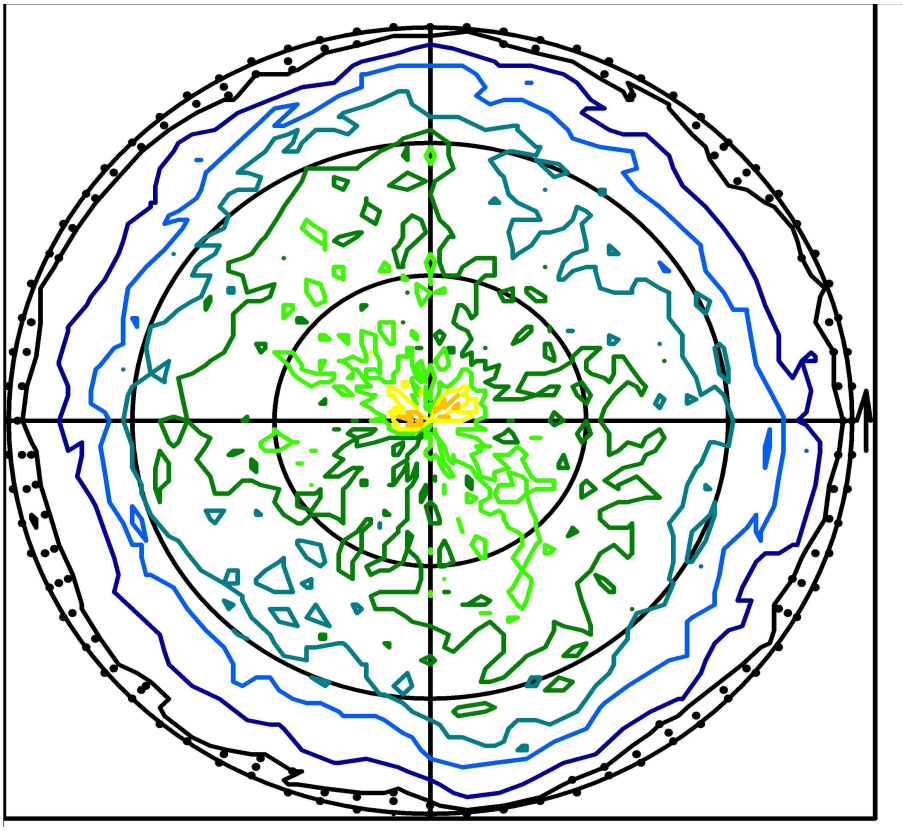

(b)

Figure 5.3-11 X-ray pole figure distribution corresponding to (a) (150) (2θ = 21.2°) and (b) (121) (2θ = 25.5°) diffraction reflections of BNT films sintered at 1450 ºC/1h

Lotgering's equation was used to calculate the degree of texture along the (2 10 0) direction: [Lotergering F. K. -1959]

$$f_i = (P_i - P_0) / (1 - P_0) \qquad (5.3\text{-}2)$$

where Pi stands for $P_i = \sum I_i / \sum I_{(hkl)}$ and $P_0 = \sum I_{0i} / \sum I_{0(hkl)}$. In this case the subscript "i" in the equation indicates (2 10 0) plane index and the subscript "0" indicates the corresponding random powder material, that is used as a standard to determine P_0. Therefore, f(2 10 0) indicates the (2 10 0) orientation on the surface of BNT thick films. ΣIi and ΣI{hkl} stand for the sums of the peak areas for the sintered specimen. Figure 5.3-12 illustrates the variation of the texture factor (f) for (2 10 0) orientation determined by equation (1) as a function of the sintering temperature. The degree of (2 10 0) preferred orientation is increased from 11% to 33% as the sintering temperature

increases from 1300 to 1450 ºC, supporting all the previous observations.

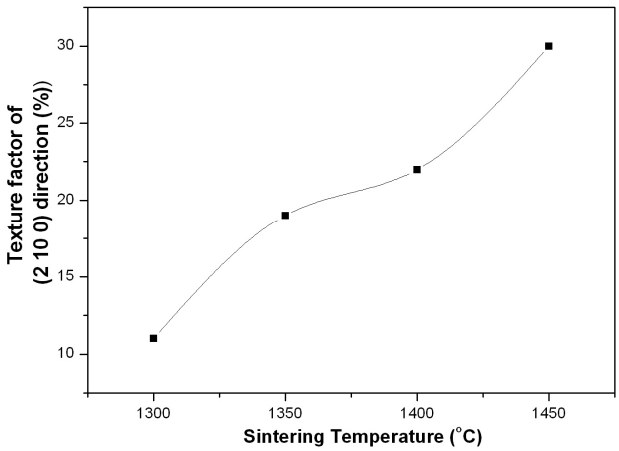

Figure 5.3-12 Texture factor of (2 10 0) direction of BNT films, calculated by Lotgerin´s equation, as a function of the sintering temperature

5.3.3.4 Electrical properties

The variation of the permittivity and loss tangent, measured in the direction normal to the substrate plane, of BNT thick films sintered at different temperatures as a function of the frequency is represented in Figure 5.3-13. As the sintering temperature increases from 1300 to 1350 ºC, the permittivity of BNT films increased moderately from 96 to 104, however, for higher sintering temperature the dielectric permittivity dropped markedly to 69 and 47, as for the films sintered at 1400 and 1450 ºC, respectively. In contrast, the loss tangent of BNT thick films did not show an obvious change when the sintering temperature was increased from 1300 to 1450 °C.

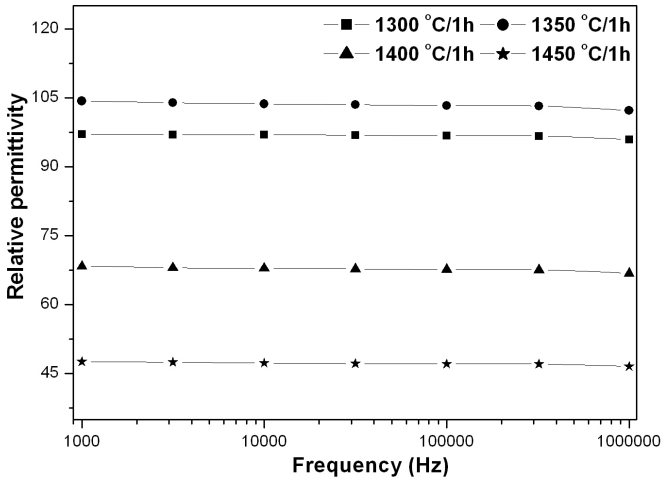

(a)

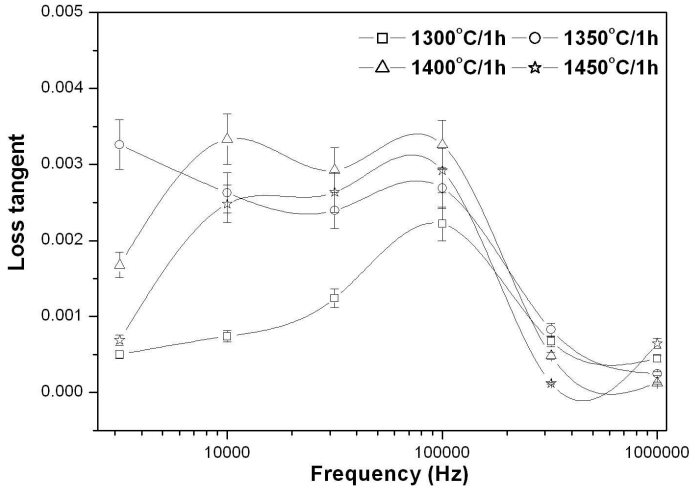

(b)

Figure 5.3-13 Relative permittivity (a) and loss tangent (b) of BNT films sintered at various temperatures as a function of the frequency

The dependence of relative permittivity and loss tangent on the applied dc voltage at 1 MHz of BNT films sintered at different temperatures is depicted in Figure 5.3-14. The relative permittivity does not show any variation with the bias voltage, while all the values of loss tangent at 1 MHz display good bias voltage stability and low losses of the order of 10^{-4}. These loss values of the BNT films imply suitability for the front-end wireless applications.

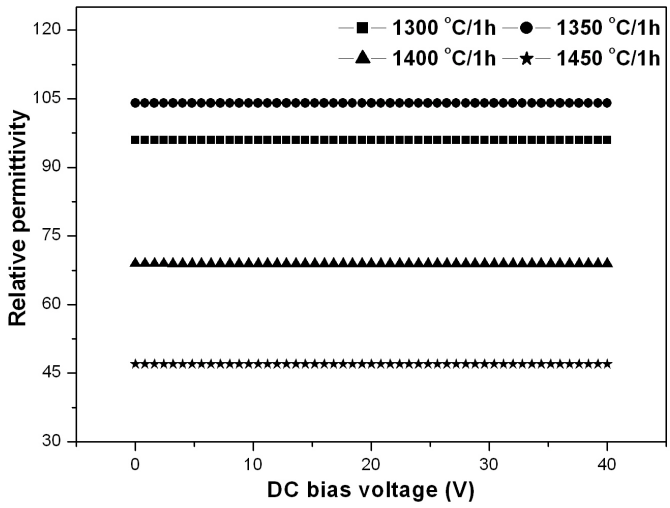

(a)

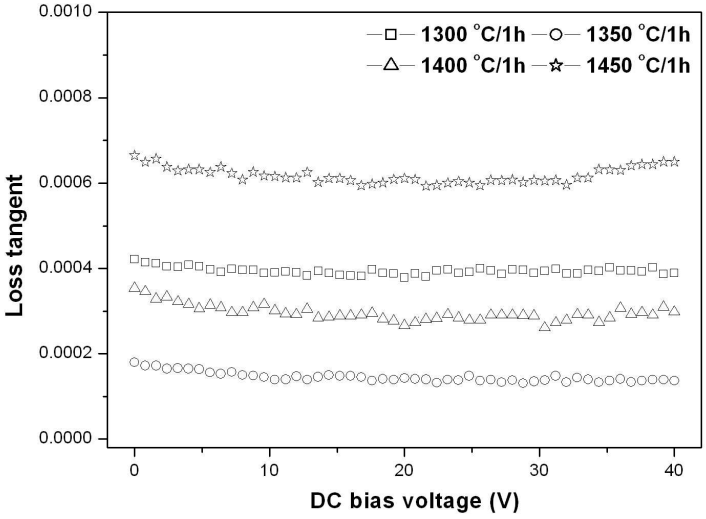

(b)

Figure 5.3-14 Relative permittivity (a) and loss tangent (b) of BNT films sintered at various temperatures as a function of the applied dc voltage at 1 MHz

Interesting is the variation of the temperature dependence of the relative permittivity of BNT films with the sintering temperature (Figure 5.3-15). The most noteworthy point here is the change of the temperature dependence of the relative permittivity from a negative to a positive value with the increase of the sintering temperature. The slope of the line is negative for films sintered until 1400 ºC and changes to positive for the films sintered at 1450 °C, which indicates that the temperature dependence of the relative permittivity of BNT thick films can be controlled to a desired value close to zero if sintered at the appropriate temperature.

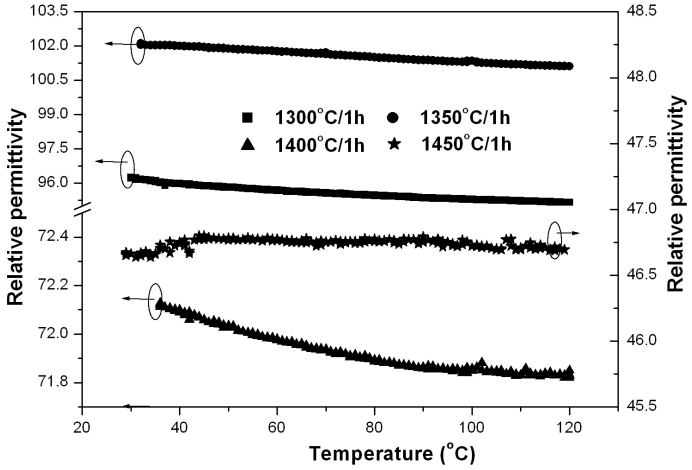

Figure 5.3-15 Temperature dependence of the relative permittivity at 1MHz of BNT films sintered at different temperatures

Figure 5.3-16 that plots the variation of temperature coefficient of relative permittivity ($TC\varepsilon_r$) and grain aspect ratio of BNT films as a function of the sintering temperature. $TC\varepsilon_r$ was computed in terms of the parameter $\Delta\varepsilon/\varepsilon_0\Delta T$, where $\Delta\varepsilon$ stands for the change in relative permittivity in relation to permittivity at 30 °C, ε_0. As the sintering temperature increases from 1300 to 1450 °C, $TC\varepsilon_r$ changes from -114 to +12 ppm/°C, associated with the increase of the aspect ratio from 5 to 23. For BNT films sintered at 1450 ºC, +12 ppm/ºC of $TC\varepsilon_r$ meets the demands for practical MW applications, in which $TC\varepsilon_r$ should be below 15 ppm/ºC. The observed relation between $TC\varepsilon_r$, measured in the direction normal to the substrate plane and the grain aspect ratio indicates that the change in $TC\varepsilon_r$ is the result of the anisotropy changes in the textured morphology of BNT films and this variation can be tailored through the sintering temperature. Moreover a linear relation between $TC\varepsilon_r$ and the relative permittivity of BNT films sintered at different temperatures is observed (Figure 5.3-17), verifying the simple relation between $TC\varepsilon_r$ and ε_r ($TC\varepsilon_r \alpha \varepsilon_r$) observed for high *Q* microwave ceramic dielectrics. [Reaney I. M. -2006] Values of $TC\varepsilon_r$ increase from -114 to +12 ppm/ºC as the relative permittivity drops from about 104 to 47.

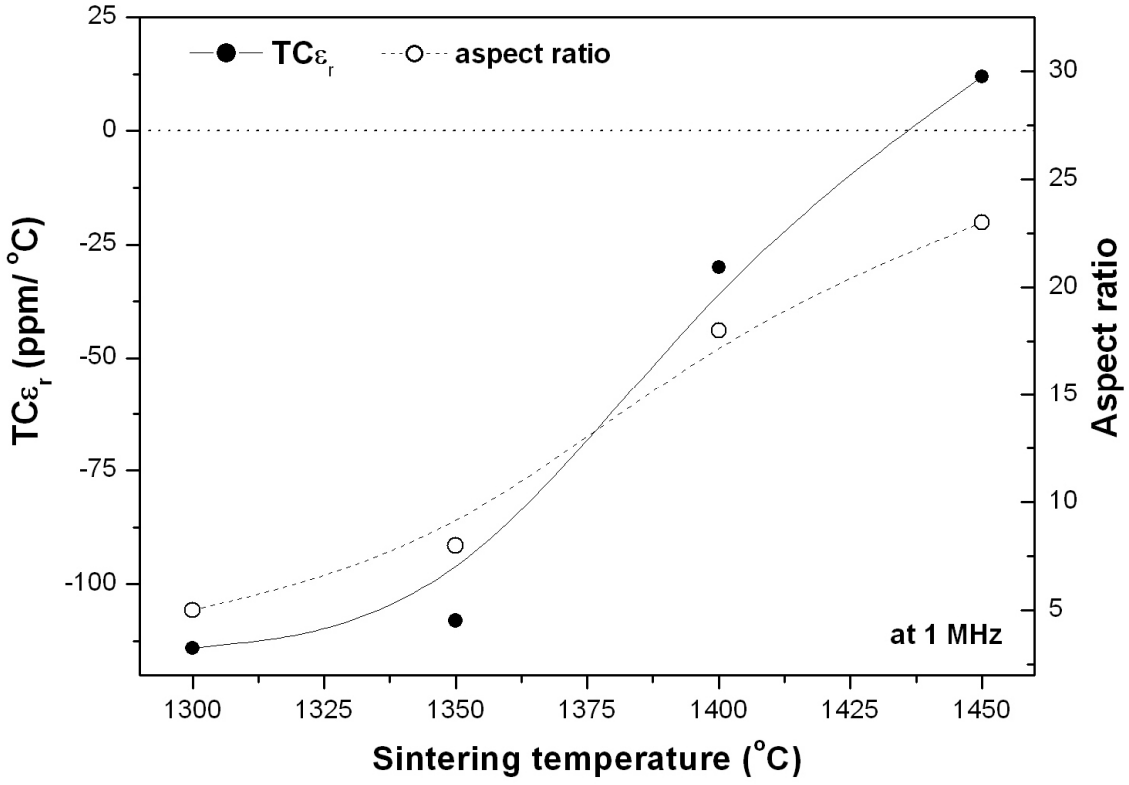

Figure 5.3-16 Dependence of $TC\varepsilon_r$ and aspect ratio of BNT thick films on the sintering temperature

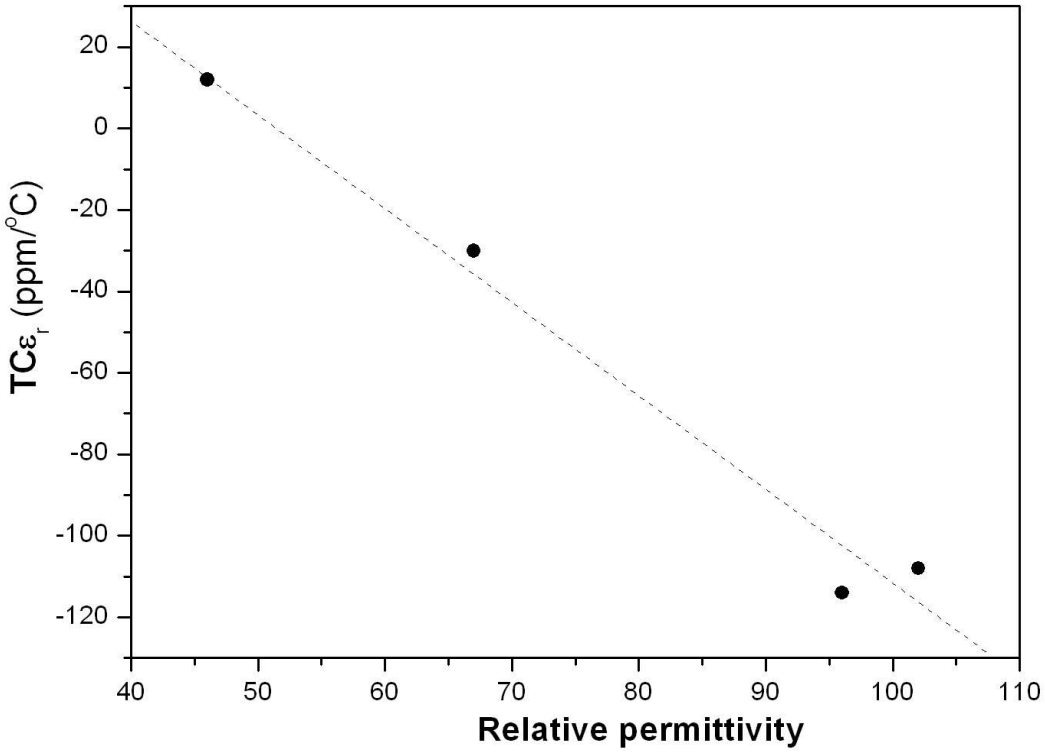

Figure 5.3-17 Relation between TCε_r and relative permittivity of BNT thick films

5.3.4 Discussions

The observed results unambiguously demonstrate that the substrate has a marked effect on the microstructure development of BNT thick films. Compared to the corresponding unconstrained ceramics and partially free-sintered BNT films deposited on carbon coated Pt substrate, BNT films on bare Pt substrate exhibit a highly textured microstructure with a high aspect ratio of the elongated grains. These results can be explained by the existing stresses in the films caused by the constrained sintering on Pt.

During the sintering of a green film on a substrate shrinkage does not take place along the substrate plane. Instead, the film shrinks appreciably in the normal direction but almost not in the plane and the total shrinkage is limited to the film thickness. [Bordia R. K. -1985, Bordia R. K. -1988] As a result, stresses will be developed in the film, particularly in the film plane that will affect the sintering process (densification mechanisms and grain growth).

A prediction of the sintering of complex green bodies is possible using a continuum mechanics model incorporating sintering stresses and sintering viscosities. [Bordia R. K. -1985, Bordia R. K. -1988] An isotropic formulation was firstly developed to understand the densification of constrained films, and according to the

relationship: [Bordia R. K. -1988, Green D. J. -2008]

$$\left(\frac{\rho^{\bullet}}{\rho}\right)^{\text{constr.}} = \frac{1+\nu^{p}}{1-\nu^{p}}\frac{1}{3}\left(\frac{\rho^{\bullet}}{\rho}\right)^{\text{free}} \tag{5.3-3}$$

where the normalized densification rate for a free sintering body is $-3\varepsilon^{free}$, the effect of the constraint is to reduce the normalized densification rate of the film, and the magnitude of this reduction depends on the viscous Poisson's ratio, ν^{p}. In fact, constrained films shrink more rapidly in the unconstrained direction in comparison with freely sintered specimens, but not at all in the other directions, so that global densification is retarded. An in-plane biaxial tensile stress develops that retards overall densification and the maximal achievable density will be lower than in the free sintering conditions. In addition processing defects, such as cracks or debonding may be induced. [Bordia R. K. -1988, Scherer G. W. -1985]

More recently it was proved that the isotropic model does not satisfactory describe the constrained sintering behaviour and a transversely isotropic formulation for a sintering of constrained bodies was developed. [Guillon O. -2007] The essential premise of the isotropic model is that the microstructures of free and constrained bodies are identical. However, this is not the case, and holds less and less as the densification increases [Guillon O. -2007]. It was recently proved that the stresses induced by constraint lead to the development of anisotropic microstructures during sintering. For cases where either a non-isotropic strain or non-isotropic stress field is applied to the sintering bodies, directional diffusional fluxes lead to elongated pores and as soon as grain growth sets in to elongated grains. [Green D. J. -2008] Indeed constrained sintered BNT films exhibit a high textured microstructure with a high aspect ratio of the elongated grains (23 for films sintered at 1450 °C / 1h) (Figure 5.3-3 (g)). On the other hand, in unconstrained BNT ceramics the shrinkage took place in all directions favouring the equiaxed grain growth [Fu Z.-2007] and restraining the elongated grain growth that is only observed at very elevated temperatures (Figure 5.3-8).

Activation energies of densifying processes were determined and showed that the retardation observed in the constrained- sintering films is primarily due to a change in the densification mechanisms (from a faster grain-boundary diffusion to a slower lattice-diffusion). [Choe J. W. -1995] This leads also to a clearly anisotropic

microstructure, as observed in this work. In the constrained situation, in which the films are stretched along the planar directions, the “necks” or contact points between BNT particles will be under dissimilar stresses depending on their orientation in the film. Some “necks” will be under tensile stresses while others under compressive ones and, as a consequence, the rate of “neck” growing is different. If “necks” will lose their curvature at low density, the driving force necessary for matter transport is diminished and sintering is retarded. In addition, if some grain boundaries will become mobile at low densities further densification is hampered or even null and porosity may be trapped within BNT grains. Though the BNT films of this study present quite dense microstructures, particularly those sintered at high sintering temperatures (Figure 5.3-4), due to the presence of the “Ti rich phase”, BNT films are actually more porous than the ceramics processed under identical conditions. In the meantime when grain growth takes place anisotropic grain growth is observed (Figures 5.3-3 and 9). The reduction in densification and anisotropic grain growth was observed in constrained films of ZnO and YSZ / Al_2O_3 composites as well. [Calata J. N. -2001, Lu X. J. -2007, Bordia R. K. -1993]

The effect of the constrained sintering is also apparent on the evolution of film’s textured microstructure with the sintering temperature. BNT films exhibit an increase of the aspect ratio and textured degree with the increase of the sintering temperature (Figures 5.3-3 and 9). The aspect ratio of elongated grains increased from 5 to 23 when BNT films are sintered from 1300 to 1450 ºC (Table 5.3-1).

Apparently the observations of the present work support the proposed transversely isotropic model [Guillon O. -2007], though there is a lack of systematic studies of grain growth and grain growth mechanisms in constrained sintered systems. Further studies on the grain growth in constrained BNT films and other systems are definitely required.

As indicated by SEM microstructures (Figures 5.3-3, and 6) some BNT elongated matrix grains are surrounded by “deformed” second phase grains that were not detected by XRD. Based on EDS analysis (Figure 5.3-6 and Table 5.3-2) this second phase is Ti rich and deficient in Ba and Nd, compared to the BNT matrix grains. Ti rich phases, in particular titanium dioxide, have been also observed in some compositions of the $BaO–Nd_2O_3–TiO_2$ system. [Ubic R.-1998, Jaakola T. -1986, Chen X. M. -1995] As reviewed in chapter 1, the composition and stoichiometry of $BaO\text{-}Nd_2O_3\text{-}TiO_2$ system, namely $BaNd_2Ti_4O_{12}$ (BNT 114) and $BaNd_2Ti_5O_{14}$ (BNT 115) have been the subject of

conflicting and ambiguous reports. And it is now accepted that BNT 114 is the correct nominal formula and is commonly referred to as 114 phase, based on the stoichiometry of its constituent oxides: $BaO\text{-}Nd_2O_3\text{-}4TiO_2$. However, because BNT 115 shows even better dielectric properties (*Qf*-6199, ε_r-91.9 at 3.5 GHz) than BNT 114 (*Qf*-3500, ε_r-80.8 at 3 GHz), BNT 115 is commercially employed in microwave devices. [Wakino K. -1984, MBRT90, FuJi Titanium Industry Co., Ltd, Japan] This is also the reason behind the choice of BNT 115 in this current study.

In current work, it was observed that the Ti rich second phase is not well crystallised. The diffuse nature of the Electron Diffraction (Figure 5.3-7) patterns points to the amorphous nature of this second phase, and it might be related to an eutectic reaction between the constituent oxides. In the studies of Cruickshank et al [Cruickshank K. M. -1996] in the $BaO\text{-}Nd_2O_3\text{-}nTiO_2$ system, for n = 4.7-5.0, besides the identification of TiO_2 as a secondary phase the authors reported that as the sintering temperature is increased from 1250 to 1400 ºC, the limits of the solid solution increase slightly for high values of n. According to the phase diagram of $BaTiO_3\text{-}TiO_2$ an eutectic point is located at 1312 ºC. [O´Bryan H. M. -1974] For temperatures higher that 1400 ºC it is then supposed that the liquid reacts with BNT grains being somehow incorporated in the structure, as observed by Cruickshank et al, [Cruickshank K. M. -1996] and at the same time promoting under the present constrained sintering conditions the anisotropic grain growth, as perceived in this work (Figures 5.3-3).

As a result of the textured microstructure anisotropic dielectric properties are developed in BNT thick films. Worth noting is the relation between the temperature coefficient of the permittivity, $TC\varepsilon_r$, measured in the direction normal to the substrate plane, and the aspect ratio of elongated grains of BNT thick films, as shown in figure 5.3-16. It is also observed that as the sintering temperature increases the dielectric permittivity decreases and as a consequence, verifying the simple relation between $TC\varepsilon_r$ and ε_r ($TC\varepsilon_r$ *a* ε_r) that holds for the majority of the MW materials, [Reaney I. M. -2006] $TC\varepsilon_r$ increases (Figure 5.3-17) which indicates that $TC\varepsilon_r$ of BNT thick films can be engineered to a desired value close to zero by choosing the appropriate sintering temperature. The decrease of ε_r with the sintering temperature might be related to the polarization and polarization dependence on the crystal growth anisotropy.

No dielectric data were found on $BaO\text{-}Re_2O_3\text{-}TiO_2$ (Re = Sm, La) single crystals, but a dependence of the dielectric response on the grain orientation is known in several of these materials. In the present case of BNT thick films when measuring the dielectric

response the applied field is normal to the plane and the dielectric response corresponds mainly to the materials reaction along the ab-direction. As a consequence, (hk0) textured films with ab-axes components in the plane (or parallel to the plane) will exhibit an average lower polarization response resulting in a lower relative permittivity when compared with the films in which the (hk0) orientation is not favoured. Indeed the films sintered at 1450 ºC in which (hk0) texture is enhanced along the plane exhibit an inferior dielectric permittivity and positive $TC\varepsilon_r$ and on the other hand the films sintered at 1300 ºC, with the development of a weaker texture along the plane, presented an average higher dielectric permittivity and a lower $TC\varepsilon_r$ as clearly shown by the linear relationship between the $TC\varepsilon_r$ and permittivity (Figure 5.3-17). Though these observations have not yet been reported for thick films it was stated that textured BaO-Re_2O_3-TiO_2 ceramics (Re = Sm, La) ceramics, by the template grain growth technique, exhibited enhanced thermal stability of the dielectric response, [Valant M.-2000, Wada K.-2003, Fukami Y.-2006] nearly “zero” temperature coefficient of resonance frequency, and equivalent permittivity and *Q* values compared to the non textured specimens. The reasons for this dependence on the texture degree of the microstructure of BaO-Re_2O_3-TiO_2 ceramics were not properly discussed. [Wang F. S. -2006, Wada K. -2006]

Several approaches have been used to tailor the $TC\varepsilon_r$ of MW materials that include doping, [Valant M.-1996] formation of composite materials, [Santha D.-2006] and composite structures. [Wu Y. J. -2003] However, for the majority of these cases at the expense of a low *Q*. In this work, the constrained sintering of BNT films by facilitating the anisotropic grain growth suppresses the out of plane polarization response and, as a consequence, increases $TC\varepsilon_r$. In randomly oriented ceramics or films the $TC\varepsilon_r$ is negative and as the sintering temperature increases and the film microstructure becomes more anisotropic, the out of plane polarization contribution decreases, the relative permittivity decreases and $TC\varepsilon_r$ increases, reaching, for the proper sintering conditions, the almost zero $TC\varepsilon_r$ value. Moreover, the use of constrained sintering is a much easier process to control the $TC\varepsilon_r$ than the complex template grain growth that requires the preparation of anisotropic seeds usually from time- and cost-consuming methods.

5.3.5 Summary

The anisotropic microstructure development in BNT thick films prepared by EPD on Pt substrate and its impact on the dielectric properties was studied in this

chapter. It is proved that the textured microstructure arises from: i) the anisotropic crystal structure of BNT materials, ii) the constrained sintering of BNT thick films, where the in-plane stress is the main contributing factor to the development of elongated grain growth and iii) in the particular case of BNT 115 composition used in the current work, the presence of a Ti-rich phase that promotes the densification and the texture development for high sintering temperatures. It was also verified that the elongated grain growth of BNT thick films is strongly dependent on the sintering temperature. On the other hand the effect of the electric field used for EPD was proved to be negligible. As a result of the textured microstructure, the temperature dependence of the relative permittivity of BNT thick films could be controllably varied from negative to positive with the increase of sintering temperature and grain aspect ratio and decrease of the permittivity. Within the sintering temperature interval [1300-1450 °C], $TC\varepsilon_r$ changed from -114 to +12 ppm/°C, associated with the increase of the grain aspect ratio from 5 to 23. As such, near zero $TC\varepsilon_r$, high *Q*, with $45<\varepsilon_r<70$ thick films can be fabricated.

By demonstrating an alternative way to tailor $TC\varepsilon_r$ of dielectric thick films these results have a significant technological impact for the future applications of BaO–Re_2O_3–TiO_2 materials in film form for high frequency devices.

5.3.6 References

1. Bordia R. K. and Jagota A. (1993) J. Am. Ceram. Soc. **76**, 2475
2. Bordia R. K. and Raj R. (1985) J. Am. Ceram. Soc. **68**, 287
3. Bordia R. K. and Scherer G. W. (1988) Acta Metall. **36**, 2393
4. Bordia R. K. and Scherer G. W. (1988) Acta Metall. **36**, 2399
5. Calata J. N., Lu G. Q., Chuang T. J. (2001) Surf. Interface Anal. **31**, 67
6. Chen X. M., Suzuki Y., Sato N. (1995) J. Mater. Sci. Mater. Electron. **6**, 10
7. Choe J. W., Calata J. N. and Lu G. Q. (1995) J. Mater. Res. **10**, 986
8. Cruickshank K. M., Jing X. P., Wood G., Lachowski E. E., West A. R. (1996) J. Am. Ceram. Soc. **79**, 1605
9. Fukami Y., Wada K., Kakimoto K., Ohsato H. (2006) J. Eur. Ceram. Soc. **26**, 2055
10. Fu Z., Wu A. Y., Vilarinho P. M., Kingon A. I., Wördenweber R. (2007) Appl. Phys. Lett. **90**, 052912.
11. Green D. J., Guillon O., Rodel J. (2008) J. Europ. Ceram. Soc. **28**, 1451
12. Guillon O., Aulbach E., Rodel J., Bordia R. K. (2007) J. Am. Ceram. Soc. **90**, 1733
13. Jaakola T., Uusimäki A., Rautioahu R., Leppävuori S. (1986) J. Am. Ceram. Soc. **69**, C234
14. Lotergering F. K. (1959) J. Inorganic Nucleation Chemistry **9**, 113
15. Lu X. J. and Xiao P. (2007) J. Euro. Ceram. Soc. **27**, 2613
16. O´Bryan H. M. and Thomson J. J. (1974) J. Am. Ceram. Soc. **57**, 522
17. Reaney I. M. and Iddles D. (2006) J. Am. Ceram. Soc. **89**, 2063
18. Santha D., Sebastian M. T., George V., Philip J. (2006) Mater. Chem. and Phys. **100**, 423.
19. Scherer G. W. and Garino T. (1985) J. Am. Ceram. Soc. **68**, 216
20. Ubic R., Reaney I. M. and Lee W. E. (1998) Int. Mater. Rev. **43**, 205
21. Wada K., Kakimoto K. I., Ohsato H. (2003) J. Eur. Ceram. Soc. **23**, 2535
22. Wada K., Kakimoto K., Ohsato H. (2006) J. Eur. Ceram. Soc. **26**, 1899
23. Wakino K., Minai K. and Tamura H. (1984) J. Am. Ceram. Soc. **67**, 278
24. Valant M., Suvorov D., Kolar D. (1996) J. Mater. Res. **11**, 928
25. Valant M., Suvorov D., Rawn C. J. (2000) Ferroelectrics **237**, 253
26. Varfolomeev M. B., Mironov A. S., Kostomarov V. S., Golubtsova L. A., Zolotova T. A. (1988) Mogeneity Zhurnal Neorganicheskoi Khimii **33**, 1070

27. Wang F. S., Hsu Y. F., Wang Y R., Cheng L. T., Hsu Y. C., Chu J. P., Huang C. Y. (2006) J. Eur. Ceram. Soc. **26**, 1629
28. Wu Y. J., Uekawa N. and Kakegawa K. (2003) Mater. Lett. **57**, 4088

Chapter 6
Fabrication of Low Loss $BaNd_2Ti_5O_{14}$ Thick Films on Alumina Substrates by EPD

Abstract:

This chapter reports a method of performing electrophoretic deposition (EPD) of BNT thick films on non-conducting substrates overcoming the requirement of a conducting substrate through the use of sacrificial graphite layer. The conductivity of the substrate is therefore no longer a limiting factor on the utilization of EPD. Uniform and dense BNT layers have been deposited on non-conducting alumina (Al_2O_3) substrates by EPD from a non-aqueous suspension. The influence of the graphite layer thickness is also considered on the morphology of the sintered BNT films. The interaction between BNT films and alumina substrates is discussed. Severe interactions were observed for sintering temperatures above 1300 °C. The diffusion of Al ions into the films resulted in the formation of neodymium aluminate and in the destabilisation of the BNT solid solution. The dielectric properties of BNT thick films on Al_2O_3 substrates are measured at low and microwave frequencies. 100 µm BNT films on alumina substrate show ε_r and Q of 146 and 1161 respectively at about 10 GHz when sintered at 1250 °C/1h. BNT films on alumina substrates possess good Q values and high ε_r, and therefore are potentially useful for high frequency applications.

6.1 Introduction

The trend in wireless and mobile communications for broader bandwidth microwave circuitry, coupled with high packaging density and low cost fabrication has triggered investigations of new circuit configurations and technologies that meet these requirements. Microstrip lines with high impedance are often required in the design of matching networks for mixers and amplifiers. [Barnwell P.-1997] Tian Z. R. reported that an improvement of the line impedance of around 25 per cent can be obtained by using a multilayer structure, compared with the conventional single layer structure (Figure 6-1), where strong capacitive coupling can easily be obtained by overlapping the end of the two tracks using a dielectric separation sheet [Tian Z. R.-2002]. It was suggested that, by using a thin layer of a dielectric film, the impedance can be increased. This is an important feature as it enables the realisation of relatively high impedance

lines on high dielectric constant substrates. The high impedance capability of this structure is suitable for the implementation of low-loss matching networks, such as band-pass microwave filters. It was then demonstrated the potential of multilayer structures to yield higher microwave performance. [Tian Z. R.-2002] The limitation on achievable fine line width and fine gap that limits the performance of conventional microwave microstrip can effectively be eliminated by using multilayer structures, thus alleviating the pressure on the fabrication process and improving the reliability. [Barnwell P.-1998]

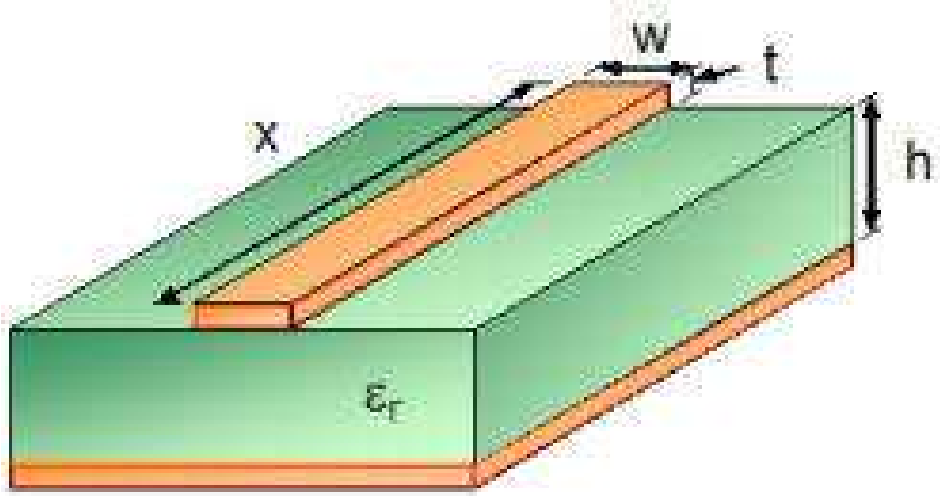

(a)

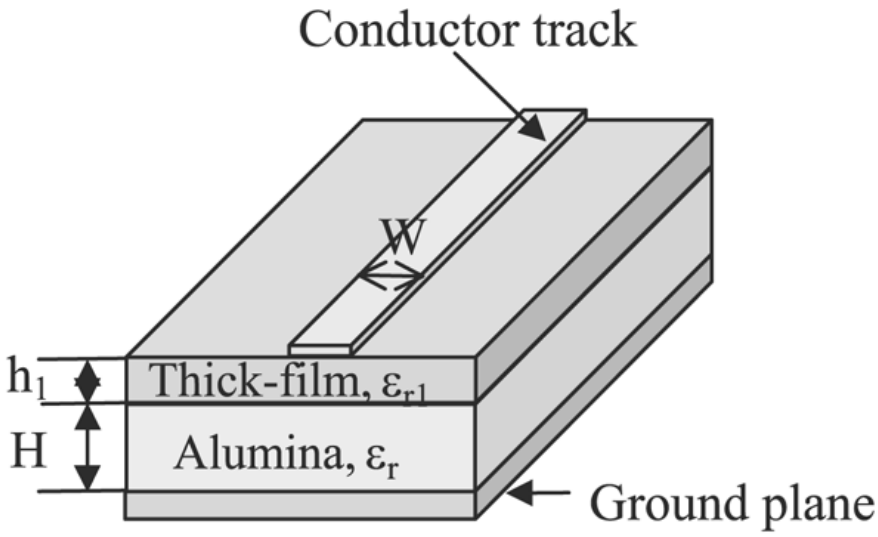

(b)

Figure 6-1 Schematic configuration of (a) a conventional microstrip and (b) of a multilayer microstrip (after Tian Z. R.-2002)

The multilayer microstrip configuration highlights that the multilayer approach to microwave structures, coupled with new thick-film technology, offers a viable and economic solution to achieve high-density, high-performance microwave circuits. By using an extra layer of thick dielectric film, some microwave components, such as high impedance line and broadband filter which are difficult to realise in the conventional single layer structure can be easily achieved with less fabrication stringency, and thus leads to lower costs and higher reliability.

In this chapter, the use of commercial non conducting alumina substrates to deposit BNT films by EPD technique is exploited to fabricate thick dielectric multilayer configurations. Polycrystalline alumina (Al_2O_3) is a universal substrate material for electronic circuits because of the low loss, good thermal conductivity and high mechanical strength of alumina, in addition to the associated fabrication low costs. For example, the high thermal conductivity coupled with the high resistivity and dielectric strength respond for its application as substrates and packaging for high power or high-density assemblies of microelectronic components. [Ma J.-2002] In the meantime, the utilization of alumina substrate antennas for mobile communication handsets has been rapidly growing due to the added advantages of compact size. [Toko America Inc, Zhong S. S. -2004]. So it is worthwhile to explore the properties of high Q dielectrics, such as BNT on Al_2O_3 substrates.

However, the utilization of insulating substrates in EPD raises difficulties, since one of the pre-requisites for EPD is that the substrate should be a conductor. In the EPD process, as mentioned in previous chapters, the charged powder particles dispersed in a liquid medium are attracted and deposited onto a conductive and oppositely charged electrode under the application of an electric field. In principle, it is not possible to carry out EPD on non-conducting substrates. In fact, most of the EPD processes reported in the literature involve electrical conductive metallic substrates. If this requisite (limitation) will be overcome and the deposition on non-conducting substrates becomes feasible, the EPD process become much more attractive for applications in a wide spectrum of materials processing and gains value.

There are only a few reports in the literature in which attempts have been made to electrophoretically deposit on non-conducting porous substrates. [Hamagami J. -2002, Matsuda M.-2005, Negishi H.-2006, Kanamura K.-2002] Among these cases, the EPD of YSZ particles on a NiO–YSZ substrate was made possible through the use of an adequately porous substrate. The continuous pores in the substrates, when saturated

with the solvent, helped in establishing a “conductive path” between the electrode and the particles in suspension. Deposition rate was found to increase with increasing substrate porosity up to a certain value. [Besra L.-2006, 2007, Hosomi T.-2007] The higher the applied voltage, the faster the deposition is. However, the limitation is that there exists a threshold porosity value below which EPD becomes practically impossible for a given applied voltage. In addition, the preparation of porous substrates with different porosity involves also considerable costs.

In the present work, thin layers of conducting graphite were coated onto the alumina substrates to facilitate the conduction on the substrate surface. The graphite coating burns out during sintering step not interfering in the final product. The novelty of the process lies in the fact that it overcomes the need for conductive substrates for EPD. The deposition has been made possible simply through the use of adequately thick temporary graphite layer previously deposited on the alumina substrates. The influence of graphite layer thickness is considered on the morphology of sintered BNT films. The compatibility of alumina substrates with BNT films is analyzed and discussed. BNT films on alumina substrate were characterized in low and microwave frequencies taking in consideration possible applications at high frequencies.

6.2 Experimental

In this chapter, all the films were prepared from home made BNT powders in acetone with I_2 based suspensions, which is proved to be optimal suspensions for EPD of BNT powders in chapter 5.2. Alumina substrates were made conductive on one side with a graphite layer, deposited by RF sputtering. The graphite interlayer acts first as the conducting electrode and then during sintering is removed. The experimental details, including preparation of BNT powders and films and graphite layers, and characterization of the prepared films are described in chapter 4.

It should be stressed that since there is no bottom electrode between BNT films and alumina substrates for the electrical measurement at low frequencies, the back of the alumina substrate was completely covered with Au coatings by sputtering. So, the measurements in this case include the alumina substrate, which means that the measured properties are a response from the composite of BNT films and alumina substrates, as shown in Figure 6.2.

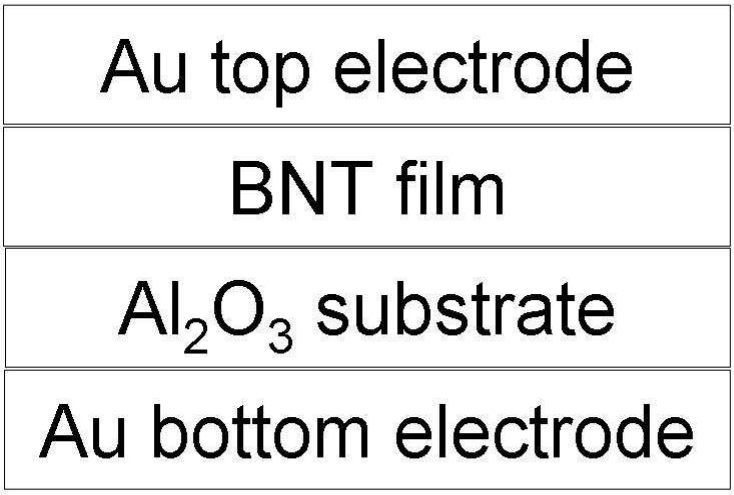

Figure 6-2 Schematic of structure for measurement of BNT on alumina substrate at low frequency

For microwave frequency characterization, the samples were analyzed without electrodes by the spit post technique and relative permittivity (ε_r) and quality factor (Q) were determined.

6.3 Results and Discussions

6.3.1 Deposit characteristics

Figure 6-3 shows the thickness of BNT films deposited on Al_2O_3 substrates as a function of the deposition time at a constant voltage of 200 V. As expected and observed in chapter 5.2 (Figure 5.2-10), the thickness of the deposited layer increases in the initial period, in which a linear relationship between the deposition thickness and time holds, followed by a decrease with the increasing of the deposition time. As mentioned before, in a constant voltage EPD, these trends are expected because while the potential difference between the electrodes is maintained constant, the electric field influencing electrophoresis decreases with deposition time because of the formation of an insulating layer of ceramic particles on the surface of the deposition electrode. The relation between deposited thickness and deposition time has been discussed in detail in chapter 5.2. In addition and noteworthy to point is that there is not obvious difference in the EPD performance between the graphite coated alumina substrates and Pt metal substrates, attesting the adequacy of insulating substrates in EPD and the strategy here developed to overcome the initial limitation.

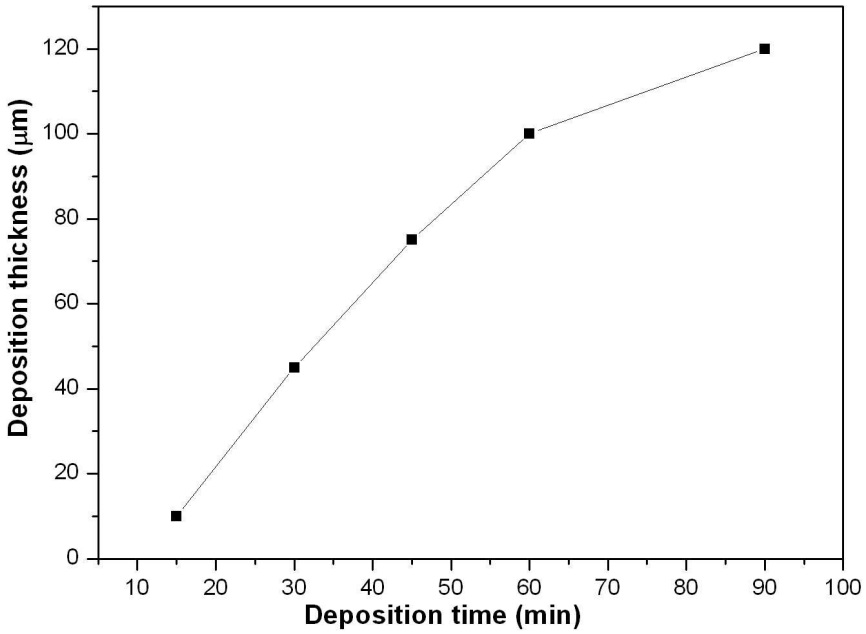

Figure 6-3 Deposition thickness of the deposited BNT films against deposition time at constant voltage of 200 V for graphite coated alumina substrates

6.3.2 Effect of graphite layer thickness

Figure 6-4 depicts the surface optical micrographs of green and sintered BNT films formed on graphite coated alumina substrates. Uniform, conformal and crack free films were obtained for dried BNT films. However, with too thin graphite layers it is difficult to deposit the BNT films because a sufficiently conductive layer is not formed to permit the deposition. It was found that graphite layers with thickness below 100 nm cannot be used as a temporary electrodes for EPD (Figure 6-4 (b)).

The conductivity of the substrate electrode is a critical parameter to the quality of films deposited by EPD. Peng et al [Peng Z. Y. -2001] observed that the low conductivity of $La_{0.9}Sr_{0.1}Mn_3$ (LSM) substrates leads to non-uniform green films of YSZ films and to a slow deposition. On the other hand, as shown in Figure 6-4 (d), in the present study thick graphite layers lowered the adhesion of BNT films to the substrates after sintering. For 500 nm thick graphite layers non conformal and non uniform films were obtained after sintering because the thick graphite layer restricted the final adhesion of BNT films to the substrate. This result indicates that there is an optimal graphite layer thickness to obtain uniform and conformal sintered BNT films on a non-conductive Al_2O_3 substrate. Sintered conformal films were obtained for graphite layer thicknesses in the range between 200 nm to 400 nm (Figure 6-4 (c)). Table 6-1 summarizes the influence of the thickness of the graphite layer on the morphology of

BNT films on alumina substrate after sintering.

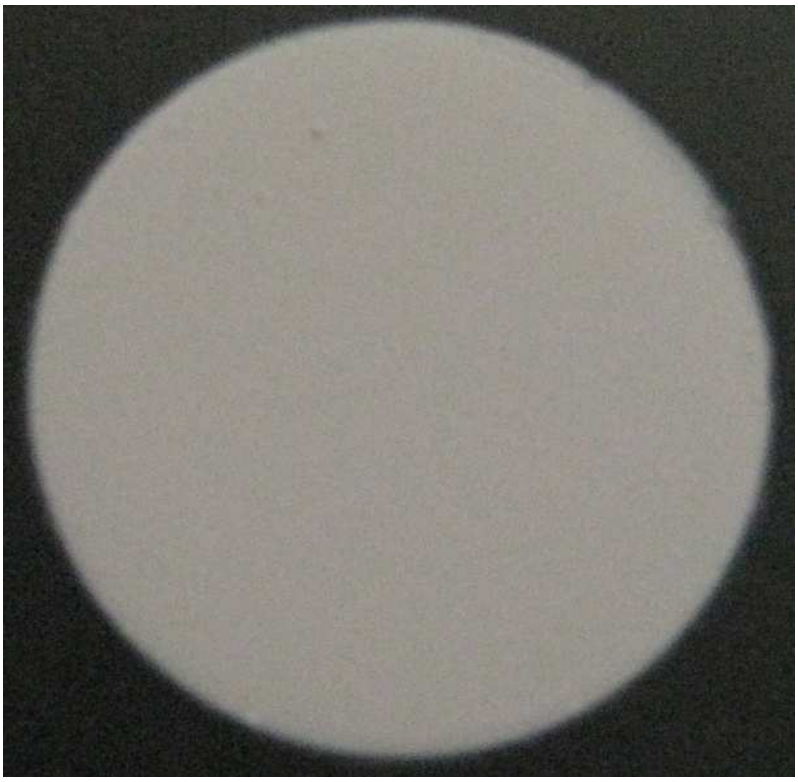

(a)

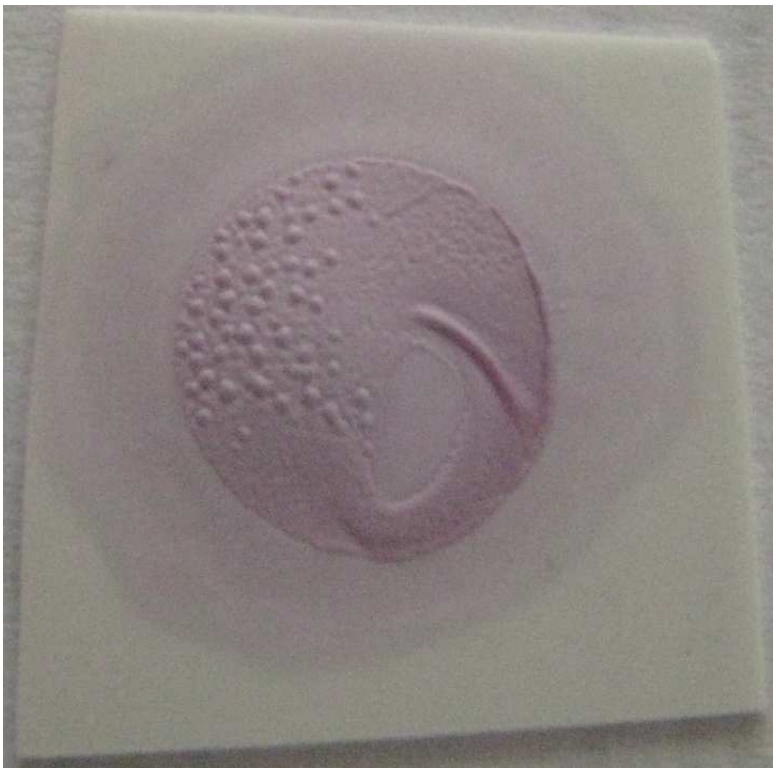

(b)

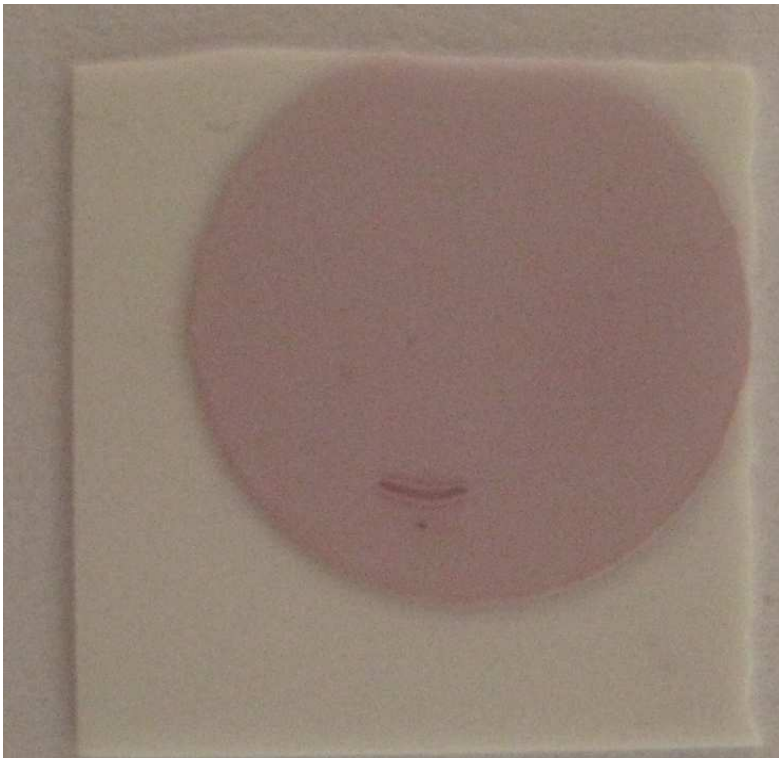

(c)

(d)

Figure 6-4 Surface optical micrographs of BNT films on graphite covered alumina substrates before sintering (a), and after sintering at 1250 °C for 1h on 100 nm-thick graphite layer (b) on 300 nm-thick graphite layer (c) and on 500 nm-thick graphite layer (d)

Table 6-1 Influence of the graphite layer thickness on the morphology of BNT films on alumina substrates sintered at 1250 °C for 1h

Thickness of graphite layer	Morphology of BNT films after sintering
<100 nm	not uniform
200-400 nm	conformal and uniform
>500 nm	films separated from alumina substrate

6.3.3 Interactions between BNT films and alumina substrates

The XRD patterns of BNT films on alumina substrate sintered at different temperatures are represented in Figure 6-5. All the samples sintered between 1200 °C – 1250 °C are single phase, being the diffraction pattern correspondent to the orthorhombic $BaNd_2Ti_5O_{14}$ phase [JCPDS card 33-0166]. However for BNT films sintered at 1300 °C, although the main phase is still the orthorhombic BNT, a neodymium aluminate phase was clearly identified. For BNT films sintered at 1350 °C mostly of the BNT phase disappeared being neodymium aluminate the dominating one. This result indicates that severe reactions took place between the films and the substrates for high sintering temperatures (1350 °C). Indeed, Shannon [Shannon R.D. -1976] and Mizuta et al. [Mizuta K.-1996] reported a reaction between alumina and BNT ceramics at sintering temperatures higher than 1300 °C.

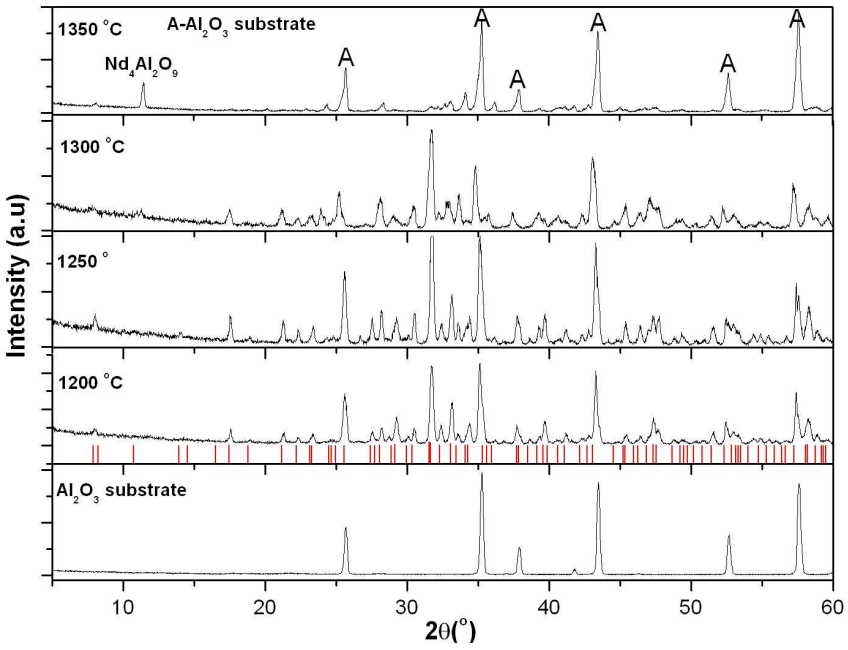

Figure 6-5 XRD patterns of BNT films on alumina substrates sintered at different temperatures (Diffraction lines from the JCPDS card 33-0166 are indicated by the red marks)

Figure 6-6 depicts the surface and cross section SEM micrographs of the BNT films sintered at temperatures from 1200 to 1350 °C. Crack free films were obtained. Films sintered at 1200 °C have low density with a considerable amount of porosity, as clearly seen in the micrographs of Figures 6-6 (a) and (b). As the sintering temperature increases to 1250 and 1300 °C, the density of the films increases markedly, as observed in the cross section micrographs (Figures 6-6 (d) and (f)). These images also reveal the good adhesion between films and the substrate. For the films sintered at 1250 and 1300 ºC elongated grains are developed and this anisotropy increases with the increase of the sintering temperature, in agreement with the observations described in chapter 5.3 for BNT films on Pt foils. The severe interactions between BNT films and alumina substrates, that took place at high sintering temperatures and were identified by XRD (Figure 6.5), are visibly illustrated in Figure 6-5 (g) in which the film morphology changed and equiaxed grains are depicted.

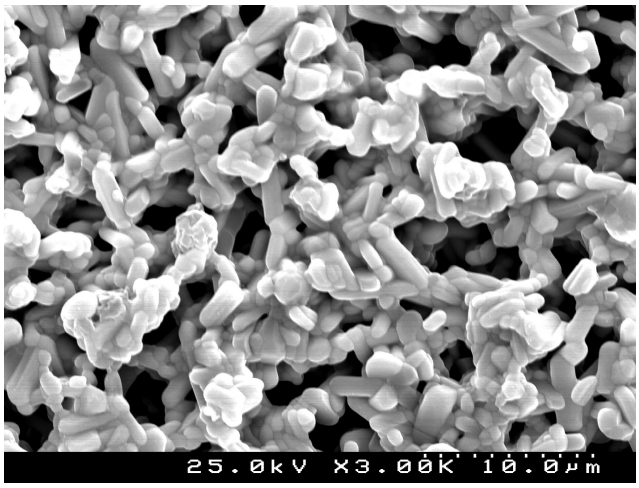

(a)

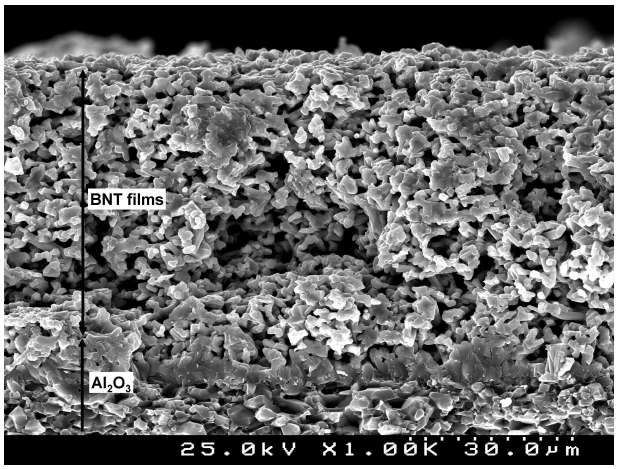

(b)

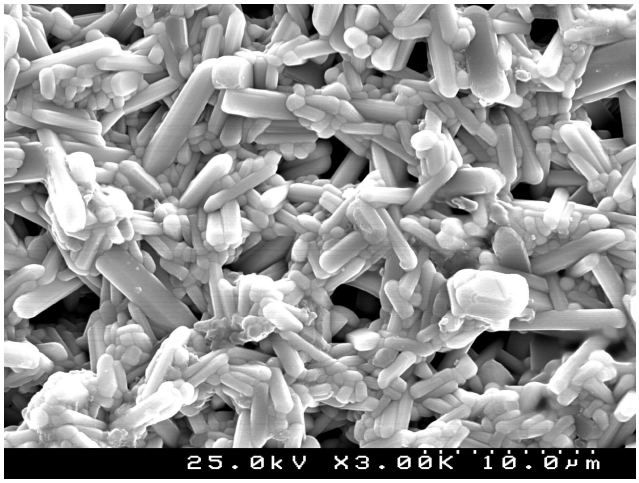
25.0kV X3.00K 10.0µm

(c)

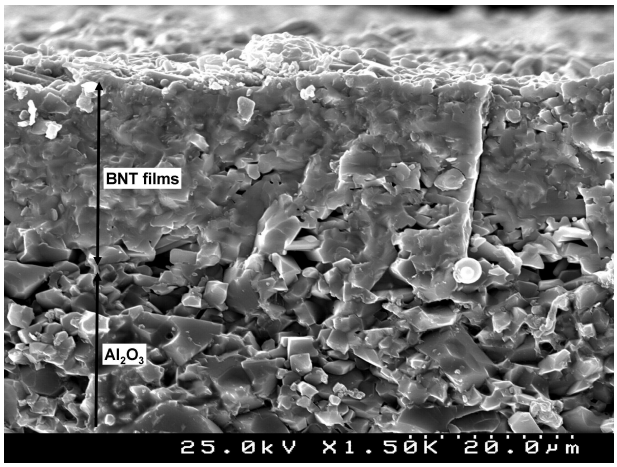
BNT films
Al_2O_3
25.0kV X1.50K 20.0µm

(d)

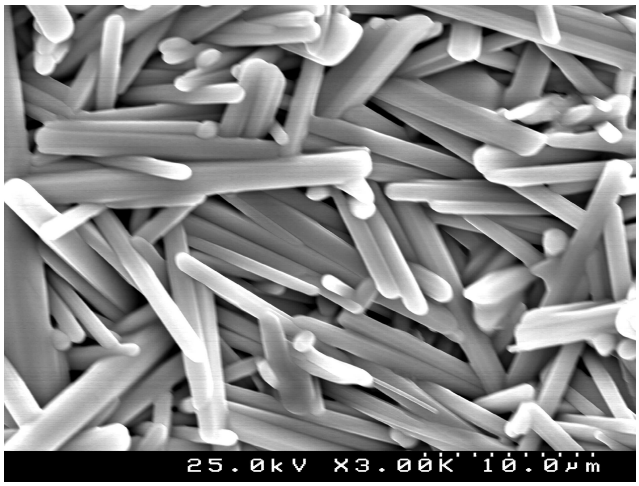
25.0kV X3.00K 10.0µm

(e)

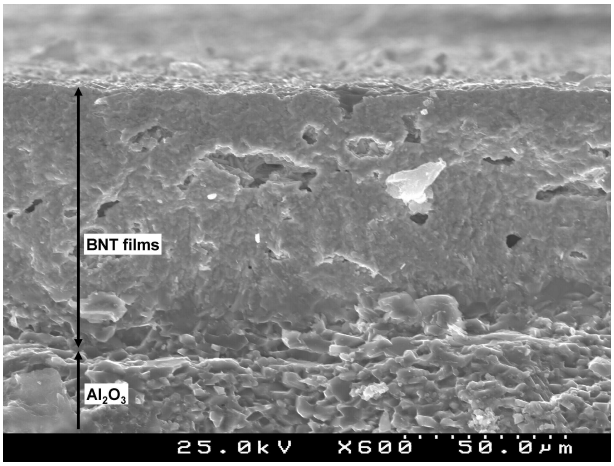

(f)

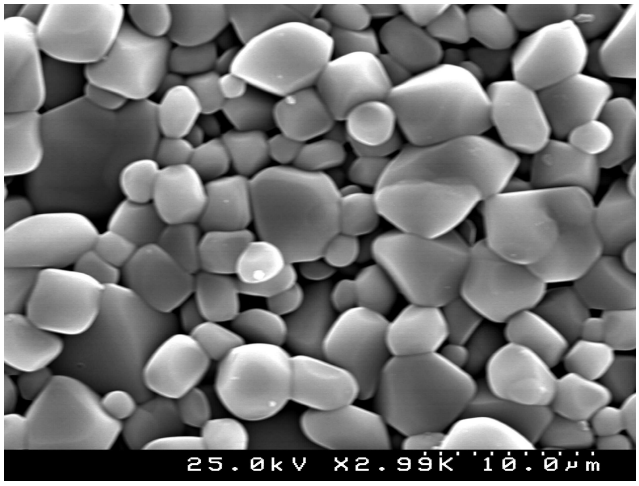

(g)

Figure 6-6 SEM surface and cross section micrographs of BNT films on alumina substrates sintered at 1200 °C for 1h (plane view (a) and cross section (b)), at 1250 °C/1h (plane view (c) and cross section d), at 1300 °C for 1h (plane view (e) and cross section (f)) and at 1350 °C for 1h (plane view (g))

Figure 6-7 illustrates the X-ray elemental profile of the cross-sections and surface X-Ray elemental map of BNT films sintered at different temperatures. No visible interactions are observed between BNT films and alumina substrates for films sintered at 1200 °C. As the sintering temperature increases to 1300 °C, Ba and Ti peaks were detected in the alumina substrates and Al^{3+} ions diffused into BNT films (Figure 6-7 (b)), in agreement with the XRD results where neodymium aluminate was detected (see Figure 6-5). In addition, X-ray map analysis revealed the intensive presence of rounded shape grains of a second phase, rich in Nd and Al (Figure 6-7 (c)). Similar results have

been reported in BST and YBCO thick films on alumina substrates by screen printing. [Su B.-2001, Matsuoka Y.-1996]

Based on the above results it was found that Nd^{3+}, Ti^{2+} and Ba^{2+} ions start to diffuse into the alumina substrates at a sintering temperature of 1300 °C and as a results a the formation of a second phase occurs that is expected to degrade the dielectric properties of BNT films.

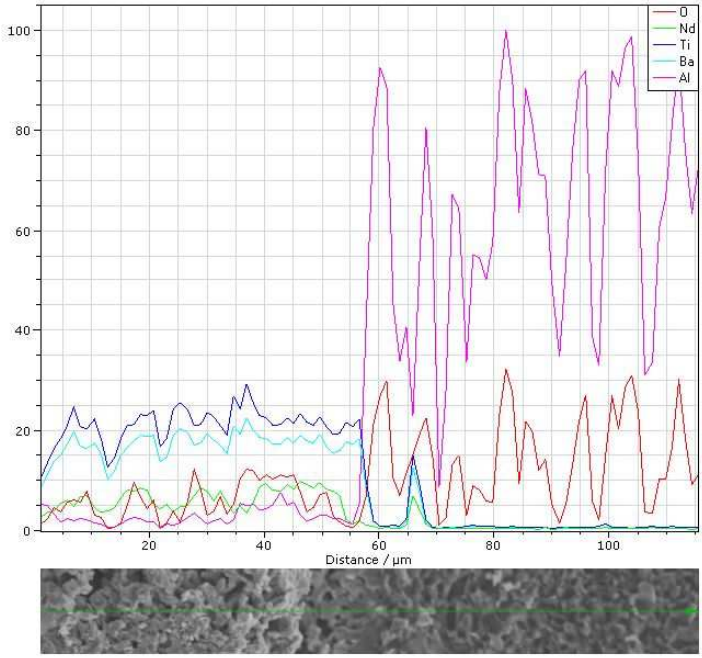

(a)

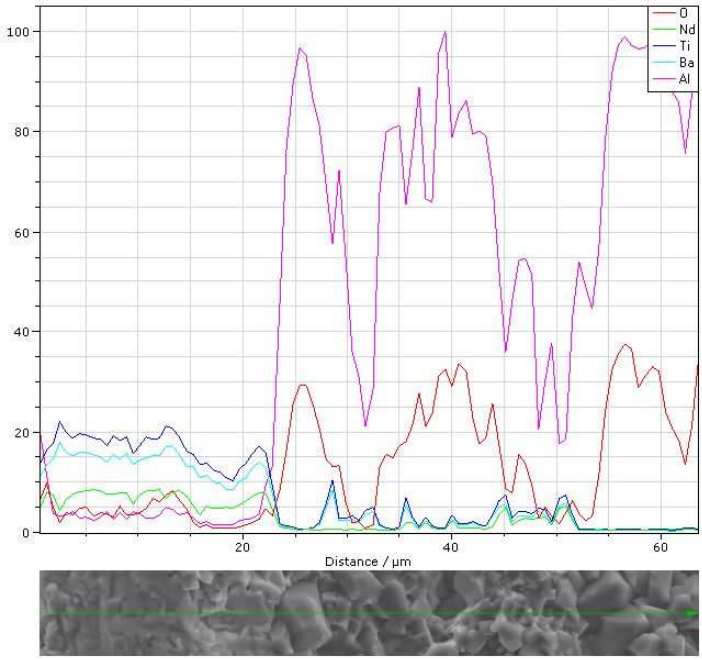

(b)

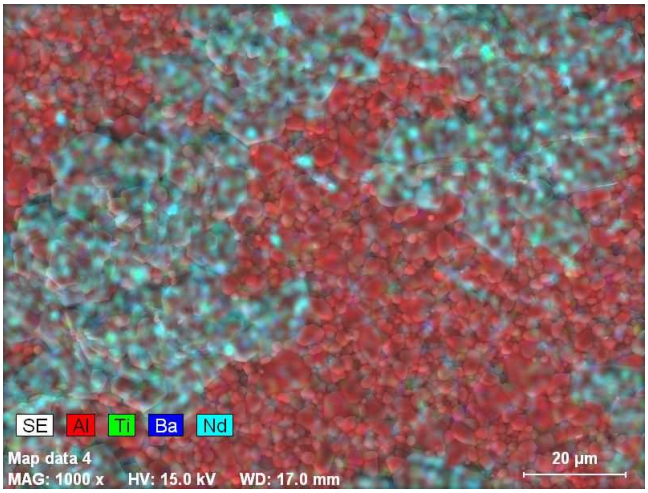

(c)

Figure 6-7 X-ray profile of a cross section of BNT films on alumina substrate sintered at (a) 1200 °C/1h, (b) 1300 °C/1h, (c) surface X-ray map of BNT films sintered at 1350 °C/1h

The analysis of the interface between BNT and Al_2O_3 substrates by TEM confirmed the interaction between films and the substrate at high sintering temperatures (Figure 6-8). For BNT films sintered at 1300 °C, EDS analysis showed the presence of Ti, Ba and Nd elements at the alumina side and the presence of Al at the film side.

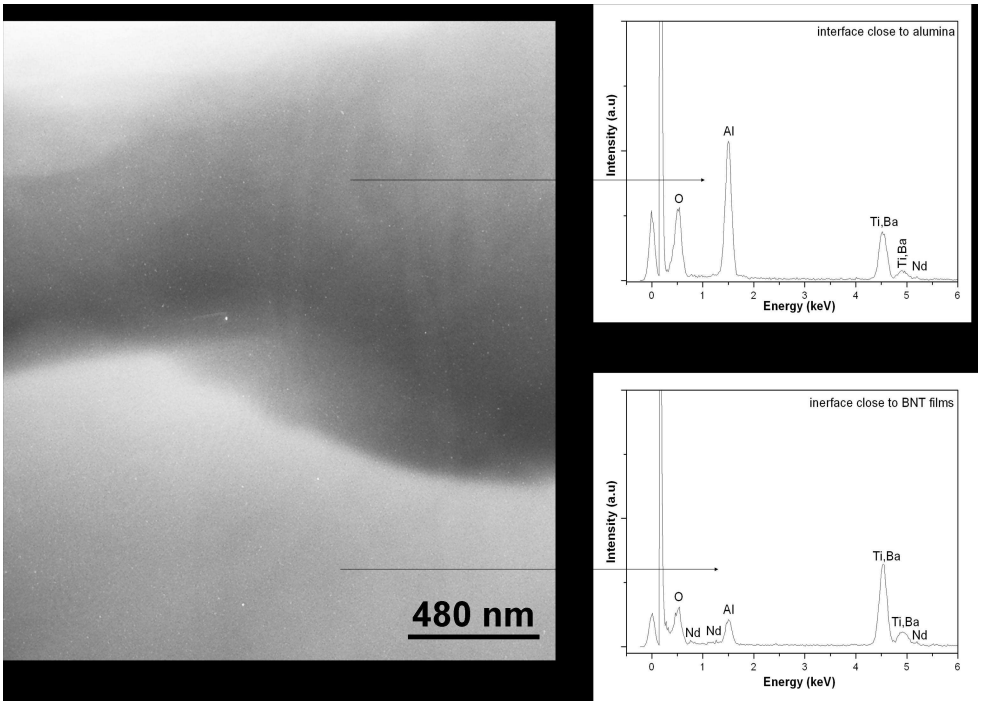

Figure 6-8 TEM micrographs and EDS analysis of the interface between sintered BNT films and alumina substrate, sintered at 1300 °C/1h

6.3.4 Dielectric properties

The dielectric properties of the BNT thick films on Al_2O_3 were analysed by the split post cavity resonator method at microwave frequencies and the results are presented in Table 6-2. 100 µm thick BNT films show ε_r of 146 and 93, and Q of 1161 and 1006 when sintered at 1250 and 1300 °C, respectively at about 10 GHz. The lower ε_r and Q value for BNT films sintered at 1300 °C should be related to reactions between film and substrate and to the presence of the second phase, above identified. Similarly, 30 µm-thick BNT films show ε_r and Q of 71 and 315, respectively when sintered at 1300 °C. The decrease of Q for thinner BNT films is related to the stronger effect of the second phase on the bulk of a thinner film than on a thicker one.

Table 6-2 Microwave dielectric properties of BNT thick films on Al_2O_3 substrate

Samples	Thickness (µm)	Sintering (℃/1h)	ε_r	Q	Frequency (GHz)
BNT films	100	1250	149	1161	9.63
BNT films	100	1300	93	1006	9.69
BNT films	30	1300	71	315	9.79

Figure 6-9 shows the relative permittivity and loss tangent of BNT films on alumina at low frequency. As mentioned the measured dielectric properties correspond to the dielectric response of the composite structure film + substrate. As shown in Figure 6-9, the relative permittivity is 39 for composites of BNT film + alumina substrate. The negative loss tangent results from a limitation of HP Bridge when measuring very low loss values.

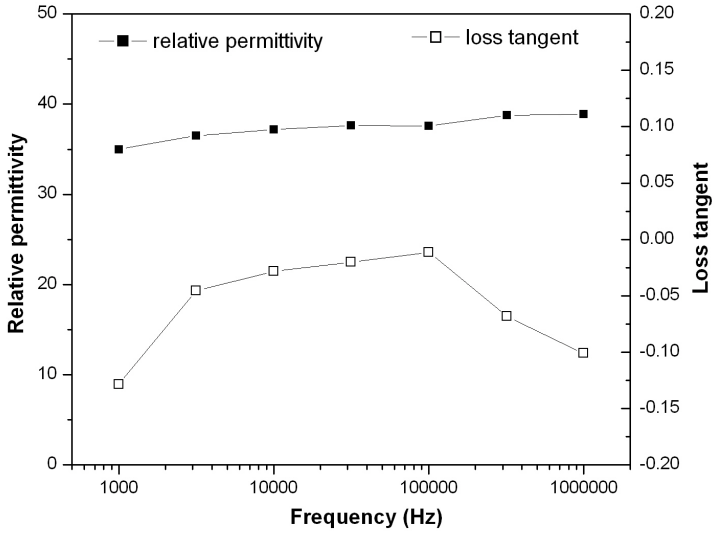

Figure 6-9 Relative permittivity and loss tangent against frequency of BNT films on alumina substrates (BNT – Al_2O_3 composite) sintered at 1250 °C/1h

Figure 6-10 depicts the temperature dependence of the relative permittivity of BNT films with alumina substrates at 1 MHz. TCε_r of the composite BNT - Al_2O_3 is 229 ppm/°C between 30-120 °C. The high Q and good thermal stability make BNT films on alumina substrate have good potential application for high frequency devices.

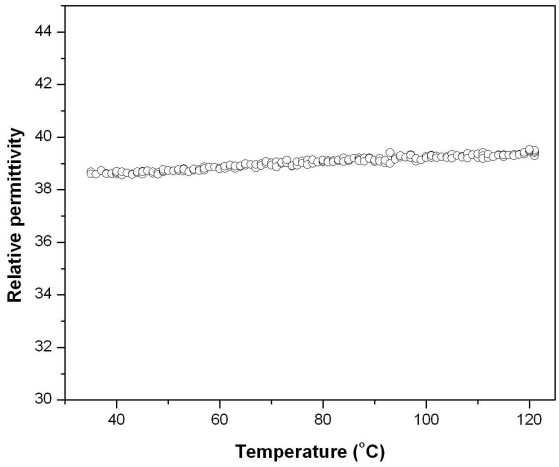

Figure 6-10 Temperature dependence of the relative permittivity of BNT films on alumina substrates (BNT – Al_2O_3 composite) sintered at 1250 °C/1h

6.4. Summary

A method to perform EPD on non-conducting substrates was developed through the use of a sacrificial graphite layer and EPD of BNT thick films on non-conducting alumina substrates was demonstrated. The thickness of the graphite layer plays a key role on the quality of the films after sintering. For sintering temperatures above 1300 °C the interaction between BNT films and alumina substrates occured with the formation of an aluminium based phase, which contributes to the degradation of the dielectric response. 100 µm BNT films on alumina substrate show ε_r and Q of 146 and 1161 at about 10 GHz when sintered at 1250 °C/1h. At 1 MHz, the relative permittivity is 39 for composite of BNT film + alumina substrate. BNT films on alumina substrates possess good Q values and high thermal stability, and therefore are potentially useful for high frequency applications. The success of EPD of BNT on alumina substrates is relevant as it enables deposition of low loss dielectrics at a low cost. It is believed that this approach of using sacrificial graphite layers for EPD on non-conducting substrates can be extended for both thin and thick film deposition of a large variety of other non-conducting substrates as well.

6.5 Reference

1. Barnwell P., Wood J. (1997) Proceedings of European Microelectronics Conference **44**, 51
2. Barnwell P., Wood J. and Reynolds, Q. (1998) Proceedings of International Electronic Manufacturing Technology Conference, 327
3. Besra L., Compsonb C., Liu M. L. (2007) J. Power Sources **173**, 130
4. Besra L., Compsonb C., Liu M. L. (2006) J. Am. Ceram. Soc. **89**, 3003
5. Hamagami J., Kanamura K., Umegaki T. (2002) Electrochem. Soc. Proc. **21**, 55
6. Hosomi T., Matsuda M. and Miyake M. (2007) J. Euro. Ceram. Soc. **27**, 173
7. Kanamura K., Hamagami J. (2002) Solid State Ionics **172**, 303
8. Matsuda M., Hosomi T., Murata K., Fukui T., Miyake M. (2005) Electrochem. Solid State Lett. **8**, A8
9. Ma J. and Hong H. H. (2002) J. Mater. Sci.: Mater. In Electronics **13**, 461
10. Matsuoka Y., Ban E., Ogawa H. And Kurosawa K (1996) J. Alloy. Compd. **239**, 55
11. Negishi H., Oshima N., Haraya K., Sakaka K., Ikegami T., Idemoto Y., Koura N. and Yanagishita H. (2006) J. Ceram. Soc. Jpn. **114**, 36
12. Peng Z. Y. and Liu M. L. (2001) J. Am. Ceram. Soc. **84**, 283
13. Shannon R. D. (1976) Acta Cryst. **A32**, 751
14. Su B. and Button T. W. (2001) J. Euro. Ceram. Soc. **21**, 2777
15. Tian Z. R., Free C., Aitchison C., Barnwell P. and James Wood J. (2002) Proceeding of international symposium on microelectronics **4931**,394
16. Toko America Inc. (1997) A miniature patch antenna for GPS application, Microwave **40**,116
17. Zhong S. S., Cui J. H., Xue R.F., and Niu J.W. (2004) Microwave Opt. Tech, Lett. **46**, 497

Chapter 7
Preparation and Dielectric Properties of $BaNd_2Ti_5O_{14}$-$(Ba_{0.5}Sr_{0.5})TiO_3$ Composite Films by EPD Combined with Sol-Gel Process

Abstract:

In this chapter, the preparation and characterization of $BaNd_2Ti_5O_{14}$ (BNT)-$Ba_{0.5}Sr_{0.5}TiO_3$ (BST) composite thick films on flexible platinum foil substrate, via an electrophoretic deposition combined with sol gel process is reported. Homogeneous, dense, and uniform BNT-BST composite thick films are fabricated on flexible Pt foils. Phase composition and microstructure of the BNT-BST thick films are characterized by X-ray diffraction and scanning electron microscopy. 9μm-thick BNT-BST composite films presented a relative permittivity and a loss tangent of 287 and 0.0013 at 1MHz, a dielectric tunability of 12% at 33kV/cm, and a temperature coefficient of relative permittivity of 0.26% between 28 ºC to 120 ºC, respectively. The results clearly indicate that the dielectric properties of BNT dielectric thick films can be modified with the incorporation of ferroelectric BST to fit the requirements of tunable devices. The good physical and electrical properties of the BNT–BST composite thick films, including very low dielectric loss tangent while retaining reasonably high relative permittivity and dielectric tunability, make them excellent candidates for integration into tunable RF and microwave devices.

7.1 Introduction

Progress in microwave communications and continuing miniaturization of integrated circuitry has resulted in a demand for tunable passive components, such as tunable oscillators, phase shifters, and varactors, among others. [Horwitz J. S.-1998, Levin I.-2000] High dielectric tunability and low dielectric loss are important and critical for these applications. [Park B. H. -2001] The main requirement for the electrical properties of ceramic materials to be used in such tunable devices is a combination of the optimal value of the relative permittivity, high level of electric field tunability, and low dielectric losses. However, low dielectric loss in conjunction with high tunability in simultaneous in a materials have been proved to be very problematic

to be achieved from the physics point of view. [Sengupta L. C.-1999] Thus, in practice, there is a trade-off between dielectric tunability and the materials dielectric loss.

Ferroelectrics such as barium–strontium titanate (BST) are well known as promising candidates for the application in microwave tunable devices including phase shifters, filters, and others. [Chang W.-2002] Ferroelectric layers can be also used as control elements for accelerating structures with dielectric loading. [Kanareykin A. D.-2003] However, many problems remain in utilizing BST for such high frequency applications. In particular, one of the major challenges is the simultaneous minimization of the material dielectric losses and maximization of the material dielectric tunability. [Gevorgian S. S. -2001] Indeed, the optimal electronic parameters of the dielectric material of choice for tunable device applications should be: moderate to low relative permittivity at microwave frequencies ($30<\varepsilon_r<1500$), low electronic loss tangents ($0.005<\tan\delta<0.01$), and high dielectric tunability (change in relative permittivity with applied voltage: >10%). [Sengupta L. C.-1999]

Intensive investigations have been performed aiming at the reduction of losses. [Chen C. L -1999] Recent efforts on improving the loss characteristics of BST materials include the doping with high-Q additives such as MgO, Al_2O_3 etc. [Wu L.-2000, Chang W.-2002, Ngo E. –2001]. However, these dopants may react with BST materials in a way that the microwave dielectric properties of the material will vary markedly with the processing parameters, resulting in inconsistency in the device performance. It has been intuitively believed that the dielectric losses of ferroelectrics can be further improved by mixing them with linear low-loss dielectrics. That is why attempts are being done in synthesizing such composite materials. Connecting a low-loss non-tunable dielectric in series with tunable BST films should result in a reduced overall loss tangent and a loss of tunability for the layered structure. [Irvin P. -2005]

In previous chapters, it was shown that $BaNd_2Ti_5O_{14}$ (BNT) thick films present very low dielectric losses. Based on this, in the present study BNT - BST composite thick films are chosen to address the possibility of improving the dielectric losses and keeping the good tunability of the relative permittivity of BST, by using high-Q BNT materials as matrix in the composite.

In this chapter, the preparation and characterization of BNT–BST composite thick films on platinum foil substrate, via an electrophoretic deposition-sol gel process is reported. Homogeneous, dense, and uniform BNT-BST composite thick films were fabricated on flexible Pt substrate. The main goal of this work was to search for new

compositions of ferroelectrics with reasonable tunability and small dielectric losses. Composite materials exhibiting relatively high tunability in combination with reduced dielectric permittivity, low loss level and good temperature stability have been experimentally obtained. The good physical and electrical properties of BNT–BST composite thick films, including very low dielectric loss tangent while retaining reasonably high relative permittivity and dielectric tunability, make them excellent candidates for integration into tunable high frequency devices.

7.2 Experimental

In this chapter, all the BNT thick films are prepared from home made BNT powders. BNT films were prepared on Pt foil in acetone with I_2 suspensions with applied voltage of 200 V. The BST sol was infiltrated into BNT thick films with Pt foil substrates by spin coating. The as spin-coated BST films onto BNT green films were pyrolyzed at 300 ºC for 5min, which process was repeated 10 times so as to acquire around 500 nm thick for upper BST films. For comparison, the BST thick films are also prepared on Pt foil by EPD. The BST powders were made from the same BST sol for the infiltration. All the BNT-BST composite films and BST thick films were sintered in air at 1300 ˚C for 1 h. The experimental details are described in chapter 4, including the preparation of BST sols, BST thick film, BNT thick films and the physical characterization.

7.3 Results and Discussions

Figure 7-1 depicts the XRD patterns of $BaNd_2Ti_5O_{14}$ (BNT)-$(Ba_{0.5}Sr_{0.5})TiO_3$ (BST) composite thick films on Pt foil sintered at 1300 °C for 1h. For comparison the XRD patterns of pure BST and BNT thick films are also included. Two crystalline phases, the cubic $Ba_{0.5}Sr_{0.5}TiO_3$ (JCPDS card 39-1395) perovskite structure and the orthorhombic $BaNd_2Ti_5O_{14}$ structure (JCPDS card 33-0166) are observed without other phases being detected for the composite thick films.

To optimize the dielectric properties of the materials by infiltrating BST into BNT, the two constituents must not react during the densification process. Fortunately, as indicated in Figure 7-1 BNT and BST materials do not interact with each even at high sintering temperatures. Both BNT and BST materials sintering temperature are around 1300˚C [Fu Z.-2007, Sengupta L. C. -1999], so their similar sintering temperature avoid the risk of very different sintering behavior and of the appearance of intermediate

reactions.

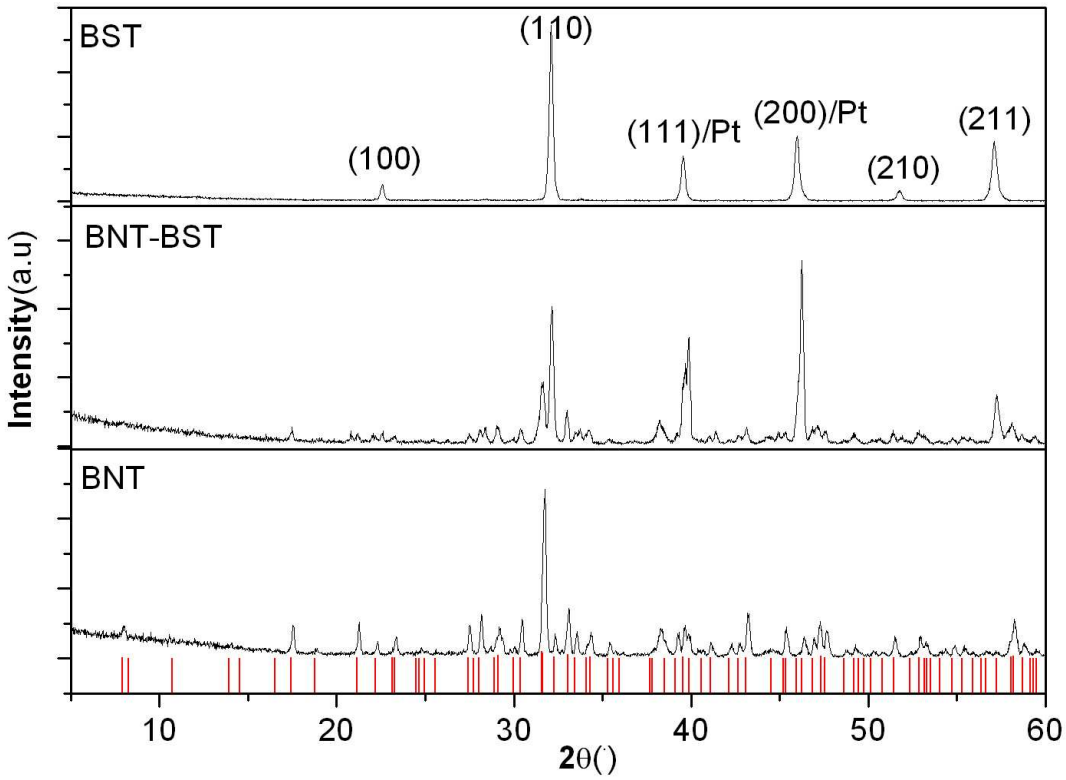

Figure 7-1 XRD pattern of BNT, BNT-BST composite and BST thick films on Pt foil, sintered at 1300 °C/1h (the diffractions lines of JCPDS card 33-0166 are indicated by red mark)

Typical microstructures of BST, BNT-BST composite and BNT thick films are depicted in Figure 7-2. Crack - free, dense, homogeneous and uniform BNT-BST composite thick films can be fabricated by EPD combined sol-gel process. BNT-BST thick films are clearly biphasic with both BNT and BST phases uniformly distributed within each other, containing need-like BNT grains and round BST (Figure 7-2 (c). From the SEM cross-section micrograph of a 9μm thick BNT-BST composite thick film sintered at 1300 °C and displayed in Figure 7-2 (d), the interface between the film and the Pt substrate is smooth and abrupt with no interfacial layers, amorphous phases or voids. The X-ray elemental mapping was employed to analyze the distribution of the BST phase in the BNT matrix of the thick films (Figure 7-2 (e) and strontium was the chosen element to identify the degree of homogeneity between the materials. As shown in Figure 7-2 (e) strontium is uniformly distributed in the BNT matrix indicating that BST phase is homogeneously infiltrated into the BNT matrix.

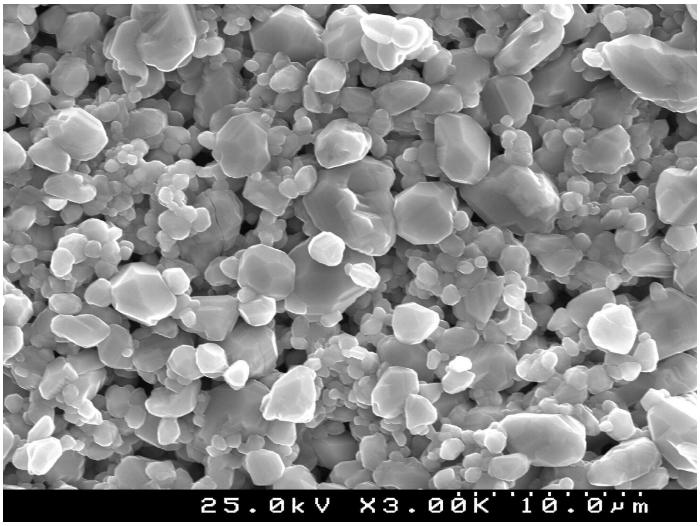
25.0kV X3.00K 10.0µm

(a)

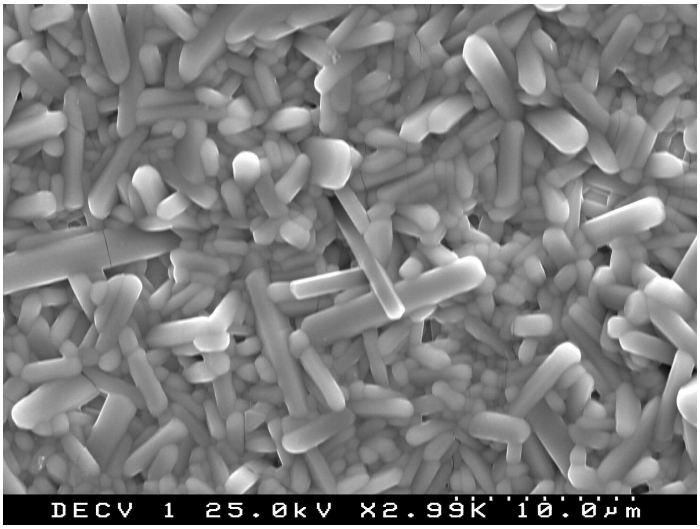
DECV 1 25.0kV X2.99K 10.0µm

(b)

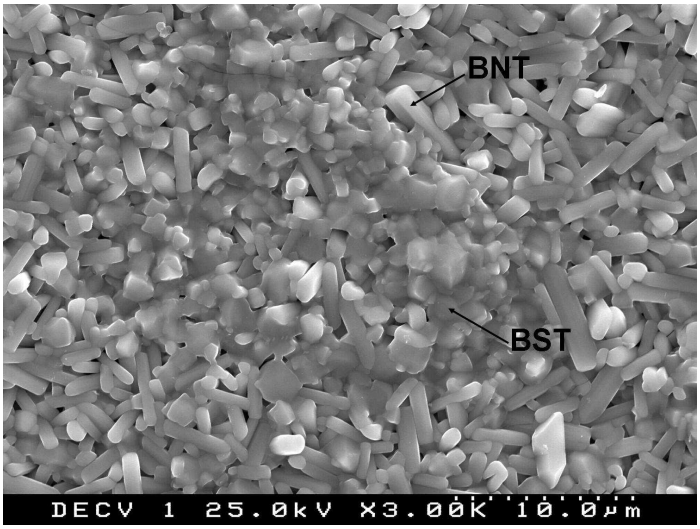
BNT
BST
DECV 1 25.0kV X3.00K 10.0µm

(c)

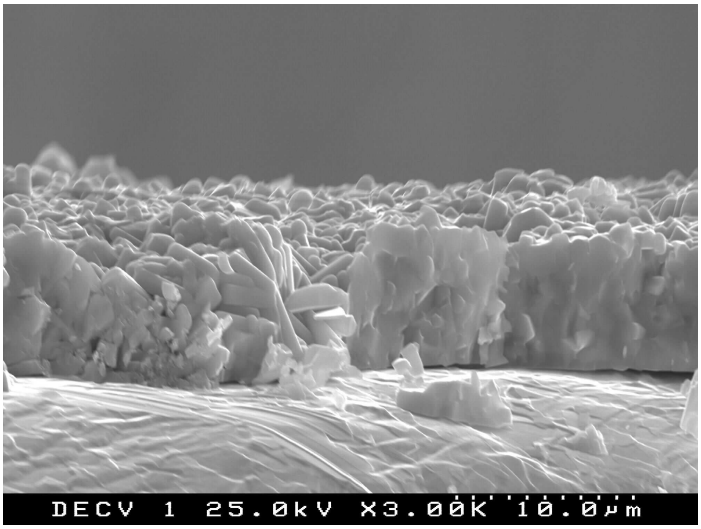

(d)

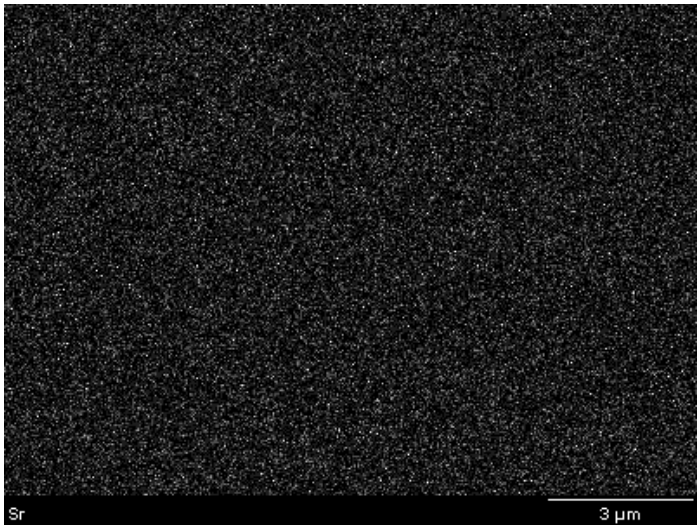

(e)

Figure 7-2 SEM surface micrographs of (a) BST, (b) BNT, (c) BNT-BST composite films, (d) cross section of BNT-BST composite films, and (e) surface X-ray Sr element mapping of BNT-BST composite thick films, all sintered at 1300 °C/1h

The comparison of the relative permittivity and loss tangent of BST, BNT-BST composite and BNT thick films as a function of frequency is shown in Figure 7-3. The relative permittivity and loss tangent of BNT-BST composite films are 287 and 0.0013, respectively at 1 MHz. Meanwhile, the absence of an appreciable dispersion of the dielectric properties with the measured frequency up to 1 MHz is indicative of an excellent film quality and the absence of internal interfacial barriers. Compared to the pure BNT (ε_r=95, tanδ=0.0004 at 1 MHz) or BST thick films (ε_r=800, tanδ=0.008 at 1 MHz), as shown in Figure 7-3, the relative permittivity and loss tangent of BNT-BST composite thick films are dramatically changed. In contrast to pure BNT thick films, the

increased relative permittivity of BNT-BST composite thick films is the result of the presence of the high relative permittivity of the BST phase in BNT, as expected for composite materials. On the other hand, in contrast to pure BST thick films, the loss tangent for the BNT-BST composite material is markedly improved (reduced) from $\tan\delta_{BST} = 0.008$ to $\tan\delta_{BNT\text{-}BST} = 0.0013$ at 1 MHz, respectively due to the introduction of the low loss BNT. The loss tangents of these composites have been reduced to enhance the overall impedance matching and thereby lowering the overall insertion loss of the device.

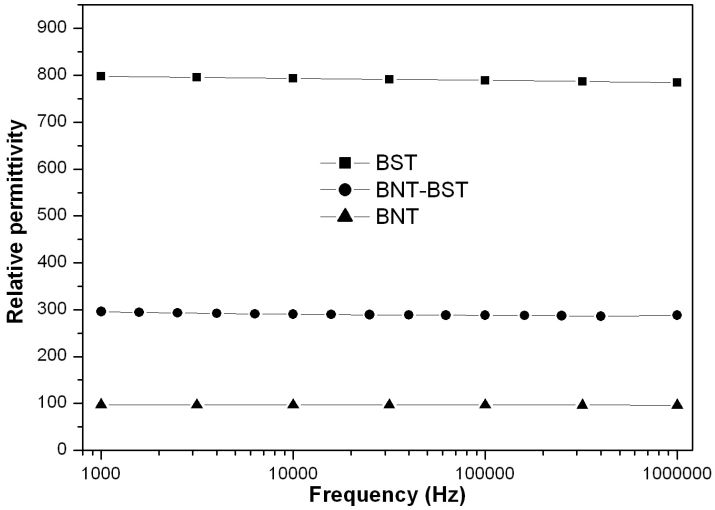

(a)

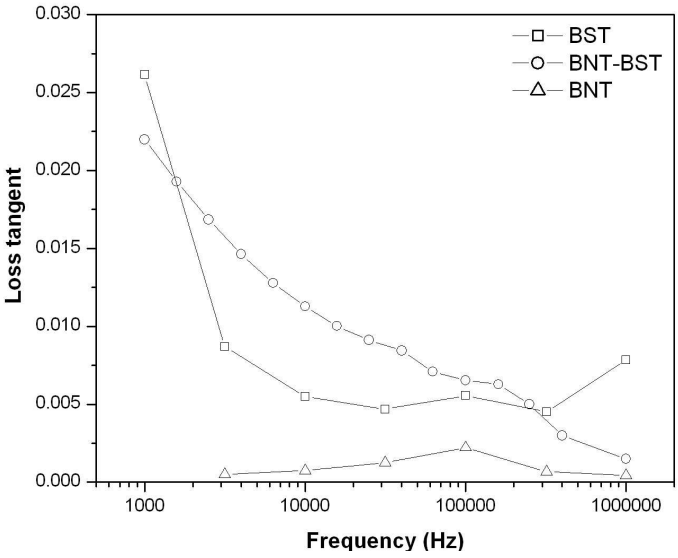

(b)

Figure 7-3 Relative permittivity (a) and loss tangent (b) of BST, BNT-BST and BNT thick films as a function of frequency

The comparison of the DC bias dependence of dielectric properties on the electric field, an indication of the tunability, for pure BST, BNT-BST composite, pure BNT thick films at room temperature is depicted in Figure 7-4. Their dielectric properties and calculated tunability are summarized in Table 7-1, as well.

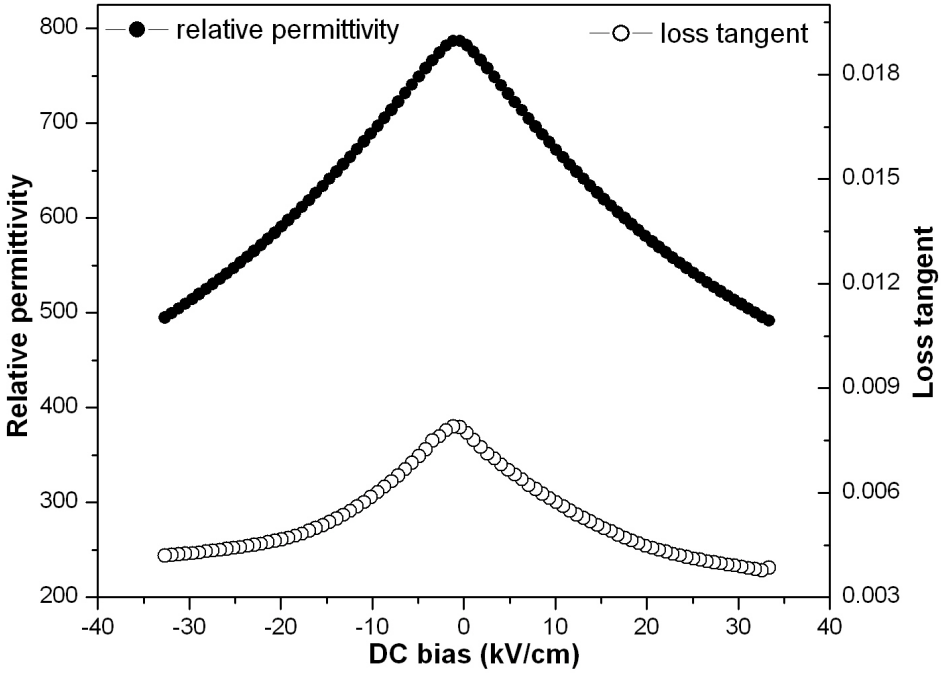

(a)

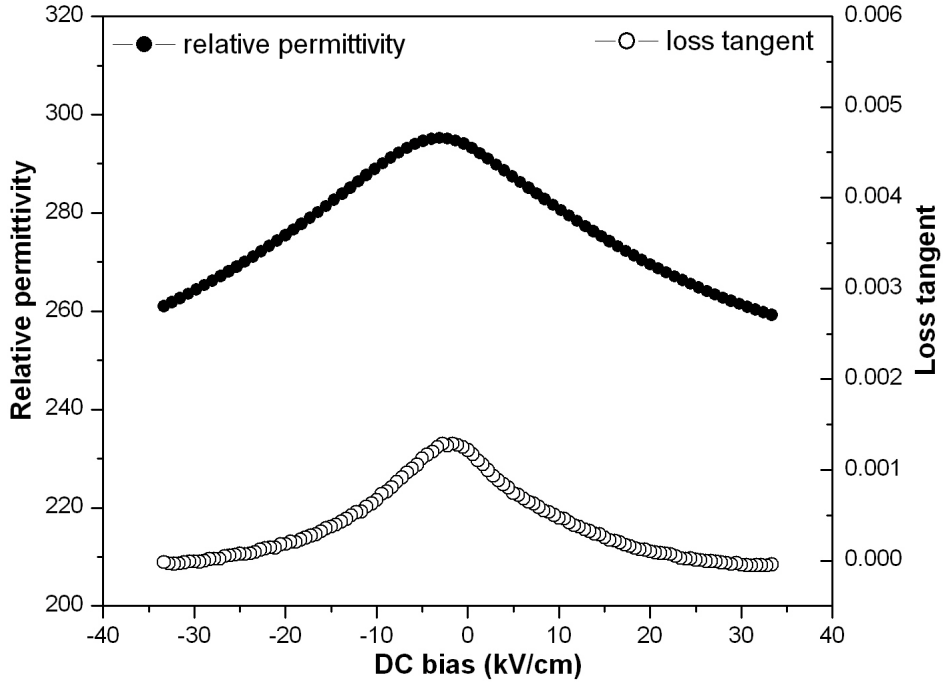

(b)

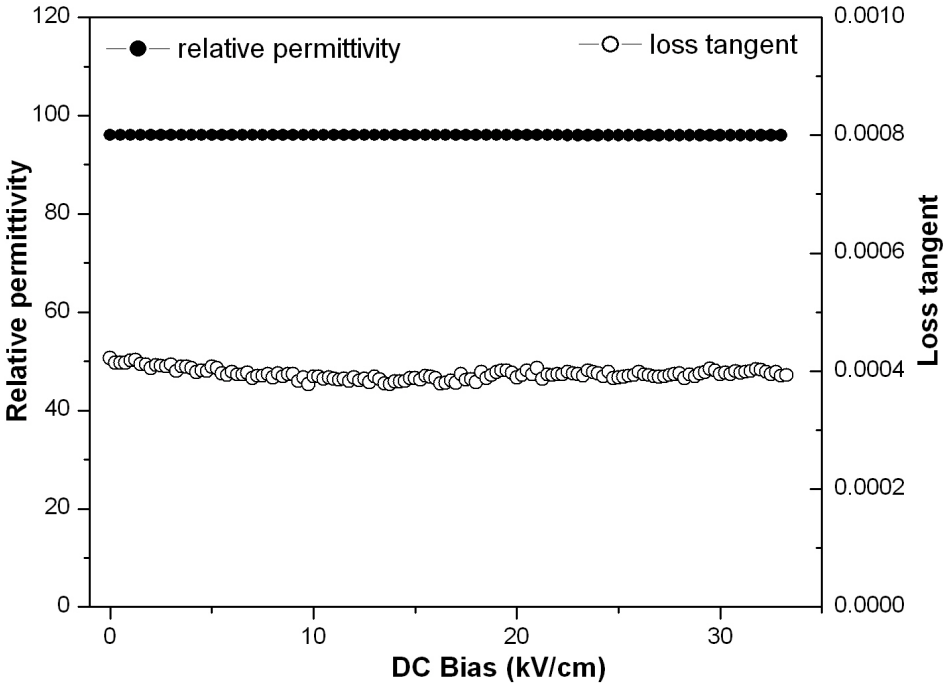

(c)

Figure 7-4 DC bias dependence of relative permittivity and loss tangent of (a) pure BST, (b) BNT-BST composite (c) pure BNT thick films, sintered at 1300 °C/1h

The dielectric tunability was calculated by the formula:

$$\text{Tunability} = \frac{\varepsilon_{r0} - \varepsilon_{rb}}{\varepsilon_{r0}} \times 100\% \qquad (7\text{-}1)$$

where ε_{r0} and ε_{rb} represent the relative permittivity value at zero applied electric field and the maximum applied electric field, respectively. Based on the formula (7-1), the relative tunability of 38% and 12% at 33 kV/cm is observed for pure BST and BNT-BST composite thick films, respectively. It is obvious that pure BNT does not show any tunable characteristics at a DC bias, as shown in Figure 7-4 (c).

In the present work composite BNT-BST thick films exhibit low losses (0.0013 at 1 MHz) and a relatively high tunability (12% at 33 kV/cm). The tunability of BNT–BST films is much lower than pure BST thick films. Since EPD films are significantly thinner than the bulk ceramics, the film tunability can be elevated by applying high dc electric fields with overall lower power consumption, compared to bulk ceramics. So, higher dielectric tunability than the measured can be easily realized by increasing the external applied electric field in the device fabrication.

As mentioned above, there is inevitably trade-off when improving the dielectric loss tangent of ferroelectric materials. In the tunable device community, the figure of merit K is usually used to compare the quality of tunable dielectrics. *K* is define as: [Chong K. B. -2004]

$$K = \frac{tunability}{\tan\delta} = \frac{(\varepsilon_{r0} - \varepsilon_{rb})/\varepsilon_{r0}}{\tan\delta} \tag{7-2}$$

where ε_{r0} and ε_{rb} have the same meanings as in formula (7-1), and tanδ is the dielectric loss tangent at zero dc applied voltage and expresses the trade-off between tunabilty and losses. According to formula (7-2), *K* factor of pure BST and BNT-BST composite thick films was calculated to be 48 and 70 at 33 kV/cm and 1 MHz, respectively. Although the effects of BNT introduction reduced the relative permittivity, loss tangent, and dielectric tunability (Figure 7-3, 4), of BST, BNT-BST composite thick films exhibit a considerably increased figure of merit as compared with pure BST thick films. The *K* factor clearly shows that the BNT introduction is successful in improving the dielectric properties of BST thick films, enhancing their suitability in tunable device applications with their low loss and high *K* factor.

Table 7-1 lists the comparison of the dielectric properties of BNT-BST composite films prepared in the current work with analog reported materials. As indicated BNT-BST composite thick films present a very high *K* factor, together with improved overall dielectric performance characterized by low dielectric loss and reasonable tunability for application in agile devices. Furthermore, high dielectric tunability can be easily obtained by increasing the external applied electric field in device fabrications. In this respect, BNT–BST composite thick films are very promising candidates for the above tunable device applications.

Table 7-1 BNT thick films prepared in this work with analog reported materials

Materials	ε_r	Tanδ	Tunability (%)	*K*	Reference
BNT-BST composite thick films	290	0.0013 at 1MHz	12 at 33.3kV/cm	70	current work
Pure BST thick films	800	0.008 at 1MHz	38 at 33.3kV/cm	48	current work
Pure BNT thick films	95	0.0004 at 1MHz			current work
BST-MgO composite thick films	327	0.002 at 1MHz	8 at 20 kV/cm	40	Ngo E.-2001
BST-Al_2O_3 composite thin films	870	0.011 at 7.7GHz	15.9 at 8.1 kV/cm	14.45	Chong K. B.-2004
BST-MgO composite thin films	222	0.007 at 100kHz	15.7 at 237 kV/cm	22.4	Cole M. W.-2003
BST-$Bi_{1.5}ZnNb_{1.5}O_7$ composite thin films	403	0.0037 at 7.7GHz	5.7 at 8.1 kV/cm	15.4	Yan L.-2004
BST-$Ba_4Ti_{13}O_{30}$ composite ceramics	110	0.0005 at 6GHz			Thomas J. P.-2004

Figure 7-5 exhibits the temperature dependence of relative permittivity of BNT-BST composite. The temperature dependence of relative permittivity of BNT-BST composite was analyzed between 28 °C to 120 °C at 1MHz and calculated to be 0.26%/°C, which indicates a relative good temperature stability of BNT-BST composite thick films.

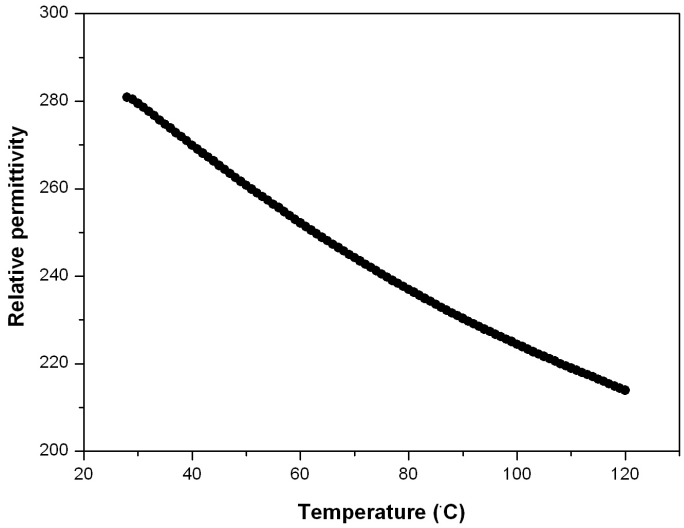

Figure 7-5 Temperature dependence of relative permittivity of BNT-BST composite films, sintered at 1300 °C/1h

7.4 Summary

Dense, homogeneous and uniform BNT-BST composite thick films were fabricated by EPD combined sol-gel process. The two components, BNT and BST, did not react at high sintering temperatures, resulting in composite thick films of BNT and BST. The dielectric loss tangent was reduced from 0.008 for BST to 0.0013 for BNT-BST at 1 MHz. Identical to the dielectric loss tangent, the relative permittivity and dielectric tunability was also reduced for BST from 800 to 280 and 37.5% to 12%, for BNT-BST, respectively. But nevertheless and more importantly, the dielectric tunability for BNT-BST composite thick film remains, for these low dielectric losses, 12% what is a very high value together with one of the highest figure of merit (70) reported until now for tunable dielectric films and temperature dependence of relative permittivity of 0.26%/˚C between 28˚C to 120˚C. The BNT introduction significantly improved the dielectric loss of BST thick films, adding a great value to BNT-BST composite thick films for tunable dielectric device applications.

7.5 References

1. Chang W. and Sengupta L. C. (2002) J. Appl. Phys. **92**, 3941
2. Chen C. L., Feng H. H., Zhang Z., Brazdeikis A., Huang Z. J., Chu W. K. and Chu C.W. (1999) Appl. Phys. Lett. **75**, 412
3. Chong K. B., Kong L. B. and Chen L. F., Yan L., Tan C. Y., Yang T., and Ong C. K., Osipowicz T. (2004) J. Appl. Phys. **95**, 3
4. Cole M. W., Nothwang W. D., Hubbard C., Ngo E., and Ervin M. (2003) J. Appl. Phys. **93**, 9218
5. Fu Z., Wu A. Y., Vilarinho P. M, Kingon A. I. and Wordenweber R. (2007) Appl. Phys. Lett. **90**, 052912
6. Gevorgian S. S. and Kollberg E. L. (2001) IEEE Trans. on Microwave Theory and Tech. **49**, 2117
7. Horwitz J. S., Chang W., Carter A. C., Pond J. M., Kirchoefer S. W., Christy D. B., Levy J., and Hubert C. (1998) Integrated Ferroelectric **22**, 799
8. Irvin P., Levy J., Guo R., and Bhalla A. (2005) Appl. Phys. Lett. **86**, 042903
9. Kanareykin A. D., Gai, W., Power J. G., Nenasheva E. A., Karmanenko S. F. and Sheinman I. (2003) A method for tuning dielectric loaded accelerating structures, In Proceedings of the Particle Accelerator Conference, PAC, 1888
10. Levin I., Leapman R. D., and Kaiser D. L., J. Mater. Res. **15**(2000)1433
11. Ngo E., Joshi P. C., Cole M. W., and Hubbard C. W. (2001) Appl. Phys. Lett. **79**, 248
12. Park B. H., Peterson E. J., Jia Q. X., Lee J., Zeng X., Si W., and Xi X. X. (2001) Appl. Phys. Lett. **78**, 533
13. Sengupta L. C. and Sengupta S. (1999) Mater. Research Innovations **2**, 278
14. Thomas J. P. (2004) Integrated ferroelectrics **66**, 213
15. Wu L., Chen Y. C., Huang C. L., Chou Y. P. and Tsai Y. T. (2000) J. Am. Ceram. Soc. **83**, 1713
16. Yan L. (2004) Appl. Phys. Lett. 85, 3522

Chapter 8
Conclusions and Future Work

8.1 Conclusions

The aforementioned works related to investigate solutions to overcome particular engineering obstacles in fabricating reliable low loss dielectric thick films for high frequency application. Our work has addressed specific engineering-based hurdles such as economical and reproducible fabrication of low loss dielectric thick films. The ideas behind these works were born as sketches on a whiteboard that grew into functional devices after careful planning and considerable lab effort. I was fortunate enough to have been given the necessary latitude to investigate these ideas, formulate the processing routes and see them to fruition and for that opportunity. I am entirely grateful to my supervisors, Prof. Paula M. Vilarinho and Prof. Angus I. Kingon.

EPD is a fast and cost-effective method of depositing films of ceramics. As interest in this method grew, we proved our contention and developed a method for depositing low loss dielectric thick films on metal foils and alumina substrates. High quality BNT thick films were prepared in the current work. It was shown that the density of EPD derived BNT films can be greatly increased by a cold isostatic pressing treatment after deposition, which resulted in considerable enhancement of the dielectric properties. Dense BNT thick films displayed a homogeneous microstructure with a characteristic needle shape grain growth when compared with equivalent ceramic samples. The dielectric Q is higher than any previously reported for thick films. The excellent dielectric properties, including good thermal stability and bias voltage independent capacitance characteristics suggest the suitability of EPD derived BNT thick films for integrated capacitor and microwave device applications. EPD has thus been proved to be a low-cost and efficient method to process low loss (high Q) coatings on metal electrodes of high frequency device.

Based on the works we have completed, we have come to the following general out puts and conclusions:

1) A novel approach to depositing low loss BNT thick films on Pt foil and alumina substrates has been developed and characterized. Success in the EPD processing is intimately related to a careful choice of solvent and additives. Suspension study revealed that the suspension stability determines whether a deposition is generated

at the electrode and the quality of the deposited films by EPD.

2) The anisotropic microstructure development in BNT thick films prepared by EPD on Pt substrate and its impact on the dielectric properties demonstrated an alternative way to tailor TCεr of dielectric thick films. These results have a significant technological impact for the future applications of $BaO–Re_2O_3–TiO_2$ materials in film form for high frequency devices. Observed anisotropic grain growth is facilitated by the constrained sintering. By controlling the sintering temperature, near – zero TCεr, high Q thick films can be fabricated. These findings are of technological relevance since they demonstrate that by controlling the substrate constraint and sintering conditions can be used to control grain anisotropy and thus microwave properties of the $BaO-Re_2O_3-TiO_2$. The thick films facilitate scaling to small device sizes for high frequency operation. Similar observations are expected in other MW systems thus opening further technological opportunities.

3) We report a method of performing EPD on non-conducting substrates overcoming the requirement of a conducting substrate through the use of sacrificial graphite layer. The conductivity of the substrate is therefore no longer a limiting factor in the application of EPD. We believe that this approach can be extended for both thin and thick film deposition on a variety of other non-conducting substrates as well.

4) Our results showed that the dielectric properties of BST ferroelectric thick films can be readily modified with BNT introduction to fit the requirements of tunable device applications. We concluded that the BNT introduction significantly improved the dielectric loss tangent of the BST thick films. The good physical and electrical properties of the BNT–BST composite thick films, including very low dielectric loss tangent while retaining reasonably high dielectric constant and dielectric tunability, make them excellent candidates for integration into tunable RF and microwave devices.

8.2 Future work

This thesis is a systematic but not complete study of the EPD of low loss BNT materials. Interesting physical phenomena were found, and possible physical mechanisms were discussed in these systems, especially in the case of sintering effect on the structure, microstructure and dielectric properties of BNT thick films. However, a better understanding and using of the EPD techniques, that will allow a further practical application of the materials, requires the following work to be carried out:

a) Systematically measure the dielectric properties of BNT thick films on Pt

foils at microwave frequencies;

b) Multi-component deposition by EPD, such as, EPD of glass sintering aids and BNT materials for low temperature sintering to take use of base meta substrate, i.e. Cu foil;

c) Composite structure pattern by EPD, such as, stripe structure of BNT based high Q composite design, to tune the dielectric properties for some specific applications.

List of Publications During PhD Period

1. Scientific papers:

1.1 Published papers

[1] **Zhi Fu**, Paula M. Vilarinho, Aiying Wu, Angus I. Kingon, "Textured Microstructure and Dielectric Properties of Low Loss $BaNd_2Ti_5O_{14}$ Thick Films Prepared by Electrophoretic Deposition", *Advanced Functional Materials*, In Press

[2] **Zhi Fu**, Aiying Wu, Paula M. Vilarinho, Angus I. Kingon, R. Wördenweber, "Low Dielectric Loss $BaNd_2Ti_5O_{14}$ Thick Films Prepared By an Electrophoretic Deposition Technique", *Applied Physics Letters*, 90, 052912, 2007

[3] **Zhi Fu**, Aiying Wu, Paula M. Vilarinho, "Effect of Seed Layer Thickness on Texture and Electrical Properties of Sol-Gel Derived $(Ba_{0.8}Sr_{0.2})TiO_3$ Thin Films", *Chemistry of Materials*, 18, 3343-3350, 2006

[4] **Zhi Fu**, Paula M. Vilarinho, Aiying Wu, Angus I. Kingon, "Development of Low Loss, Temperature Stable $BaNd_2Ti_5O_{14}$ Thick-Film Dielectrics by Electrophoretic Deposition Techniques", *IMAPS/ACerS 4th International Conference on Ceramic Interconnect and Ceramic Microsystems Technologies Proceedings*, Munich, Germany, CICMT 2008, 140 – 147

1.2 Papers to be submitted

[5] **Zhi Fu**, Aiying Wu, Paula M. Vilarinho, Angus I. Kingon, "Effect of Suspension Medias on Electrophoretic Deposition of $BaNd_2Ti_5O_{14}$ Thick Films", to be Submitted to *Chemistry of Materials*

2. Patents:

[6] Paula M. Vilarinho, **Zhi Fu**, Aiying Wu, Angus I. Kingon, "Tunable Low Loss (High Q) Dielectric Composite Thick Films and Method of Making the Same", *Portuguese Patent*, Submitted

[7] Paula M. Vilarinho, **Zhi Fu**, Aiying Wu, Angus I. Kingon, "the Employment of Graphite Interlayer for Insulator Substrates and Electrophoretic Deposition of High Q Dielectric Thick Films on That", *Portuguese Patent*, Submitted